

KILOWATT ISOTOPE

POWER SYSTEM

PHASE II PLAN

VOLUME IV

TELEDYNE FSCD vs. GDS

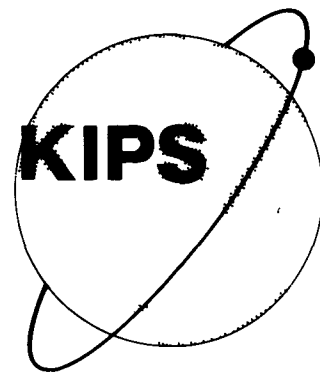
PREPARED BY

TELEDYNE ENERGY SYSTEMS

UNDER

SUBCONTRACT 282566

MASTER



Sundstrand Energy Systems

ROCKFORD, ILLINOIS 61101
unit of Sundstrand Corporation



C00-4299-025

DISTRIBUTION OF THIS DOCUMENT IS UNCLASSIFIED

DISCLAIMER

This report was prepared as an account of work sponsored by an agency of the United States Government. Neither the United States Government nor any agency Thereof, nor any of their employees, makes any warranty, express or implied, or assumes any legal liability or responsibility for the accuracy, completeness, or usefulness of any information, apparatus, product, or process disclosed, or represents that its use would not infringe privately owned rights. Reference herein to any specific commercial product, process, or service by trade name, trademark, manufacturer, or otherwise does not necessarily constitute or imply its endorsement, recommendation, or favoring by the United States Government or any agency thereof. The views and opinions of authors expressed herein do not necessarily state or reflect those of the United States Government or any agency thereof.

DISCLAIMER

Portions of this document may be illegible in electronic image products. Images are produced from the best available original document.

KILOWATT ISOTOPE POWER SYSTEM

PHASE II PLAN

**VOLUME IV
TELEDYNE FSCD VS GDS
PREPARED BY
TELEDYNE ENERGY SYSTEMS
SUBCONTRACT 282566**

To

DEPARTMENT OF ENERGY

From

**SUNDSTRAND ENERGY SYSTEMS
4747 HARRISON AVENUE
ROCKFORD, ILLINOIS 61101**

DISCLAIMER

This book was prepared as an account of work sponsored by an agency of the United States Government. Neither the United States Government nor any agency thereof, nor any of their employees, makes any warranty, express or implied, or assumes any legal liability or responsibility for the accuracy, completeness or usefulness of any information, apparatus, product, or process disclosed, or represents that its use would not infringe privately owned rights. Reference herein to any specific commercial product, process, or service by trade name, trademark, manufacturer, or otherwise, does not necessarily constitute or imply its endorsement, recommendation, or favoring by the United States Government or any agency thereof. The views and opinions of authors expressed herein do not necessarily state or reflect those of the United States Government or any agency thereof.

**C00-4299-025
15 MARCH 1978**

DISTRIBUTION OF THIS DOCUMENT IS UNLIMITED

NOTICE

“This document was prepared as an account of work sponsored by the United States Government. Neither the United States nor the United States Department of Energy nor any of their employees, nor any of their contractors, subcontractors, or their employees, make any warranty, express or implied, or assumes any legal liability or responsibility for the accuracy, completeness or usefulness of any information, apparatus, product or process disclosed, or represents that its use would not infringe privately-owned rights.”

TELEDYNE FSCD VS. GDS

FOREWORD

This report was written to satisfy the requirements of Task 10.0 of the Statement of Work to Sundstrand Energy Systems under the Department of Energy Contract Number EN-77-C-02-4299. The report is contained in five volumes:

Volume I	Phase II Program Plan
Volume II	Flight System Conceptual Design (FSCD)
Volume III	Ground Demonstration System (GDS) FSCD vs. GDS Comparison Evaluation Criteria Comments
Volume IV	Teledyne, FSCD and GDS
Volume V	Safety Quality Assurance Reliability

INTRODUCTION

This Volume IV contains Teledyne's input to the Kilowatt Isotope Power System Phase II Plan. Included is a description of the Flight System Heat Generation System, Flight System Radiator, Thermal Insulation Stability, GDS Heat Generation System and GDS Radiator.

The paragraph numbers of this volume correspond to the overall KIPS Phase II paragraph numbers.

INPUT TO FINAL REPORT

TABLE OF CONTENTS

2.5.1	FLIGHT SYSTEM HEAT GENERATOR SYSTEM
2.5.1.1	Introduction
2.5.1.2	Summary
2.5.1.3	Thermal Environment of Heat Source
2.5.1.4	Emergency Cooling System
2.5.1.5	Venting/Gas Management
2.5.1.6	Reliability
2.5.1.7	Structural Analysis
2.5.2.6	FLIGHT SYSTEM RADIATOR
2.5.2.6.1	Configuration
2.5.2.6.2	Tradeoff Studies and Analyses
2.5.2.6.3	Flow Distribution
2.5.2.6.4	Structural Analysis
2.5.2.6.5	Fabrication and Inspection
2.5.2.6.6	Critical Characteristics
2.5.2.6.7	Reliability
2.5.2.8	THERMAL INSULATION STABILITY
2.5.2.8.1	Foil Insulation
2.5.2.8.2	Fibrous Insulation

TABLE OF CONTENTS (CONTINUED)

3.5.1	GDS HEAT GENERATION SYSTEM
3.5.1.2	Summary
3.5.1.3	Thermal Environment of Heat Source
3.5.1.4	Emergency Cooling System
3.5.1.5	Venting/Gas Management
3.5.1.6	Reliability
3.5.2.6	GDS RADIATOR
3.5.2.6.1	Configuration
3.5.2.6.2	Analyses
3.5.2.6.2.1	Thermal/Hydraulic
3.5.2.6.2.2	Meteoroid
3.5.2.6.2.3	Structural
3.5.2.6.3	Tests
3.5.2.6.3.1	Coating Tests
3.5.2.6.3.2	Thermal/Hydraulic Test Program
3.5.2.6.4	Fabrication and Inspection
A. DIX A	Thermoelectric Topping Cycle for KIPS Organic Rankine Power System

LIST OF FIGURES

<u>TITLE</u>	<u>FIGURE NO.</u>
SECTION 2.0 FLIGHT SYSTEM CONCEPTUAL DESIGN	
KIPS Isotope Heat Source Assembly (HSA)	2.5.1.2-1
System Mount Schematic	2.5.1.2-2
MHW Heat Source	2.5.1.2-3
MHW Vent Design	2.5.1.2-4
Physical Model for Heat Source Temperature Calculations	2.5.1.3-1
Heat Source Response to Low Emissivity Boiler and Radiation Shield	2.5.1.3-2
KIPS Heat Source Assembly - MHW Heat Source Temperature	2.5.1.3-3
EHSA Thermal Model	2.5.1.3-4
Typical Sector Cross Section	2.5.1.3-5
Thermal Model of Heat Source Assembly (Steady State Analysis)	2.5.1.3-6
Thermal Model of Heat Source Assembly (Reentry Thermal Analysis)	2.5.1.3-7
Temperature Distribution of Heat Source Assembly (IHS)	2.5.1.3-8
Temperature Distribution of Heat Source Assembly (IHS)	2.5.1.3-9
Temperature Distribution of Heat Source Assembly (IHS)	2.5.1.3-10
Peak Surface Temperature During Reentry	2.5.1.3-11
Peaks PICS Temperature During Reentry	2.5.1.3-12
Total Surface Recession	2.5.1.3-13
Maximum PICS Temperature at Impact	2.5.1.3-14
Minimum PICS Temperature at Impact	2.5.1.3-15
PICS Temperature Range at Impact vs. Initial Surface Temperature of IHS	2.5.1.3-16
PICS Temperature Range at Impact vs. Initial Path Angle	2.5.1.3-17
Temperature and Recession Histories During Reentry	2.5.1.3-18
One Dimensional Tap II in Multifoil Transient Model	2.5.1.4.1
Heat Source Assembly Temperatures After Boiler Fluid Flow Stoppage	2.5.1.4-2
Measured Heat Flux Through Zirconia Coated Aluminum Multifoil Insulation System	2.5.1.4-3
Sample Assemblies for Compatibility Test	2.5.1.4-4
Meltdown Assembly Simulating KIPS Heat Source	2.5.1.4-5

LIST OF FIGURES (CONT.)

<u>TITLE</u>	<u>FIGURE NO.</u>
Test Arrangement for Meltdown	2.5.1.4-6
Temperature-Time Profile for KIPS Meltdown Assembly	2.5.1.4-7
EHSA Multifoil Meltdown Test Flow Diagram	2.5.1.4-8
Temperature Response of Single Thermocouple Attached to the EHSA Components	2.5.1.4-9
Temperature Response of EHSA Components Averaged in the Axial Direction	2.5.1.4-10
Electrical Heat Source Assembly (EHSA) Inside the Thermal Vacuum Chamber After the Meltdown Test	2.5.1.4-11
Heater Block Assembly Removed from the EHSA	2.5.1.4-12
A view Inside the Lower End of the Heater Block Assembly	2.5.1.4-13
The Remaining Foil Outside the Boiler Shows Signs of Partial Melting	2.5.1.4-14
Single Failure Points - IHSA	2.5.1.6-1
Cylinder and Rib Stiffened End Cover	2.5.1.7-1
Cylindrical Portion of the HSA Housing	2.5.1.7-2
KIPS Radiator	2.5.2.6-1
Effect of Tube Diameter and Flow Rate on KIPS Radiator Pressure Drop	2.5.2.6-2
Flight System Radiator Tube Armor	2.5.2.6-3
Two-Tube Model Schematic	2.5.2.6-4
Flow Percentage Versus Total Flow Rate	2.5.2.6-5
Tube Outlet Temperature Versus Total Flow Rate	2.5.2.6-6
Radiator Loads	2.5.2.6-7
Radiator Panel Section	2.5.2.6-8
Radiator Leak Single Point Failure Locations	2.5.2.6-9

SECTION 3.0 GROUND DEMONSTRATION SYSTEM

Electrical Heat Source Assembly	3.5.1.2-1A
Electrical Heat Source Installation	3.5.1.2-1B
EHSA Housing	3.5.1.2-2
Boiler Tube Penetration Assembly Installation	3.5.1.2-3
Electrical Heater	3.5.1.2-4
Schematic Electrical Heater	3.5.1.2-5
Boiler Assembly	3.5.1.2-6
Boiler Assembly Instrumentation	3.5.1.2-7

LIST OF FIGURES (CONT.)

<u>TITLE</u>	<u>FIGURE NO.</u>
EHSA Power Supply Console	3.5.1.2-8
EHSA Power Supply Console (Interior View)	3.5.1.2-9
Heat Loss from Housing and One End Cover	3.5.1.3-1
Heat Radiated from Boiler to Inside Surface (Can) of Multifoil Insulation	3.5.1.3-2
Heat Transferred Through Multifoil Insulation	3.5.1.3-3
Heat Transferred Through MIN-K End Insulation	3.5.1.3-4
Heat Transferred from Tube to End Cover	3.5.1.3-5
Side View of Mounting Structure	3.5.1.3-6
Top View of Mounting Structure	3.5.1.3-7
Conduction Heat Transfer from EHSA Support Structure	3.5.1.3-8
Radiation Heat Transfer from EHSA Support Structure	3.5.1.3-9
Radiation Heat Transfer from EHSA End Cover	3.5.1.3-10
Heat Loss from EHSA Housing Lower End Cover to Mounting Plate and Shroud	3.5.1.3-11
KIPS Heat Source Vacuum Test Power Lead Temperatures	3.5.1.3-12
KIPS Heat Source Cumulative Heat Loss (Within Heat Source)	3.5.1.3-13
Heat Balance Applied to Differential Element	3.5.1.3-14
KIPS Heat Source Vacuum Test Thermocouple Wire Temperatures	3.5.1.3-15
KIPS Heat Source Cumulative Thermocouple Wire Heat Loss	3.5.1.3-16
Heater Cartridge Test Set-up	3.5.1.3-17
KIPS Electrical Heater Cartridge Circuit Resistance Versus Operating Time	3.5.1.3-18
Test Set-up in TM Vacuum Furnace	3.5.1.3-19
EHSA Test Flow Diagram	3.5.1.3-20
Heater Block Temperature Profile	3.5.1.3-21
KIPS GDS Electric Heat Source Assembly Enclosure Gas Seal Leak Failure Points	3.5.1.6-1
Ground Demonstration System Radiator Assembly	3.5.2.6-1
Extrusion/Adaptor to Header Termination Extrusion	3.5.2.6-2
Header/Tube Termination 4-Tube Panel Test	3.5.2.6-3
KIPS Radiator Thermal Hydraulic Characteristics	3.5.2.6-4
Radiator Structure Weight Versus Skin Thickness for Various Diameters	3.5.2.6-5
Minimum (Constrained) Radiator Weight	3.5.2.6-6
Sensitivity of Header Weight to No-Puncture Probability	3.5.2.6-7
	3.5.2.6-8

LIST OF FIGURES (CONT.)

<u>TITLE</u>	<u>FIGURE NO.</u>
Relationship of Tube Weight to No-Puncture Probability	3.5.2.6-9
Relationship of Radiator Weight to Tube and Header Probability	3.5.2.6-10
Armor Requirement as a Function of No-Puncture Probability	3.5.2.6-11
Spectral Directional Reflectance of Two White Paint Specimens	3.5.2.6-12
Hemispherical Emittance of White Paint Specimens at Temperatures from -160°F to 266°F	3.5.2.6-13
KIPS Isothermal Tube Test Pressure Drop Between Radiator Tube Pressure Taps Versus Reynolds Number	3.5.2.6-14
KIPS Flow Test-Moody Friction Factor Versus Reynolds Number	3.5.2.6-15
Radiator Short Panel in T/V Chamber	3.5.2.6-16
KIPS Short Panel T/V Test Heat Rejection Versus Mass Flow Per Tube	3.5.2.6-17
Radiator Long Panel in-Air Test	3.5.2.6-18
KIPS Long Panel Flow Test Total Pressure Drop Versus Mass Flow Per Tube	3.5.2.6-19
KIPS Long Panel Flow Test Extrusion Pressure Drop Versus Mass Flow Per Tube	3.5.2.6-20
KIPS Long Panel Flow Test Header Pressure Drop Versus Mass Flow Per Tube	3.5.2.6-21
Extrusion/Adapter to Header Termination	3.5.2.6-22
Radiograph Technique Weld Specimen	3.5.2.6-23
NDT Radiograph Technique	3.5.2.6-24
Extrusion/Header to Header Weld Test Sample	3.5.2.6-25
Extrusion/Adapter Weld	3.5.2.6-26
Adapter to Extrusion Weld (Obsolete Design)	3.5.2.6-27
Metallography of Extrusion/Adapter Subassembly to Header Weld	3.5.2.6-28
Metallography of Extrusion/Adapter Subassembly to Header Weld	3.5.2.6-29

LIST OF TABLES

<u>TITLE</u>	<u>TABLE NO.</u>
 SECTION 2.0 FLIGHT SYSTEM CONCEPTUAL DESIGN 	
Components, Materials, and Weight	2.5.1.2-I
Predicted HSA Steady State Operational Temperatures OF	2.5.1.3-I
Thermal Properties of Heat Source	2.5.1.3-II
Summary of Results - Thermal Model No. 2	2.5.1.3-III
Steady State EHSA Performance Prior to Meltdown	2.5.1.4-I
Pre and Post Meltdown Equilibrium Temperatures of the EHSA Components	2.5.1.4-II
Failure Mode Likelihood Rank	2.5.1.6-I
Failure Effects Categories and Ranking	2.5.1.6-II
Failure Mode and Effects Analysis - IHSA	2.5.1.6-III
Radiator Weight Breakdown	2.5.2.6-I
Flight System Radiator Design Performance Criteria and Design Constraints	2.5.2.6-II
Failure Mode and Effects Analysis	2.5.2.6-III
Radiator Leak Single Point Failures	2.5.2.6-IV
Candidate Fibrous Insulation	2.5.2.8-I
 SECTION 3.0 GROUND DEMONSTRATION SYSTEM 	
EHSA Weight	3.5.1.2-I
Summary of Heat Loss Characteristics	3.5.1.3-I
Heat Flow Path and Environment Characteristics	3.5.1.3-II
Heat Flow Path and Environment Characteristics	3.5.1.3-III
KIPS Electrical Heater Cartridge Thermal Test Program	3.5.1.3-IV
Summary of Statistical Evaluation of Heater Cartridge Circuit Resistance	3.5.1.3-V
Summary of the Test Results	3.5.1.3-VI
A Summary of Heat Losses from EHSA Based on Various Component Temperatures	3.5.1.3-VII
EHSA Acceptance Test Data	3.5.1.3-VIII
Failure Mode and Effects Analysis	3.5.1.6-I
KIPS GDS Heat Source Enclosure, Gas Seal Leak Points	3.5.1.6-II
Radiator Weight Breakdown	3.5.2.6-I
GDS Radiator Design Performance Requirements and Design Constraints	3.5.2.6-II
Accoustic Spectrum	3.5.2.6-III

LIST OF TABLES (CONT.)

TITLE

TABLE NO.

Expected Load Environments	3.5.2.6-IV
Aluminum Alloys Based on Load Environment	3.5.2.6-V
Structural Design Criteria	3.5.2.6-VI
Radiator Structure Weight	3.5.2.6-VII
Values of Solar Absorption and Normal and Hemispherical Emittance of White Paint Specimens	3.5.2.6-VIII

2.5.1 Heat Generation System

2.5.1.1 Introduction

The KIPS utilizes an organic working fluid with a Rankine thermodynamic power conversion cycle and consists of two major subsystems: three Heat Source Assemblies (HSA) and power conversion machinery. Each HSA consists of one MHW-type isotope heat source (IHS), a fin/tube heat exchanger, heat source support system, emergency cooling system, insulation, housing, and a gas management device.

The isotope heat source is in the shape of a right circular cylinder and consists of 24 fuel containers having individual impact protection, the aeroshell and the ablation sleeve exterior to the aeroshell. The heat producing radioisotope Plutonium-238 is in the form of the oxide, PuO_2 . The fuel containers consist of a fuel sphere, a metallic shell which serves to contain in the fuel, and a graphite impact shell which provides the primary resistance to mechanical impact loads. The graphite aeroshell serves as an ablator during reentry as well as an attenuator of reentry heating to the heat source interior. The Pyrocarb ablation sleeve protects the POCO aeroshell from excessive thermal stress during reentry.

The remainder of the HSA is in the shape of a right circular, stepped cylinder and consists of an outer aluminum housing, which is the main support structure for the isotope heat source, the end closures, the aluminum foil emergency cooling system, the stainless steel boiler tube/copper fin heat exchanger, the radiation barrier, and the required insulation necessary to support the isotope heat source and to maintain heat losses at a tolerable level. There are three HSA's in the KIPS. Each serves as a portion of the support structure for the power conversion machinery and each is mounted to the spacecraft structure through a shock-mount.

2.5.1.2 Heat Source Assembly (IHSA)

The Isotope Heat Source Assembly (IHSA) is a right circular, stepped cylinder which measures 11.34 inches diameter at the non-loading end, 10.13 inches diameter at the midpoint, 11.94 inches diameter at the loading end, 24.62 inches overall length from the fixed end of the housing to the pressure relief device and weighs 73.5 pounds. See Figure 2.5.1.2-1. There are three IHSA's in the flight system, each supplying 2400 W(t) input to the flight system for conversion to output power.

Each IHSA serves as the mounting structure for a portion of the power conversion system (PCS) and is attached to the spacecraft structure by means of a single shock-mount. See Figure 2.5.1.2-2. Inlet and outlet connections to the heat exchanger tubes are made at the fixed end of the unit while loading of the MHW heat source takes place through the loading end, which is at the opposite end of the unit. HSA fuelling operations can be accomplished without having to disturb either of the heat exchanger tube connections.

To facilitate on-site ground checkout of the flight system prior to launch, the HSA is initially assembled using an electrical heater as the power source. After successful checkout, the electrical heater, center insulation disc and lower cover are removed and replaced with the MHW heat source, flight-type insulation disc and end cover.

LEGEND

- 1 MHW HEAT SOURCE
- 2 RADIATION BARRIER
- 3 HEAT EXCHANGER
- 4 EMERGENCY COOLING SYSTEM
- 5 INSULATION-THERMAL STRUCTURAL
- 6 HOUSING
- 7 FIXED END CLOSURE
- 8 LOADING END CLOSURE
- 9 PRESSURE RELIEF DEVICE
- 10 SYSTEM SHOCKMOUNT ATTACHMENT
- 11 PCS STRUT ATTACHMENT
- 12 PCS ATTACHMENT
- 13 RADIATOR ATTACHMENT

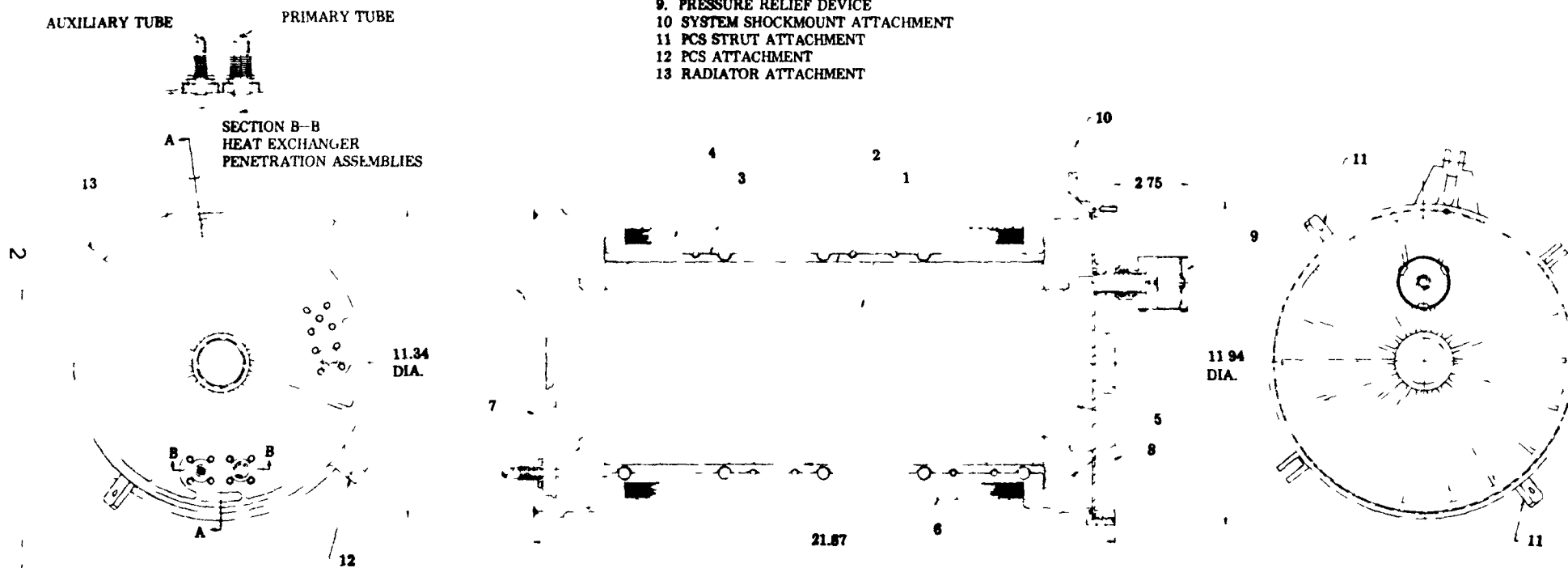


FIGURE 2.5.1.2-1 KIPS ISOTOPE HEAT SOURCE ASSEMBLY

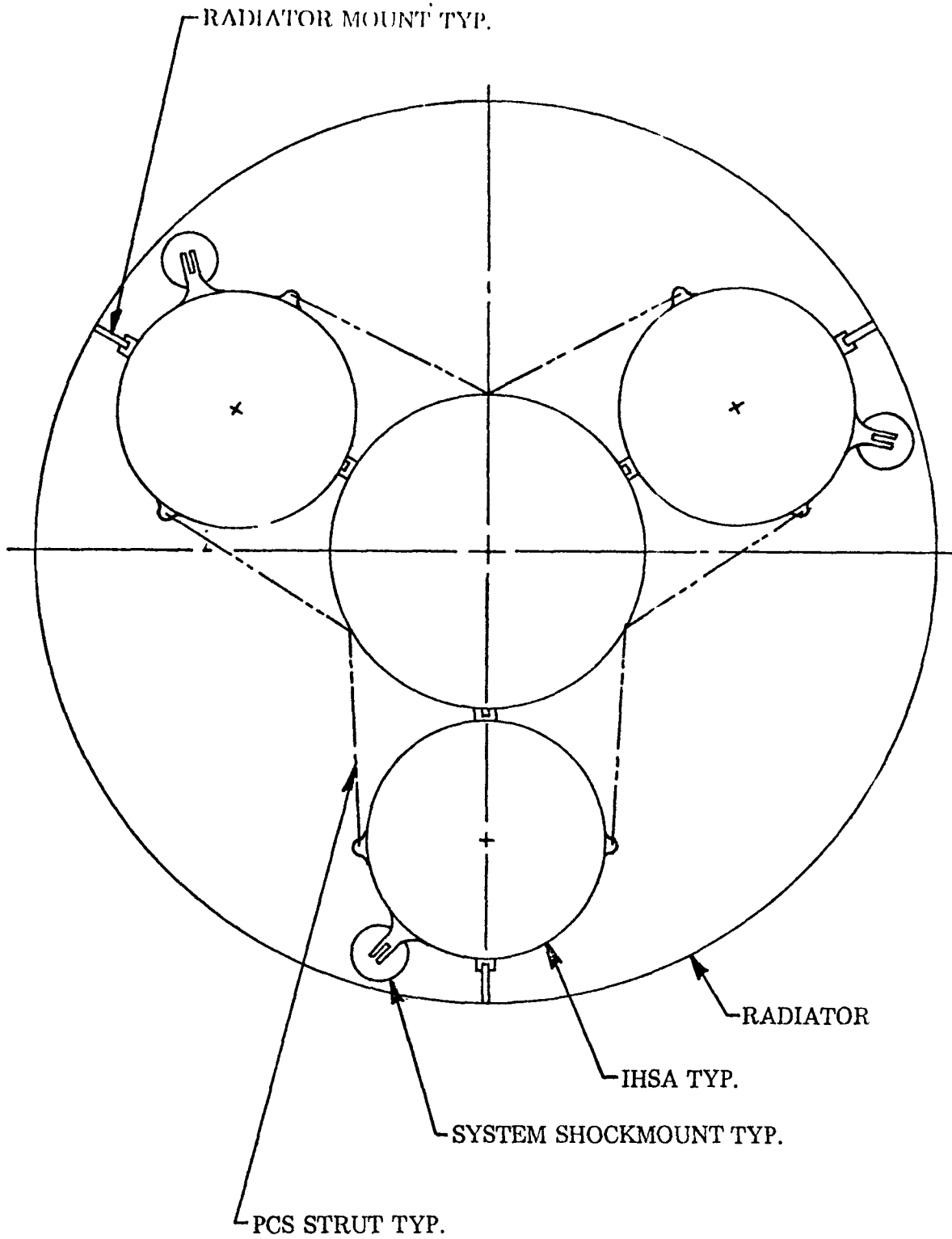


FIGURE 2.5.1.2-2
SYSTEM MOUNT SCHEMATIC

Loading of the MHW heat source takes place in a facility designed for this operation, using conventional fueling techniques and tooling.

Each of the IHSA's in the flight system is identical except for the heat exchanger center-body. The major components of an IHSA are the MHW heat source, radiation barrier, heat source heat exchanger, emergency cooling system, fibrous insulation, heat exchanger tube penetration fitting assemblies, upper and lower end covers, housing and pressure relief device. See Table 2.5.1.2-1 for a listing of individual components, materials and weights.

MHW Heat Source (HIS)

The MHW Heat Source (Figure 2.5.1.2-3) is in the shape of a right circular cylinder measuring 7.42 inches diameter and 16.53 inches in length and weighs approximately 42 pounds. The primary heat source element is the Fuel Sphere Assembly (FSA) which is a self-contained modular fuel element. The FSA's are arranged in six (6) planes of four (4) spheres each; adjacent planes are rotated 45° to achieve nesting and to minimize length. The FSA's are held in place in groups of eight (8) by segmented graphite retaining rings with conical seats. Woven graphite cloth compliance pads are positioned between each FSA plane to achieve a tight fit without tight tolerance control. Three (3) FSA/retaining ring subassemblies are inserted into the graphite crush-up material which is provided at both ends for additional FSA impact protection, graphite end caps, which are captivated by an expandable ring, complete the assembly. A woven graphite emissivity sleeve is placed over the cylindrical portion of the aeroshell.

The Fuel Sphere Assembly (FSA) is the basic heat source fuel element. The FSA is comprised of the fuel sphere, the Post Impact Containment Shell (PICS), two vent hole filter subassemblies, a weld shield, and the Graphite Impact Shell (GIS). The FSA is designed to provide impact protection and post-impact containment for the fuel.

Each fuel sphere contains an initial thermal inventory of 100 watts nominal. A total of 24 spheres provides a nominal thermal power of 2400 watts for the heat source at beginning of life. The physical form of the fuel is a sphere shaped, solid ceramic compact of plutonium dioxide, PuO₂. The individual sphere diameter is 1.465 inches.

The PICS consists of two welded, 0.024 thick, 1.550 inch internal diameter, iridium hemispheres, which encapsulate the fuel sphere. Each PICS is designed with the following: (1) vent hole (0.005 inch diameter) and vent hole filter subassembly in each hemisphere which permits the helium gas to vent but prevents release of particulates from the interior of the PICS; (2) a burst disc, which is welded over the vent hole to seal the PICS hermetically, thus permitting decontamination after fuel encapsulation; and (3) a weld shield, mounted on one hemisphere of the set, to provide thermal protection to the fuel during closure welding and to prevent contamination of the weld by the fuel. The vent hole filter subassembly is welded around its periphery to the hemisphere; the weld shield is attached to one of the hemispheres by welding at its three tabs. When assembled, these components (the iridium hemispheres with vent holes, the vent hole filter subassemblies, the burst discs, and the weld shield) comprise the Post-Impact Containment Shell (PICS); all components of the PICS are made of iridium. The hemispheres are grit blasted on their exterior surface to increase emissivity and thus enhance radiative heat transfer.

TABLE 2.5.1.2-I

<u>Component</u>	<u>Material</u>	<u>Weight (lbs)</u>
Housing	Aluminum Alloy 6061-T6	8.75
Cover, Upper	Aluminum Alloy 6061-T6	2.51
Cover, Lower	Aluminum Alloy 6061-T6	1.99
Lock Ring	Aluminum Alloy 6061-T6	.76
Penetration Assembly (.50 diameter tube)	Stainless Steel 304/321	.29
Penetration Assembly (.25 diameter tube)	Stainless Steel 304/321	.26
Gasket	Viton	.01
Heat Exchanger	Copper Shell/Stainless Steel Tubes	7.31
MHW Heat Source		42.00
Emergency Cooling System	Aluminum Alloy 1100	3.10
Insulation - Thermal/ Structural	Min-K TE-1400	4.36
Radiation Barrier	Nickel 201	1.40
Pressure Relief Device	Aluminum Alloy/Stainless Steel	.50
Miscellaneous Hardware		.26
		<hr/> 73.5

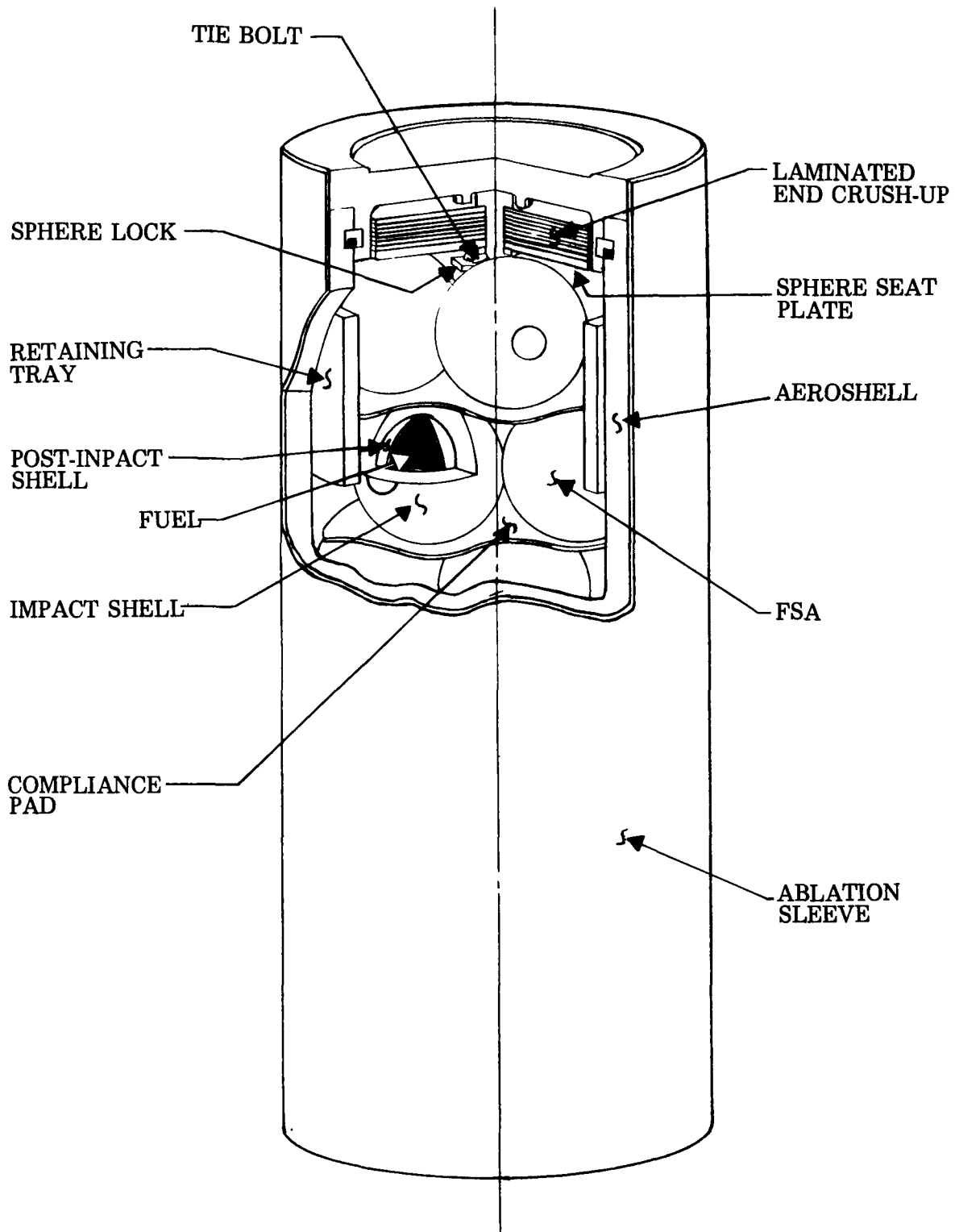


FIGURE 2.5.1.2-3
MHW HEAT SOURCE

Figure 2.5.1.2-4 shows the arrangement of the vent hole filter subassembly. The filter medium is a frit of iridium powder bonded to a circular weld disk and also to a circular cover disk. There is a 0.125 inch diameter hole in the weld disk that acts as an exit plenum for the helium diffusing through the frit. The circular periphery of the frit provides a relatively large area through which the helium can enter.

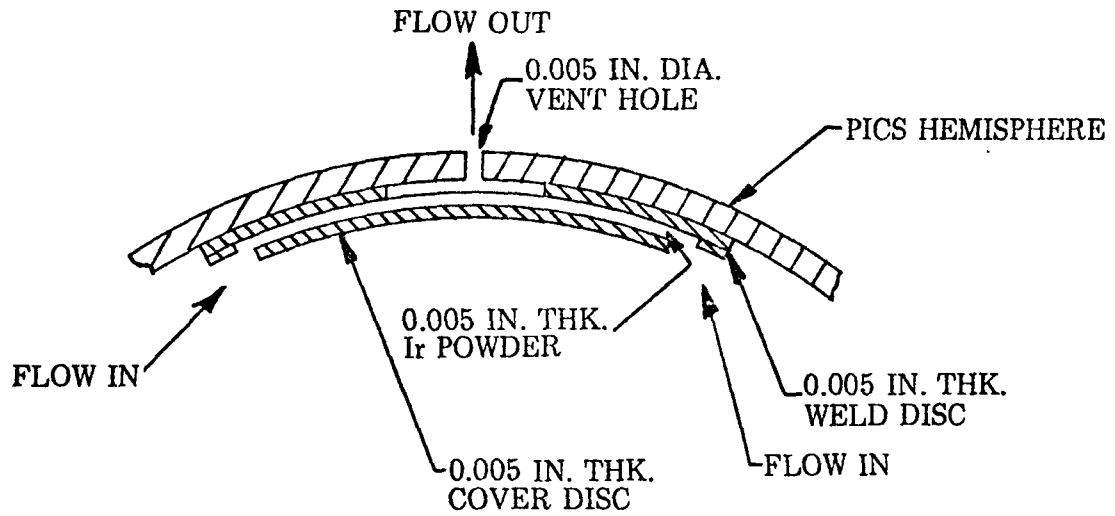


FIGURE 2.5.1.2-4
MHW VENT DESIGN

The Graphite Impact Shell (GIS) is designed to provide impact protection to the fuel sphere and to the Post-Impact Containment Shell under impact conditions associated with Heat Source terminal velocity. The GIS consists of a body and a cap which are produced by resin impregnating randomly wound spheres of Thornel-50 yarn and then pyrolyzing at 2500° F. The cap and body are threaded to provide a means of retention of the cap. The impact shell thickness is nominally 0.460 inches. A flat surface is machined on the impact shell for alignment with the retaining ring. However, the graphite retaining ring used to assemble groups of eight (8) FSA's provides the added thickness needed to compensate for the thinner flat spot.

The Heat Source is designed to be protected from the severe aerothermodynamic heating environment that may be encountered during reentry by the graphite aeroshell; the aeroshell also acts as the primary heat source structural member. The aeroshell is comprised of a cylindrical section and two end caps which are attached to the cylinder during the heat source assembly procedure. A purified poly crystalline graphite, POCO AXF-5Q1, is used for the aeroshell material.

The ablation sleeve is a cylindrical shell made of Pyrocarb-406 graphite with a wall thickness of 0.130 inch. The sleeve enhances radiative heat transfer to the heat exchanger during normal operation and provides additional strength and protection for the aeroshell against excessive thermal stress during steep angle superorbital re-entries.

Support and Preload Requirements

During the initial assembly of the MHW heat source by the Fueling Agency, a preload of approximately 800 pounds is placed upon one end of the heat source, while each heat source end plug is locked to the aeroshell by means of a graphite snap ring. Since the mating snap ring grooves in the aeroshell and end plug are made oversize in height because of the possible accumulation of tolerances during manufacturing and assembly operations, the initial 800 pound preload relaxes slightly. Because an 800 pound (minimum) preload is required to preclude excessive movement of the fuel sphere assemblies during the launch environment, it must be reapplied by the mounting of the heat source into its individual HSA.

The MHW heat source is supported by a compressive load applied to both ends of the heat source through Min-K TE-1400 support discs. Loads from the heat source are ultimately transmitted to the housing through each end cover. Preloading of the heat source takes place after it has been installed into the individual HSA.

Radiation Barrier

The radiation barrier, which is located in the annular space between the MHW heat source and heat exchanger, is required in order to raise* the temperature of the

* The need for increasing the MHW operational temperature for impact conditions will be described in a later section.

MHW heat source during normal operation. It is attached to each end of the heat exchanger with sheet metal screws.

The radiation barrier is a formed, thin wall, hollow, right circular cylinder which measures 7.57 inches outside diameter by 0.010 inch thick by 16.53 inches long and is made from nickel 201 sheet. After forming, the two edges of the sheet, which are butted together, are seam welded along their entire length, to form a continuous cylinder. Each side of the cylinder is grit blasted with aluminum oxide grit to provide the desired emissivity characteristics. Nickel 201 was selected as the material primarily because in a vacuum environment it does not form an oxide thereby enabling stable emissivity characteristics to be achieved and it has a low carbon content which precludes embrittlement at operational temperatures.

Heat Source Heat Exchanger

The heat source heat exchanger consists of a 0.020 inch thick copper shell that is formed around the primary and auxiliary cooling tubes. The primary cooling tube is 0.500 inch outside diameter by 0.035 inch wall stainless steel and the auxiliary cooling tube is 0.250 inch outside diameter by 0.035 inch wall stainless steel. Each tube is in a reverse spiral shape to enable the inlet and outlet portions of the tubes to exit at the same end of the shell. The tubes and shell are joined together by brazing. The entire assembly is coated on the inside and outside diameter with an iron titanate coating which is intended to assist in controlling the isotope heat source temperature.

The three flight system heat exchangers are connected in series to form three fluid flow zones: Subcooled, two phase and superheated. The inside of the primary cooling tube, on each heat exchanger, is fitted with a special insert which is intended to increase the film coefficient of the working fluid and to induce a high radial acceleration to maintain fluid contact on the tube wall even under the most extreme g loads. There is a different insert inside each heat exchanger.

The minimum inside diameter of the heat exchanger shell is 7.63 inches and the maximum outside diameter, at the cooling tubes, is 8.81 inches. The shell flange-to-flange length is 16.53 inches. The heat exchanger fits in the annular space between the radiation barrier and the emergency cooling system and is supported at each end by clamping flanges between Min-K insulation rings. The shell flanges are hand formed at assembly, by making a series of cuts through the shell wall, and bent to rest upon the insulation.

The primary and auxiliary cooling tubes exit from the same end of the heat exchanger shell. They pass through the HSA upper end cover and through the penetration assemblies where they are joined to the inter-HSA tubing.

Emergency Cooling System

An aluminum multifoil insulation system is used in the flight system to assure that isotope heat source temperatures are maintained within tolerable limits, should Dowtherm cease to flow through the heat exchanger, by acting as an emergency heat

dumping system. In such an accident situation, the heat source temperature would rise, resulting in the melting of the multifoil insulation, thereby allowing the heat source to radiate heat through the heat exchanger walls to the housing thereby maintaining tolerable heat source temperatures. In addition to its ECS function the multifoil system (because of its excellent insulation properties) limits radial heat losses to the housing walls. The multifoil insulation system is located in the annular space between the outside of the heat exchanger and the inside of the housing.

The multifoil insulation system is a hollow right circular cylinder measuring 8.895 inches inside diameter by approximately 0.42 inch thick by 15.00 inches long. It consists of one continuous length of 0.001 inch thick type 1100 aluminum alloy foil loosely wrapped sixty times around an 0.010 inch thick type 1100 aluminum alloy foil can. Spacing between wraps is intended to be approximately 0.007 inch. The foil material is lightly coated on one side with zirconium oxide (ZrO_2). The primary purpose of the coating is to insure a separation between wraps of the foil. Aluminum was selected as the foil system material because of its compatibility with the heat exchanger operating temperature and its low density.

The multifoil system is purchased as an assembly from ThermoElectron Corporation, located in Waltham, Massachusetts. Tests which were conducted and analysis performed to support this design are described in another section.

Fibrous Insulation

Most of the insulation in an HSA is Min-K TE-1400, and serves three purposes: to minimize longitudinal and radial heat losses to the housing/end covers, to provide sufficient end preload for the isotope heat source and to support the heat exchanger and emergency cooling system. Min-K TE-1400 was selected because of its temperature, thermal conductivity and compressive strength properties.

Heat Exchanger Tube Penetration Assemblies

The penetration assembly fittings have two functions: to minimize the heat losses from the heat exchanger tubes to the end cover (where the tubes penetrate the cover) and to form a vacuum tight closure between these tubes and the end cover. The penetration assembly consists of a type 321 stainless steel formed bellows welded to a type 304 stainless steel flange. Stainless steel was selected because of its compatibility with the type 304 stainless steel heat exchanger tube material and for its relatively low thermal conductivity properties. There are four penetration assemblies in each HSA, two for the primary cooling tubes and two for the auxiliary cooling tubes.

The lower end of the bellows is pre-welded to the flange and is sized to allow the heat exchanger tube to pass through the bellows at assembly with approximately 0.06 inch radial clearance. The upper end of the bellows contains a reducing collar which is sized so the tube can be easily welded to the collar. This weld joint is made prior to outgassing the entire HSA.

There is a recess in each cover which is slightly larger than the outside diameter of the penetration assembly flange. The flange is isolated from the cover by a Viton rubber gasket and the radial clearance between the cover recess and the flange body. The only metal-to-metal contact in the penetration assembly/cover connection is through the four machine screws which attach the penetration assembly flange to the cover.

End Covers

Each of the end covers is machined from a disc of 6061-T6 aluminum alloy plate. Based upon structural analysis, aluminum was chosen for the cover material because of its strength to weight characteristics. Each end cover is circular shaped, with a flat, smooth underside to assist in the sealing and insulation preload process and has ribs for added stiffness, machined as an integral part of the outside surface.

A single piece cover closes the upper end of the HSA and contains the inlet and outlet connection fittings for the heat exchanger. This cover is joined to the housing, at assembly, by welding. The lower end of the HSA is also closed with a single piece cover which is joined to the housing by means of a specially machined lock ring. This feature provides access to the inside of the HSA thereby enabling the electrical heat source to be removed and the isotope heat source to be installed.

Housing

The housing is machined from a hollow tube, 6061-T6 aluminum alloy forging which initially measures 14.00 inches outside diameter by 2.50 inches wall thickness by 23.00 inches long. Based upon structural analysis aluminum was chosen for the housing material because of its strength to weight characteristics. Because the physical properties of such a large diameter billet of material are not covered in existing commercial specifications, room temperature tests will be performed in accordance with ASTM E8-69 on test rings taken from the billet, in each of three directions, to verify that ultimate and yield strengths as well as elongation characteristics of the basic forged material will meet the properties which were used in the structural analysis to determine various wall thicknesses in the housing.

One end of the housing has an Acme thread which allows an end cover to be attached using a specially machined lock ring, the other end has a weld flange for attachment of the other end cover. The system attachment fittings are machined as an integral part of the housing. The upper end of the housing has two attachment fittings: one for attaching the PCS, the other for the radiator. The lower end has three attachment fittings: two for attaching the PCS (using struts), the third for attaching (through a shockmount) to the spacecraft structure.

Pressure Relief Device (PRD)

The pressure relief device (PRD) is a device used to vent the internal pressure of the HSA. It is attached to the lower cover, during the pre-launch preparation cycle by means of a Swagelok-type fitting. The PRD has two primary functions: (1) maintain an hermetic seal, isolating the internal HSA from the air environment during

handling and launch pad operations, (2) vent the HSA to space during the ascent period of launch and thereafter provide an orifice adequately large enough to maintain the HSA internal vacuum environment. The seal prior to launch is maintained by a puncture diaphragm which is welded into the PRD penetration assembly. The HSA is vented after launch by the action of a lance piercing the puncture diaphragm. This is caused by the expansion of an evacuated bellows/spring system which is activated by the reduction of atmospheric pressure subsequent to launch.

2.5.1.3 Thermal Environment of the Isotope Heat Source

The purpose of the heat source assembly is to provide support and containment with an acceptable environment for the isotopic heat source. Also, the heat source assembly must provide an efficient means for transporting the isotopic decay heat to the working fluid. Analyses of the heat source assembly have verified that both high and low temperature constraints on the isotope heat source are met for normal operation and emergency (malfunction) conditions, including separate reentry conditions. These same analyses have demonstrated low heat losses to the surroundings with tolerable temperatures for all components.

System requirements and pertinent specifications are as follows:

Thermal Inventory	2400 W per HSA
Maximum Iridium PICS Temperature	1300°C (2372°F)
Minimum Iridium PICS Temperature	1050°C (1922°F)
Nominal Heat Exchanger Surface Temperature	400°C average value (752°F)

Heat Flow Path Analysis

Considerable effort was required to develop a method of transferring heat from the isotopic heat source surface to the heat exchanger that would assure the proper operating temperatures despite normal manufacturing tolerances. With heat transport by direct radiation from the heat source surface to the heat exchanger, very precise and stable values of thermal emittance would be necessary. Any slight variation in emittance due to variation in coating thickness or degradation could result in the heat source surface (hence PICS) temperature moving outside the acceptable limits. This implied that a very low emittance coating would have to be developed because no known material or coating appeared to have the necessary emittance. Thus, an approach to lessen temperature sensitivity to surface characteristics was incorporated into the design. A radiation barrier was placed between the heat source surface and the heat exchanger. This barrier increased the number of radiating surfaces between the heat source and the heat exchanger. Thus, for a given overall emittance the sensitivity to individual surface variations from nominal was greatly reduced. Likewise, the need for very low emittance coatings was eliminated, allowing use of commercially available surface treatments and coatings. Figure 2.5.1.3-1 gives a cross section of the heat source assembly showing the heat flow path from the heat source to the boiler.

Variation of surface emittances and the consequent effect on heat source temperatures was investigated by computer analyses. These analytical results are shown in Figure 2.5.1.3-2. Figure 2.5.1.3-2 shows the range of surface emittance values that are acceptable during normal operating of the HSA. In the event of a loss of coolant accident (LOCA), the multifoil insulation will melt away. Under these conditions, the same temperature limits apply to the heat source components. Thus, the choice of surface treatments and coatings is even further restricted. Figure 2.5.1.3-3 shows the effect of these restrictions on the possible choices of surface characteristics.

FIGURE 2.5.1.3-1

PHYSICAL MODEL FOR HEAT SOURCE TEMPERATURE CALCULATIONS

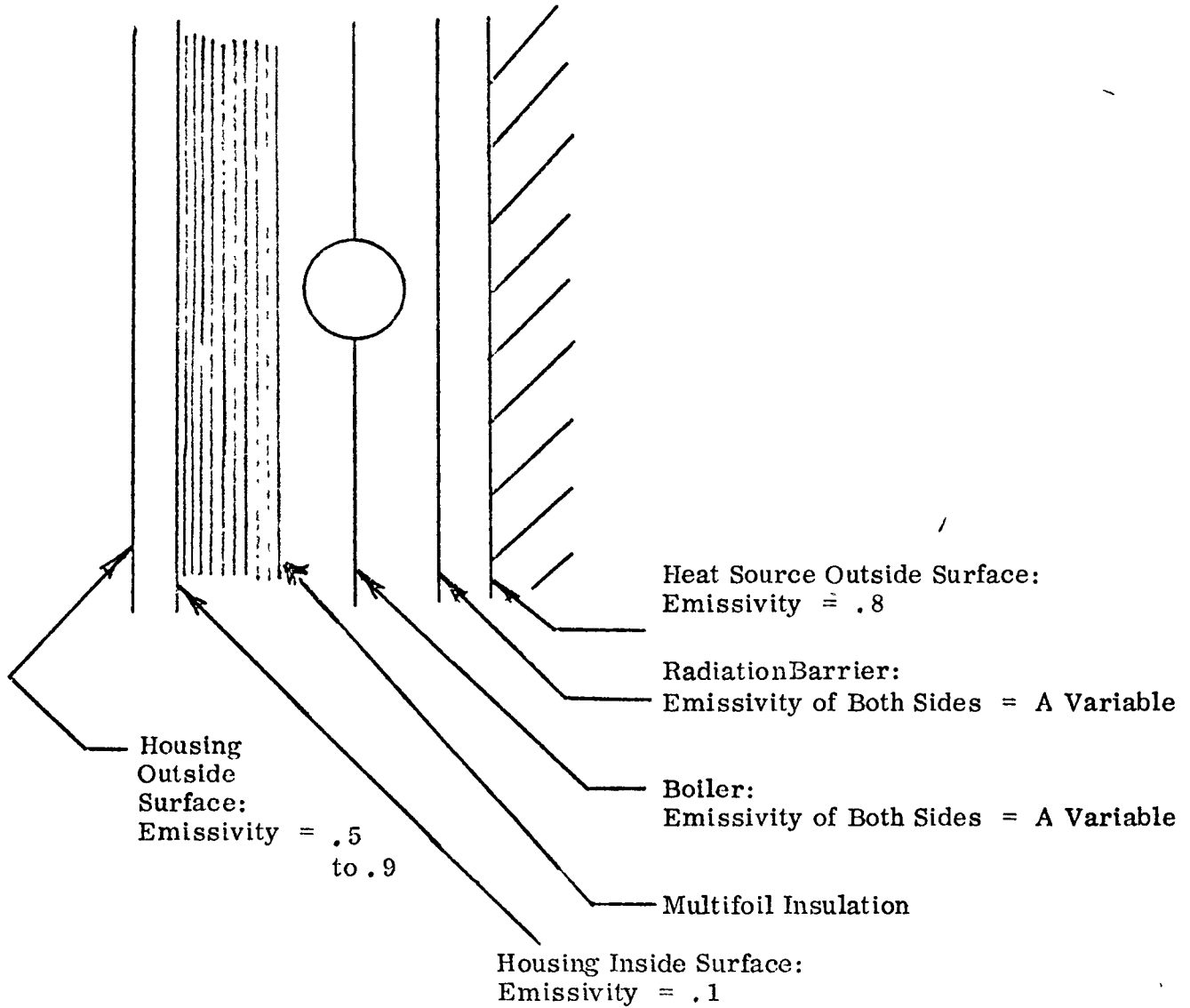


FIGURE 2.5.1.3-2
HEAT SOURCE RESPONSE TO LOW EMISSIVITY BOILER AND RADIATION SHIELD (NORMAL OPERATING CONDITION)

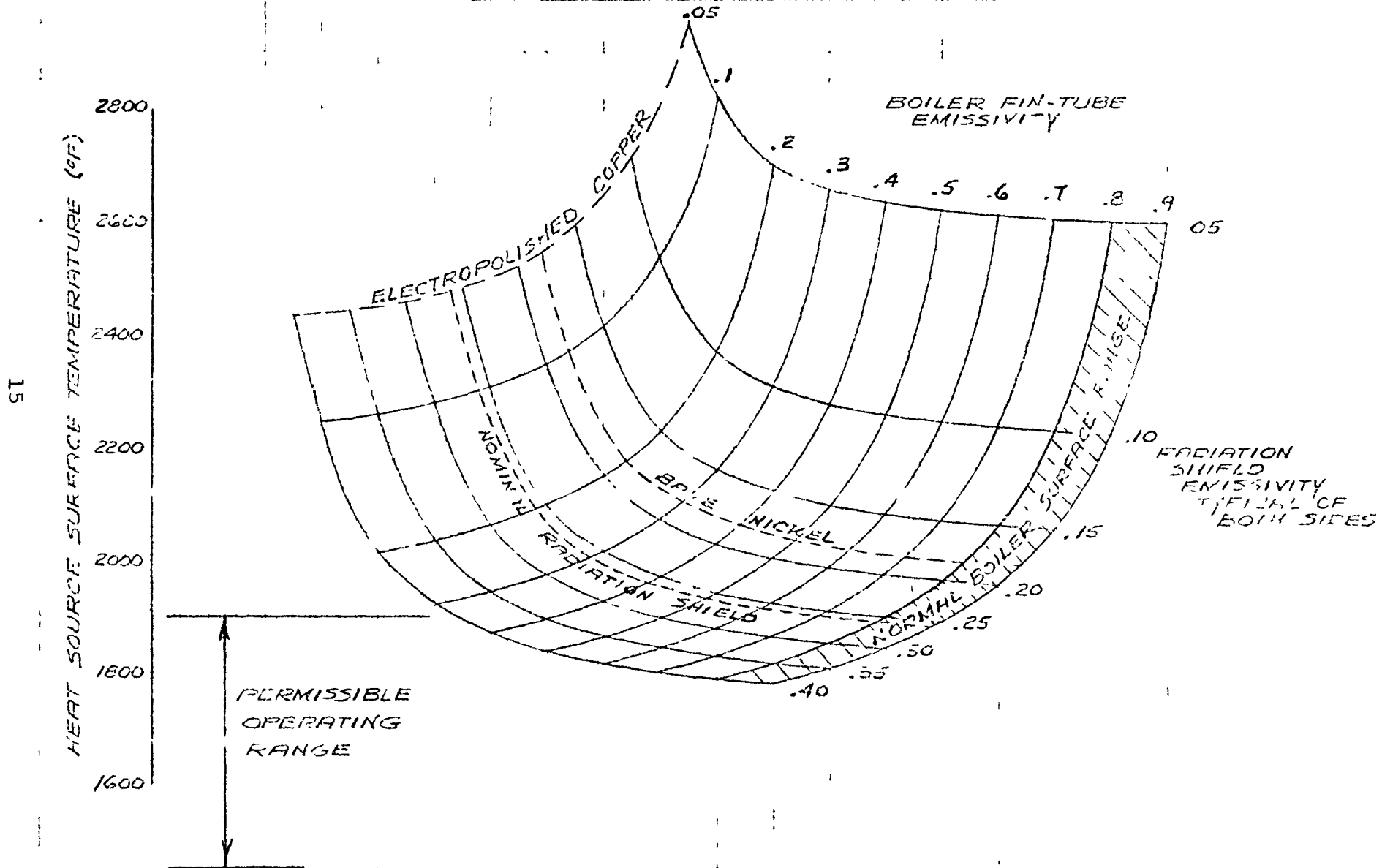
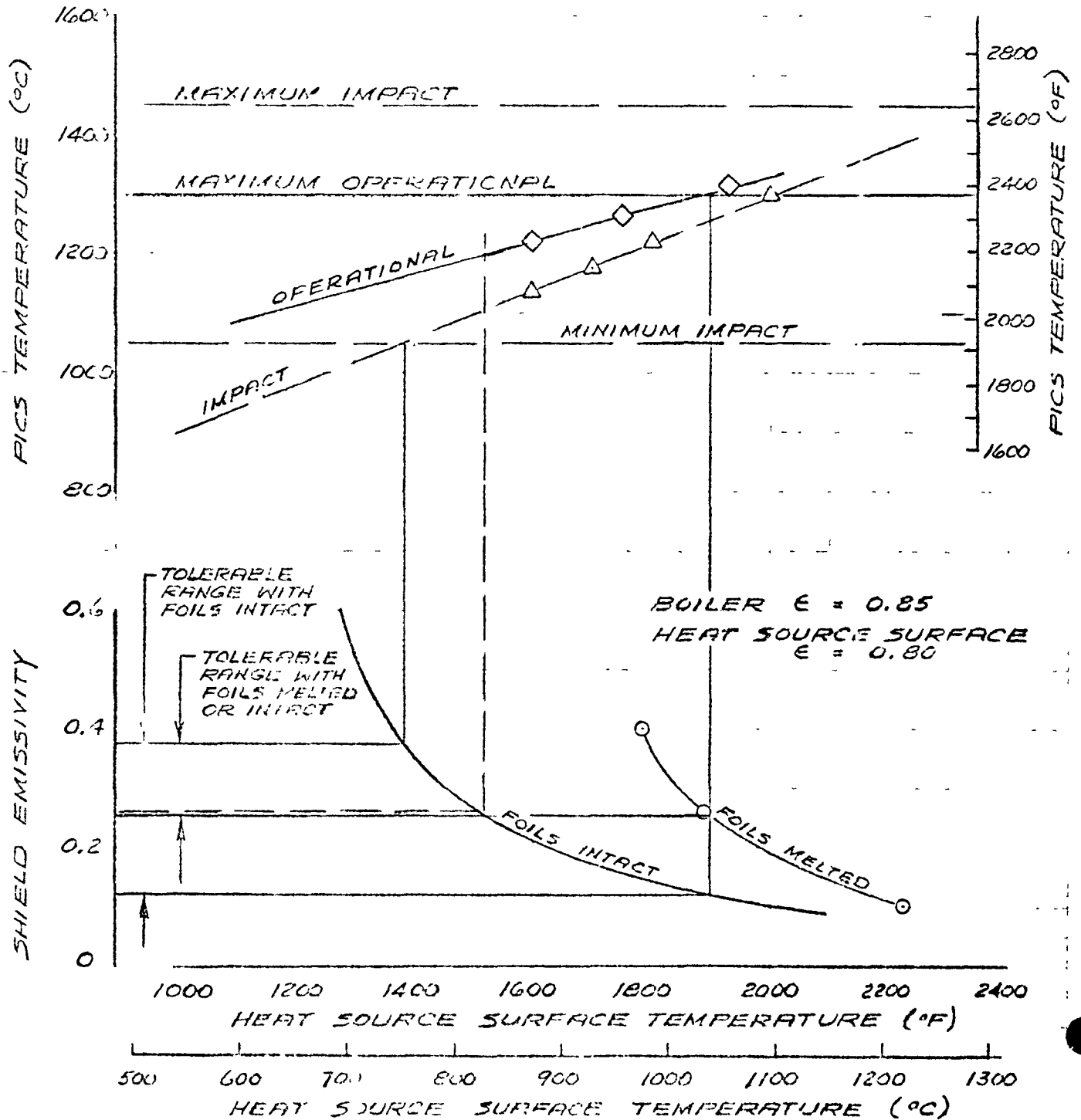


FIGURE 2.5.1.2-3
KIPS HEAT SOURCE ASSEMBLY
MHV HEAT SOURCE TEMPERATURES



The final choice of surface emittance, based on capability to satisfy requirements of both operating and malfunction environments, is 0.26 for both sides of the radiation barrier.

Steady State Temperatures

A computer thermal model of the HSA was constructed to determine the steady state operational temperatures at significant locations throughout the HSA. The HSA was assumed to be thermally symmetrical about a plane normal to the cylindrical axis passing midway between (and parallel to) the end covers. Also, symmetry was assumed about a plane containing the cylindrical axis and passing through the central axis of the housing inlet tube for the working fluid. Thus, one-fourth of the HSA was examined in detail. Figure 2.5.1.3-4 shows the section of the HSA chosen for computer analysis. This portion of the HSA was divided into six radial pie-shaped sectors with nodes assigned to the significant locations within each sector. A cross section view of sector 6 containing the fluid inlet tube is shown in Figure 2.5.1.3-5. A total of 166 nodes were used for the model. The predicted operational temperatures are summarized in Table 2.5.1.3-I.

Heat Flow Analysis

The computer code determined the heat flow in each nodal linkage. Appropriate linkage flows were summed by the program to determine net heat flow across a significant boundary. Considering the heat flow from housing and end cover nodes to space, and the heat flow through the fluid inlet tube, the thermal efficiency was calculated to be approximately 97.5%. Thus, the heat loss from one 2400 W(t) HSA is about 60 watts(t) during normal steady state operation.

Reentry Thermal Analysis

This study was conducted to determine the reentry and impact temperature and ablation response of the MHW heat source for the KIPS mission.

The IHS will experience surface recession in the 0.04 - 0.12 inch range and PICS impact temperatures in the 2000 - 2600°F range due to synchronous earth orbit malfunctions which result in prompt side-stable reentries. Temperature and ablation safety margins appear to be adequate for prompt reentries into the earth's atmosphere.

Two thermal models were developed for this study. One model represents the IHS for the steady state phase of the analysis, and the other is used for transient response analysis. The models represent sections that are approximately repetitive along the length of the IHS with respect to temperature and geometry. Within the retaining ring, the models represent a set of 2.554 inch diameters FSA's. From the retaining ring outward, the models are 2.21 inches thick. This dimension equals the distance between the centers of two adjacent sets of FSA's and hence implicitly accounts for the nesting of the FSA's and the inclusion of the compliance pads. The models are necessarily simplified representations of the actual hardware. Simplifications here include the omission of the compliance pads and tie bolt/lock ring

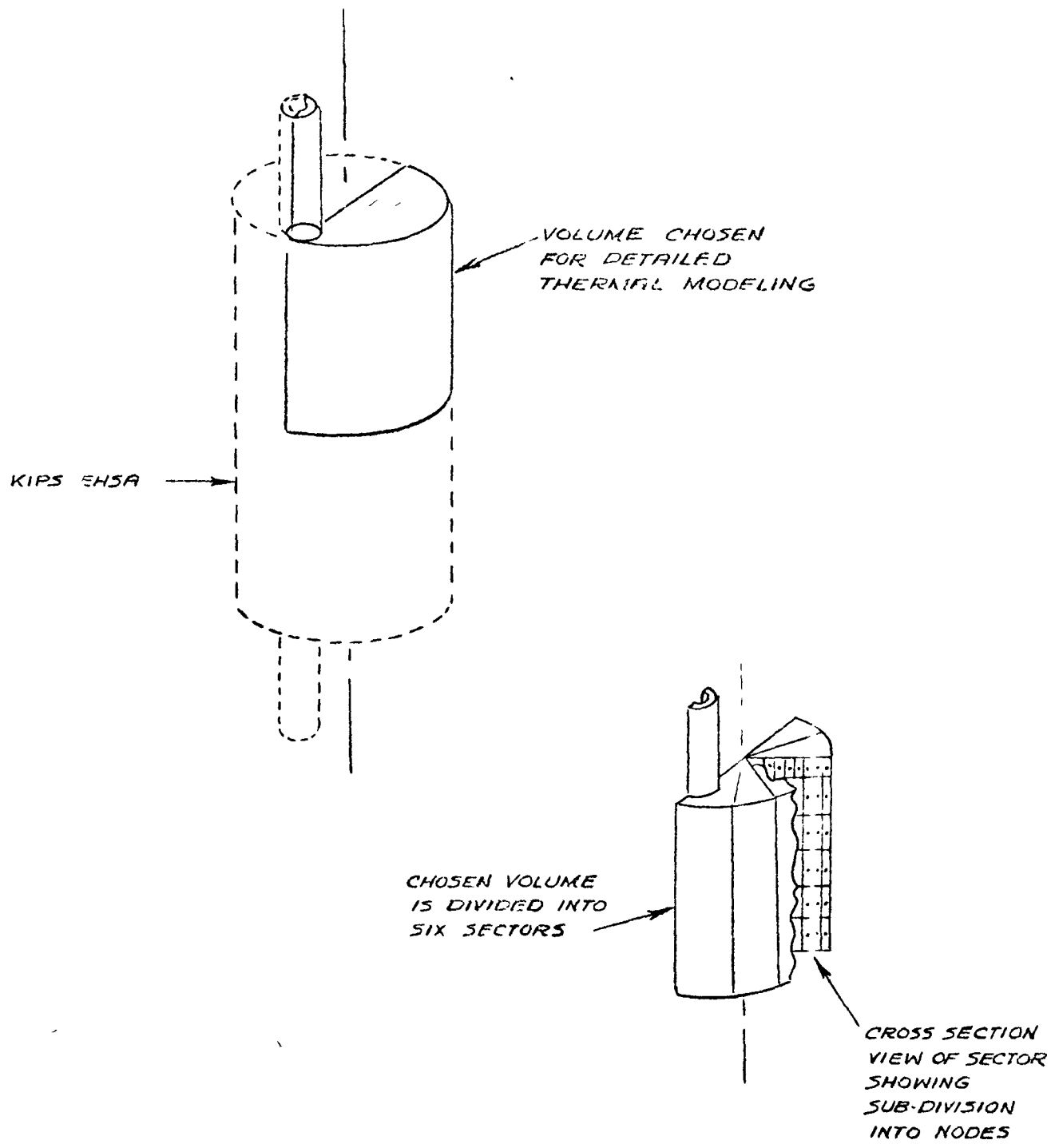
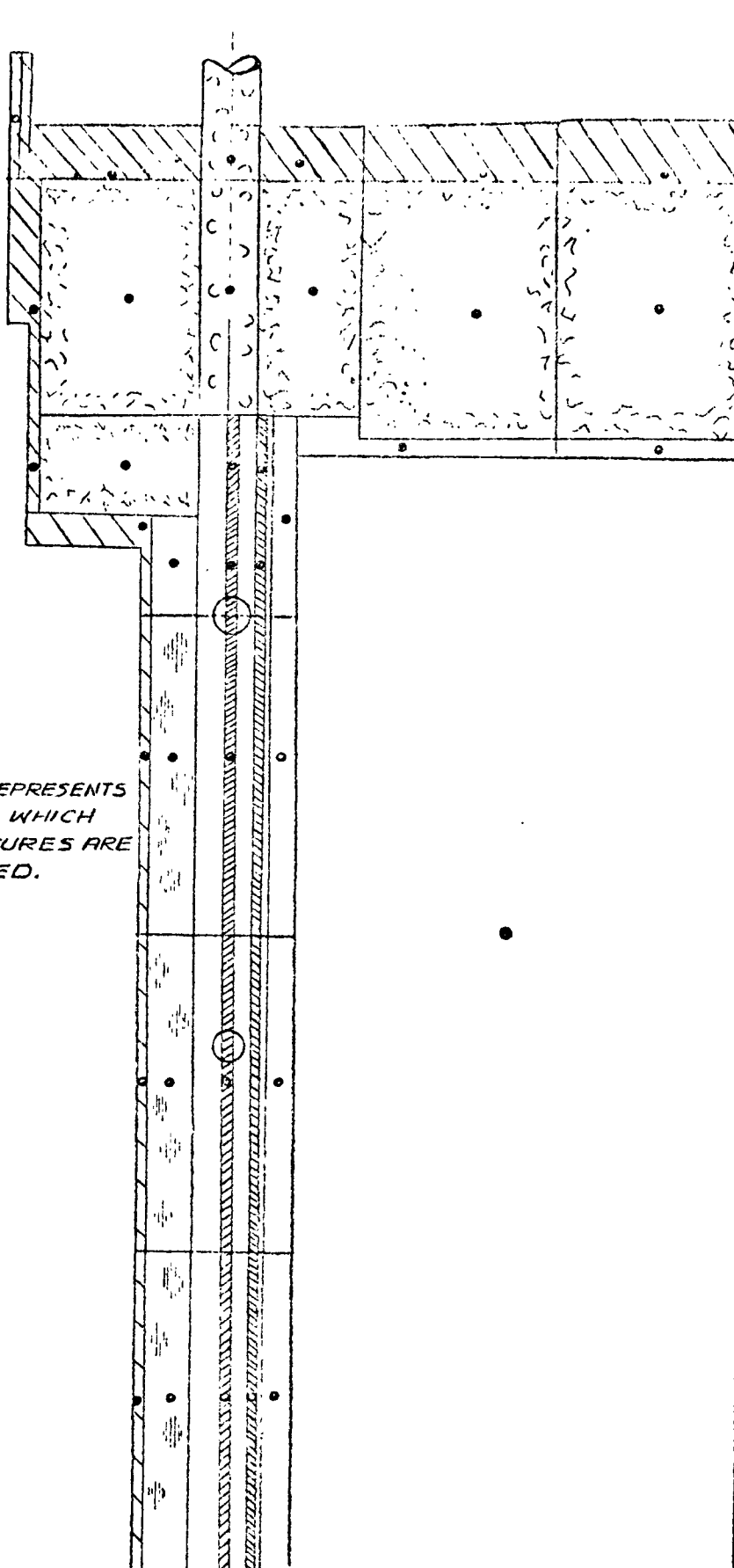


FIGURE 2.5.1.3-4
EWSA THERMAL MODEL

NOTE :

EACH DOT REPRESENTS
A NODE AT WHICH
TEMPERATURES ARE
CALCULATED.



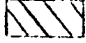
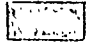
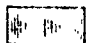


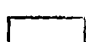
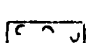
-  HOUSING
-  FIBROUS INSULATION
-  MULTIFOIL INSULATION
-  BOILER
-  RADIATION BARRIER
-  HEAT SOURCE
-  FLUID TUBE

FIGURE 2.5.1.3-5
TYPICAL SECTOR CROSS SECTION

TABLE 2.5.1.3-I
PREDICTED HSA STEADY STATE
OPERATIONAL TEMPERATURES (°F)

<u>Location</u>	<u>Highest</u>	<u>Typical</u>	<u>Lowest</u>
Upper End Cover	203	180	163
Housing Side	178	165	154
Fibrous Insulation*	1018	700	306
Multifoil**	799	790	782
Heat Exchanger	836	750	663
Radiation Barrier	1537	1420	1338

* These temperatures represent values at the centers of nodal volumes. Appreciable gradients exist in the insulation particularly so surface temperatures differ appreciably from values given.

** These temperatures represent values along the foil inside surface just opposite the heat exchanger surface.

assembly and the assumption of one continuous retainer ring per IIS. Also, heat conduction through the gas that immediately surrounds the FSA's was assumed to be zero. Further details of individual models are now described.

Model #1 (IIS - Steady State)

Model #1 shown in Figure 2.5.1.3-6, represents a 90° section of the IIS for the computation of steady state temperatures. The boundary condition for this model is the outer surface temperature which was held uniform.

Two different conditions were evaluated regarding the gap fill. One condition considered helium being in all gaps. The other condition considered evacuated gaps except the fuel/PICS gap which contained helium. The former condition is a representation of a helium filled and sealed IIS such as is used in some space T/E generator applications. The latter condition is a representation of an unsealed IIS such as is used in the KIPS.

Model #2 (IIS - Transient)

Model #2, shown in Figure 2.5.1.3-7, represents a 180° section of the IIS for the computation of temperatures from the time the heat source is released from the assembly until it impacts on the earth's surface. The boundary conditions for this model are convective and radiative heat fluxes on the outer surface. The heating distributions used were for a side stable reentry mode with element 1 being on the windward side. The model can be used equally well for side spin reentry modes for which the side stable heating distributions would be averaged and applied uniformly over the external surface.

Continuum air is assumed to be in all gaps during reentry except the fuel/PICS gap which is assumed to contain helium.

Surface recession is computed for oxidation and sublimation of the ablation sleeves. The heat balance at the surface is modified to account for these reactions. The model, however, does not account for the shrinking of the ablation sleeve elements due to surface recession.

Thermal Properties

Conventional thermal properties used in this study are given in Table 2.5.1.3-II. In addition, reaction rate constants reported in Ref. 1 for Poco AXF-Q1 graphite were assumed to apply for the computation of oxidation rates of the Pyrocarb 406 ablation sleeve. The reason for this substitution is that reaction rate oxidation data for Pyrocarb 406 apparently does not exist since no reference to such data is made in the Updated Safety Analysis Report for the MJS-II Mission (GE #76SDS4241 dated June 1976).

FIGURE 2.5.1.3-6
THERMAL MODEL OF HEAT SOURCE ASSEMBLY
(STEADY STATE ANALYSIS)

THERMAL MODEL NO.1
MODEL THICKNESS = 2.21" EXCEPT FSA'S

HELIUM FILLED GAPS

ABLATION SLEEVE
(PYFOCARB 406 GRAPHITE)

AEROSHELL (POCO AXF 5Q1
GRAPHITE)

RETAINING RING
(FOCO AXF 5Q1
GRAPHITE)

FUEL SPHERE
ASSEMBLY

CONTACT RESISTANCE
(1600 BTU/FT²·HR·°F)

GRAPHITE IMPACT
SHELL (THORNEL 50)

FUEL (PRESSED PLUTONIUM
OXIDE)
100 WATTS / SPHERE

POST IMPACT CONTAINMENT
SHELL (IRIDIUM)

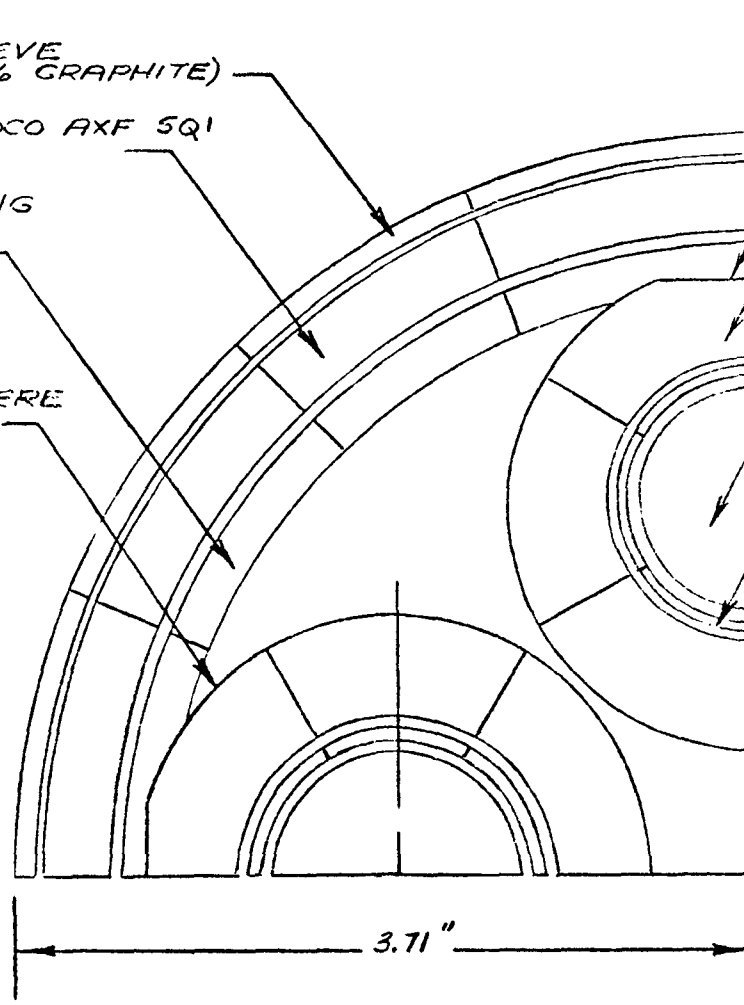


FIGURE 2.5.1.3-7
THERMAL MODEL OF HEAT SOURCE ASSEMBLY
(REENTRY THERMAL ANALYSIS)

MODEL NO. 2

MODEL THICKNESS = 2.21" EXCEPT
 FSA'S

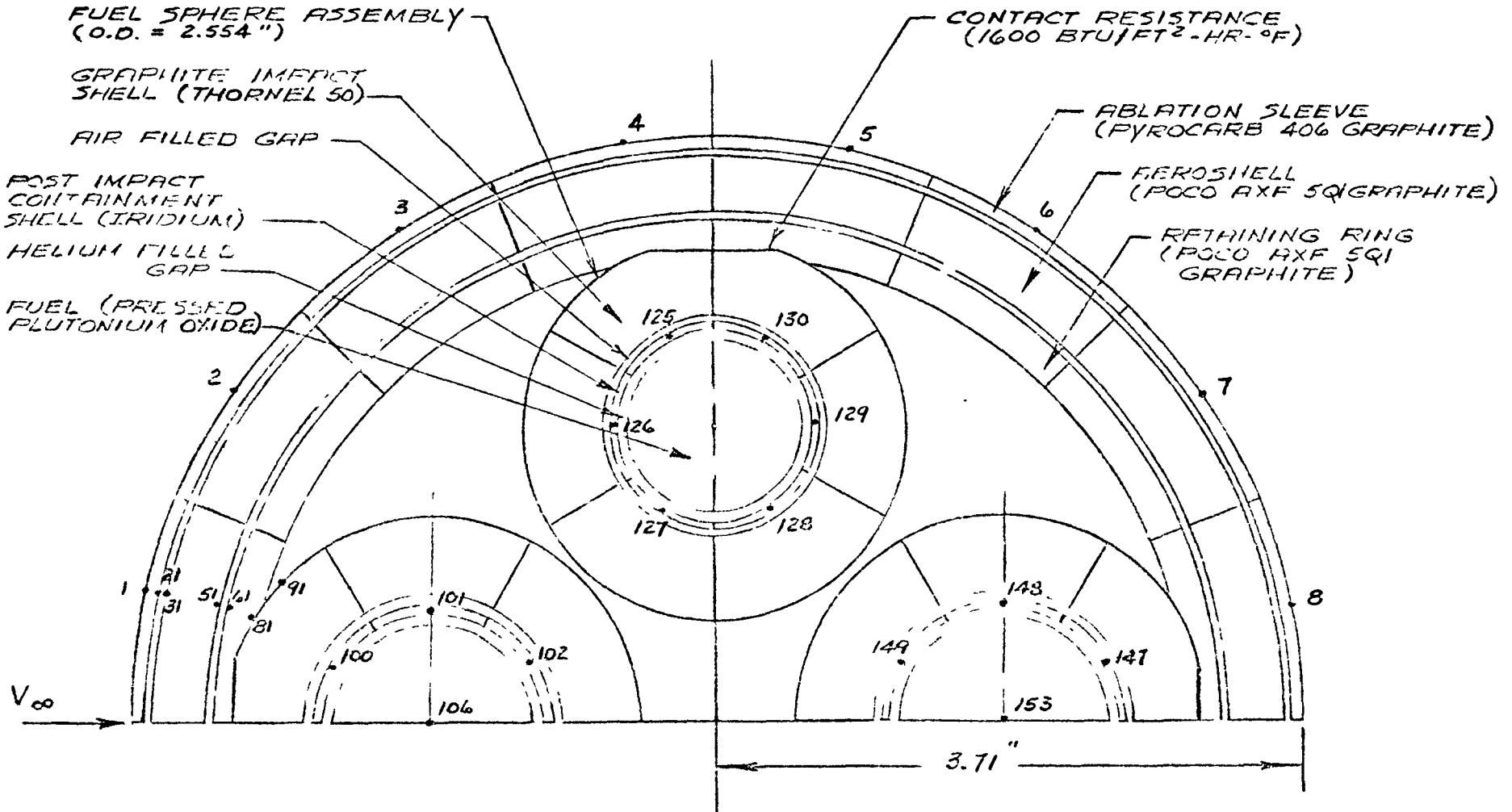


TABLE 2.5.1.3-II

THERMAL PROPERTIES OF HEAT SOURCE

Material (Component)	Temp. (°F)	Conductivity (Btu/in-sec-°F)	Emissivity	Density X Specific Heat (Btu/in ³ -°F)	Reference	
Helium (Gaps)	40	1.924 x 10 ⁻⁶			NASA TR-R-132	
	980	4.108 x 10 ⁻⁶				
	1520	5.209 x 10 ⁻⁶				
	3140	8.282 x 10 ⁻⁶				
	4940	11.416 x 10 ⁻⁶				
	5840	12.833 x 10 ⁻⁶				
Air (Gaps)	0	3.12 x 10 ⁻⁷			NASA TRR-132; M. Thomas, ARS Dynamic Symposium August, 1961.	
	1500	9.5 x 10 ⁻⁷				
	2060	10.35 x 10 ⁻⁷				
	3140	1.415 x 10 ⁻⁶				
	3141	1.570 x 10 ⁻⁶				
	4040	3.356 x 10 ⁻⁶				
	4500	4.421 x 10 ⁻⁶				
	4940	4.930 x 10 ⁻⁶				
	6740	5.270 x 10 ⁻⁶				
Pressed Plutonium Oxide (Fuel) 82.5% of theoretical density	0		0.59	0.0212	LES 8/9 FSAR Vol. 1, GESD, dated 3/75.	
	100	5.822 x 10 ⁻⁵		0.0213		
	1000		0.68			
	1112	3.910 x 10 ⁻⁵		0.0277		
	2000		0.77			
	2012	2.657 x 10 ⁻⁵		0.0283		
	3000	2.269 x 10 ⁻⁵	0.685	0.0286		
T _m = 4350°F ρ = 0.3414 lb/in ³ Q = 0.0415 Btu/in ³ - sec	4000	2.222 x 10 ⁻⁵	0.956	0.0287		
	Iridium (PICS)	0	1.968 x 10 ⁻⁵	0.23	0.0249	LES 8/9 FSAR, Vol. 1, GESD, dated 3/75.
		1000	1.829 x 10 ⁻⁵	0.20	0.0282	
		2000	1.771 x 10 ⁻⁵	0.18	0.0315	
		3000	1.513 x 10 ⁻⁵	0.19	0.0349	
4000		1.513 x 10 ⁻⁵	0.21	0.0382		
POCO AXF 5Q1 Graphite (Aero shell and retaining ring)	100	0.00134	0.80	0.0109	LES 8/9 FSAR Vol. 1, GESD, dated 3/75.	
	500	0.00111	0.80	0.0193		
	1000	0.00088	0.80	0.0248		
	1500	0.00071	0.80	0.0282		
	2000	0.00059	0.80	0.0303		
ρ = 0.0642 lb/in ³	2500	0.00050	0.85	0.0315		
	3000	0.00043	0.90	0.0320		
Thornel 50 (GIS)	100	2.407 x 15 ⁻⁵ (C)	0.8	0.0074	LES 8/9 FSAR Vol. 1, GESD, dated 3/75.	
		1.925 x 10 ⁻⁴ (A,B)				
	1000	2.847 x 10 ⁻⁵ (C)	0.8	0.0168		
ρ = 0.0433 lb/in ³	2000	2.277 x 10 ⁻⁴ (A,B)	0.8	0.0205		
		3.657 x 10 ⁻⁵ (C)				
	3000	2.925 x 10 ⁻⁴ (A,B)	0.8	0.0216		
		4.375 x 10 ⁻⁵ (C)				
	4000	3.500 x 10 ⁻⁴ (A,B)	0.8	0.0221		
4.630 x 10 ⁻⁵ (C)						
		3.704 x 10 ⁻⁴ (A,B)				

TABLE 2.5.1.3-II (Continued)

THERMAL PROPERTIES OF HEAT SOURCE

Material (Component)	Temp. (°F)	Conductivity (Btu/in-sec-°F)	Emissivity	Density X Specific Heat (Btu/in ³ -°F)	Reference
Pyrocarb 406 Graphite (Ablation Sleeve)	0	1.532 x 10 ⁻⁴ (C)	0.8	0.0082	MJS-77 SAR GE76 SDS 4241, dated 3/76
	1000	3.064 x 10 ⁻⁴ (A,B)	0.8	0.0213	
		1.641 x 10 ⁻⁴ (C)			
		3.282 x 10 ⁻⁴ (C)			
$\rho = 0.05468 \text{ lb/in}^3$	2000	1.676 x 10 ⁻⁴ (C)	0.8	0.0257	
	3000	3.352 x 10 ⁻⁴ (A,B)	0.9	0.0268	
		1.583 x 10 ⁻⁴ (C)			
	4000	3.166 x 10 ⁻⁴ (A,B)	0.95	0.0273	
		1.583 x 10 ⁻⁴ (C)			
Min-K 1400 Vacuum	0				SIG-EAS-1209
	392	2.08 x 10 ⁻⁷			
	842	2.73 x 10 ⁻⁷			
	1202	3.54 x 10 ⁻⁷			
	1560	4.68 x 10 ⁻⁷			

Analytical Methods

Both steady state and transient solutions were obtained using finite difference equations that exist in the Thermal Analyzer Program (TAP-3) described in Ref. 2. The thermal characteristics of each model and the boundary conditions for each case were provided as input.

Hypersonic laminar convective and hot gas radiative heat fluxes, velocities, free stream temperatures and pressures during reentry were obtained from References 5 and 6. Below Mach 2, the convective heating distribution was assumed to be uniform with heating levels computed as a function of Reynolds number in accordance with Ref. 7.

Radiation heat transfer across small gaps in the models was approximated by using configuration factors that were computed for infinite parallel plates. Radiation interchange between surfaces within the confines of the retaining ring, however, required a more complex evaluation. In this region view factors were first evaluated. These were either obtained from standard view factor analytical curves or they were estimated. Using view factors as an input, the IRLIMP program, described in Ref. 8, was then used to compute the radiation absorption factors for all multireflecting elements representing the inner surface of the retaining ring and the outer surfaces of the IHS's. These absorption factors were subsequently used to determine the radiant interchange in the TAP-3 solutions.

Oxidation and sublimation at the graphite surface were computed in accordance with techniques described in Refs. 1 and 9. The heat balance at the wall accounted for these surface reactions. The product of combustion was assumed to be CO and CO₂, varying linearly with mass flux rate ratio (\dot{m}/\dot{m}_{DL}) from 100% CO₂ at the threshold of oxidation to 100% CO at the threshold of diffusion limited oxidation.

The input convective heat fluxes were modified during the course of the solution to account for hot wall and mass addition effects. The input radiative heat fluxes were modified during the course of the solution to account for mass addition effects in accordance with Ref. 10.

IHS - Steady State

Steady state IHS studies treated the outer boundary temperature as a parameter that was varied within the range of 1600 - 2000° F.

Figures 2.5.1.3-8 through 2.5.1.3-10 show temperature distributions that account for vacuum gaps except in the fuel/PICS gap which is filled with helium. These results are representative of unsealed heat sources in outer space. As such, these results represent the MIW IHS used in the KIPS.

As will be shown later, the higher steady state temperature levels of the vacuum gap IHS will permit the KIPS IHS to operate at low surface temperatures ($\approx 1450^\circ\text{F}$) and still have its PICS remain ductile at the time of impact.

FIGURE 2.5.1.3-8
TEMPERATURE DISTRIBUTION OF HEAT SOURCE ASSEMBLY (HSA)
(STEADY STATE ANALYSIS)

VACUUM GAPS EXCEPT FOR FUEL / PICS
GAP WHICH IS FILLED WITH HELIUM

$T_{SURFACE}$ IS 1600 °F

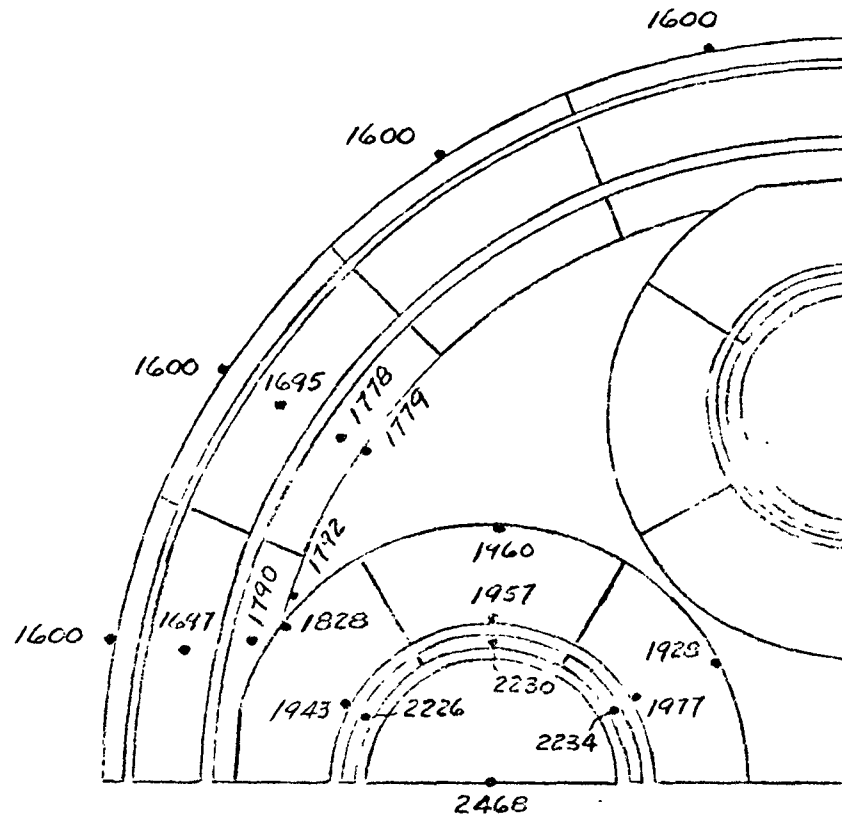


FIGURE 2.5.1.3-9
TEMPERATURE DISTRIBUTION OF HEAT SOURCE ASSEMBLY (IHS)
(STEADY STATE ANALYSIS)

VACUUM GAPS EXCEPT FOR FUEL / PICS
GAP WHICH IS FILLED WITH HELIUM

$T_{SURFACE} = 1800\text{ }^{\circ}\text{F}$

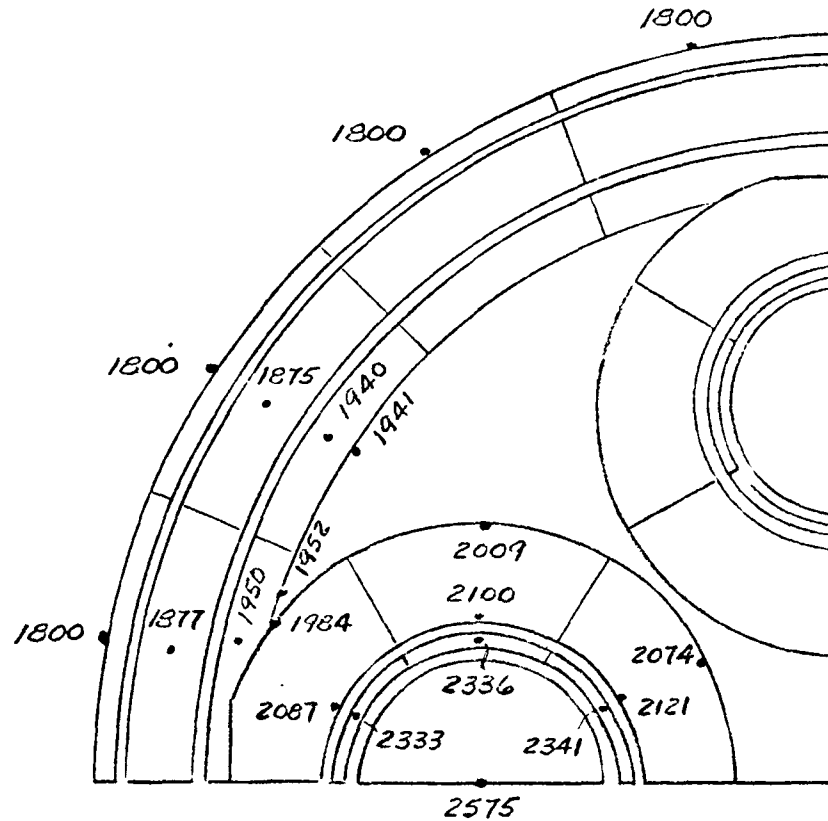
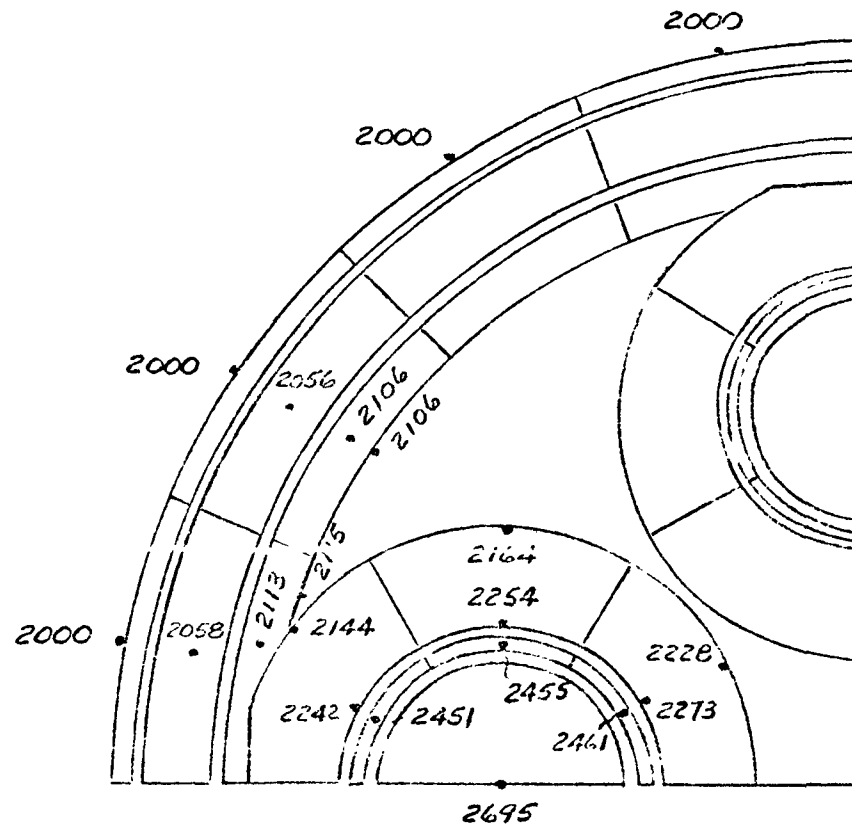


FIGURE 2.5.1.3-10
TEMPERATURE DISTRIBUTION OF HEAT SOURCE ASSEMBLY (HSA)
(STEADY STATE ANALYSIS)

VACUUM GAPS EXCEPT FOR FUEL / PICS
GAP WHICH IS FILLED WITH HELIUM

$T_{SURFACE} = 2000^{\circ}F$



IHS - Transient

A total of 89 reentry heating cases were evaluated. Results pertinent to KIPS are summarized in Table 2.5.1.3-III. The parameters that were varied are: (1) initial path angle ($\gamma_i = -8, -10, -15, -30$ degrees), (2) velocity ($V = 25K, 30K, 35K, 40K$ fps), (3) release altitude ($h_i = 400K, 200K, 100K$ ft), (4) initial IHS surface temperature ($T_i = 1600^\circ F, 1800^\circ F, 2000^\circ F$, and (5) gap fill during normal operation (helium and vacuum).

Carpet plots are shown in Figures 2.5.1.3-11 through 2.5.1.3-15 to graphically depict several IHS temperatures and ablation as a function of V_i , T_i and h_i . Figures 2.5.1.3-11 and 2.5.1.3-12 are peak surface and PICS temperatures during reentry. Figure 2.5.1.3-13 is maximum recession (El 1) during reentry. Figures 2.5.1.3-14 and 2.5.1.3-15 are maximum and minimum PICS temperatures at impact. The influence of initial IHS temperature on the PICS temperature at impact is shown in Figure 2.5.1.3-16. The results show the range of impact temperatures for the two steady state gap fill assumptions, i. e., helium and vacuum. The influence of release altitude and initial path angle on the PICS temperature at impact is shown in Figure 2.5.1.3-17 for the vacuum gap/1600° F IHS surface temperature initial condition. An orbital decay case (Table 2.5.1.3-II - Case 21) was also included in this study because of its frequent use as a "bench mark." Temperature and ablation histories are presented for this case in Figure 2.5.1.3-18. From the results of the reentry thermal study, it is apparent that the thickness of the ablation sleeve (0.130 inches) is adequate to accommodate the ablation of all prompt reentries with initial velocities equal to or less than 40,000 fps. The largest computed ablation thickness was 0.121 inches (Table 2.5.1.3-II - Case 20).

An interesting characteristic of the IHS design is the high level of insulation it provides the PICS. For example, the PICS temperature never exceeded 2752° F in any case evaluated. This is well below the iridium-carbon eutectic melt temperature values (3830-4160° F) noted in ORNL-TM-1383.

Impact temperatures of the iridium PICS are required to stay in the range of 1050 to 1450°C. Below this range, iridium becomes brittle and undesirable fuel property changes also occur. Above this range the iridium strength falls off and grain growth may also occur (Ref. 11). The Figure 2.5.1.3-16 results show 1600° F is the lowest helium filled IHS surface temperature that will satisfy this impact temperature requirement. An extrapolation of Figure 2.5.1.3-16 data also shows a KIPS IHS (vacuum) can satisfy this requirement with surface temperatures of $\approx 1450^\circ F$. These lower temperature bounds are expected to hold for the entire range of initial velocities and release altitudes considered in this study even though Figure 2.5.1.3-16 results are limited to $V_i = 25K$ fps and $h_i = 100K$ ft.

TABLE 2.5.1.3-III

SUMMARY OF RESULTS

THERMAL MODEL #2

Case	Vel. (K fps)	Path Angle (deg.)	Peak Temperature (°F)				PICS Impact Temperature (°F)		Surface Recession @ E1 I (inches)	Initial HIS Surface Temperature (°F)
			E1 1	E1 31	E1 61	E1 100	Max. (E1 102)	Min. (E1 147)		
<u>Release Alt. = 400 K ft., Initial Temperature Model #1, helium filled gaps</u>										
52	25	-30	----	2506	2007	2013	2048	1947	.033	1600
53	↓	-20	4453	2637	2060	2069	2072	1950	.038	↓
54	↓	-15	4278	2744	2141	2093	2092	1954	.041	↓
55	↓	-10	4169	2859	2281	2130	2122	1960	.048	↓
56	↓	-8	4055	2918	2335	2150	2139	1964	.051	↓
57	↓	-30	----	2669	2190	2196	2198	2091	.037	1800
58	↓	-20	4465	2789	2220	2219	2216	2090	.041	↓
59	↓	-15	4391	2871	2275	2237	223	2090	.043	↓
60	↓	-10	4161	2966	2432	2273	2253	2091	.050	↓
61	↓	-8	4069	3020	2482	2293	2265	2092	.054	↓
62	↓	-30	----	2864	2367	2354	2353	2236	.043	2000
63	↓	-20	4480	2946	2407	2376	2363	2230	.046	↓
64	↓	-15	4405	3010	2404	2394	2373	2227	.048	↓
65	↓	-10	4177	3067	2577	2419	2384	2221	.054	↓
66	↓	-8	4085	3119	2623	2436	2391	2217	.057	↓
<u>Release Alt. = 400 K ft., Initial Temperature Model #1, Vac. gaps except helium in fuel/PICS gap</u>										
67	25	-30	----	2569	2098	2159	2158	2053	.035	1600
68	↓	-20	----	2688	2133	2182	2175	2050	.039	↓
69	↓	-15	4383	2790	2249	2201	2189	2049	.042	↓
70	↓	-10	4152	2905	2359	2232	2211	2049	.049	↓
<u>Release Alt. = 100 K ft., Initial Temperature Model #1, helium filled gaps</u>										
71	25	-30	----	1957	1809	1978	1990	1938	.023	1600
72	↓	-20	----	1973	1816	1981	1995	1938	.022	↓
73	↓	-15	----	1985	1821	1983	1994	1938	.022	↓
74	↓	-10	----	1999	1826	1985	1996	1938	.022	↓
75	↓	-8	----	2006	1829	1986	1997	1938	.022	↓
76	↓	-30	----	2141	1992	2133	2143	2085	.025	1800
77	↓	-20	----	2157	1999	2135	2143	2083	.024	↓
78	↓	-15	----	2167	2003	2137	2143	2081	.023	↓
79	↓	-10	----	2180	2009	2139	2143	2079	.023	↓
80	↓	-8	----	2186	2012	2140	2142	2078	.023	↓
81	↓	-30	----	2345	2171	2299	2304	2256	.027	2000
82	↓	-20	----	2359	2178	2301	2301	2230	.026	↓
83	↓	-15	----	2368	2183	2303	2299	2226	.026	↓
84	↓	-10	----	2376	2189	2304	2295	2222	.025	↓
85	↓	-8	----	2379	2192	2305	2293	2221	.025	↓
<u>Release Alt. = 100 K ft., Initial Temperature Model #1, Vac. gaps except helium in fuel/PICS gap</u>										
85	25	-30	----	2016	1886	2230	2110	2052	.023	1600
86	↓	-20	----	2031	1893	2230	2103	2047	.023	↓
87	↓	-15	----	2043	1898	2230	2106	2044	.022	↓
88	↓	-10	----	2057	1903	2230	2105	2041	.022	↓
89	↓	-8	----	2064	1906	2230	2104	2040	.022	↓

PEAK SURFACE TEMPERATURES DURING REENTRY

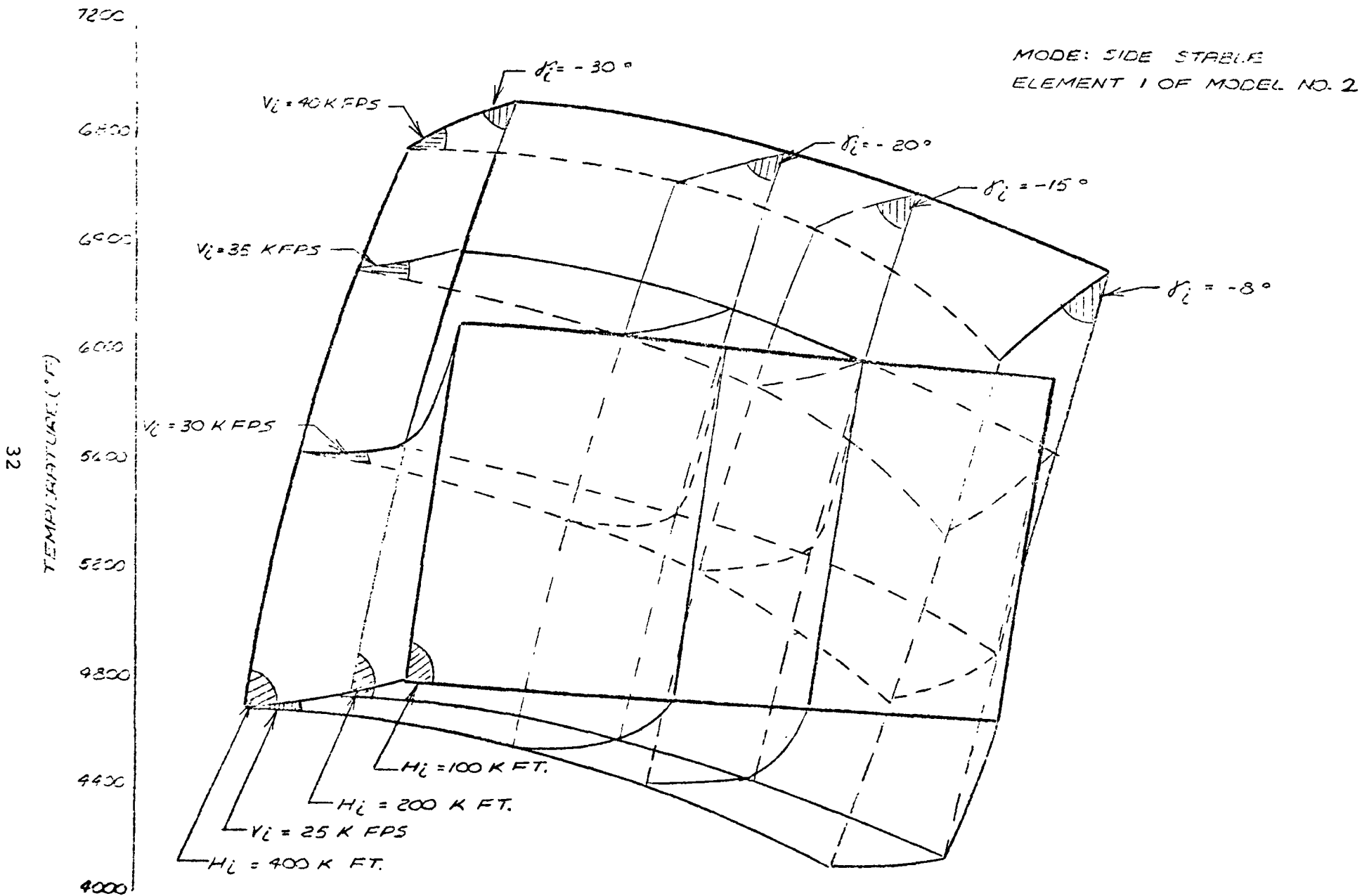


FIGURE 2.5.1.3-12
PEAK PICS TEMPERATURE DURING
REENTRY

MODE: SIDE STABLE
ELEMENT 100 OF MODEL NO. 2

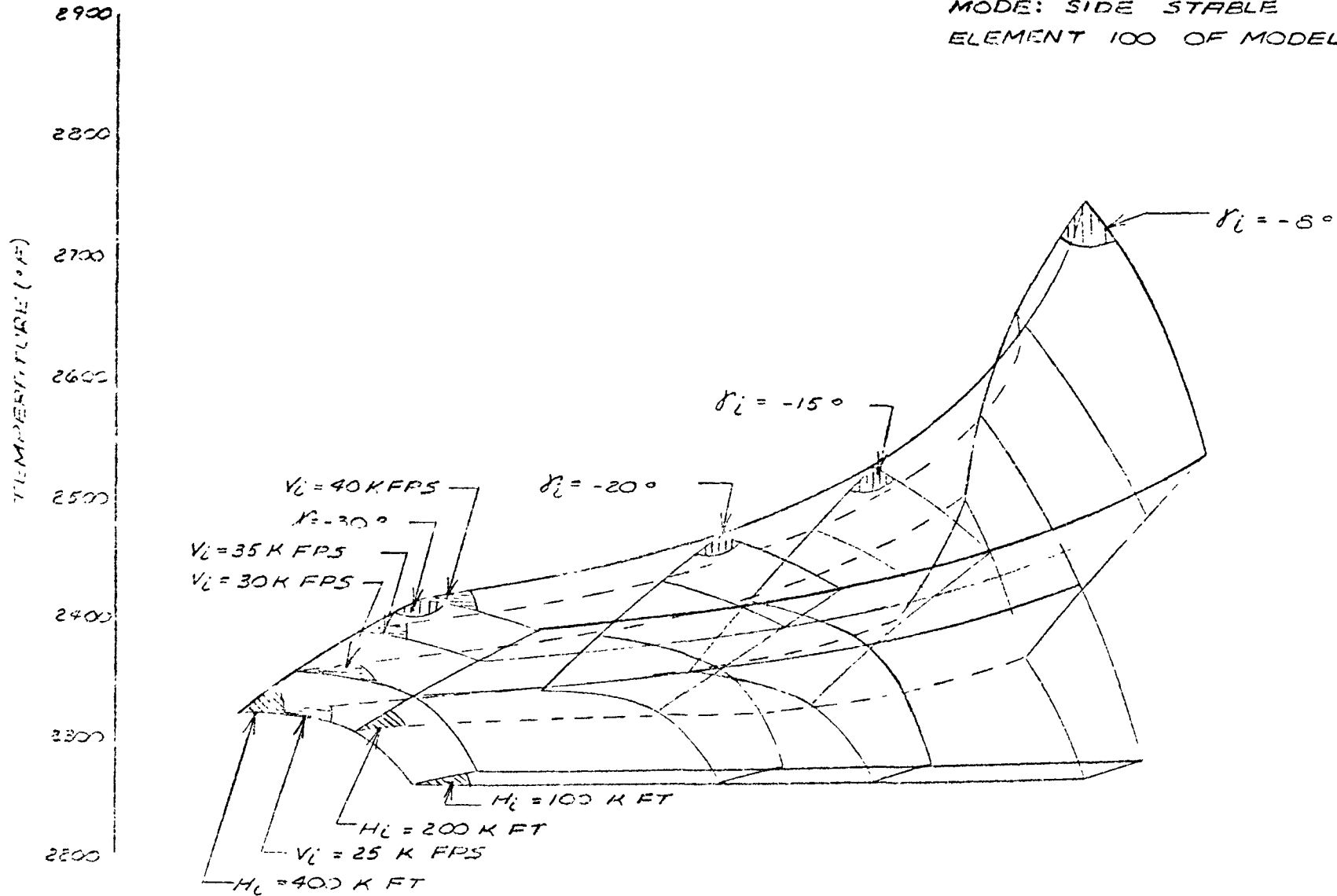


FIGURE 2.5.1 3-13
TOTAL SURFACE RECESSION

MODE: SIDE STABLE
MODEL: 2-D
ABLATED ELEMENT: 1

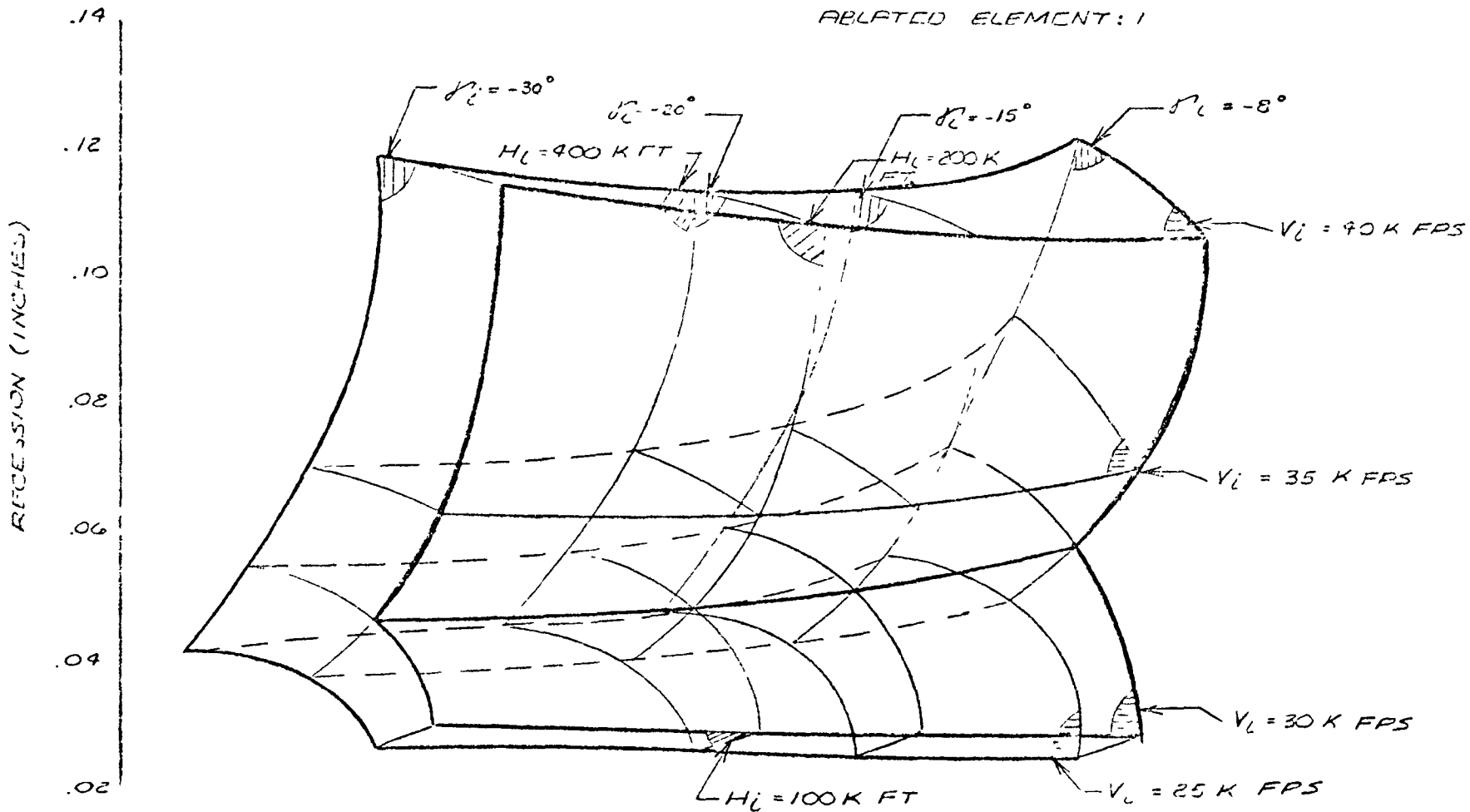


FIGURE 2.5.1.3-14
MAXIMUM PICS TEMPERATURE AT IMPACT

MODE: SIDE STABLE
ELEMENT 102 OF MODEL NO. 2

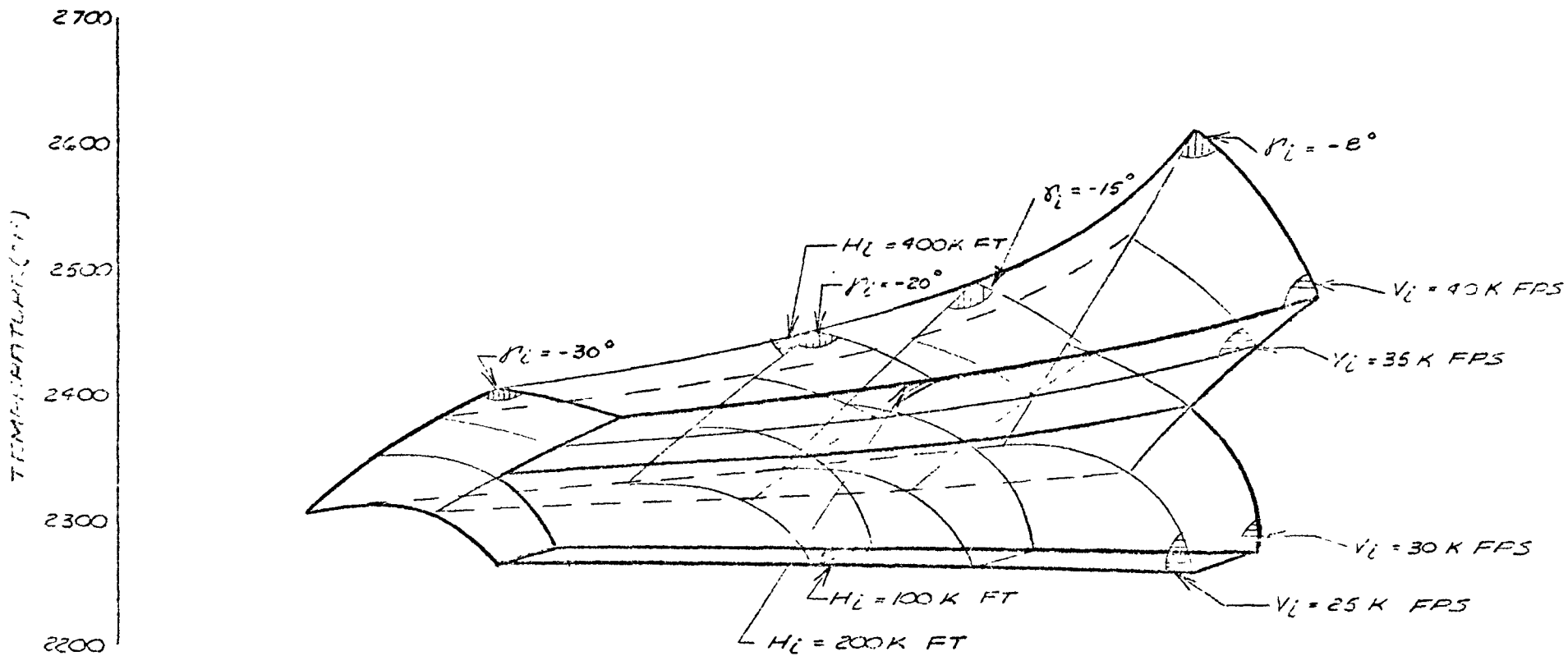


FIGURE 2.5.1.3-15
MINIMUM PICS TEMPERATURE AT IMPACT

MODE: SIDE STABLE
ELEMENT 147 OF MODEL NO. 2

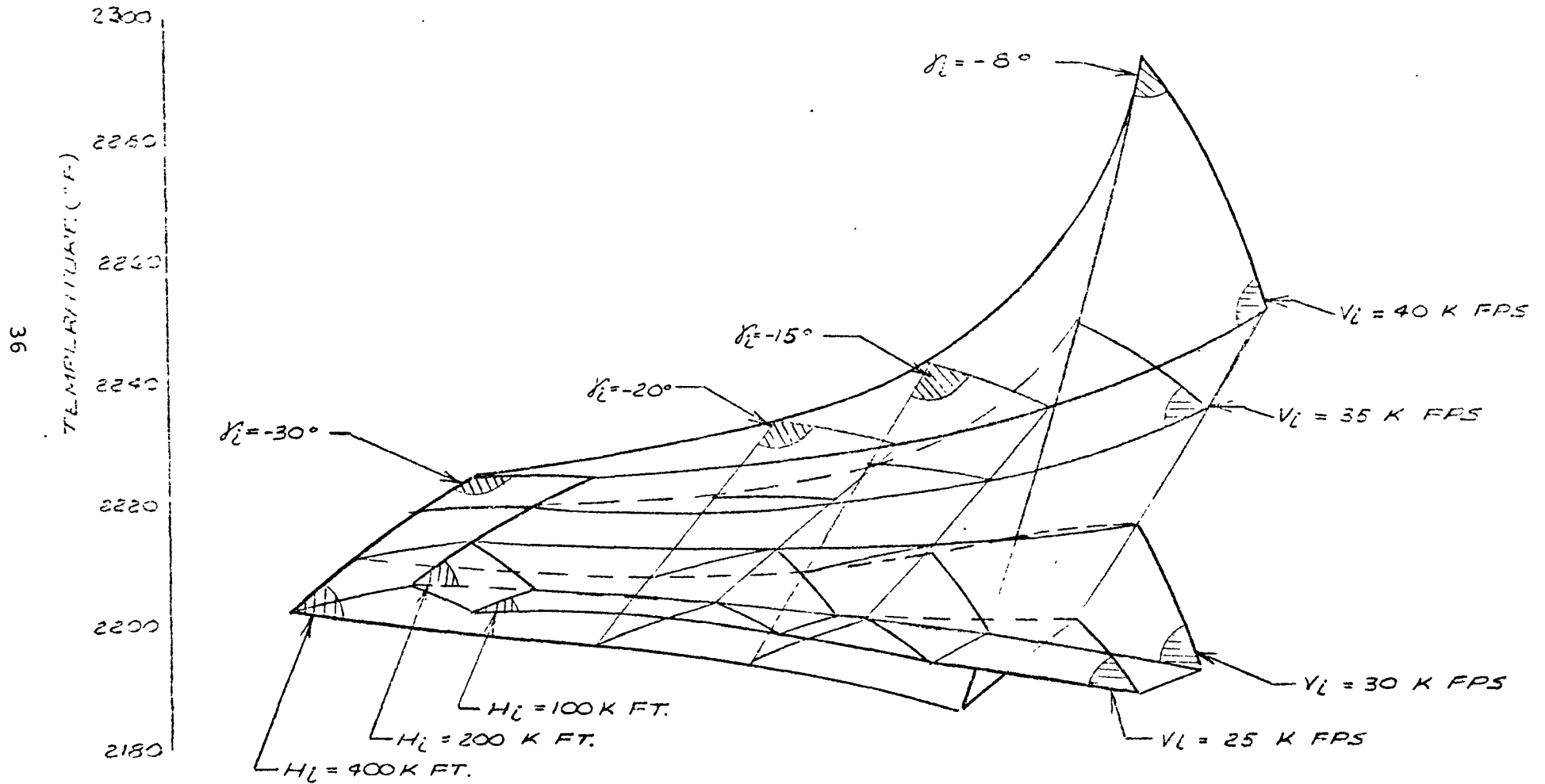
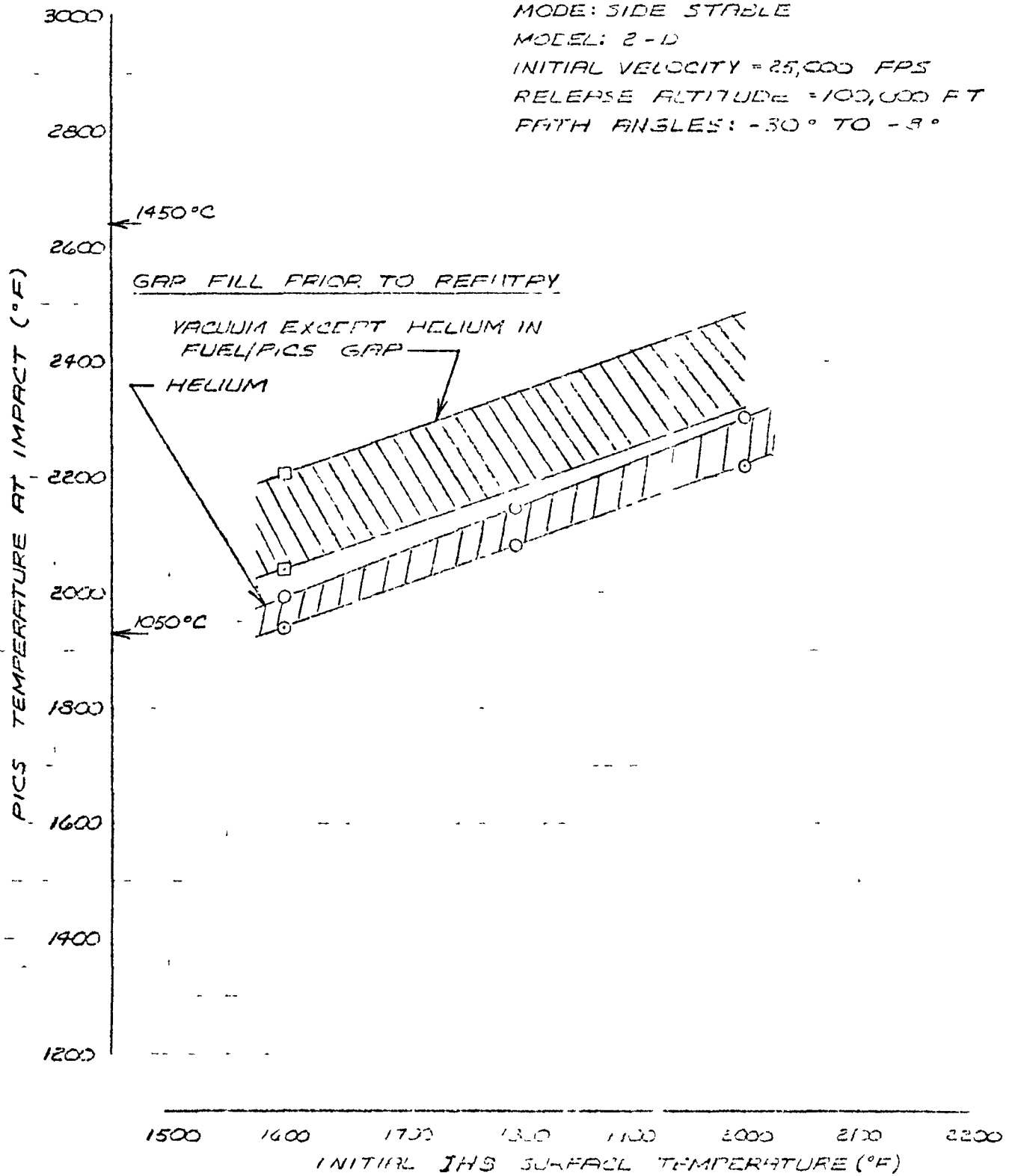
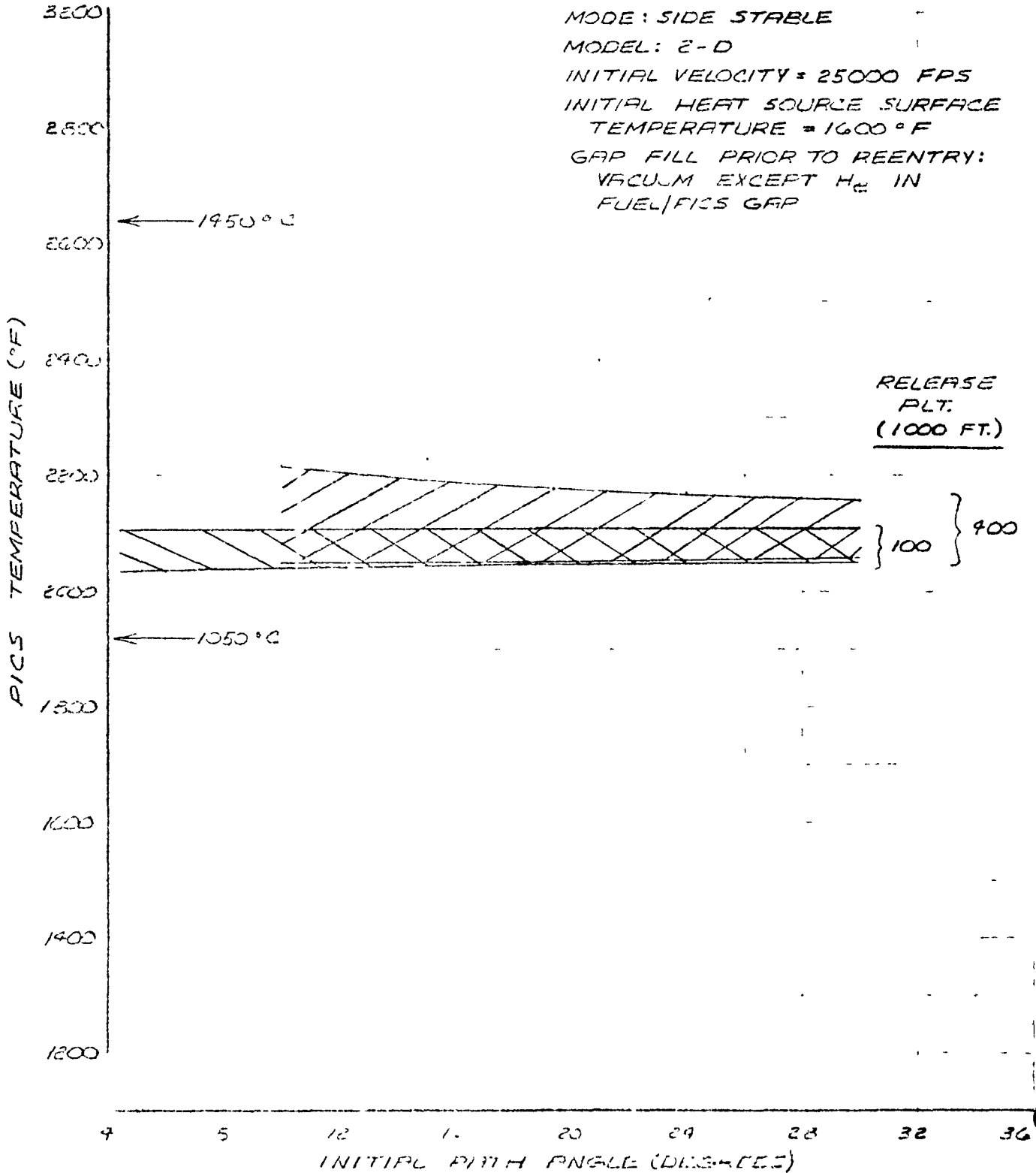


FIGURE 201-11
PICS TEMPERATURE - FUEL-PICS IMPACT
VS INITIAL SURFACE TEMPERATURE - IHS



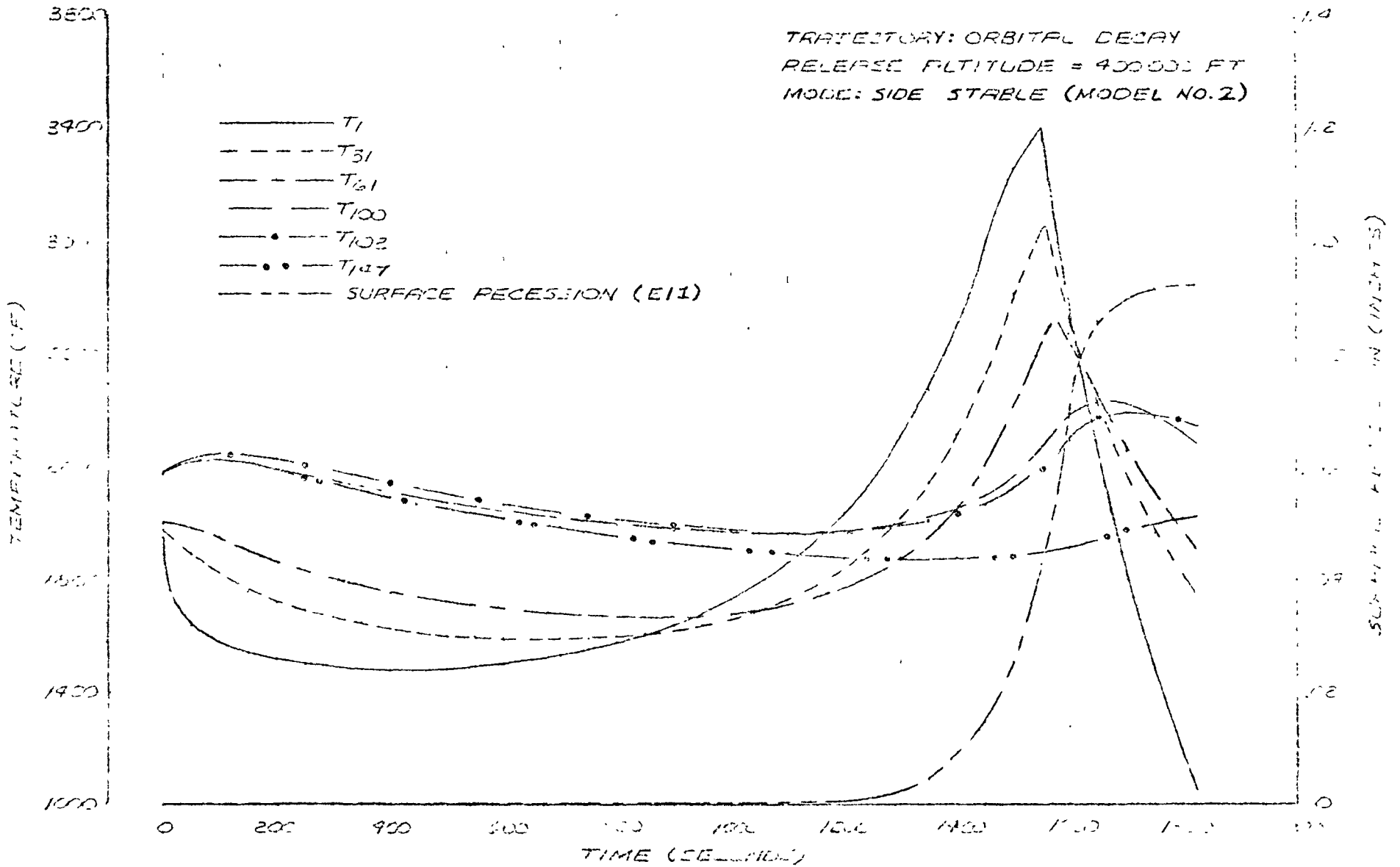
AAH 12-27-76

FIGURE 2.5.1.3-17
PICS TEMPERATURE PROFILE AT IMPACT VS.
INITIAL PATH ANGLE



KAM 10-22-76

FIGURE 2.5.1.3-18
TEMPERATURE AND RECESSON HISTORIES DURING REENTRY



2.5.1.4 KIPS Emergency Cooling System

Introduction - KIPS Heat Source Assembly (HSA) consists of a radiation barrier, boiler, multifoil insulation and a Multi Hundred Watt (MIHW) radioisotope heat source. Heat from MIHW heat source is carried away by "Dowtherm A" coolant flowing through the boiler and is eventually utilized in an organic Rankine conversion cycle to produce electrical power. Nuclear safety considerations require that the MIHW heat source temperature be maintained within narrow limits for normal operation and in the event of "loss of coolant accident" (LOCA). In order to achieve this, a melting multifoil insulation system is used in the HSA, which not only limits the heat losses from it to very low values, but also acts as an emergency heat dumping system when the heat source temperatures rise above operational limits. Preliminary parametric design, thermal and structural studies were conducted to determine the weight versus parasitic heat loss tradeoffs for the KIPS system. As a result of these studies and a survey of candidate foil materials, the tentative selection of a multifoil system was made. This system was composed of 60 layers of 1 mil pure aluminum foil. Separation of the foils is achieved by micron size zirconia particles as proposed by the multifoil system vendor, ThermoElectron Corporation (TECO).

The spacer particles are selected on the basis of low thermal conductivity and compatibility with the foil material chosen for this application (usually a choice dependent on temperature). The oxide particles are optimized with regard to particle size and coating density to minimize thermal transport. The oxide particles provide a high thermal impedance to conduction by: (a) selection of oxides with low thermal conductivity, (b) high thermal interface resistance between the foils and particles, and (c) low conduction path area. The multiple foils are effective radiation shields. The vacuum environment eliminates gas conductor and convective heat transport.

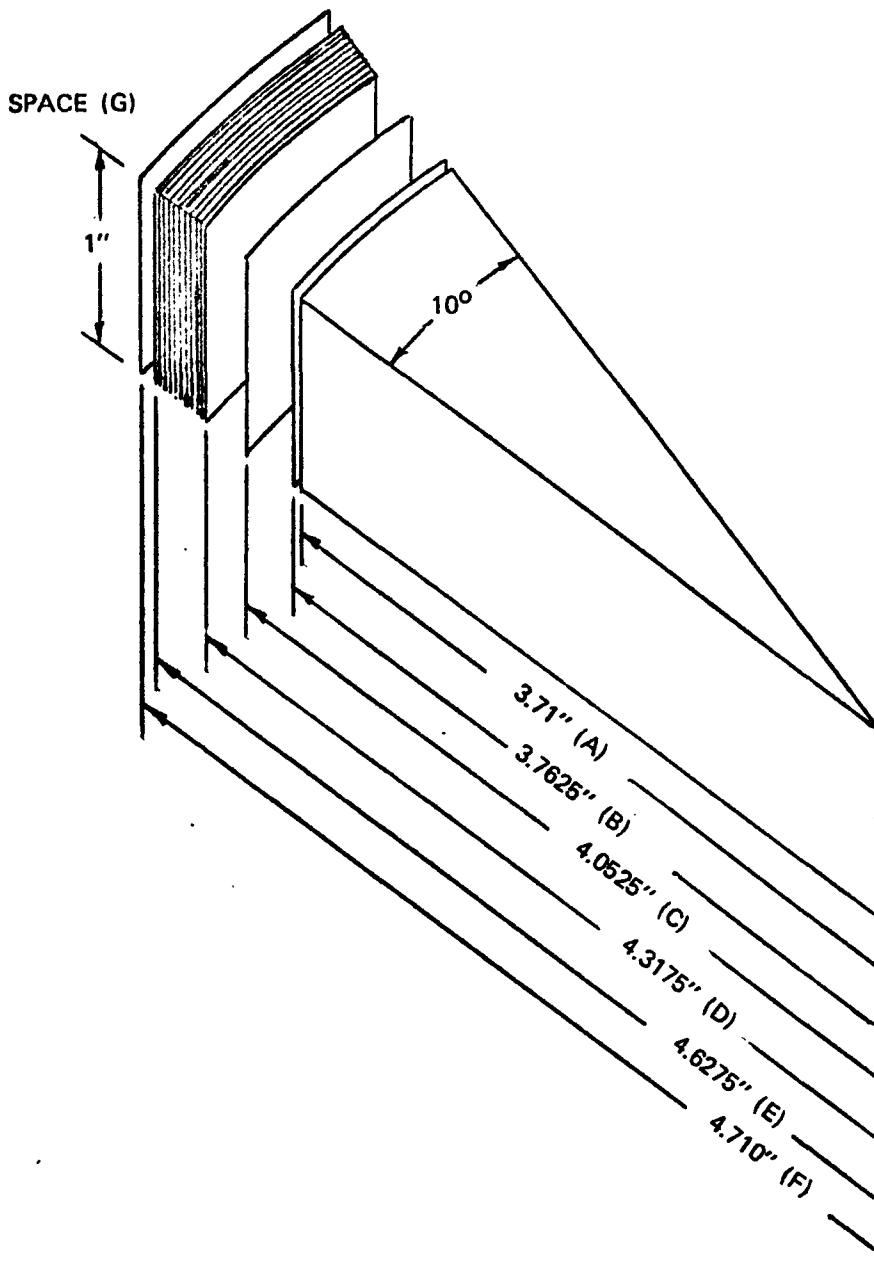
A mathematical model of the entire KIPS heat source assembly was constructed to determine the transient thermal response in the event of loss of coolant accident. TECO subjected a scale model of the foil insulation system to a meltdown test to verify the design concept. This model was tested in an evacuated bell jar apparatus, by first simulating the foil system inner boundary temperatures and heat flux at predicted steady state operational conditions. Meltdown was then accomplished by increasing the heat flux at the inner boundary of the foil system to simulate the heat flux expected if the coolant stopped flowing through the boiler. Test results showed that the foils melted progressively one at a time and the system approached equilibrium temperatures. In order to verify the ability of the emergency cooling system, a full scale Electrical Heat Source Assembly (KIPS1020020-039), which had earlier been utilized for performance testing, was subjected to an actual LOCA test.

Mathematical Model

A TAP III model was constructed to study the transient thermal behavior of the KIPS heat source assembly. The one-dimensional model as shown in Figure 2.5.1.4-1 consists of a pie shaped segment of the heat source assembly. The node map, radial dimensions of various components and the emissivities assumed for the component materials are also shown in Figure 2.5.1.4-1. All heat transfer is assumed to

FIGURE 2.5.1.4-1

ONE DIMENSIONAL TAP III MULTIFOIL TRANSIENT MODEL



LOCATION	COMPONENT	MATERIAL	EMISSIVITY	NODE NUMBER
A	HEAT SOURCE OUTSIDE SURFACE	GRAPHITE	0.80	1
B	RADIATION SHIELD INSIDE SURFACE	NICKEL .010" THICK	0.26	2
C	BOILER FIN INSIDE SURFACE	COPPER .020" THICK	0.85	3
D	MULTIFOIL INSULATION CAN INSIDE SURFACE	ALUMINUM .010" THICK	0.12	4
	INDIVIDUAL FOILS	ALUMINUM .005" PITCH	0.12	5-63
E	LAST (60TH) FOIL OUTSIDE SURFACE	ALUMINUM .001" THICK	0.12	64
F	HOUSING OUTSIDE SURFACE	ALUMINUM .060" THICK	VARIABLE	65
G	SPACE		1.0	66

be by radiation except between layers of multifoil insulation, where conduction through the spacer material was also considered. The equivalent thermal conductivity of the spacer material was assumed to be 0.00012 Btu/hr-ft-°F. Nominal operating conditions were assumed prior to flow stoppage.

The Thermal Analyzer Program (TAP III) solves n-dimensional transient problems in networks of conductors and capacitors by forward finite difference numerical technique. Thus, for nodes having finite capacities, the equation used is:

$$T_{2, \theta + \Delta \theta} = T_{2, \theta} + \frac{\Delta \theta}{C_i} \left[Q_i + \sum_j Y_{i, j} T_{j, \theta} - T_{i, \theta} \sum_j Y_{i, j} \right]$$

where $Y_{i, j}$ is the reciprocal of thermal resistance between nodes i and j.

The solution is obtained when steady state temperatures are reached.

The results of the computer code for nominal design temperatures are shown in Figure 2.5.1.4-2. For the assumed thermal capacity of the heat source, it is found that the rise in its temperature is gradual and linear after the flow is stopped. The boiler temperature rises rapidly after the flow is stopped and then gradually levels off as the foils start to melt. The first foil starts to melt approximately 3 minutes after the flow is stopped and the subsequent sequential melting of foils is complete in approximately 24 minutes. The housing rejects heat to the surroundings according to its temperature. All the components reach 98% of their steady state temperatures in less than 6 hours. The final equilibrium temperature of the housing depends on its surface emissivity. The calculated value is for an emissivity of 0.92. Also, it should be noted that the transient response time of various components is dependent on the accuracy with which their thermal capacities can be determined. On the whole, the performance of the multifoil insulation seems very promising in limiting the heat losses during normal operation and as an emergency heat dump system.

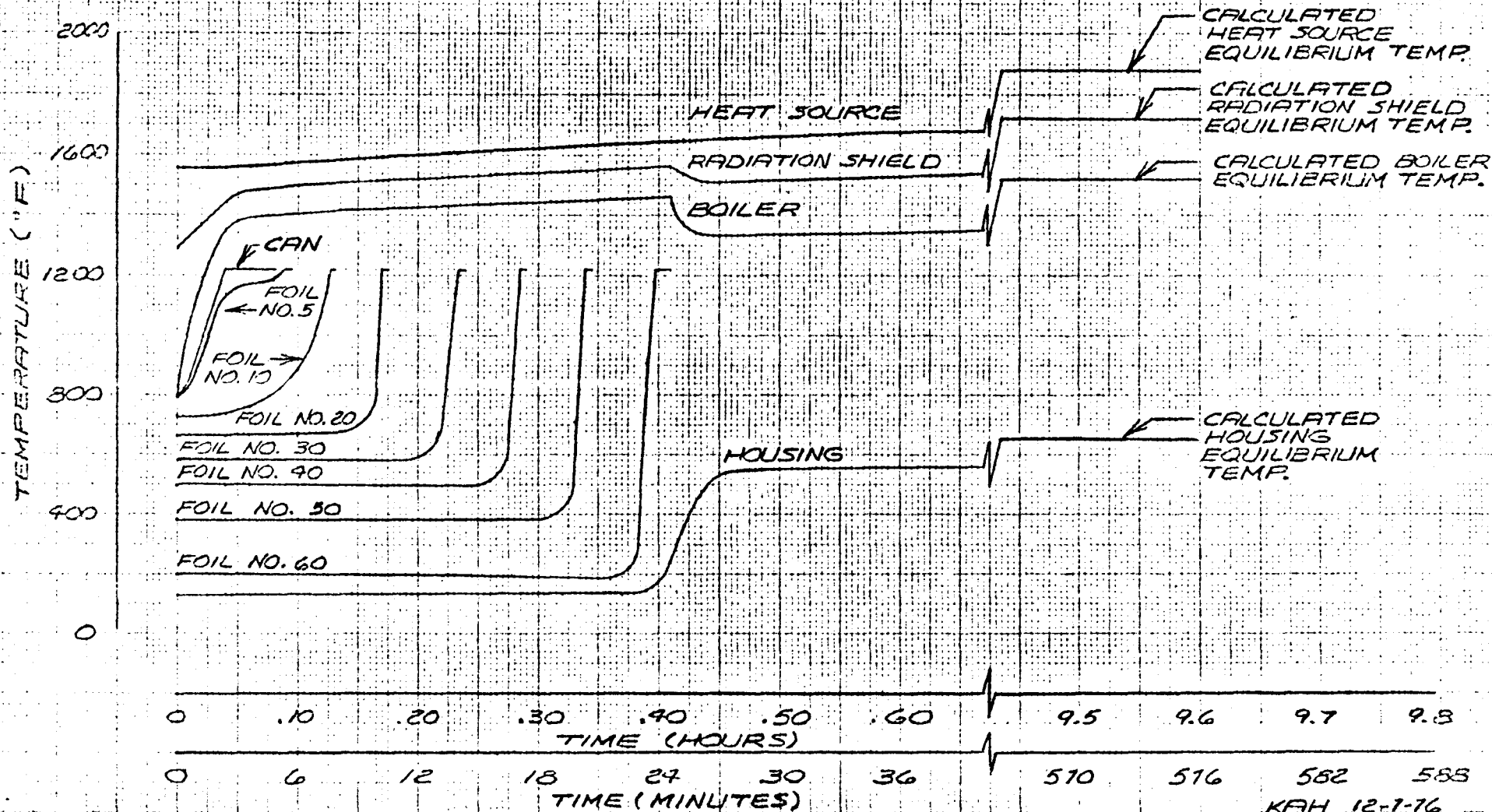
Scale Model Tests

Heat Flux Measurement - The heat flux through a given foil-particle system is a function of heat source temperature (T), heat sink temperature (T_c), and number of foil layers (N). Assuming radiation to room environment, the heat flux was measured as a function of T and N for optimized values of the characteristic dimension of particles (d), particle density per unit area (σ), and spacing between foil layers (s). The heat flux was measured using a cylindrical heat source approximately 2.5 inches in diameter and 3.0 inches in height. A tantalum filament (0.2 inch diameter) radiantly heated the cylinder.

FIGURE 2.5.1.4-2

HEAT SOURCE ASSEMBLY TEMPERATURES AFTER BOILER
FLUID FLOW STOPPAGE

NOTES: (1) FLUID FLOW CEASES AT TIME ZERO
(2) TIME FOR HEAT SOURCE TO RISE 98% OF THE WAY FROM INITIAL TO FINAL EQUILIBRIUM TEMPERATURE IS ABOUT 5.7 HOURS



The heat flux data for aluminum/zirconia Multifoil Insulation system are given in Figure 2.5.1.4-3 as a function of temperature. It is extremely difficult to measure such a low heat flux accurately. The heat losses at the relatively low temperature under consideration are smaller than the extraneous heat losses (i. e., filament and the edge of the cylindrical and planer assemblies). These data are in reasonable agreement with the earlier measurements performed by the vendor on nickel/zirconia system. It is noticed that for the expected nominal hot side temperature of multifoil insulation even the gross heat flux through the insulation is extremely small.

Compatibility Studies

The objective of this test was to obtain information on the compatibility among materials which shall be, or might be, used in the thermal insulation around the KIPS heat exchanger. The materials concerned were Min-K TE-1400, aluminum, nickel and stainless steel.

The testing conditions were 500°C for 1000 hours in a vacuum of 1×10^{-5} torr or better. All materials were cut into one inch squares and all metal foils were coated with 0.06 ± 0.02 mg/cm² of ZrO₂ powder by the ThermoElectron binder spray process for Multi-Foil Insulation System. These squares were arranged in various combinations and each set was separately enclosed in 2" x 2" x 1/2" molybdenum boxes. Molybdenum is practically inert at the testing condition. The material combinations and the sample arrangements of the test coupons are shown in Figure 2.5.1.4-4. These boxes were stacked inside a 6" x 6" vacuum furnace. During the 1000 hour test, the temperature of the inside of the furnace was maintained at $500 \pm 2^\circ\text{C}$ by an automatic temperature control. The vacuum of the system was maintained around 10^{-7} torr except for a period of system shut-down due to a power failure during a weekend. This power failure occurred after about 850 hours.

All tested materials indicated no observable deterioration except for slight discolorations of the aluminum and the stainless steel foils which were probably due to an air exposure at a relatively high temperature during the power failure. No weight changes were measureable for any tested samples. Photomicrographs gave no evidence that the zirconia particles interacted with the aluminum foil substrate.

In order to ascertain that the discoloration was due to an air leakage during the power failure, a second set of samples were tested for 100 hours. These samples showed no discoloration.

Meltdown Test (Scale Model)

A scale model of the proposed Multi-Foil Insulation System was subjected to a meltdown test to determine its capabilities prior to manufacturing the full scale prototype system.

The design of the meltdown assembly is shown in Figure 2.5.1.4-5. The Multi-Foil insulation consists of 60 layers of Zirconia coated (nominal 0.06 mg/cm²) aluminum foil (one mil thick) with a layer spacing of 10 mils/layer. The planar ends are

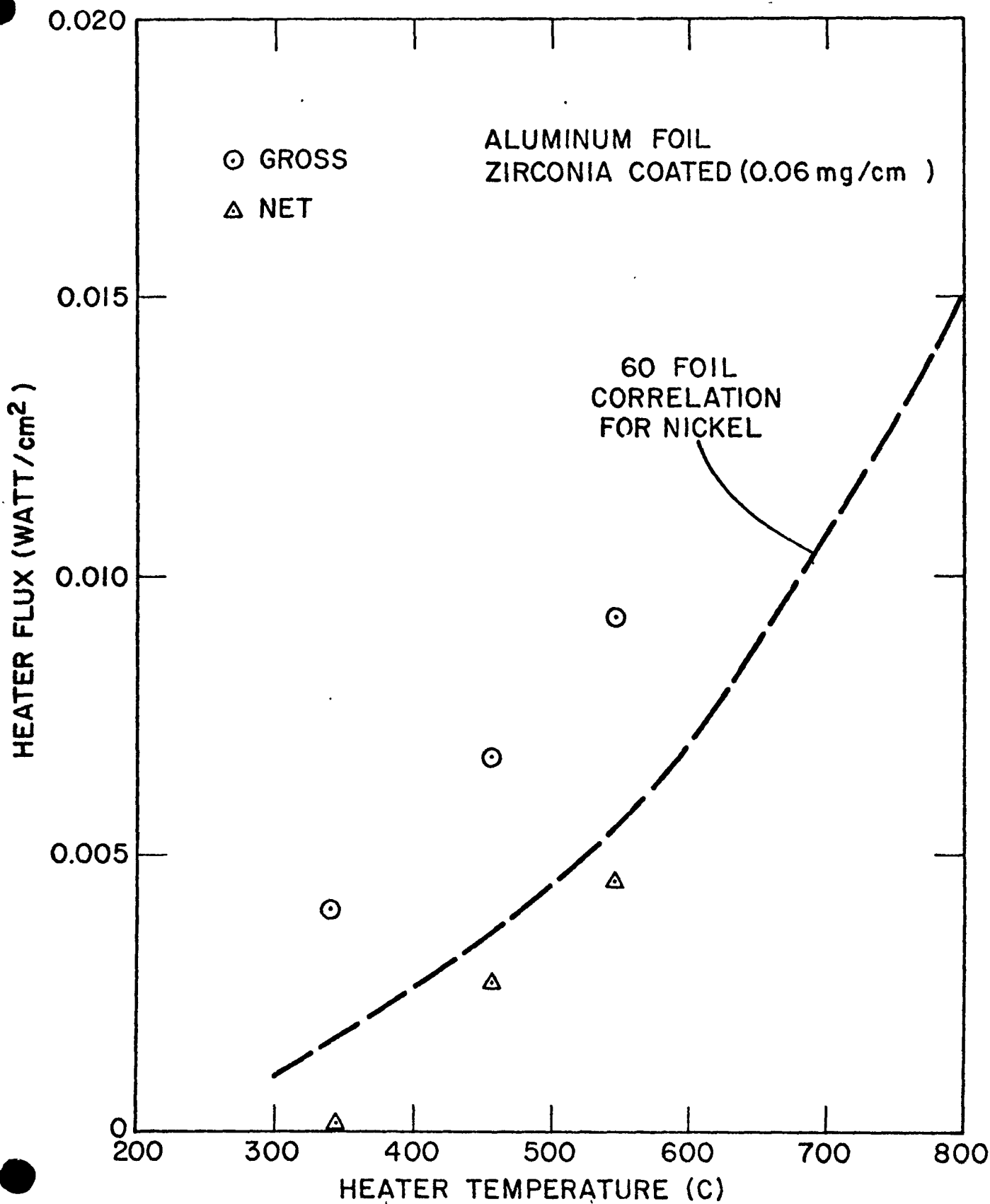


Figure 2.5.1.4-3: Measured Heat Flux Through Zirconia Coated Aluminum Multi-Foil Insulation System

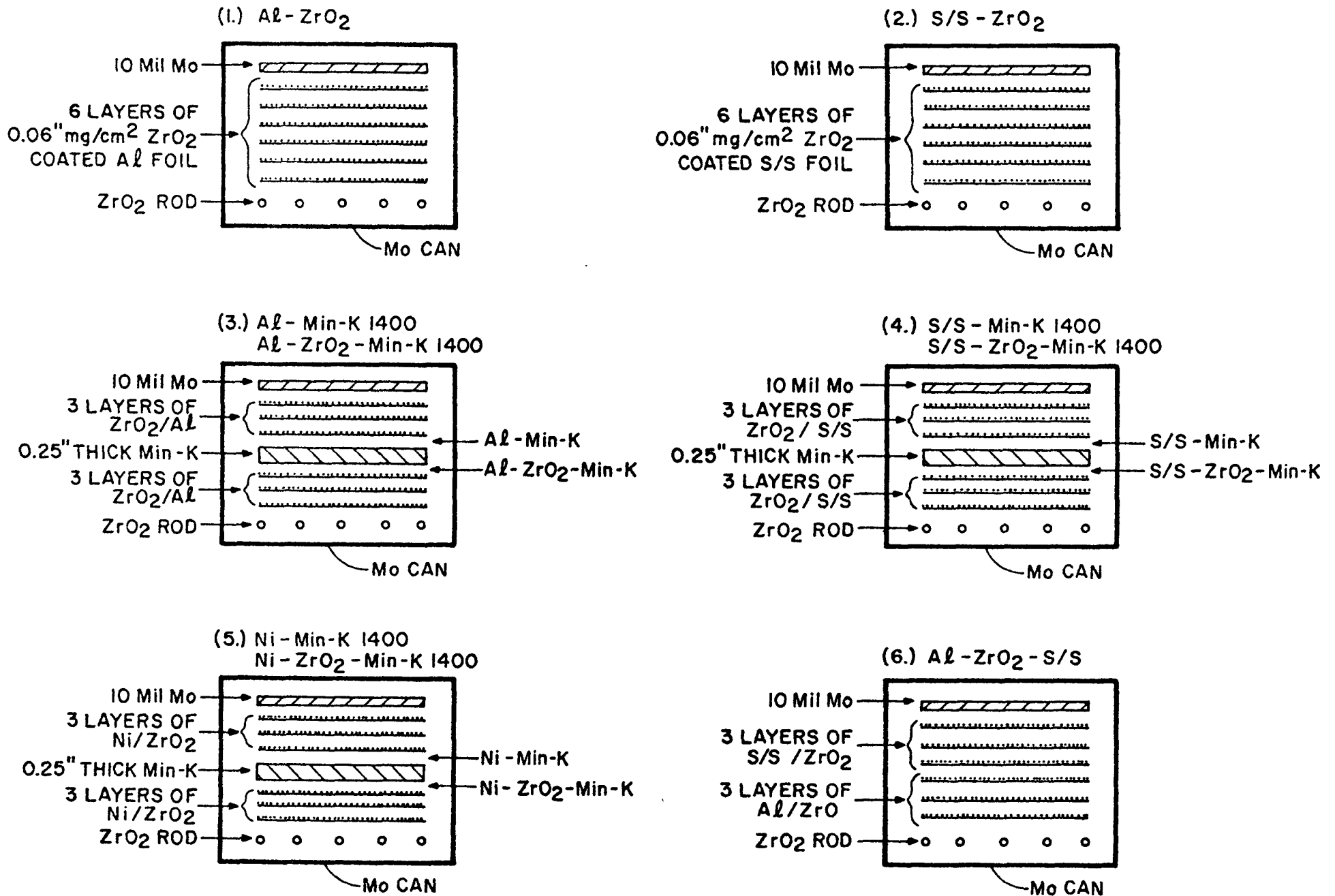


Figure 2.5.1.4-4:

Sample Assemblies for Compatibility Test

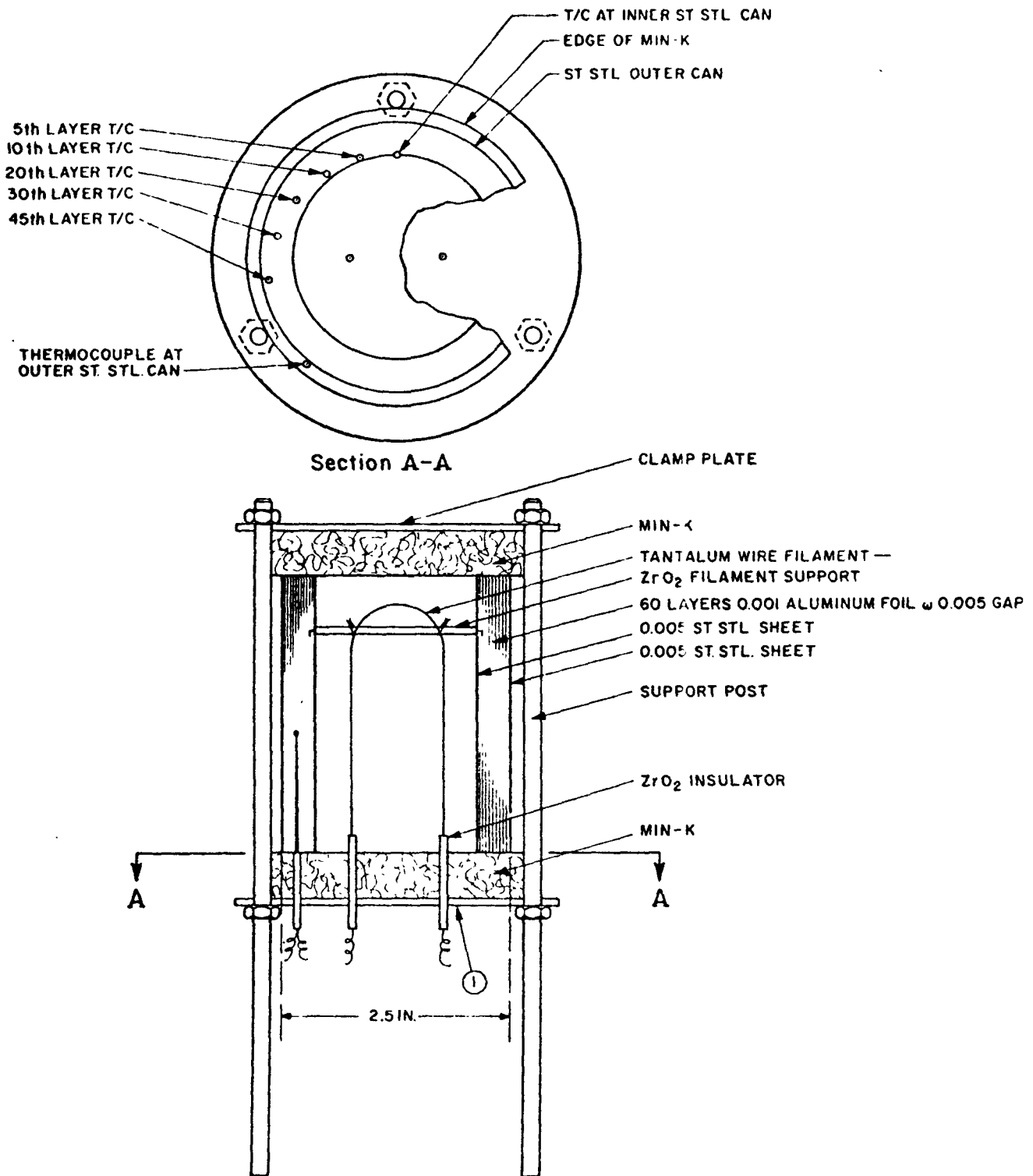


Figure 2.5.1.4-5: Meltdown Assembly Simulating KIPS Heat Source

Min-K TE-1400. The tantalum filament is 0.020 inch in diameter. The heater body is made of stainless steel.

The experimental arrangement is shown in Figure 2.5.1.4-6. The vacuum system pressure throughout the test was approximately 10^{-5} torr.

The assembly was equilibrated at a temperature of 662°F prior to the start of the meltdown. The equilibrium power input was 3.75 watts. The power input was then given a step increase to 68 watts for the duration of the test.

The temperature-time profile for the meltdown test is given in Figure 2.5.1.4-7. The thermocouple locations are indicated in Figure 2.5.1.4-5. After the start of the temperature ramp, the aluminum foils sequentially reach their melting point (1220°F), melt, and are removed from the insulation system. Sequential melting of the foils continues until the increased heat flux through the remaining foils matches the heater input such that the temperature of the inner surviving foil never reaches the melting point.

The temperature-time profile is not difficult to interpret since only the thermal properties of aluminum are involved. Because aluminum has an unusually low vapor pressure (approximately 10^{-6} torr) at its melting point, vapor transport is not a consideration in this test. The discreteness of the data is aided by the oxide film which forms on the aluminum and aids in isolating each foil.

Inspection of the foil assembly after meltdown showed only three intact foils. These foils exhibited no fusion and were easily separable. The aluminum from the molten foils formed a well defined disk on the bottom Min-K slab.

The surface of the unmelted foils were examined with a metallurgical microscope. There was no observable interaction of the zirconia particles with the aluminum.

Electrical Heat Source Assembly Emergency Cooling System Meltdown Test

The test was conducted inside a thermal vacuum chamber, with "Dowtherm A" as the working fluid to achieve the equilibrium operating temperatures. The test setup as indicated in Figure 2.5.1.4-8 was used to maintain steady conditions at the EHSA. Dowtherm A coolant flow through the EHSA was initially maintained at a nominal flow rate of 0.029 lbs/sec. The temperature at the inlet to the boiler was stabilized at 400°F and the thermal vacuum chamber was evacuated to less than 1.1×10^{-4} mm Hg pressure. The other equilibrium conditions which were maintained for a period of 4 hours prior to the start of meltdown are indicated in Table 2.5.1.4-I. After 4 hours of steady state operation the Dowtherm flow through the boiler was abruptly stopped (in less than 15 seconds) while maintaining the 2400 watt thermal input to the EHSA

* It was believed that an abrupt flow stoppage could result in more severe catastrophe as compared to gradual flow stoppage, due to thermal shock. Besides, an abrupt flow stoppage is more amenable to mathematical analysis.

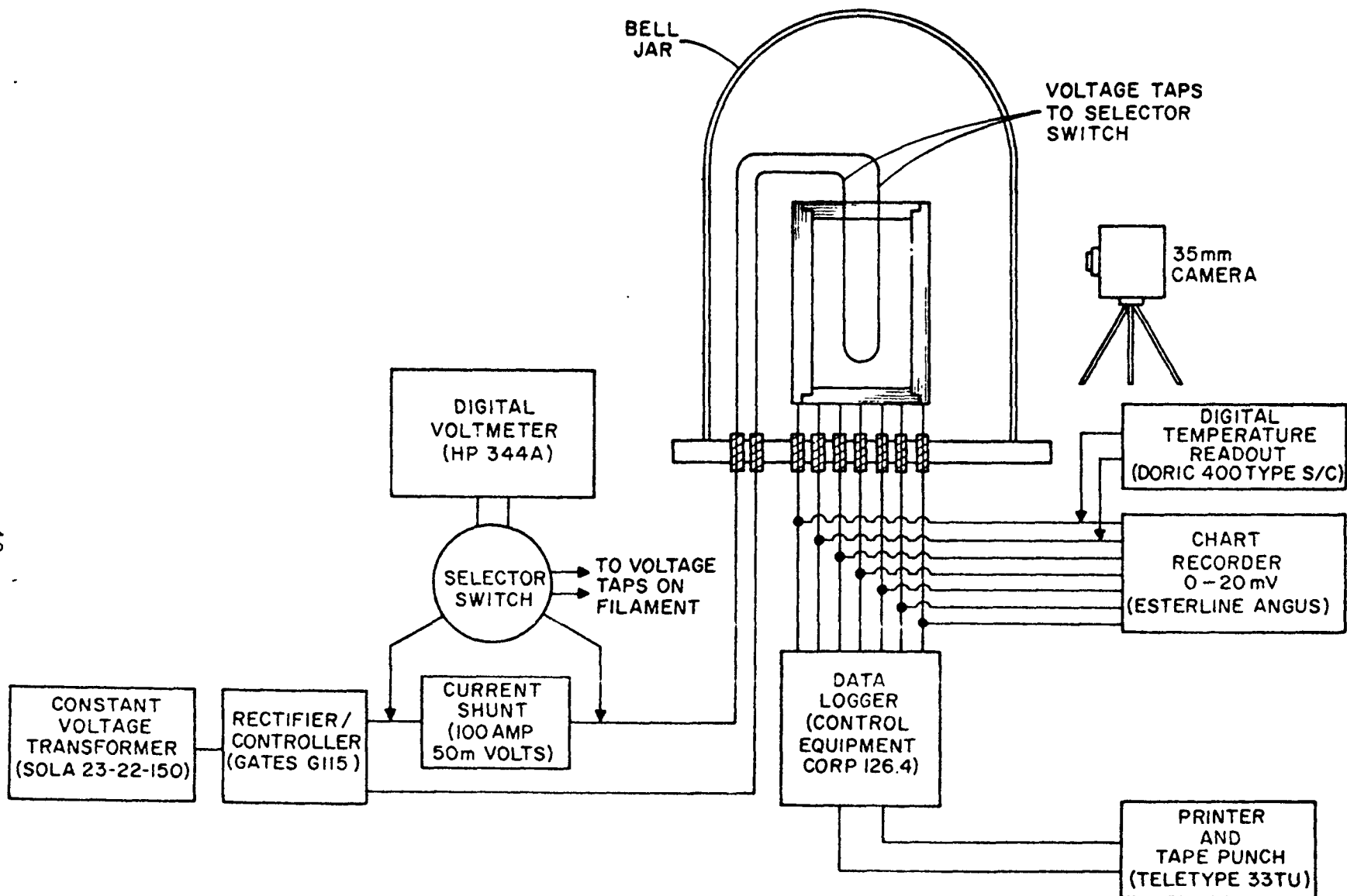


Figure 2.5.1.4-6: Test Arrangement for Meltdown

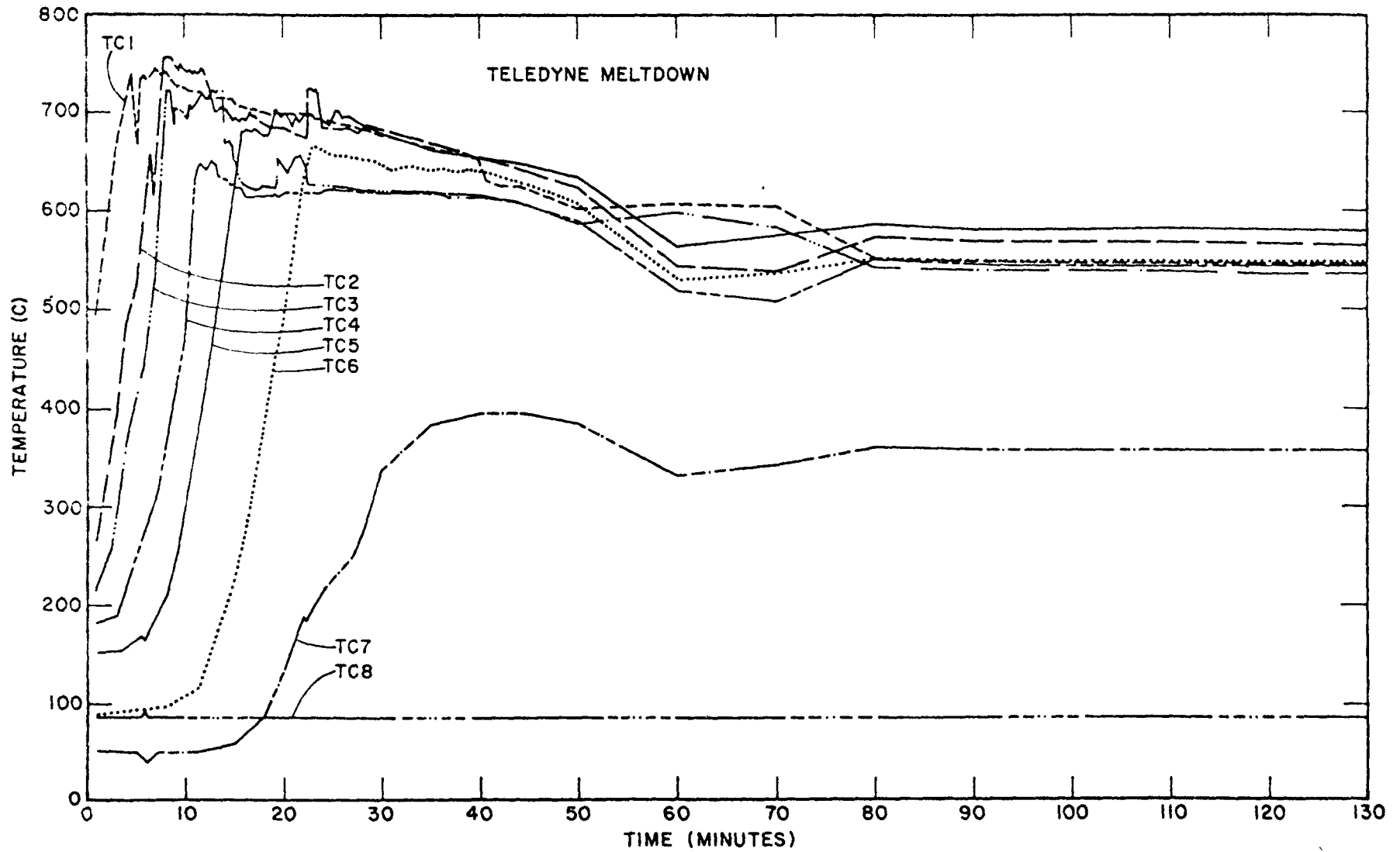
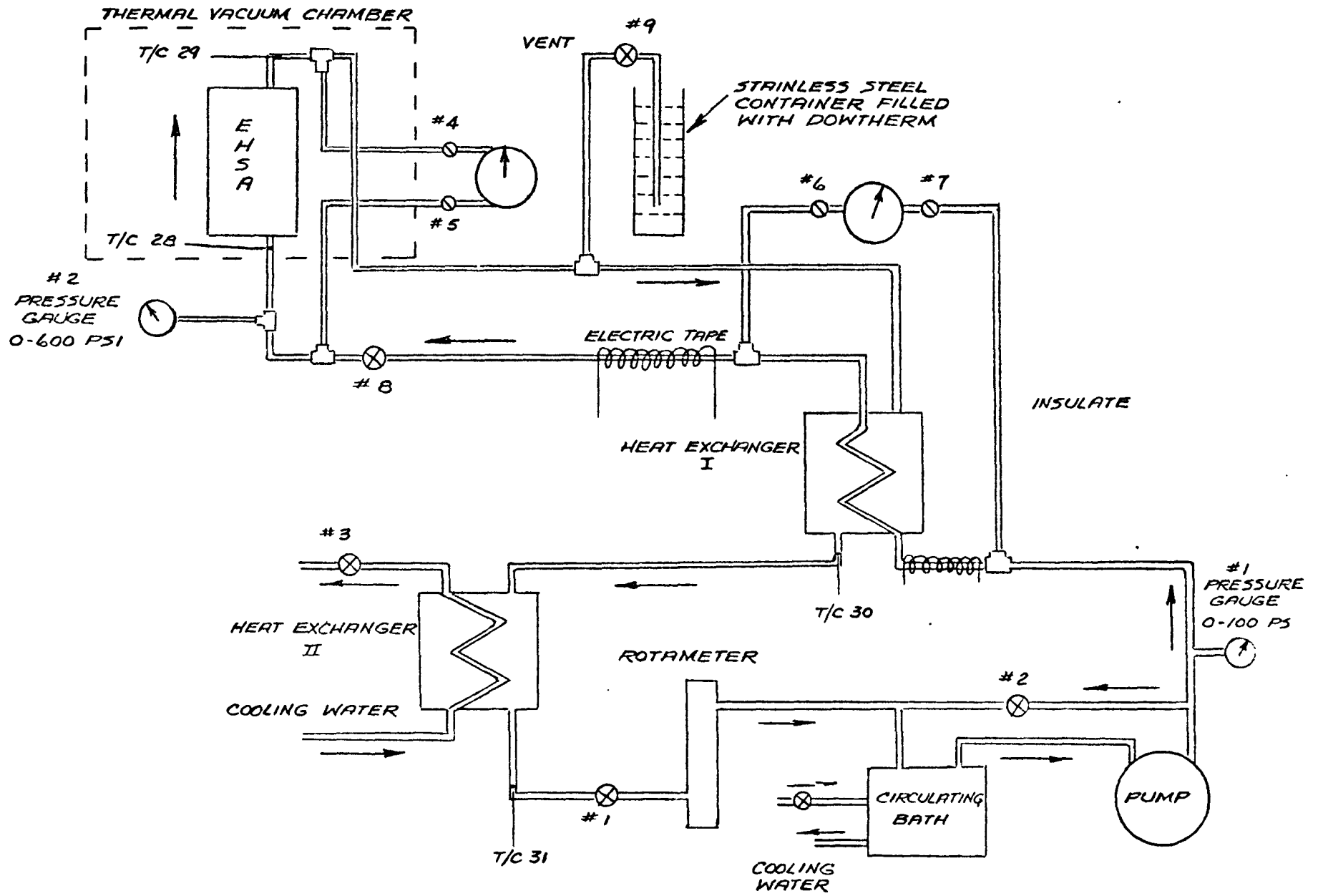


Figure 2.5.1.4-7: Temperature-Time Profile for KIPS Meltdown Assembly

FIGURE 4-8
EHSA MULTIFOIL MELTDOWN TEST FLOW DIAGRAM



TABL 1.4-I

STEADY STATE EHSa PERFORMANCE PRIOR TO MELT-DOWN

Vacuum Chamber Pressure mm Hg	Avg. Vacuum Chamber Temperature °F	Flow Rate lbs/sec	Boiler Inlet Fluid Temperature °F	Boiler Outlet Fluid Temperature °F	ΔT °F	Average Heater Block Temperature (1 + 2 + 3*)/3 °F
1.1 x 10 ⁻⁴	116	.0285	396	530	134	1363

Avg. Radiation Barrier Temp. (4 + 5 + 6)/3 °F	Avg. Boiler Temperature (7 + 8 + 9 + 13)/4 °F	Avg. Multifoil Can Temperature (10 + 11)/2 °F	Avg. Housing Temperature (15 + 16 + 17)/3 °F	Avg. Sp. Heat Btu/lb °F	Heat Carried Away by Boiler Watts
1066	605	648	213	.525	2097

52

NOTE: * Numbers inside the parentheses indicate thermocouple locations

heaters. Most significant thermocouple readings were recorded by the chart recorder, while others were read every 15 minutes for the first two hours and every 30 minutes thereafter for an additional 6 hours.

Results

During and after the meltdown it was noticed that some of the thermocouples either became open-circuited or detached from the surface. However, sufficient redundancy in the number of thermocouples allowed the determination of appropriate temperature response. No difference was observed in the temperatures recorded by the chart recorder and that indicated by the readout thermometer. The error in the temperature measurement, due to the presence of dissimilar material (Deutsch connector) in the thermocouple circuit, was determined by bringing the thermocouple wires from some of the adjacent locations, out directly through a Conax fitting. This error was found to remain less than 20°F for the boiler and less than 40°F for the heat source. All other thermocouples internal to the EHSA are believed to have comparable errors. The results of the test are plotted in Figures 2.5.1.4-9 and 10. Temperatures recorded by only one thermocouple attached to each component are plotted in Figure 2.5.1.4-9, the average temperatures in the axial direction are plotted in Figure 2.5.1.4-10. Temperatures of the heat source, radiation barrier, boiler, multifoil insulation and the housing are seen to be well stabilized prior to the flow stoppage.

Temperatures of all the components start rising immediately after the flow is stopped. The boiler and multifoil insulation temperatures rise most rapidly. Because of its high thermal inertia the heater block temperature rises gradually but monotonically during the meltdown period. When the aluminum can inside the multifoil insulation melts, the rate of rise in boiler temperature is sharply reduced. The response of boiler and multifoil can temperature is identical until the can starts to melt, when part of the heat leaving the boiler is used as latent heat of fusion for the can and its temperature seems to level off at the melting point of aluminum (the response of multifoil thermocouples after meltdown becomes superficial). It is noticed that the can inside the multifoil insulation melts 15 ± 3 minutes after the flow is stopped. After the first few foils have melted, the housing temperature starts to rise rapidly. During this period boiler temperature is seen to fluctuate slightly, which is believed to signify the sequential melting of foils. After all the foils (or the number of foils necessary to allow sufficient heat flux to pass through, so that the temperature of the remaining foil does not rise above its melting point) have melted, the boiler temperature sharply drops and after a short period (< 15 minutes) continues to rise again until equilibrium is reached. The complete meltdown occurs 45 ± 5 minutes after the flow is stopped. The heat source and radiation barrier temperatures also drop slightly upon complete melting, while the housing temperature continues to rise throughout the melting and thereafter. Two hours after the flow is stopped, all the temperatures start to level off and after an additional two hours all the components reach their steady state temperatures (less than 1% difference). The pre meltdown and the post meltdown steady state temperatures are given in Table 2.5.1.4-II.

FIGURE 2.5.1.4-9

TEMPERATURE RESPONSE OF SINGLE THERMOCOUPLE ATTACHED TO THE EHSA COMPONENTS

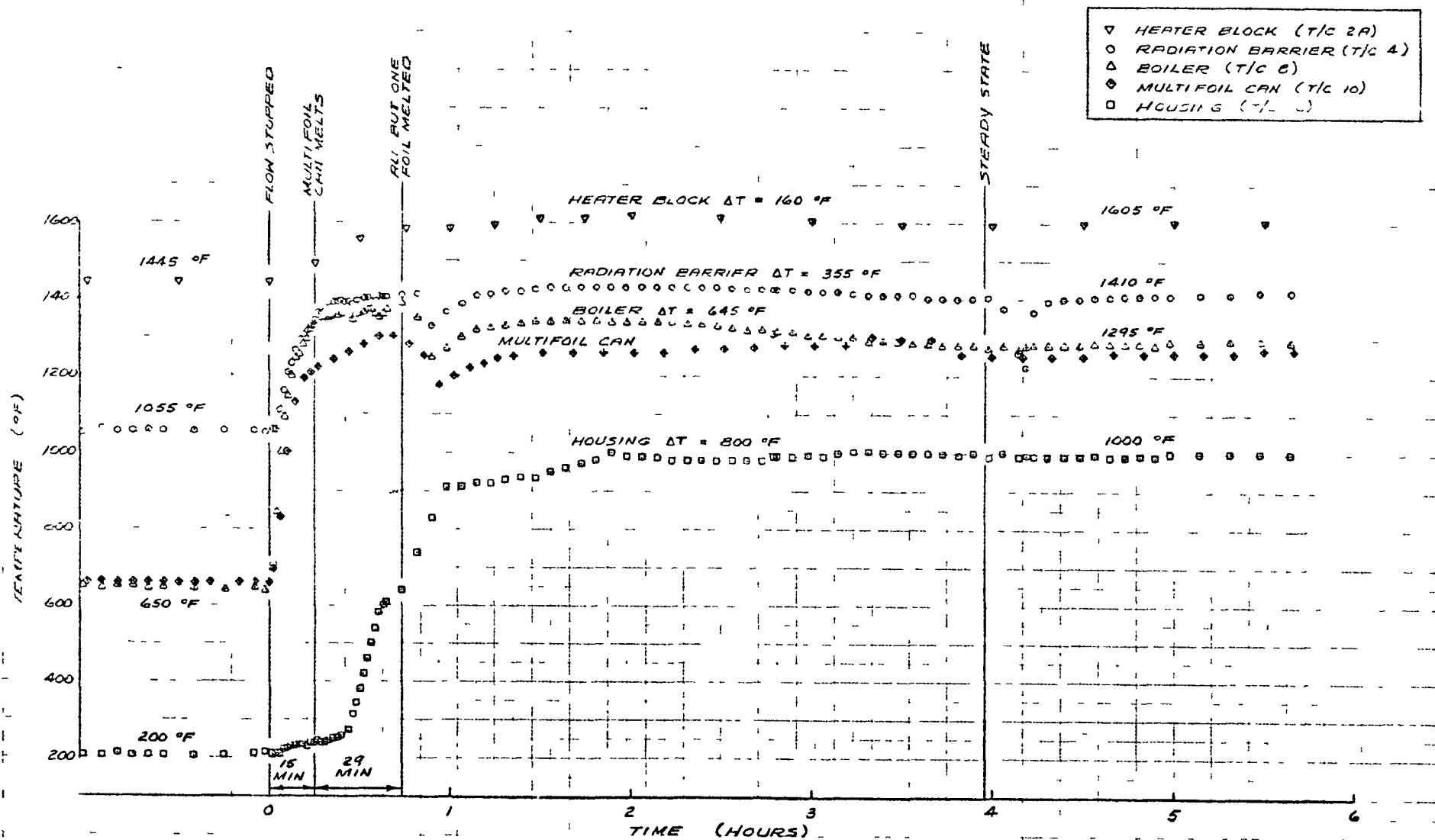
 ΔT = RISE IN TEMPERATURE FROM PRE-MELT DOWN EQUILIBRIUM CONDITION

FIGURE 2.5.1.4-10
 TEMPERATURE RESPONSE OF EHSR COMPONENTS AVERAGED IN THE AXIAL DIRECTION

ΔT = RISE IN TEMPERATURE FROM PRE-MELT DOWN EQUILIBRIUM CONDITION

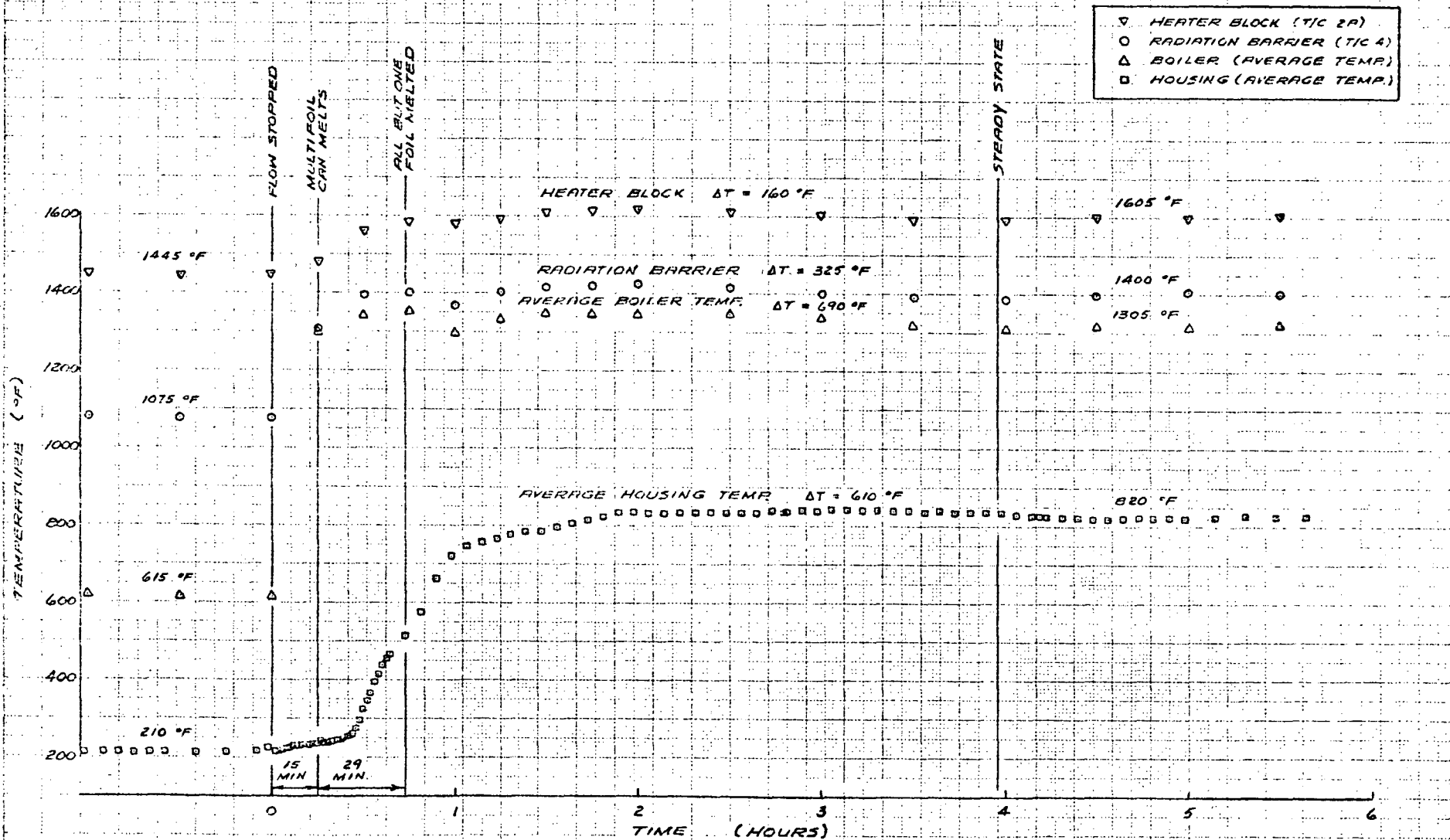


TABLE 2.5.1.4-II

PRE AND POST MELT-DOWN EQUILIBRIUM
TEMPERATURES OF THE EHSA COMPONENTS

<u>EHSA</u> <u>Components</u>	<u>Pre-Melt-Down</u> <u>Equilibrium</u> <u>Temperature</u> <u>°F</u>	<u>Post-Melt-Down</u> <u>Equilibrium</u> <u>Temperature</u> <u>°F</u>	<u>Rise in Temperature</u> <u>Due to Melt-Down</u> <u>°F</u>
Heater Block	1445	1605	160
Radiation Barrier	1075	1400	325
Boiler	615	1305	690
Multifoil Can	648*	1240	592
Housing	210	820	610

NOTE: * The higher temperature of the multifoil can as compared to the average boiler temperature is due to the specific locations of the thermocouples.

Discussion of Test Results

The final equilibrium temperature of the heater block is 1600°F which is approximately 160°F higher than the premeltdown equilibrium temperature of 1440°F. This temperature increment is well within the allowable rise in temperature of 270°F, from an initial PICS temperature of 1900°F. The boiler temperature stabilizes at 1300°F, after the meltdown; a rise of almost 700°F. The most severe rise is seen to occur in the average housing temperature which reaches 820°F (with a peak temperature of 1000°F, from an average initial temperature of 200°F. Although the environmental temperature (average thermal vacuum chamber temperature) was 300°F, which is higher than the real case temperature of 150°F (average KIPS radiator temperature); this factor is not believed to influence the housing temperature significantly under equilibrium conditions, because of strong non-linearity of the radiative heat transfer process. The fact that the average premeltdown equilibrium housing temperature is also slightly higher than that assumed for normal operation, suggests that the emissivity of the housing surface is lower than expected. The effect of lower housing emissivity is reflected in significantly higher post meltdown housing temperature; because of much greater post meltdown heat transfer rate through the housing.

The fact that the housing temperature starts to rise immediately after the flow is stopped and before the first foil melts (see Figures 2.5.1.4-9 and 10) suggests that the amount of heat rejected from the housing, increases and continues to increase even more rapidly after only a few foils have melted. The effective thermal conductivity of the multifoil insulation system in this test unit was higher than expected because of dimensional changes. This results in substantially higher rate of rise in housing temperature than predicted in Figure 2.5.1.4-2. Further, this seems also to be the cause for the longer time, after the flow is stopped that "multifoil can" takes to start melting and the complete melting of multifoil insulation. Contrary to the gradual and linear rise in temperature of the heat source predicted in Figure 2.5.1.4-2, the test data shows that the heater block temperature starts to increase rather sharply during the meltdown process. This is thought to be due to less than assumed thermal capacity of the heater block. Part of the difference in the results predicted in Figure 2.5.1.4-2 and those obtained during the test, is due to different initial equilibrium conditions. The rise in temperatures of the heater block and the radiation barrier are observed to be much less than those predicted. Nevertheless, the trend in the temperature response of most components is mostly in agreement with the study of Figure 2.5.1.4-2.

Substantial temperature gradient was observed along the housing, after the meltdown. Whereas before meltdown the temperature difference between the center of the housing and at 6.65" away from it, was less than 25°F; after the meltdown this temperature gradient was seen to have increased to approximately 150°F. This would be capable of sustaining a heat transfer rate of about 134 watts in the axial direction along the housing. It appears that the multifoil insulation continued to provide large thermal resistance, near the ends of the EHSA in the radial direction. This in turn suggests the possibility that the multifoil insulation melted only near the center of the housing. Additional evidence to this possibility is obtained from the post meltdown disassembly of the EHSA, when one of the foils (which remained unmelted) indicated only partial melting near the center.

Post Meltdown Disassembly of the EHSA

Upon completion of the meltdown test, the EHSA was disassembled using the same tooling and techniques which were used for assembly. Care was taken to preserve the integrity of individual components, where possible, throughout the disassembly process. The EHSA was removed from the thermal vacuum chamber (see Figure 2.5.1.4-11) and attached to a support structure maintaining its vertical test position. The upper end of the EHSA (outlet side of the boiler) was disassembled first as the test was performed with the EHSA in this position.

Disassembly of the EHSA was relatively easy. The housing and end-cover materials seem to have yielded due to very high housing temperature; thus, requiring very little torque and/or load to unthread the lock rings and remove the screws. The lower outer cover was difficult to remove because of a burr in one of the threads, which could have been caused during the assembly process. Multifoil insulation after melting, dropped to the bottom of the EHSA and seems to have travelled through a path of least resistance down the outgassing tube. Part of molten multifoil was collected in a tray underneath the EHSA. As a result of collection of the melted multifoil system near the bottom of the EHSA, portions of the boiler (copper), radiation barrier (nickel) and sheathed thermocouples (inconel and platinum) which came into contact with it appeared to have been dissolved by the molten multifoil system. This phenomenon seems to be dependent on concentration of the molten aluminum in contact with other surfaces and its rate of melting; surface tension effects would control the movement of molten aluminum in a zero-gravity situation. The rate of vaporization of aluminum remains extremely low in vacuum at the temperature of melting, as compared to the rate of melting. Otherwise, most of the components remained in good condition after the meltdown. "Dowtherm A" that remained inside the boiler tubes after the flow was stopped appeared to have completely burnt out and became a thick black and sticky substance.

The heater block assembly, except for discoloration near the ends of the thermocouples, appeared to be in good shape. The condition of the wiring splices, ceramic beads and Varflex sleeving on each end was excellent. See Figures 2.5.1.4-12 and 13. The mica and fibrous insulation (A-100) pads which rest on top of the heater wirings and in contact with the underside of the end plug were also in excellent condition. The total circuit resistance of the heater circuit remained the same before and after the test.

The appearance of the upper end of the boiler assembly was about the same as at the time of the assembly; except that the individual copper flanges were slightly softer than during assembly; see Figure 2.5.1.4-13. The iron titanate coating on the boiler had flaked off at some places. One of the foils remained largely unmelted, but showed patches where melting had occurred; especially a large hole on one side of the foil. See Figure 2.5.1.4-14. The outer portion of the boiler had become discolored, but showed no sign of fusion with molten aluminum. This shows that as the foils melted, the molten aluminum fell to the bottom without any transverse migration. The outside of the middle portion of the housing had become discolored (bluish). This and some other discolorations appear to have been caused by the back streaming of oil from the large vacuum pump, which inadvertently was not rapidly quenched after shutdown.

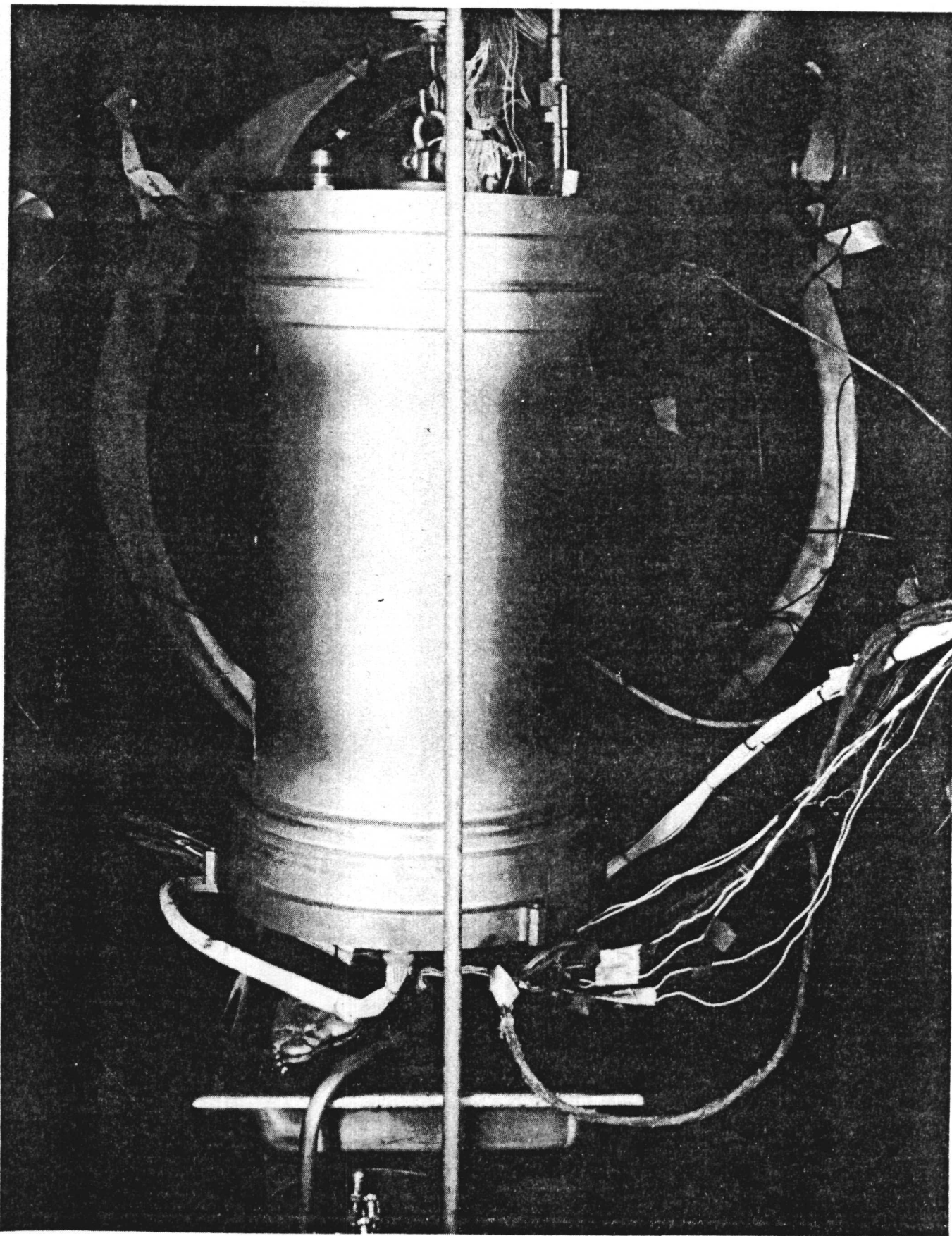


FIGURE 2.5.1.4-11. ELECTRICAL HEAT SOURCE ASSEMBLY (EHSA) INSIDE THE THERMAL VACUUM CHAMBER AFTER THE MELT-DOWN TEST. NOTE DISCOLORATION OF THE HOUSING.

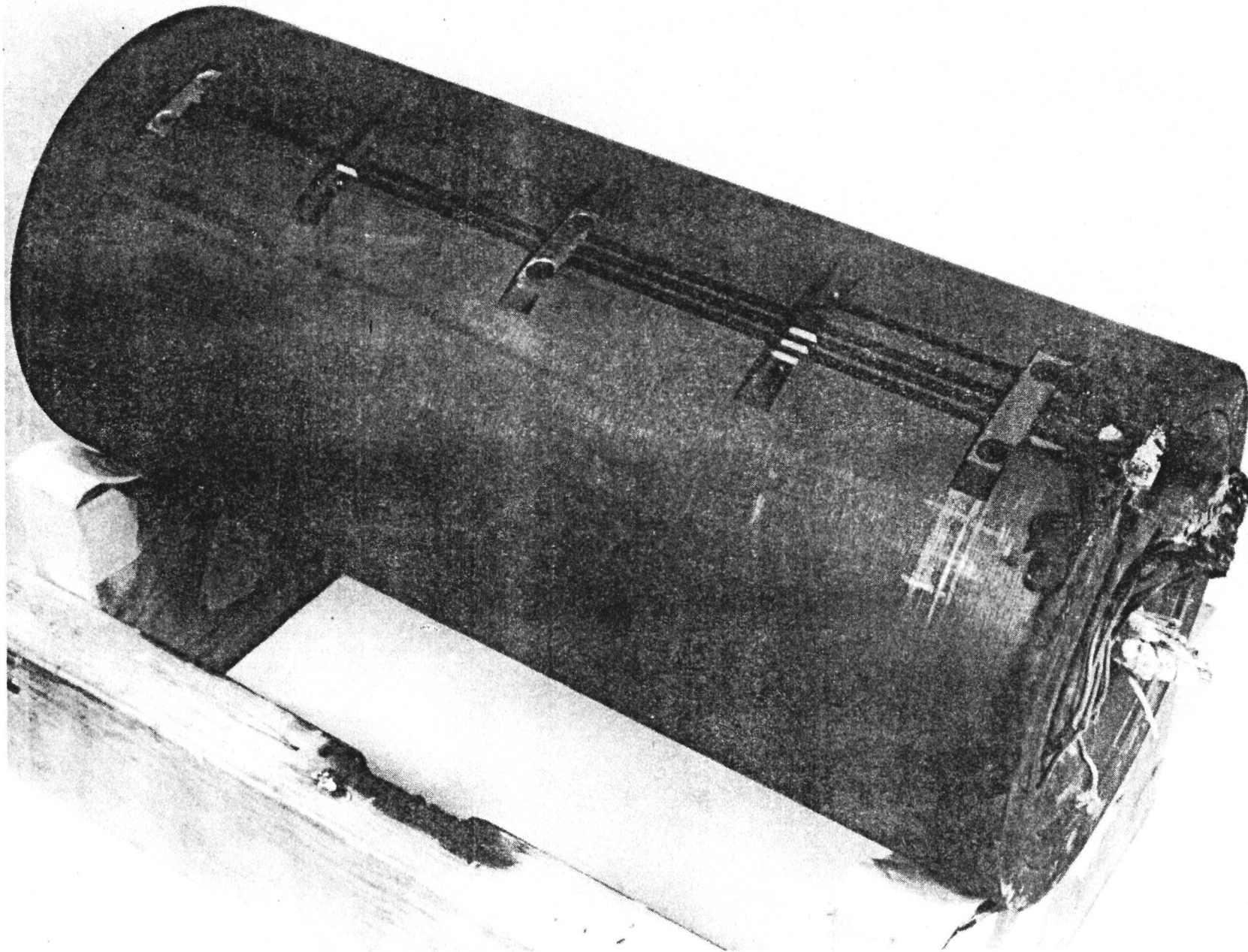


FIGURE 2.5.1.4-12. HEATER BLOCK ASSEMBLY REMOVED FROM THE EHSA. THE DETERIORATION OF THE LOWER END CAN BE SEEN.

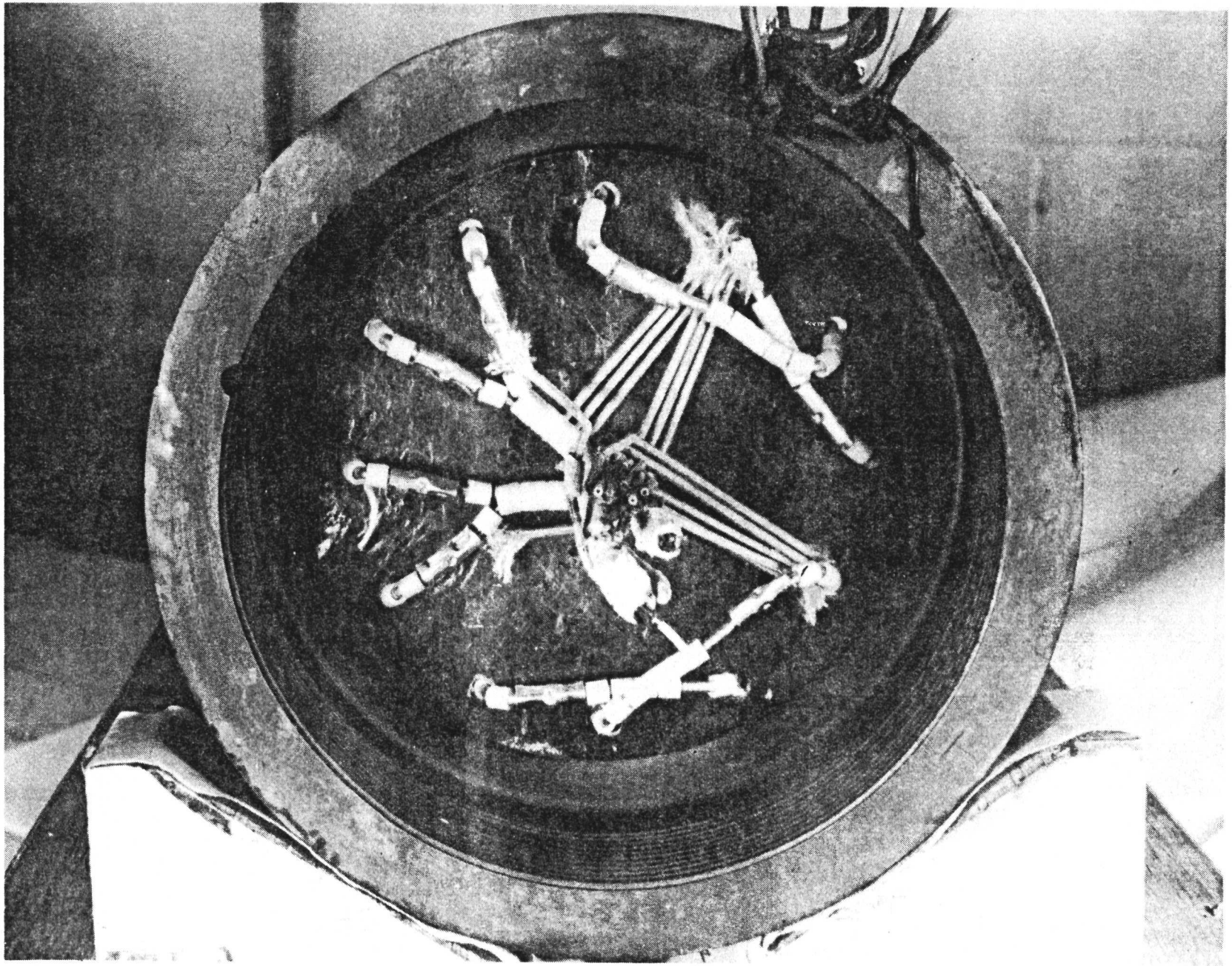


FIGURE 2.5.1.4-13 A VIEW INSIDE THE LOWER END OF THE HEATER BLOCK ASSEMBLY.

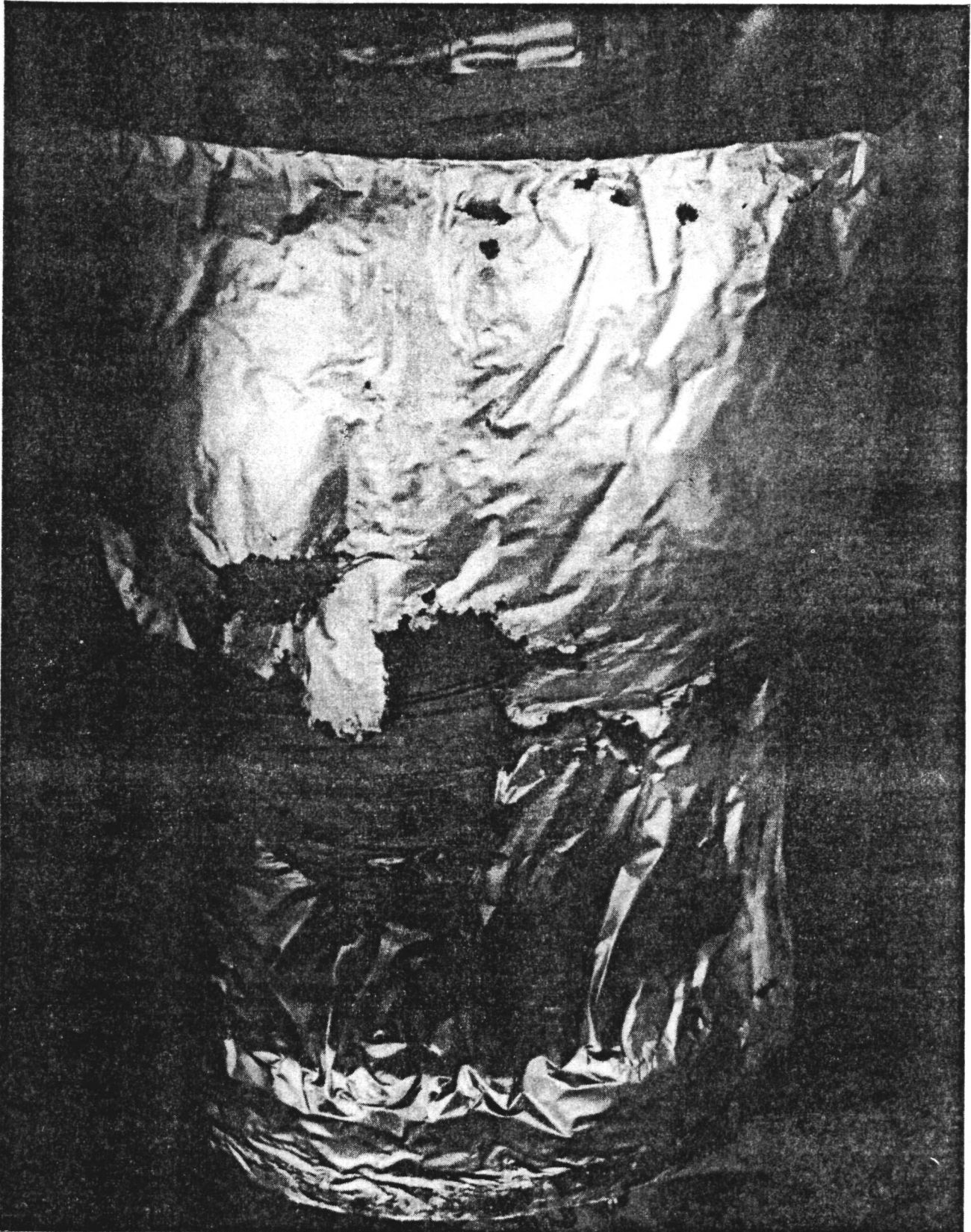


FIGURE 2.5.1.4-14. THE REMAINING FOIL OUTSIDE THE BOILER SHOWS SIGNS OF PARTIAL MELTING.

2.5.1.5 Venting/Gas Management

The gas management system for the Isotope Heat Source Assembly consists of a pressure relief device (PRD) which is attached to the outgassing port prior to launch. Prior to launch the IHS is protected from the atmosphere by an argon gas environment within the HSA. The system can be started and operated at partial power with the argon gas environment within the HSA's, but full power cannot be achieved because of the higher parasitic heat losses from the HSA's. After launch the drop in atmospheric pressure during ascent activates the PRD and the argon gas backfill is vented to space. In addition, the helium generated by the fuel decay process is thereby continuously vented throughout the mission. The PRD has been described in some detail earlier in Section 2.5.1.2 and is shown in Figure 2.5.1.2-1. The PRD is considered to be a fail-safe system in that should the lance fail to pierce the aluminum diaphragm during launch, the diaphragm will subsequently open from creep stresses (resulting from temperature and internal pressure).

2.5.1.6 Reliability

The reliability effort on the flight system has been concentrated on a preliminary Failure Mode, Effects and Criticality Analysis (FMECA) and Single Point Failures (SPF) identification. The purpose of the analysis is to provide a baseline for development of the flight system design and testing. Analysis of the isotope heat source is not included since it has been qualified on the MHW program and is government furnished. The failure modes for the Isotope Heat Source Assembly (IHSA) are primarily safety consequences and are listed as input to safety analysis.

The ground rules for the FMECA are:

1. Failure Mode, Effects and Criticality Analysis (FMECA)

The FMECA is a systematic examination of all components of the system to identify their function, how they can fail and to determine the effects of each component failure on the system. It is an on-going analysis, continually updated as the program and design progresses.

2. Failure modes/effects are ranked in the FMECA according to the severity of the failure effect.

Table 2.5.1.6-I lists guidelines for assigning failure mode likelihood "1" on the FMECA work form. Table 2.5.1.6-II lists guidelines for assigning failure effects ranking "2" on the FMECA work form.

TABLE 2.5.1.6-I

FAILURE MODE LIKEHOOD RANK

<u>Rank</u>	<u>Rationale for Ranking</u>
100	Most likely failure mode
75	Very likely failure mode
50	Likely Failure mode
25	Minor failure mode
10	Unlikely failure mode
5	Highly unlike failure mode
1	Improbably failure mode

TABLE 2.5.1.6-II

FAILURE EFFECTS CATEGORIES AND RANKING

<u>Category</u>	<u>Failure</u>	<u>Rank</u>
I	Results in catastrophic or imminent loss of power performance and mission	100
II	Results in a reduction in power resulting in a partial mission failure	50
III	Results in failure or out of specification condition not affecting power	5

Isotopic Heat Source Assembly (IHSA)

The IHSA is described in Section 2.5.1.2. Table 2.5.1.6-III presents the IHSA Failure Mode Effects and Criticality Analysis (FMECA) work sheet.

The failure modes for the IHSA and the emergency cooling system are primarily safety consequences and are listed as input to safety analysis. Figure 2.5.1.6-1 and Table 2.5.1.6-IV presents the single point failures relating to these failure modes.

② PLACES — PENETRATION ASSEMBLY

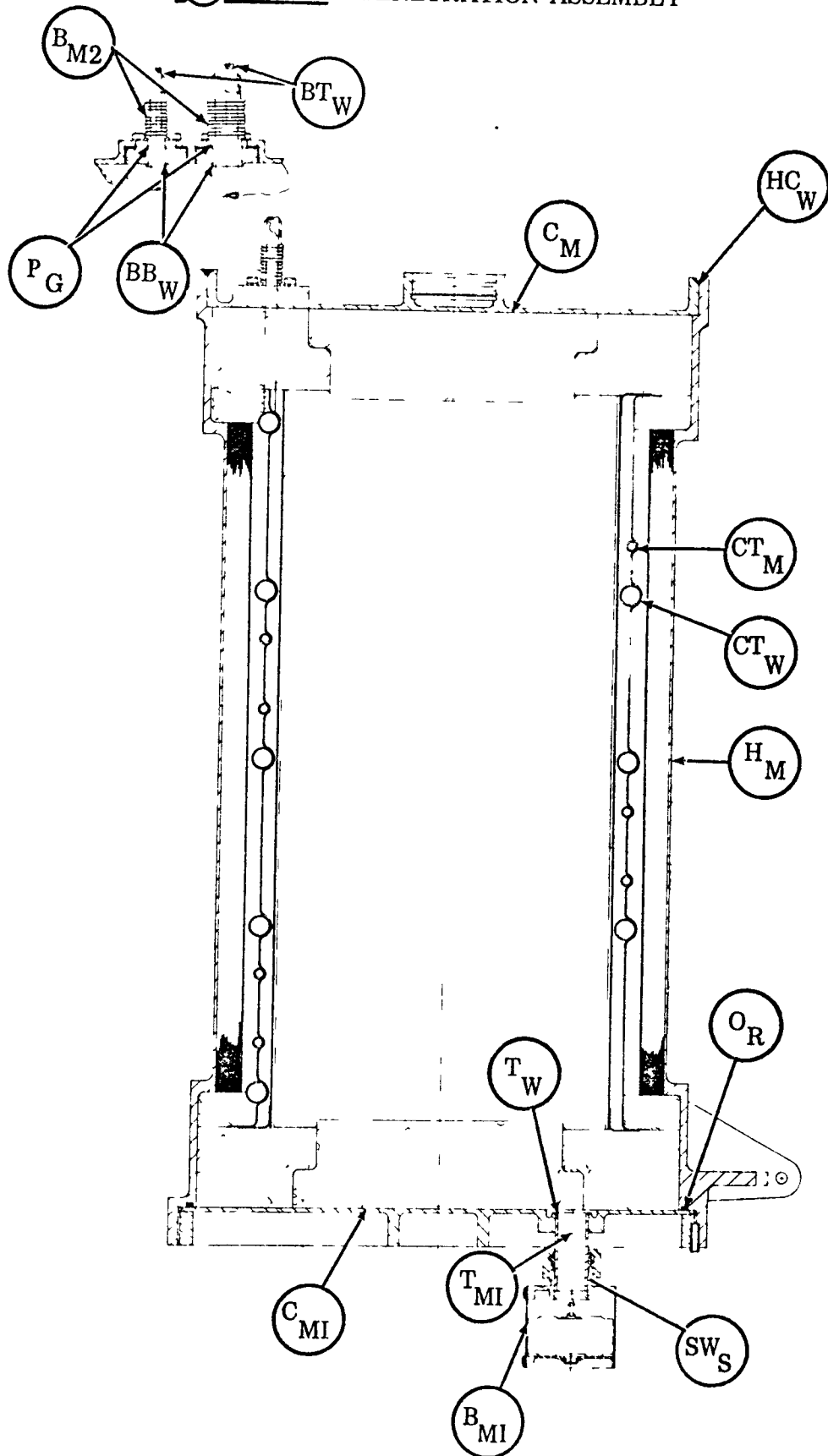


FIGURE 2.5.1.6-1
SINGLE FAILURE POINTS—I.H.S.A.

TABLE 2.5.1, 6-III

FAILURE MODE AND EFFECTS ANALYSIS - IHS

NO.	COMPONENT & FUNCTION	FAILURE MODES (FM)	POSSIBLE FAILURE CAUSES	FAILURE EFFECT (FE)	③ CRITICALITY RANK ① x ② = ③ ② FE RANK ① FM LIKEHOOD			
					DESIGN/SAFETY CONSIDERATIONS	①	②	③
1.0	<u>Emergency Cooling System</u>							
1.1	Automatically removes thermal insulation from around the Heat Source Assembly (HSA) whenever the temperature exceeds a pre-determined value.	Insulation fails to melt	Insulation material does not melt at specification temperature	Temperature rise is secondary failure and the consequence is related to safety (and mission accomplishment). The primary failure is loss of radiator fluid circulation	Insulation meltdown provides control of IHS temperature rise to preserve integrity of fuel containment structure	*	*	*
67		Inadvertant meltdown of Insulation	Insulation material melts below specification temperature Insulation failure	Increased heat loss and therefore reduced system efficiency		1	50	50
	2.0	<u>HSA Enclosure</u>						
2.1	Provide a sealed enclosure for containment of an inert cover gas surrounding the HSA during ground operation	Seal leaks at a rate greater than makeup capability at inert gas supply	Seal failure	No effect on loss of performance (thermal heat). Consequence relates to safety, i.e., life of IHS (IHS exposed to air)	Leak test a part of acceptance criteria Radiograph inspection and leak test of welds. Seals not required for space operation (chamber vented to space)	*	*	*
3.0	<u>Pressure Release Device (PRD)</u>							
3.1	Provides a means for releasing IHS enclosure cover gas in space	PRD Pre-maturely operates in air environment PRD fails to operate in space environment	Bellows seal failure Binding Mechanism, cutter head shaft bends/breaks, cutter head fails to yield	No effect on loss of performance (thermal heat). Consequences relates to safety, i.e., life of IHS. Increased heat loss and therefore reduced system efficiency until cover gas diffuses through seals to space	Design concept will follow MHW qualified design	*	*	*
						5	50	250

TABLE 2.5.1.6-IV

ISOTOPIC HEAT SOURCE ASSEMBLY ENCLOSURE
SEAL LEAK SINGLE POINT FAILURES

C _{M1}	-	Cover material - lower	1
B _{M1}	-	Bellows - Pressure Release Device (PRD)	1
T _{M1}	-	Tube material - PRD	1
SW _S	-	Swageloc seal	1
O _R	-	O-ring - lower cover	1
H _M	-	Housing material	1
CT _{M1}	-	Cooling tube material - normal	1
CT _{M2}	-	Cooling tube material - ground	1
HC _W	-	Housing/cover weld - upper	1
C _{M2}	-	Cover material - upper	1

PENETRATION ASSEMBLY

BB _W	-	Bellows/block weld	4
P _G	-	Penetration assembly gasket	4
B _{M2}	-	Bellows material	4
BT _W	-	Bellows/tube weld	4

2.5.1.7 Structural Analysis

The analysis of the KIPS HSA housing subjected to an axial load involves an integral structure composed of a cylinder and rib stiffened end cover (Figure 2.5.1.7-1). The loading arises from the 42 lb internal heat source subjected to a 30G acceleration and reacting against the end cover through the Min-K insulation. It is assumed that the insulation subjects the end cover to a uniform load distributed over a circular area of radius $a = 2.72$ inches. Then the pressure loading is,

$$p_o = \frac{42 \times 30}{\pi \times (2.72)^2} = 54.21 \text{ psi}$$

The methodology of the analysis assumes a displacement function for the end cover of the form:

$$y = A_1 (L + b - r) + A_2 (L + b - r)^2 + A_3 (L + B - R)^3 + A_4 (L + b - r)^4 + A_5 (L + b - r)^5 \quad (1)$$

where:

A_1, A_2, A_3, A_4 and A_5 are constants to be determined.

L, b and r are defined in Figure 2.5.1.7-1.

Equation (1) satisfies the condition that y at $r = L + b$ is equal to zero. To satisfy the condition of zero slope at $r = b$ we must have:

$$A_1 = -L (2 A_2 + 3 A_3 L + 4 A_4 L^2 + 5 A_5 L^3) \quad (2)$$

The strain energy of the plate is obtained from two components. In the radial direction we have the rib-plate combination with a linearly varying cross sectional moment of inertia given by:

$$I_x = \frac{t_r H_r^3}{12} + H_r t_r \left[t_p + \frac{H_r}{2} - y_{c.g.} \right]^2 + 2 t_p (C + x \tan \Theta) \left(y_{c.g.} - \frac{t_p}{2} \right)^2 \quad (3)$$

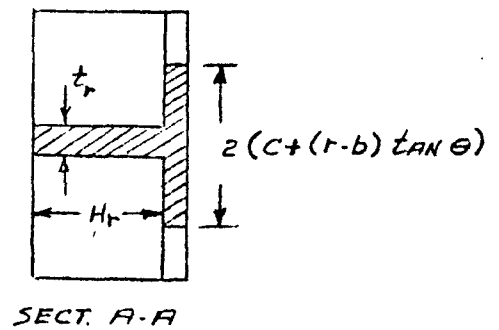
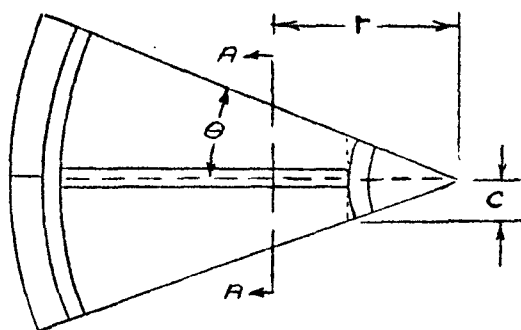
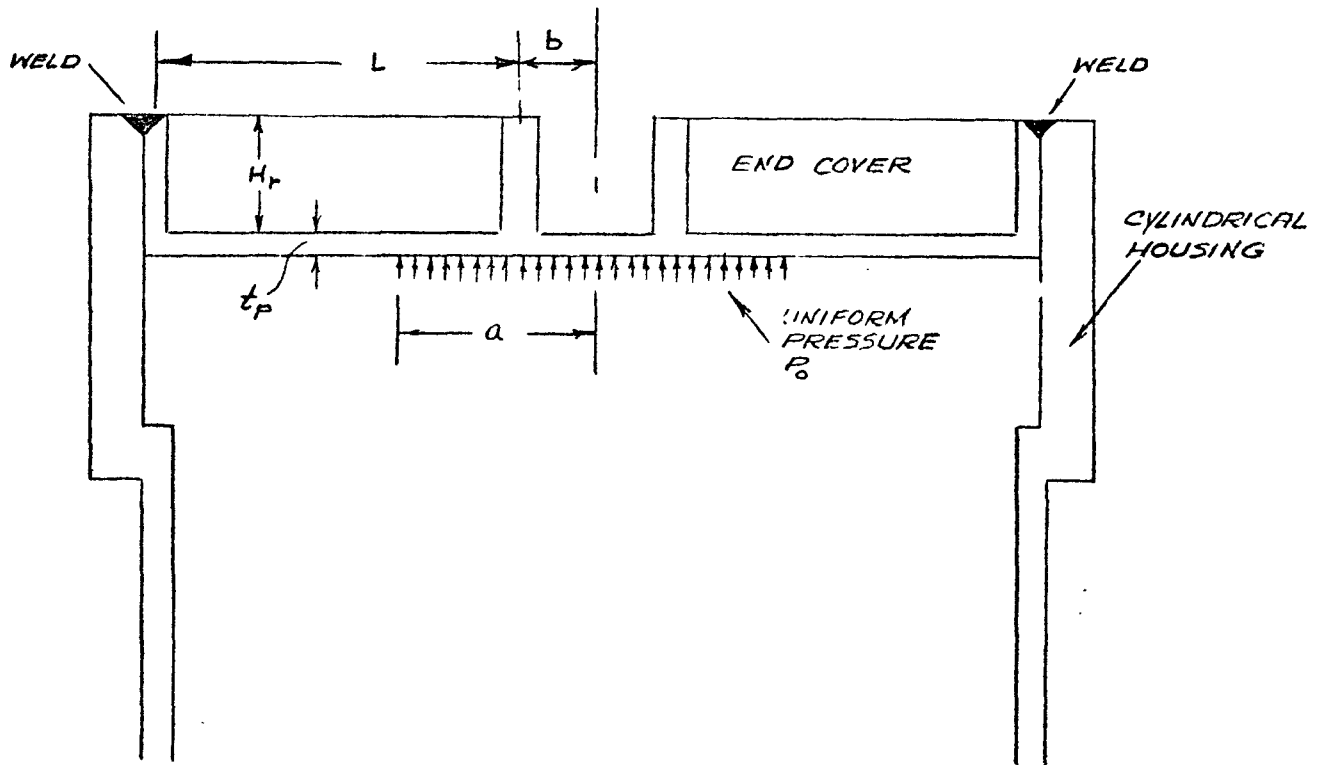
where:

$$y_{c.g.} = \frac{H_r t_r \left(t_p + \frac{H_r}{2} \right) + t_p^2 (C + x \tan \Theta)}{H_r t_r + 2 t_p (C + x \tan \Theta)} \quad (4)$$

$$x = r - b$$

FIGURE 2.5.1.7-1

$L = 4.315 \text{ IN.}$ $H_r = .750 \text{ IN.}$
 $b = 1.125 \text{ IN.}$ $t_r = .150 \text{ IN.}$
 $c = .195 \text{ IN.}$ $\Theta = 20^\circ$
 $t_p = .100 \text{ IN.}$



and, H_r , t_r , t_p , Θ and C are defined in Figure 2.5.1.7-1.

The strain energy due to the rib-plate combined structure in bending is given by:

$$V_B = \frac{E}{2} \int_0^L I_x \left(\frac{d^2 y}{dx^2} \right)^2 dx \quad (5)$$

In the tangential direction the strain energy involves the plate alone. We have:

$$V_p = \frac{E t_p^3}{48 (1 - \nu^2)} \int_0^{2\pi} \int_0^{L+b} \left[\frac{1}{r} \frac{dy}{dr} \right]^2 + \nu \frac{dy}{dr} \frac{d^2 y}{dr^2} \Big] dr d\Theta \quad (6)$$

where:

E = Young's Modulus and ν = Poisson's ratio

The total strain energy is then,

$$V = 18 V_B + V_p \quad (7)$$

According to the theory of minimum potential energy the virtual work done by the load p_o in a virtual displacement δy is equal to the variation of the strain energy due to the displacement δy . Then,

$$\frac{\partial V}{\partial A_2} \delta A_2 = \delta (W_{p_o})_{A_2} \quad (8)$$

$$\frac{\partial V}{\partial A_3} \delta A_3 = \delta (W_{p_o})_{A_3} \quad (9)$$

$$\frac{\partial V}{\partial A_4} \delta A_4 = \delta (W_{p_o})_{A_4} \quad (10)$$

$$\frac{\partial V}{\partial A_5} \delta A_5 = \delta (W_{p_o})_{A_5} \quad (11)$$

where:

$$\delta (W_{p_o})_{A_n} = \left[2\pi p_o \int_0^a r \left(\frac{\partial y}{\partial A_n} \right) dr \right] \delta A_n \quad (12)$$

Using equations 1, 5, 6, 7, 8, 9, 10, 11, 12 we arrive at four equations in four unknowns; i. e., in matrix form:

$$\begin{bmatrix}
 -.21285 & 18.46798 & 128.5947 & 705.6151 \\
 18.46798 & 196.0034 & 1274.812 & 7210.6447 \\
 128.5947 & 1274.812 & 8651.35 & 50930.481 \\
 705.6151 & 7210.6447 & 50930.481 & 309190.063
 \end{bmatrix}
 \begin{bmatrix}
 A_2 \\
 A_3 \\
 A_4 \\
 A_5
 \end{bmatrix}
 = -\frac{2}{E} p_o
 \begin{bmatrix}
 413.036 \\
 3503.78 \\
 22358.739 \\
 127127.65
 \end{bmatrix}$$

Using a value for E of 9.8×10^6 psi the solution for these equations is:

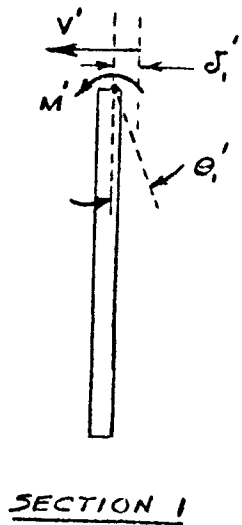
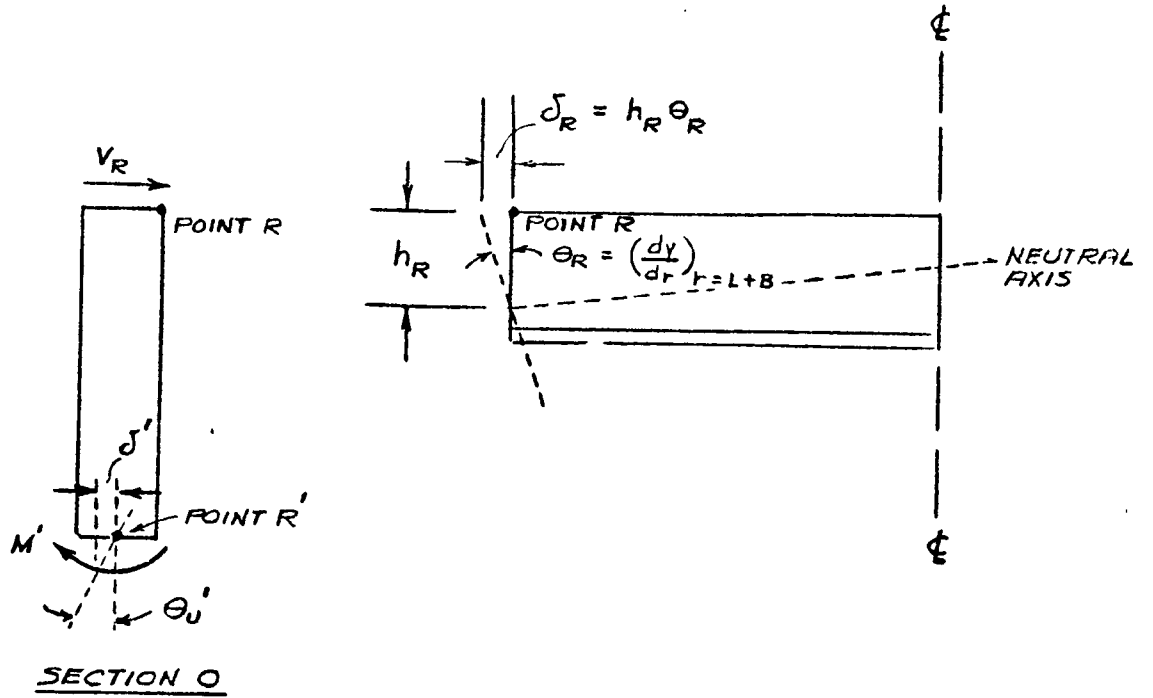
$$\begin{aligned}
 A_1 &= 1.757413 \times 10^{-4} p_o \\
 A_2 &= 9.32796 \times 10^{-6} p_o \\
 A_3 &= 5.25776 \times 10^{-6} p_o \\
 A_4 &= 2.023653 \times 10^{-7} p_o \\
 A_5 &= 1.591633 \times 10^{-8} p_o
 \end{aligned}
 \tag{13}$$

Figure 2.5.1.7-2 shows the breakdown of the cylindrical portion of the HSA housing in determining the reaction of that portion to the deformation of the end cover. The reaction is assumed to arise from the radial displacement δ_R of the end cover at point R. To determine the reaction V_R the expressions for radial displacements and angular changes at points R and R^1 on the cylinder must be determined. We have:

$$\Theta_1^1 = \frac{C_{61} M^1}{\lambda_1 D_1} + \frac{C_{41} V^1}{2 D_1 \lambda_1^2} \tag{Ref. 12}$$

$$\delta_1^1 = \frac{C_{31} V^1}{2 D_1 \lambda_1^3} + \frac{C_{51} M^1}{2 D_1 \lambda_1^2}$$

FIGURE 2.5.1.7-2



$$\Theta_0^1 = \frac{C_{40}^* V_R}{2 D_0 \lambda_0^2} - \frac{C_{40} V^1}{2 D_0 \lambda_0^2} + \frac{C_{60} M^1}{\lambda_0 D_0}$$

$$\delta_0^1 = \frac{C_{30}^* V_R}{2 D_0 \lambda_0^3} - \frac{C_{30} V^1}{2 D_0 \lambda_0^3} + \frac{C_{50} M^1}{2 D_0 \lambda_0^2}$$

$$\delta_R = \frac{C_{30} V_R}{2 D_0 \lambda_0^3} - \frac{C_{10}^* V^1}{2 D_0 \lambda_0^3} + \frac{C_{50}^* M^1}{2 D_0 \lambda_0^2}$$

Where:

$$\lambda = \sqrt[4]{\frac{3(1-\nu^2)}{R^2 t^2}}$$

$$D = \frac{E t^3}{12(1-\nu^2)}$$

Subscripts 0 and 1 refer to the thick wall and thin wall sections respectively
 M^1 , V^1 , V_R , Θ_1^1 , δ_1^1 , Θ_0^1 , δ_0^1 and δ_R are defined in Figure 2.5.1.7-2.

$$C_{30} = 1.03$$

Ref. 12

$$C_{30}^* = -.150$$

$$C_{40} = 1.05$$

$$C_{40}^* = .11$$

$$C_{50} = 1.05$$

$$C_{50}^* = -.19$$

$$C_{60} = 1.02$$

$$C_{60}^* = .10$$

$$C_{31} = 1$$

$$C_{41} = 1$$

$$C_{51} = 1$$

$$C_{61} = 1$$

Equating slopes and deflections at point R^1 allows us to solve for M^1 and V^1 in terms of V_R . The results are:

$$M^1 = 2.15936 \times 10^{-2} V_R \frac{\text{in.} \cdot \text{lb}}{\text{in.}}$$

$$V^1 = -6.31011 \times 10^{-2} V_R \frac{\text{lb}}{\text{in.}}$$

Using these results we have for δ_R :

$$\delta_R = 4.92742 \times 10^{-5} V_R$$

or

$$V_R = K \delta_R \quad \text{where } K = 2.02946 \times 10^4 \frac{\text{lb}}{\text{in.}^2} \quad (14)$$

Differentiating equation (1) and using the results of (13) we have for the slope at $r = L + b$

$$\left(\frac{dy}{dr} \right)_{r=L+b} = 1.7574 \times 10^{-4} p_o$$

The radial displacement of point R is then

$$\delta_R = h_R \left(\frac{dy}{dr} \right)_{r=L+b} = 1.12859 \times 10^{-4} p_o \quad (15)$$

where h_R is the distance from the neutral axis to the extreme fiber; i. e., $h_R = .642$ in.

Using (14) and (15) we have for V_R :

$$V_R = 2.02946 \times 10^4 \times 1.128259 \times 10^{-4} p_o = 124.127 \text{ lb/in.}$$

The maximum longitudinal stress on the cylinder is given by

$$\sigma_L = \frac{1.932 V_R}{\lambda t^2} + \frac{\pi p_o a^2}{2 \pi (R) t}$$

where

$$\lambda = 1.3269 \quad t = .170 \quad R = 5.52 \text{ in.}$$

then,

$$\sigma_L = 6467 \text{ psi}$$

The yield point for 6061-T6 aluminum alloy at 220°F is 32.4×10^3 psi. Then the margin of safety is

$$\text{M. S.} = \frac{32400}{6467} - 1 = 4.01$$

The maximum hoop stress in the cylinder is given by

$$\sigma_h = \frac{2 V_R}{t} \lambda R = 10696 \text{ psi}$$

The margin of safety is:

$$\text{M. S.} = \frac{32400}{10696} - 1 = 2.03$$

For the stress on the end cover we have: at $r = b$

$$\left(\frac{d^2 y}{dr^2} \right)_{r=b} = 9.7828 \times 10^{-5} p_o$$

$$\sigma = E \left(\frac{d^2 y}{dr^2} \right)_{r=b} h_b = 9.8 \times 10^6 \times 9.7828 \times 10^{-5} \times 54.21 \times .484 = 25154 \text{ psi}$$

The margin of safety is:

$$\text{M. S.} = \frac{32400}{25154} - 1 = .288$$

At $r = L + b = 5.44$ in.

$$\frac{d^2 y}{dr^2} \Big|_{r=L+b} = 1.865592 \times 10^{-5} p_o = 1.01134 \times 10^{-3}$$

The margin of safety is

$$\text{M. S.} = \frac{32400}{6363} - 1 = 4.09$$

2.5.2.6 Radiator

2.5.2.6.1 Radiator - Configuration

The flight system radiator assembly is an aluminum, welded/riveted assembly in the shape of a hollow right circular cylinder measuring 48.00 inches outside skin diameter by 96.00 inches header to header length and weighs 77.0 pounds. See Table 2.5.2.6-I for component weight breakdown. It has three mounting points which extend approximately 3.25 inches toward the inside to enable attachment to the Isotope Heat Source Assembly (IHSA). The radiator is spaced approximately 2.9 inches above the space-craft mount structure to provide clearance for header connections, etc. See Figure 2.5.2.6-1.

The radiator employs a forced convection heat transfer loop. The organic fluid passes through eighteen vertical tube extrusions which are connected, at each end, through an adaptor fitting, to a common header. Each extrusion serves three purposes: as a passageway for the organic fluid, as the required frontside and backside meteoroid armor protection and as vertical stiffening for the radiator shell. Each header is made from a 0.500 inch outside diameter by 0.062 inch wall tube which is formed to a circular shape. They are protected from meteoroid puncture by a shadow shield which is riveted to the radiator structure.

The 0.025 inch thick radiator skin is spliced together by means of splice plates which are riveted in place. The extruded radiator tubes are seam welded to the skin prior to the sections being spliced together. Nine circumferential channel frames are riveted to the skin for structural support.

After the radiator has been fabricated and inspected, the exterior surfaces are coated with IITRI* Z-93 thermal control coating. Z-93 is an inorganic type coating developed by IITRI which is based on a zinc oxide (ZnO) pigment with a potassium silicate (K₂SiO₄) binder and offers acceptable beginning of life performance related material properties coupled with good reproducibility. However, future work will enable determination of radiation hardness requirements and a different coating may be required for some flight applications.

The radiator also serves as the mounting structure for several other components. The electronic controller and auxiliary cooling tube are both attached to the inside of the radiator support structure and the parasitic load resistor is attached through the skin to the support structure as shown in Figure 2.5.2.6-1.

* IITRI - Illinois Institute of Technology Research Institute; as discussed subsequently in Section 2.5.2.6.6, this may not be the final flight system coating.

TABLE 2.5.2.6-I
RADIATOR WEIGHT BREAKDOWN

<u>Component</u>	<u>Weight (lbs)</u>
Radiator Skin	35.6
Skin Splices (5)	2.3
Frames (9)	10.3
Meteoroid Shields (2)	3.4
Tube Extrusions (18)	14.2
Headers and Interconnecting Fittings	3.5
Emissive Coating	3.3
Mounting Provisions (3)	4.1
Miscellaneous	.3
Total	77.0 lbs (dry)

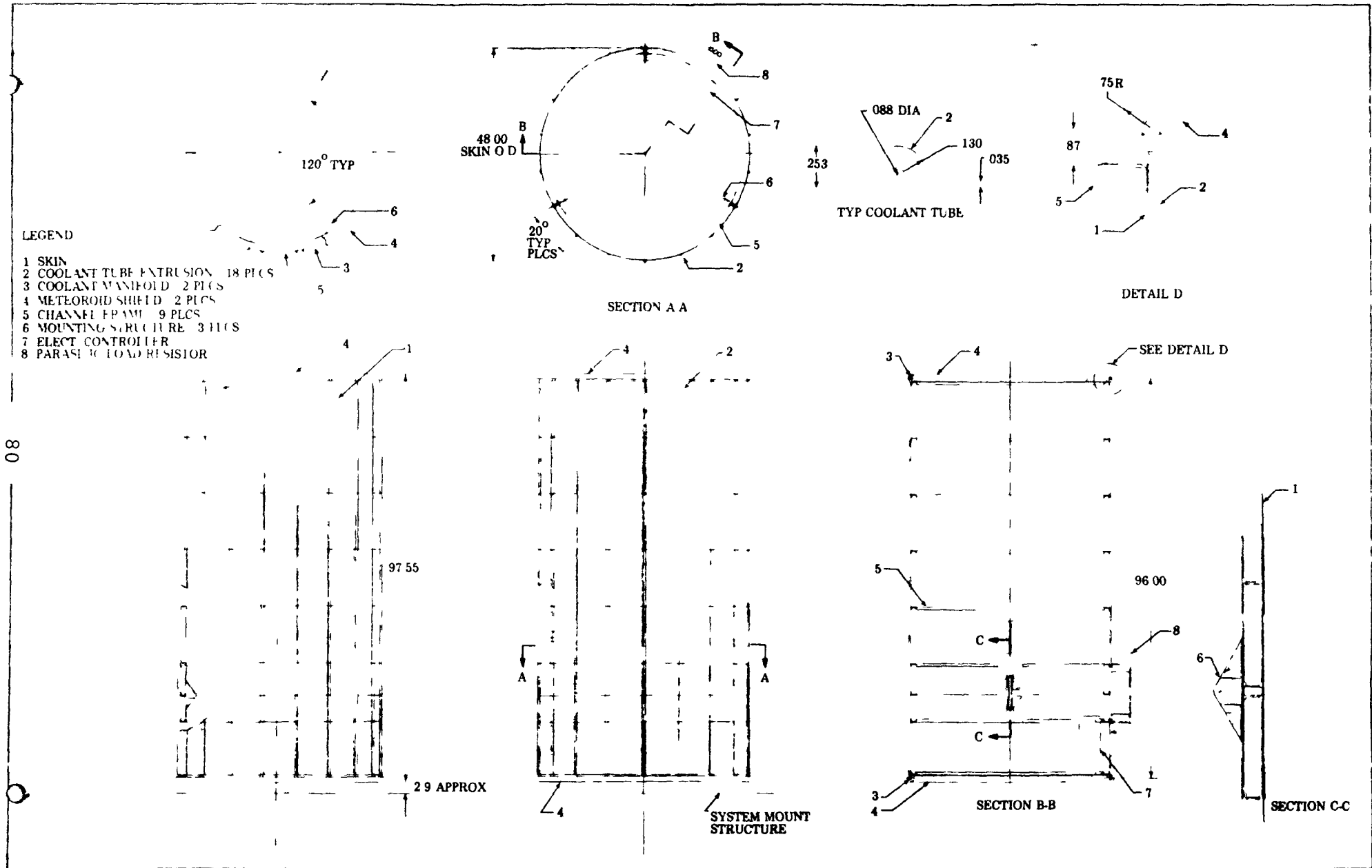


FIGURE 2.5.2.6-1 KIPS RADIATOR

2.5.2.6.2 Tradeoff Studies and Analyses

The updated flight system radiator design differs somewhat from the previous flight system/GDS radiator design. There are two primary factors responsible for the design change; these are revised performance criteria and revised design constraints. The revised criteria are presented in Table 2.5.2.6-II, wherein changes from previous values or constraints are noted. As noted in Table 2.5.2.6-II, the major changes lie in an increase in the waste heat rejection requirement, a decrease (one-half) in the allowable pressure drop and a limit to the allowable radiator length.

Based on the parametric studies performed for the previous flight system (and GDS) radiator design, it was shown that the decreased pressure drop requirement (10 psi) could be accommodated by increasing the number of flow tubes from 16 to 18 together with increasing the flow tube inside diameter from 0.085 inch to 0.088 inch (see Figure 2.5.2.6-2). This was accomplished while maintaining the exit Reynolds number for the tube flow at 3000 or higher.

The change from 16 to 18 tubes results in a higher efficiency radiator design (i. e., fin efficiency). The higher fin efficiency together with the better (measured) coating properties results in an overall radiator design efficiency as good as the GDS design despite its reduced length (8 vs 9.27 ft). However, the increase in the design waste heat rejection rate of approximately 10% over the previous design requires that advantage be taken of the ability of the inside surface of the radiator to reject heat to space through the open end of the cylinder. This effect was ignored in the GDS design for conservatism; the effect was estimated to be equivalent to a 10% increase in radiator area. For the present flight system radiator design this effect is calculated to be more than a 10% increase in effective radiator area so the design heat loads can be readily rejected.

The use of the inside surface of the radiator to reject heat results in greater vulnerability of the flow tube backsides to puncture by meteoroids. In the present design the backsides of the tubes are protected by only 60 mils of aluminum armor against direct strikes through the open end of the cylinder. The tube backsides are protected against micro meteoroids striking the outer surface of the cylinder because of the "bumper effect" of the radiator skin. The most vulnerable portion of the tube backside area to meteoroids streaming through the open end is the tube area near the top of the cylinder. For the portion of the tube area on the lower half of the radiator (nearer the base), the present 60 mils of armor is adequate protection because the "view factor" for direct strikes are small (see Figure 2.5.2.6-3). Therefore, based on the present meteoroid environmental criteria the upper portions of the tubes would require the addition of thin bumpers to insure complete protection if the cylinder end is open. The weight penalty would be minimal for these thin bumpers in any event.

A preliminary investigation was made of a spirally wound radiator which would obviate any tendency for flow maldistribution in the radiator by ensuring that all flow would see both hot and cold sides of the radiator. It was estimated that three parallel tubes would meet the pressure drop and heat transfer requirements with a greatly reduced number of tube joints and an increased fin efficiency with a resultant decrease in radiator size. The spirally wound tube is not as convenient from a structural standpoint compared to the axial tube version and a slight increase in structural weight would be needed. Further studies of this configuration will be performed in Phase II.

TABLE 2.5.2.6-II

FLIGHT SYSTEM RADIATOR DESIGN PERFORMANCE
CRITERIA AND DESIGN CONSTRAINTS

<u>Item</u>	<u>Design Value</u>	<u>Previous Value</u>
Waste Heat Load	20027 Btu/hr	18255 Btu/hr
Dowtherm Flow Rates	Maximum - 0.418 lbs/sec	0.359 lbs/sec
	Nominal - 0.268 lbs/sec	0.249 lbs/sec
	Minimum - 0.107 lbs/sec	0.158 lbs/sec
Assumed Radiator Coating Properties (IITRI Z-93)	Emissivity 0.925* Solar Absorptivity 0.25*	0.90 0.3465
Solar Heat Load	Geosynchronous Orbit Average Solar Load 35.25 Btu/hr-ft ²	Same 48.89 Btu/hr-ft ²
Dowtherm Inlet Temperature	212° F (Nominal)	Same
Desired Overall Pressure Drop	≤ 10 psi (Nominal)	≤ 20 psi (Nominal)
Reynolds Number at Exit of Flow Tubes	≥ 3000	Same
Meteoroid Penetration Criterion (Total Radiator)	P ₍₀₎ = 0.99	Same
Operational Lifetime	7 Years	Same
Radiator Length Limit	8 Feet	None
Acoustic Noise/Spectrum	145 db Overall (See Table 3.5.2.6-III)	Same
Acceleration/Vibration/Shock	(See Table 3.5.2.6-IV)	Same

* Properties measured by TRW (see Section 2.5.1.3)

FIGURE 2.5.2.6-2
EFFECT OF TUBE DIAMETER AND FLOW RATE ON
KIPS RADIATOR PRESSURE DROP

RADIATOR DIAMETER = 4 FT.
 RADIATOR LENGTH = 8 FT.
 NUMBER OF TUBES = 18
 SURFACE EMISSIVITY = 0.925
 SOLAR HEAT LOAD = 35.25 BTU/HR-FT²
 INLET TEMPERATURE = 212 °F
 SKIN THICKNESS = 0.25 IN.

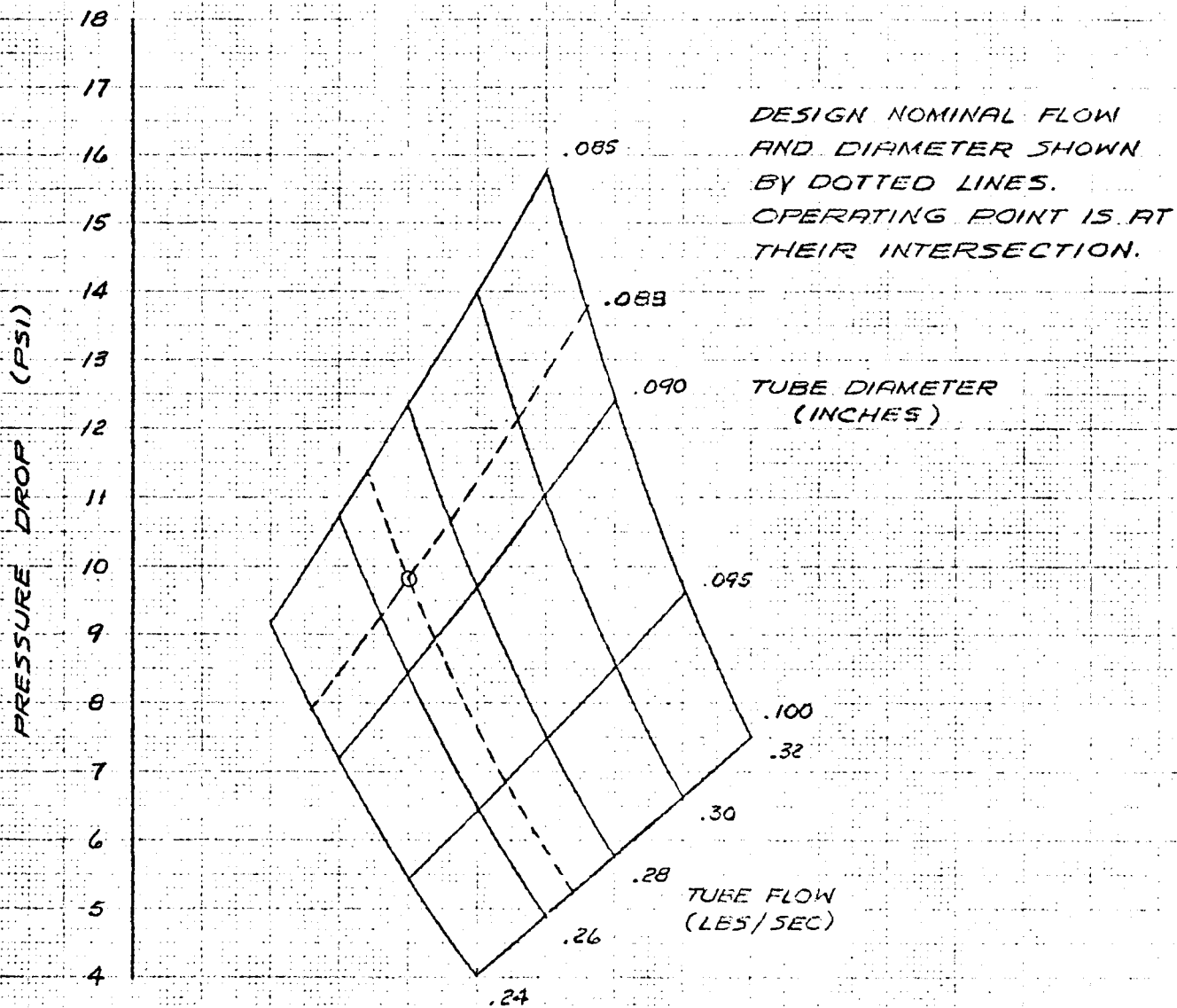
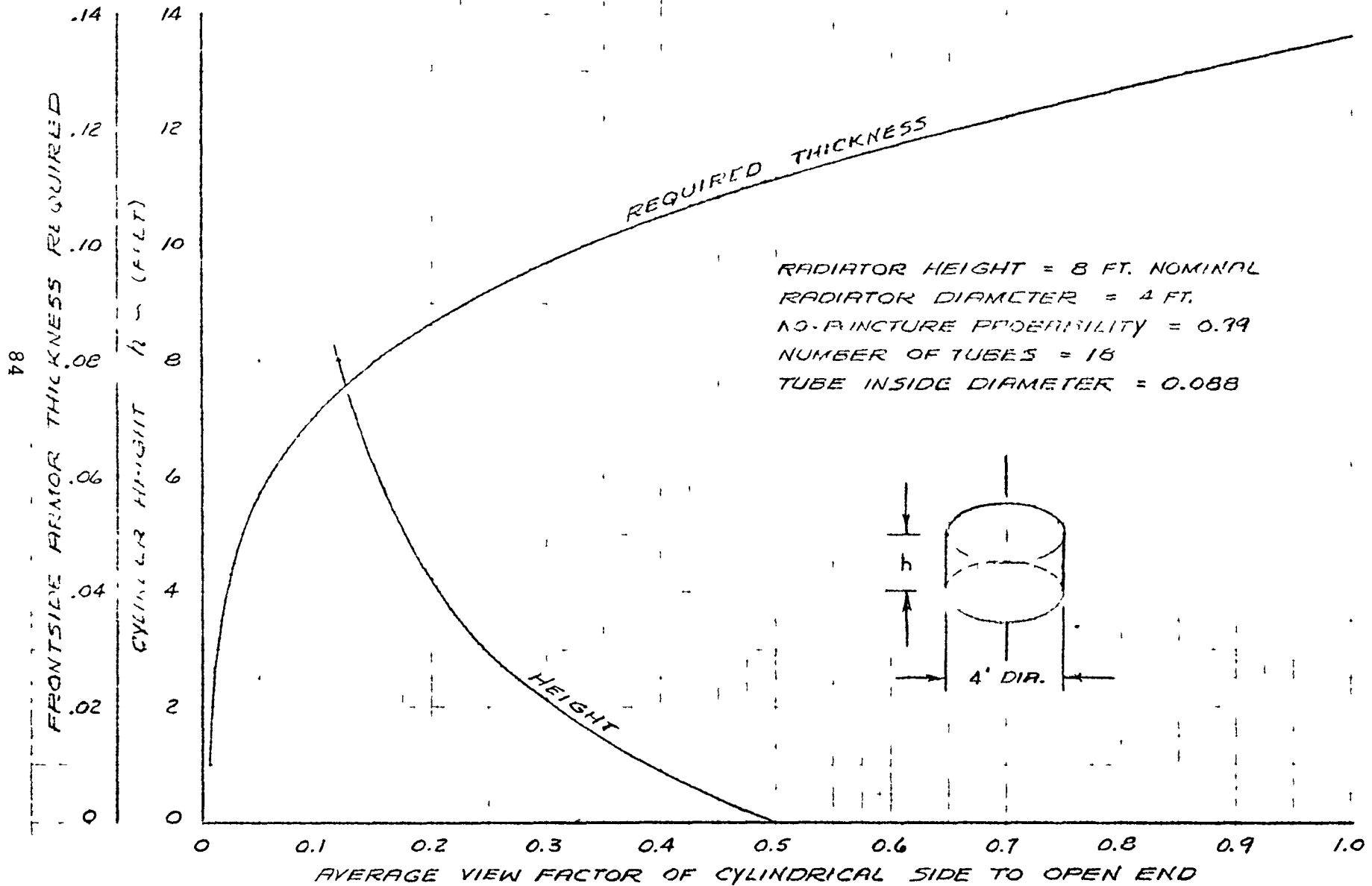


FIGURE 2.5.2.6-3
FLIGHT SYSTEM RADIATOR TUBE ARMOR



84

2.5.2.6.3 Flow Distribution

Because of the possibility that asymmetric solar heating of the radiator skin will cause some flow redistribution in the radiator an analysis was performed to study the potential for Dowtherm A fluid freezing under solar loading. A finite element computer analysis of the complete radiator proved to be prohibitive in cost, so a simplified two-tube model was selected to give a conservative indication of the "worse-case" radiator performance under solar loading. The two tube model (see Figure 2.5.2.6-4) simulated sections of the radiator whose surfaces were respectively normal to and shaded from the solar flux. The flow system model accounted for frictional pressure drop in both the manifolds and tubes, and for the turning pressure drops from the manifold to the tube and vice versa. The heat rejection and pressure/flow characteristics were taken into account by first modeling the thermal/vacuum and in-air pressure/flow GDS component tests in order that the model be as realistic as possible. For conservatism, the model flow pattern was arranged to maximize the flow resistance to the shaded tube such that the flow redistribution would be maximized.

Results of the analysis show freezing to be no danger (see Figure 2.5.2.6-6) except with extreme off-design low flows (lower than anticipated). Also, only moderate flow redistribution occurs (see Figure 2.5.2.6-5) when projected worst case values for emissivity (0.9) and solar absorptance (0.35) of the radiator coating are used. At minimum flow (0.116 lbs/sec for the total radiator), the solar absorptance (α_s) was varied from zero to one while holding the inlet temperature at 205°F and the emissivity at 0.9 to find the sensitivity of the system to changes in the solar load. The minimum fluid temperature, at the outlet of the shaded tube, was 116°F at an α_s of 0.7, well above the fluid freezing temperature of 53.6°F, the flow was divided between the heated and unheated side tubes in the ratio of 58% to 42% respectively.

FIGURE 2.5.2.6-4
TWO-TUBE MODEL SCHEMATIC

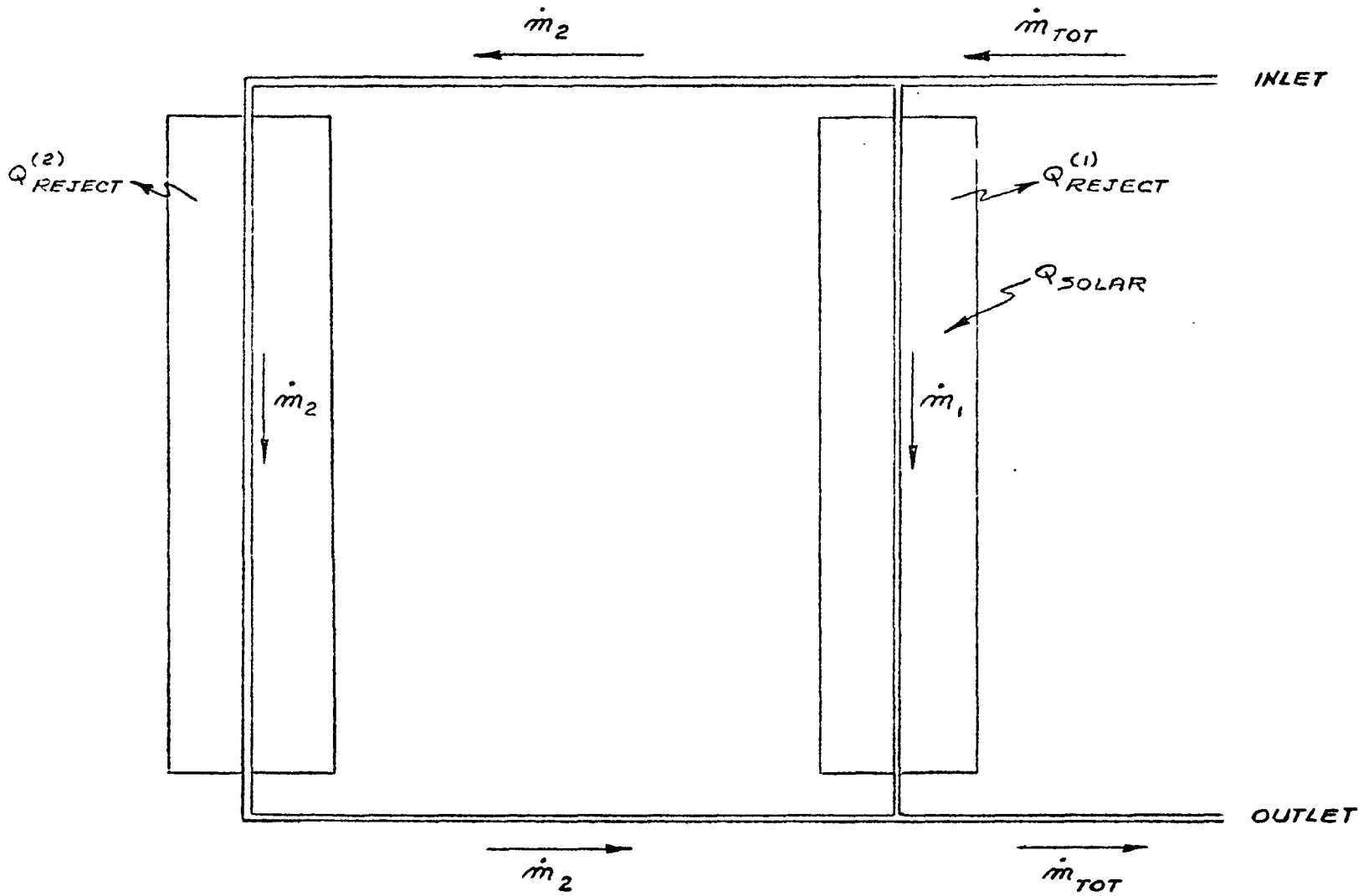


FIGURE 2.5.2.6-5

FLOW PERCENTAGE VERSUS TOTAL FLOW RATE

$$\text{FLOW PERCENTAGE} = \frac{\text{HEATED (UNHEATED) FLOW}}{1/8 \text{ OF TOTAL FLOW}} \times 100$$

$$\epsilon = 0.9$$

$$K_s = 0.35$$

INLET TEMPERATURES
(°F)

○ 205

△ 215

□ 225

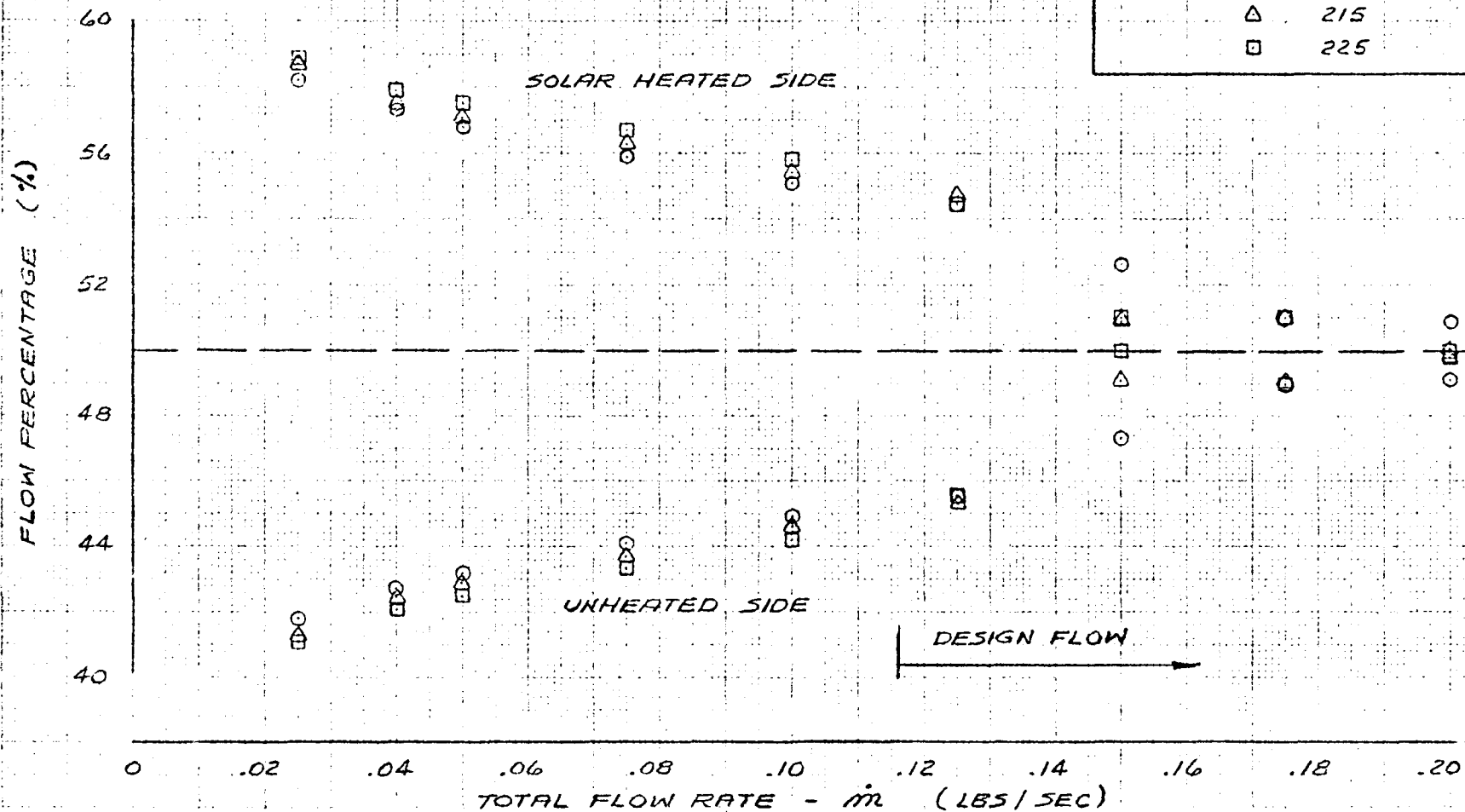
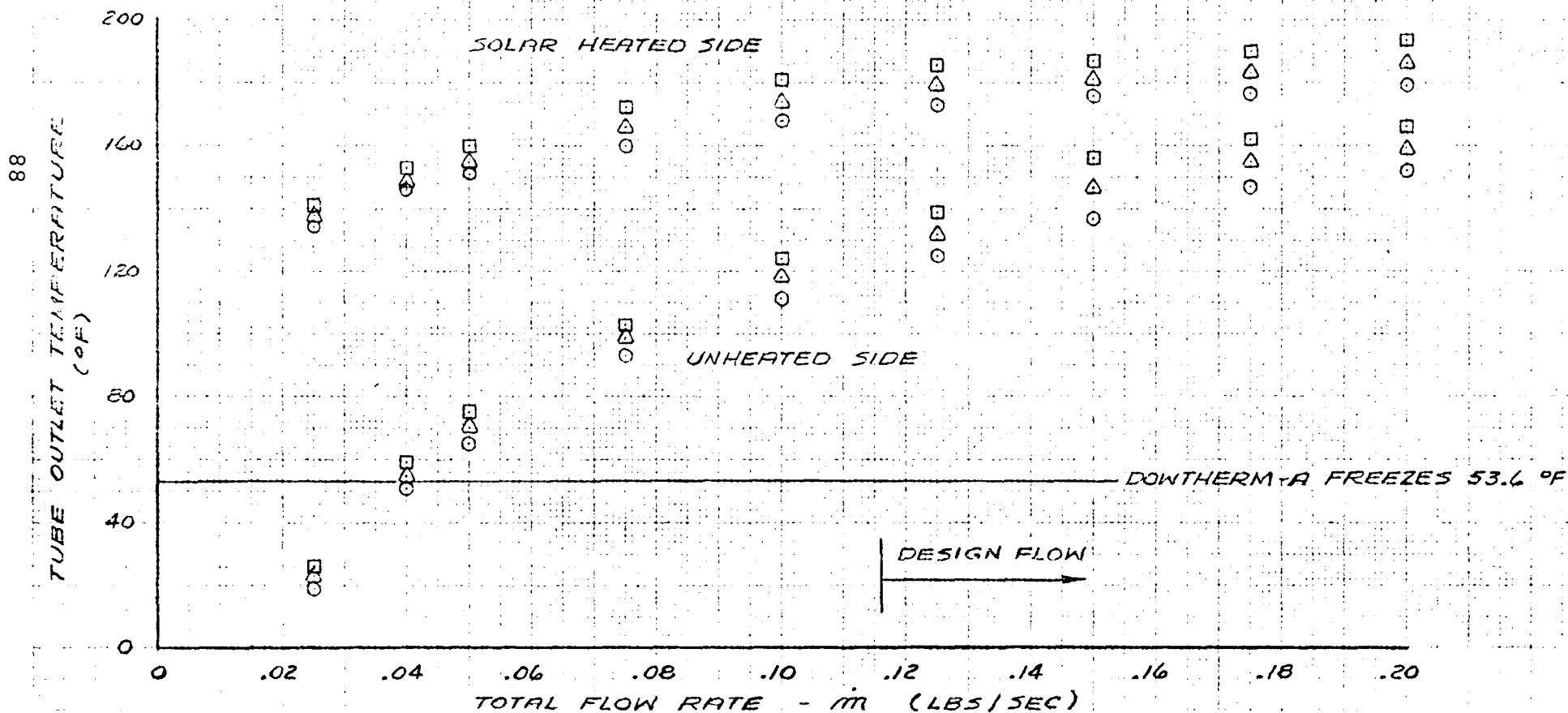


FIGURE 2.5.2.6-6

TUBE OUTLET TEMPERATURE VERSUS TOTAL FLOW RATE

$\epsilon = 0.9$
 $\alpha_s = 0.35$

INLET TEMPERATURES (°F)	
○	205
△	215
□	225



2.5.2.6.4 Structural Analysis

The radiator is a thin-skinned right circular, aluminum cylinder with eighteen (18) longitudinal and nine (9) circumferential stiffeners (see Figure 2.5.2.6-1). The longitudinal stiffeners are 6063-T5 aluminum coolant tube extrusions which are seam welded to the outside of the .025 inch 6061 T-6 aluminum (skin) panels. Four individual panels are spliced and riveted together to form the cylinder. Eight of the nine circumferential stiffeners are aluminum, .032 inch thick open channel sections which are riveted to the inside of the radiator skin. The ninth circumferential stiffener is a heavier .063 inch thick closed box frame positioned opposite the three support points located at the top of each heat source assembly housing. This frame is located at the center of the second panel bay (from the bottom). The three radiator mount points are 120° apart and attach the radiator to the heat source assembly housing at the box frame which is located 24.7 inches above the spacecraft baseline. The analysis involved an evaluation of: (1) the loads on the radiator at the support points (considered the most critical area; (2) the potential for buckling of the thin skin panels between the stiffeners; (3) the acoustical loading on the panels; (4) and the potential for shearing of the rivets (not covered herein but found not to be a problem). The expected load environment is the same that was used for the GDS design and is presented in Tables 3.5.2.6-III and IV.

Based on dynamic analysis supplied by Sundstrand (see Ref. 14) the maximum loads on the radiator are at the three support points and these are as follows: 13.9 g's radial; 19.6 g's tangential; and 13.5 g's axial. The indicated directions are shown in Figure 2.5.2.6-7A. These loads were derived by analysis of Sundstrand's estimates of the response of the radiator mounts to a shock input at the system mounts. The calculated response was based on a 775 g design shock input and assumed the entire power system is shock mounted and tuned to $f_n = 12.5$ Hz.

Analyses of the radiator structure shows that the most critical portion of the structure is the circumferential ring frame to which the supports attach. The required section for this frame is determined by the load resulting from the calculated 13.9 g acceleration in the radial direction. Note that, in the sketch of Figure 2.5.2.6-7B, the ring is supported at three points and loaded as shown thereon. The greatest stress occurs at point A (Figure 2.5.2.6-7B) as a result of a bending moment given by:

$$M_A = \frac{2 w R^2}{3} \left[\alpha - 2\beta - \frac{\pi}{4} + 2\pi \sin\Theta \right]$$

where

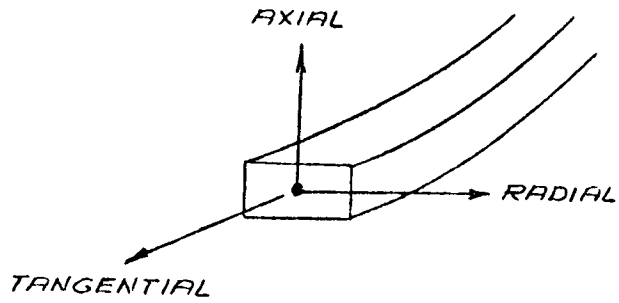
$$\alpha = -.0638$$

$$\beta = 1/4$$

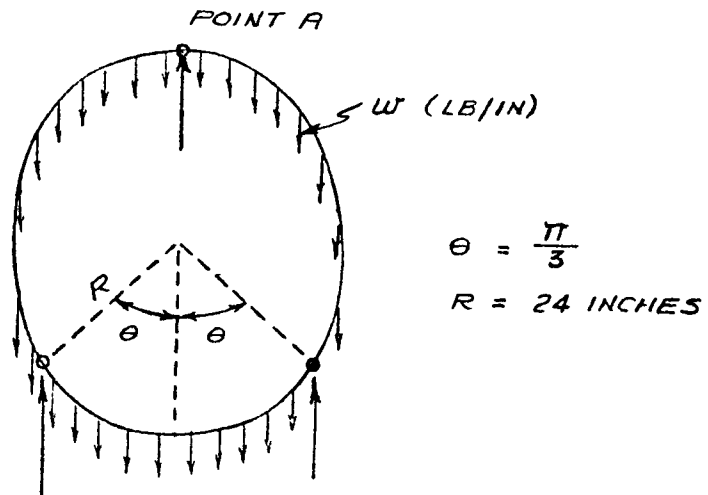
The ring frame section is presented in Figure 2.5.2.6-7C and its cross sectional moment of inertia about line 0-0 is, $I_{0-0} = .0417$. Conservatively assuming a 90 pound weight radiator, the loading per inch on the ring frame is:

FIGURE 2.5.2.6-7

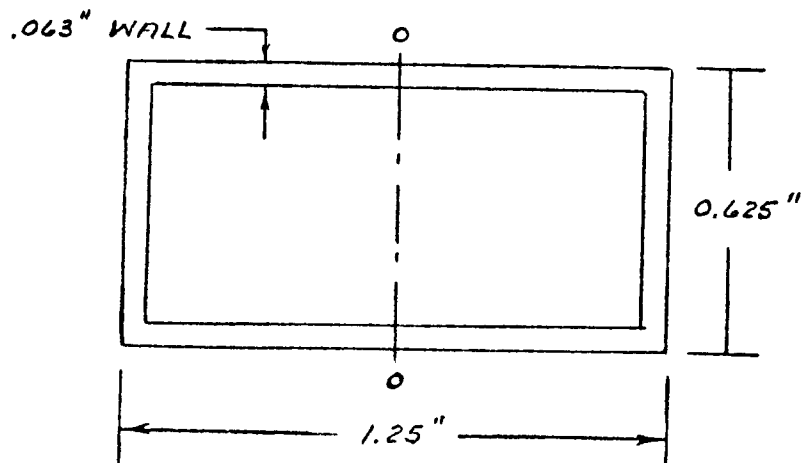
a.



b.



C. SUPPORT RING FRAME SECTION



$$w = \frac{90 \times 13.9}{2 (24)} = 8.296 \text{ lbs/inch.}$$

Therefore the maximum bending stress at point A is $\sigma_A = 28757$ psi. For 6061-T6 aluminum therefore, the margin of safety is calculated to be a minimum of

$$\text{M.S.} = \frac{36000}{28757} - 1 = 0.252$$

The other potentially critical stress is the critical buckling stress of the thin-skin radiator panels due to the calculated axial acceleration of 13.5 g's. The stiffeners break the radiator shell into eight panel sections longitudinally and 18 sections circumferentially. Thus, each panel is 12 inches by 8.38 inches having a radius of curvature of 24 inches. The worst case panels are these panels just above the three supports. Each of these panels has to support the weight of the sections of the radiator above it. Assuming all edges as simply supported, the critical stress is given by:

$$\text{Maximum stress} = S^1 = \frac{1}{6} \frac{E}{1 - \nu^2} \left[\left(\sqrt{12 (1 - \nu^2) \left(\frac{t}{R} \right)^2 + \left(\frac{6t}{R} \right)^4} \right) + \left(\frac{6t}{R} \right)^2 \right]$$

$$S^1 = 6249 \text{ psi}$$

where:

$$R = 24 \text{ inches}$$

$$E = 9.8 \times 10^6 \text{ psi}$$

$$\nu = 0.3$$

$$t = 0.025 \text{ inch}$$

The corresponding critical load is thus:

$$P = S^1 t b = S^1 t \frac{\pi}{6} R = (6249) (.025) \frac{\pi}{6} (24) = 1963 \text{ lbs}$$

The actual load on this panel is $3.75 \times 13.5 \text{ g} = 50.6 \text{ lbs}$ with a resulting margin of safety of $\frac{1963}{50.6} - 1 = 37.8$. Thus the panel thickness is determined primarily by thermal weight considerations and secondarily by the acoustical loading rather than by the acceleration forces.

The corresponding critical load is thus:

$$P = S^1 t b = S^1 t \frac{\pi}{6} R = (6249) (.025) \frac{\pi}{6} (24) = 1963 \text{ lbs}$$

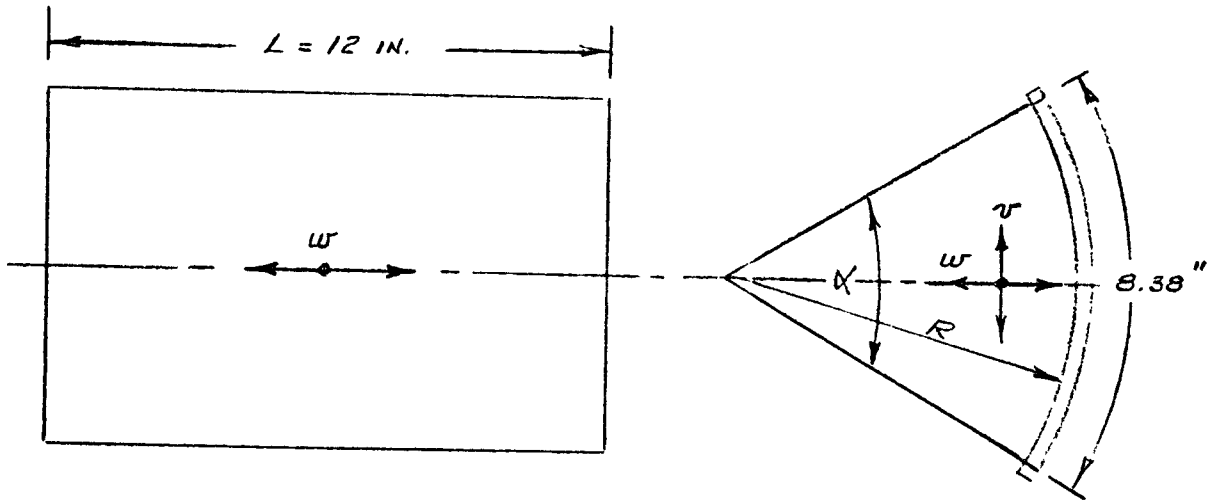
The actual load on this panel is $3.75 \times 13.5 \text{ g} = 50.6 \text{ lbs}$ with a resulting margin of safety of $1963/50.6 - 1 = 37.8$. Thus the panel thickness is determined primarily by thermal/weight considerations and secondarily by the acoustical loading rather than by the acceleration forces.

To evaluate the stress on the curved panel resulting from pressure due to exposure to the anticipated acoustic spectrum, the panel is assumed simply supported on all edges and the first mode natural frequency is evaluated using the modified Rayleigh-Ritz method. Referring to Figure 2.5.2.6-8, the total strain energy resulting from the combined directional displacements of the panel is equated to the maximum kinetic energy of the panel to determine the first mode angular first mode angular frequency. Ref. 15 presents the derivation of the two equations. The resulting solution for the first mode angular frequency for the flight system panel dimensions (12" long by 8.38") is 4325, thus the first mode frequency is $f_0 = P/2\pi = 4325/2\pi = 688 \text{ Hz}$. Thus, using Franken's method the resulting pressure on the curved panel is $q_{\text{acoustic}} = 0.20 \text{ psi}$. The critical pressure on the curved panel is given by:

$$P_{\text{crit}} = 0.93 E \left(\frac{t}{L} \right)^{3/2} \left(\frac{t}{L} \right) = 0.651 \text{ psi}$$

and therefore the ratio of actual to critical pressures is 0.307.

FIGURE 2.5.2.6-8.
RADIATOR FINEL SECTION



2.5.2.6.5 Fabrication and Inspection

The flight system radiator will be inspected to verify that fabrication processes and techniques are within specifications. All welds in fluid flow areas will be subjected to the non destructive testing technique developed during the GDS fabrication (see Section 3.5.2.6.4). A comprehensive program for establishing weld quality criteria consistent with overall design philosophy, will be developed and applied to these weld joints. Fluid flow tube openings will be inspected to assure they have not been violated as a result of fabrication processes.

2.5.2.6.6

Critical Characteristics

Two radiator design characteristics are possibly critical with regard to satisfying overall system performance objectives. These are flow tube inside diameter and radiator coating properties. The required flow tube diameter is relatively small (.088 inch) and this requires that the extruded tube dimensions be held to very close tolerances if the design radiator pressure drop is to be achieved. The pressure drop through the radiator tubes is proportional to the inside diameter of the tube to the fifth power (i. e., d_i^5) and therefore is very sensitive to manufacturing tolerances. For example, a reduction of 1 mil on the tube diameter will increase the pressure drop by 6%, and 2 mils by approximately 12%. Two factors, however, tend to mitigate this sensitivity in the present design. First, based on our experience in fabricating the GDS radiator and several test panels (which utilized slightly smaller diameter (.085 inch ID tubes) the tube extrusion fabricator (Minalex Corporation, White House Station, New Jersey), was able to hold the tube ID dimensions to very close tolerances. The specification to the vendor was a hole diameter of $0.085 \pm .002$ and based on a number of samples of a 700 ft run, most of the tubing sampled was right on the nominal dimension with none outside the tolerance range. The holding of these dimensions depends primarily on the wear of the extrusion tooling which could be monitored for large tubing runs. Second, because the vendor has confidence that he can hold rather close tolerances, the nominal dimensions can be set to insure that the pressure drop criteria will be met. Note that a lower pressure drop will not significantly affect the radiator performance.

The second area of concern are the radiator coating properties at the end-of-mission (EOM). A number of coating systems are capable of providing the desired beginning of mission properties, but insufficient data exist to predict EOM (7 years) properties for most coatings. The selected coating for the KIPS program must resist not only the potential degradation mechanisms of ultraviolet exposure and space particle impacts, but also must satisfy the additional criteria that it be a nuclear hardened coating. The IITRI Z-93 coating used for the GDS radiator, and assumed presently for the flight system radiator is expected to be as resistant to U.V. degradation as any coating which might be selected but it is not a "radiation hardened" coating. Data for the so called "hardened coatings" are classified, and therefore if the "hardening" requirement remains as a criteria for KIPS missions, these coatings will have to be evaluated in Phase II for possible application.

The effects of loss of radiator coating on system performance due to nuclear radiation were investigated. Two basic cases were investigated, both using the Z-93 radiator emissivity coating. One case considered the loss of coating exposing bare aluminum with an emissivity of 0.25 and absorptivity of 0.53. The other investigated the use of hard coated anodize under the Z-93. The anodized surface would be exposed after irradiation and would have an emissivity of 0.845 and absorptivity of 0.923.

The effects on system output are dramatic. The exposure of bare aluminum over half the radiator to direct sunlight would result in radiator outlet temperatures so high that the system would deliver very low electrical output and may even shut down. The use of an anodized surface under the same conditions gives a significant improvement due to the higher emissivity and as much as 900 watts output would be available.

If a nuclear hardened coating were used, even higher output would be expected.

One additional result of the loss of coating would be an increase in temperature maldistribution from coated to uncoated sides. From this standpoint, a spirally wound tube would be superior since all fluid would see both hot and cold radiating surfaces.

2.5.2.6.7 Reliability

The radiator is described in Section 2.5.2.6.1; Table 2.5.2.6-III presents the radiator FMECA worksheet.

The FMECA indicates that the most probable failure mode is a fluid leak caused by defective material or weld. The second most likely is a clogged cooling tube caused by internal corrosion or other loose foreign matter. Emphasis on detail design, manufacturing procedures and quality control are critical factors in achieving reliability goals.

Failures which result in loss of working fluid flow would allow the heat source to overheat if backup provisions were not incorporated. In space the emergency cooling system (ECS) will melt down to control the heat source temperature. On the ground and in the space shuttle bay, the heater temperature control module will provide emergency cooling flow to control the heat source temperature in event of loss of the normal system flow.

TABLE 2.5, 2.6-III

FAILURE MODE AND EFFECTS ANALYSIS

NO.	COMPONENT & FUNCTION	FAILURE MODES (FM)	POSSIBLE FAILURE CAUSES	FAILURE EFFECT (FE)	DESIGN SAFETY CONSIDERATIONS	③ CRITICALITY RANK ① x ② = ③ ② FE RANK ① FM LIKELIHOOD		
						①	②	③
1.0	<u>Radiator</u> Provides for waste heat rejection onto space from circulated fluids							
1.1	<u>Structural Parts</u> Skin, splice plates, fittings, channel frames, angle frames, and meteoroid shield, rivets, welds	Structural failure	Handling damage, launch or transport dynamic forces	Twisted/distorted radiator resulting in a coolant system leak	All basic structural type static components having no moving or operating parts. Experience data and Q. C. controllable	5	100	500
1.2	<u>Emissive Coating</u> Improve heat rejection characteristics (high emissivity and low solar absorptivity)	Loss of coating	Dynamic Environments - shock, vibration Vacuum vaporization	Significant reduction in radiation heat rejection	Dynamic and vacuum tests	5	50	250
		Chipping	Thermal cycling Bending and torsion loading during handling Improper coating application Environments - humidity, salt air, ultra violet light	Partial reduction in radiator heat rejection	Surface may be cleansed and refinished	10	50	500
		Cracking	Same as chipping	Minor effect on heat rejection		5	50	250
		Degradation	Solar absorptivity	Significant reduction in radiation heat rejection		10	50	500
1.3	<u>Cooling Lines, Coolant Manifolds and Connecting Tubes</u> 90 welds - maximum length = approximately 1.5" Approximately 150 ft of 0.065 I. D. tubing Approximately 25 ft of 0.50 I. D. tubing	Rupture in tube wall or weld leak failure	Fatigue, material defect, defective weld Meteoroid Penetration	Leakage resulting in loss of cooling fluid. System overheats and over temperature shutdown (aluminum foil melts) Potential fire hazard in ground operation	Vacuum leak checked Radiograph inspection of welds .063/ .065 wall al alloy tubing .063 al alloy meteoroid shields for tube header protection Dowtherm A has narrow flame-ability limits - low explosion probability	50	100	300
		Clogged or partially clogged line	Corrosion of tubing intersurface, spalling upstream, meteoroid dent	Lose part of cooling surface	Filters down-stream	50	50	2,500

Table 2.5.2.6-~~IV~~ and Figure 2.5.2.6-9 presents the radiator leak single point failure locations.

TABLE 2.5.2.6-IV
RADIATOR LEAK SINGLE POINT FAILURES

Code		<u>Quantity</u>
H _M	Header manifold tube material	2
HF _W	Header/fitting weld	36
FT _W	Fitting/extruded tube weld	36
T _W	Extruded tube material	18
HS _W	Header/splice fitting weld	18
	Total	<u>110</u>

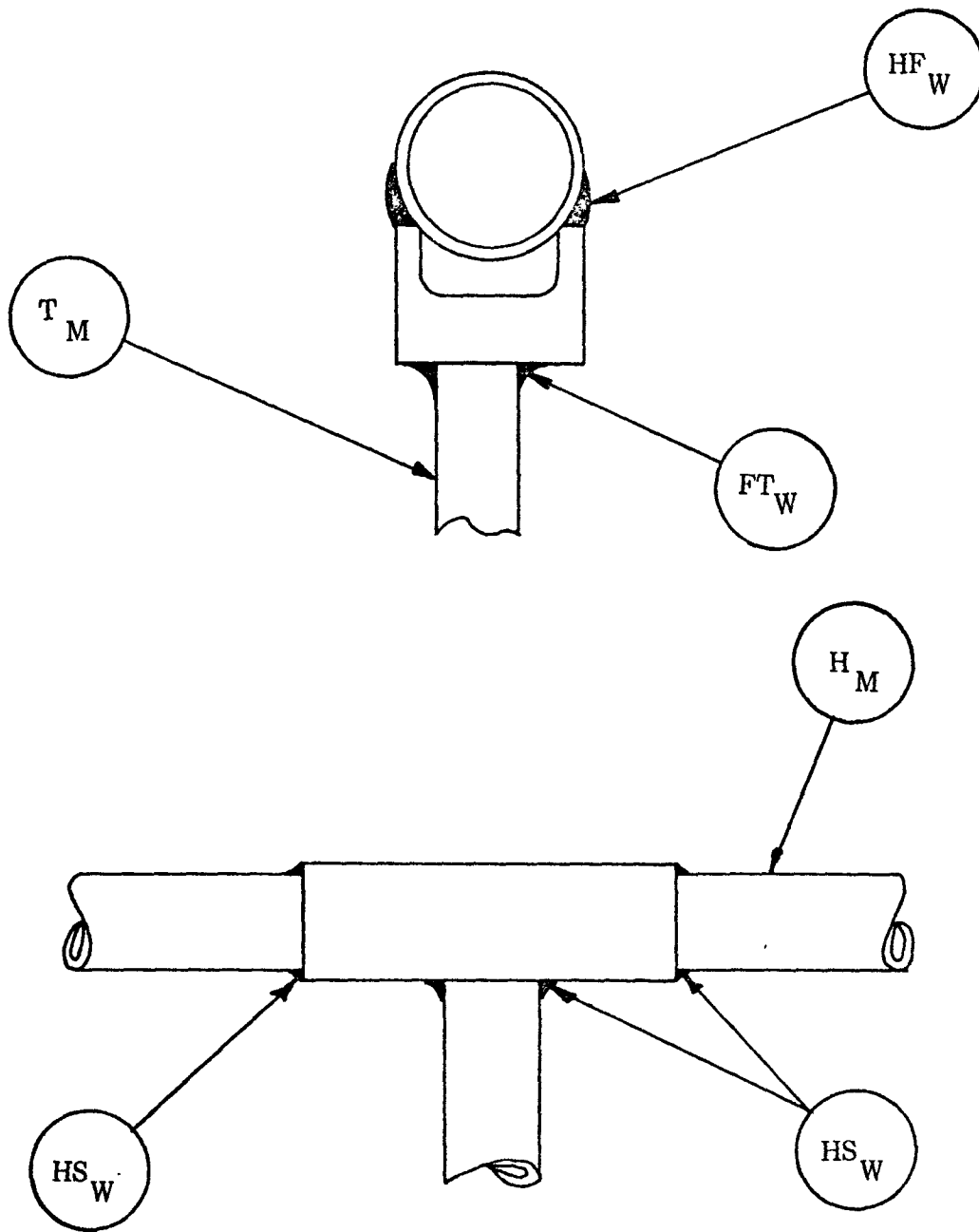


FIGURE 2.5.2.6-9
 RADIATOR LEAK SINGLE POINT FAILURE
 LOCATIONS

2.5.2.8 Thermal Insulation Stability

2.5.2.8.1 Foil Insulation

The multilayer vacuum foil system which serves the dual purpose of limiting the parasitic heat losses during normal operation and acting as an emergency cooling system in the event of a LOCA has been described in considerable detail in Sections 3.5.1.2 and 2.5.1.4. The foil insulation system is a very simple system consisting of a continuous spiral wrap of one (1) mil pure aluminum foil around an open-ended cylindrical aluminum can. The foils are separated from one another by a spray coating of micron-size zirconia particles, a process patented by the foil system vendor, the ThermoElectron Company of Waltham, Massachusetts. The foil system is confined between the outer boiler wall and the inner wall of the aluminum housing, and the can is supported top and bottom by Min-K insulation. Because the foil system is trapped in this location, its potential movement and change in configuration is limited to minor changes in the local density (or number of foil layers per inch of thickness). While these minor changes can affect the parasitic losses somewhat, the effect is expected to be minor because the total number of layers will not change and therefore, the important radiation thermal resistance will not be appreciably affected. That is, while the conduction component of the heat transfer can be changed by altering the density of the foil system, the conduction component is expected to be very small in a zero-g environment when the foil system is properly installed initially. Even more important, however, is the insensitivity of the emergency heat dump capabilities of the HSA to potential minor variations in the foil system configuration. This results from the fact that the selected foil material (1100 series aluminum) melts at a temperature considerably below the operational temperature of the heat source. Thus, in the event of an emergency (LOCA) the heat source temperature merely rises at varying rates (depending on the foil system meltdown time) to its final steady state temperature and does not have an excursion above this final temperature. The time that the foil system takes to melt down is dependent on its assembled condition, but as discussed above the emergency protection feature is insensitive to this condition.

Although materials other than aluminum were considered for the foil system, it was selected because other candidate pure foil materials melt at higher temperatures than the heat source operational temperature and therefore potentially dangerous heat source temperature excursions would be experienced during a meltdown situation.

Other aluminum alloys, however, were also considered and some of these are considered to be viable alternatives to the more pure 1100 series aluminum foil. These alternative materials include 3003, some of the 2000 series (2219, 2011, 2014, 2017), 6063, and possibly 6061, but tests should be conducted for compatibility with other heat source materials. The major reason for considering other aluminum alloys is to improve the handling characteristics of the foil system prior to and during installation.

The foil system is purchased from the vendor, ThermoElectron Corporation, by a specification which delineates the cleaning, handling and quality assurance procedures to be applied in the fabrication of the foil system. Quality checks include a verification of the zirconia coating density and uniformity by scanning electron microscope (SEM) analysis and weight measurements.

2.5.2.8.2' Fibrous Insulation

The fibrous insulation Min-K TE-1400 (Johns Manville) is used to support the heat source assembly at its ends and simultaneously limit heat losses to a minimum value. The location and description of this insulation is presented in Section 2.5.1.2. The load bearing capability of Min-K TE-1400 is utilized to apply a preload to the heat source assembly. This preload, plus the interlocking shape of the insulation discs, serves to positively locate the heat source during the launch vibration environment as well as steady state space operation. No preload force is required once the system stabilizes in orbit, however.

A number of insulating materials were considered for the end discs. Load bearing capability, low thermal conductivity, and suitability for long-term use in a vacuum were the principal criteria used in selecting the Min-K TE-1400. Table 2.5.2.12-I presents certain physical properties of and the results of thermal conductivity testing of candidate materials. This data was obtained from ASTM-C177 guarded hot plate tests performed by Dynatech R/D Company under contract to Teledyne Energy Systems for the Selenide Isotope Generator (SIG) program.

Preliminary tests of the load bearing capability of Min-K TE-1400 insulation have been completed by TES for the SIG program. Insulation specimens were tested with a 1472°F hot face and 300°F cold face and an initial compressive stress of 150 psi. The load retention was continuously monitored. These preliminary test results indicate that after about 10,000 hours the load capability of the insulation is approximately 40 to 45% of the initial value.

Choice of Min-K TE-1400 was based on several factors. First, among load bearing fibrous type insulations the Min-K insulations possess the lowest thermal conductivity properties. Second, the temperature capability is within the range of anticipated hot side temperatures. Third, the reported load bearing capability was adequate to provide heat source support loads. In addition, the Min-K TE series of insulations were developed especially for use in thermoelectric generators, where low outgassing and low levels of impurities are desirable.

Slabs of Min-K are purchased from the manufacturer, Johns Manville Corporation. These slabs are then machined to the required shapes. Vacuum bake-out of the insulation at or near normal operating temperature assures removal of all moisture and volatile impurities present in the insulation. At assembly, spaces, joints and instrumentation wire routing grooves in the Min-K are stuffed with a high temperature micro quartz insulation wherever practical. Material certification from Johns Manville assure slab quality.

TABLE 2.5.2.8--I

CANDIDATE FIBROUS INSULATIONS

Material Properties	Min-K TE-1400	Min-K TE-1800	Min-K 2000	Microtherm 20 CR	Cotronics 360 HS	CBCF-3	CBCF-4
Thermal Conductivity $\frac{\text{Btu-ft}}{\text{ft}^2\text{-hr-}^\circ\text{F}}$.0090	.0081	.0099	.0072	.0220	.0578	.0110
392°F (< 10 ⁻⁴ torr)							
842°F (< 10 ⁻⁴ torr)	.0118	.0116	.0144	.0144	.0300	.0664	.0176
1202°F (< 10 ⁻⁴ torr)	.0153	.0156	.0217	.0240	.0410	.0751	.0254
1652°F (< 10 ⁻⁴ torr) (1560°F)*	.0202*	.0202	.0355*	.0445	.0774	.0896*	.0364*
Density lbs/cubic ft	20	20	20	20	20	14	
Continuous Service Temperature (°F)	1400	1800	2000	1832	2300		
Compressive Strength (psi)							
5% Compression	75	Non Load	80	50			
8% Compression	145	Bearing	170				Non Load Bearing
Limit	150				350	150	
Average Transverse Strength (psi)	65	50	55				
Modulus of Rupture (psi)	80	68		16-20	55		
Modulus of Elasticity (psi)	2300			1150			

3.0 - GROUND DEMONSTRATION SYSTEM

3.5.1 Heat Generation System

3.5.1.2 Summary

The Electrical Heat Source Assembly (EHSA) is a circular, stepped cylinder which measures 12.70 inches diameter at the mounting end (13.60 inches diameter at the three mounting lugs), 10.22 inches diameter at the midpoint, 12.02 inches diameter at the upper end, 28.84 inches overall length from boiler tube inlet to outlet fitting and weighs 80 pounds. See Figures 3.5.1.2-1A and B. There are three EHSA's in the Ground Demonstration System (GDS) each supplying 2400 W(t) input to the GDS system for conversion to output power.

Each EHSA is attached to the GDS baseplate by means of a triangular shaped, three legged support structure. Electrical power input and instrumentation receptacles, as well as the inlet connections to the boiler assembly, are located in the mounting (lower) end of the unit. The outlet connections to the boiler assembly are located in the upper end of the unit. The EHSA is designed to permit end loading/unloading of the electrical heat source without having to disturb either of the boiler assembly tube connections. The unit also has the capability of being suspended from its upper end by using a special fitting which threads into the center of the upper cover.

Each of the EHSA's in the GDS is identical except for the boiler centerbodies and the location of instrumentation on each boiler assembly. The major components of an EHSA are the housing, upper and lower end covers, penetration fitting assemblies, fibrous insulation, multifoil insulation system, radiation barrier, electrical heat source and the boiler assembly. See Table 3.5.1.2-1 for a listing of individual components, materials and weights.

Housing

The housing is machined from a hollow tube, 6061-T6 aluminum alloy forging which initially measures 14.00 inches outside diameter by 2.50 inches wall thickness by 2.50 inches wall thickness by 23.00 inches long. See Figure 3.5.1.2-2 for final machined configuration and dimensions. Based upon structural analysis aluminum was chosen for the housing material because of its strength to weight characteristics. Price per forging and availability were other selection factors. Because the physical properties of such a large billet of material are not covered in existing commercial specifications, room temperature tests were performed in accordance with ASTM E8-69 on test rings, in each of three directions, to document ultimate and yield strengths as well as elongation characteristics of the basic forged material. These properties were then substituted for the properties used in the structural analysis to determine wall thicknesses at various points in the housing.

In each end of the housing there is an Acme thread which allows each end cover to be attached by using a specially machined lock ring. After machining and cleaning operations, a glass bead finish is applied to all exterior surfaces to remove machine tool marks and to improve surface appearance. The housing weight is 10.13 pounds.

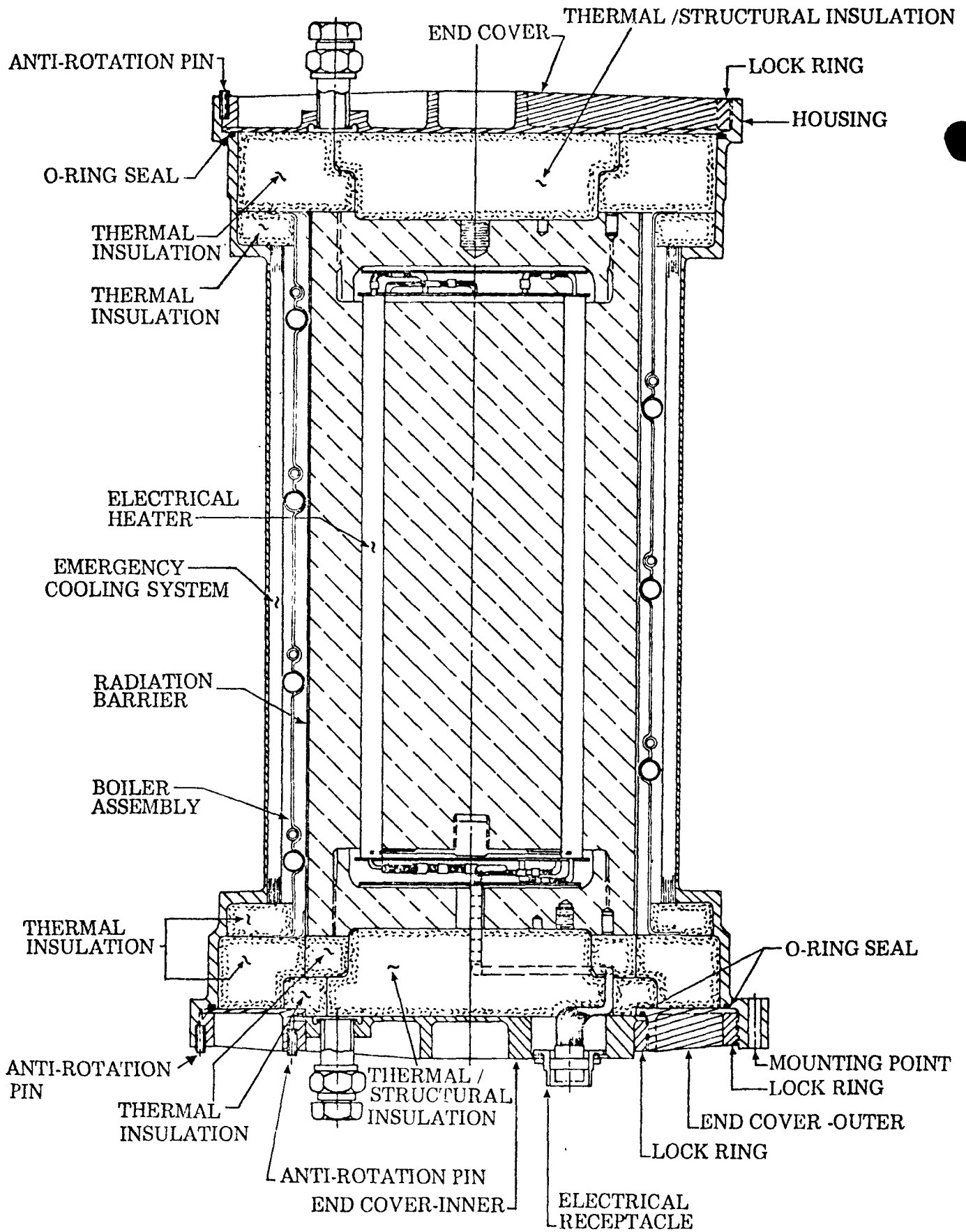


FIGURE 3.5.1.2-1A
 ELECTRICAL HEAT SOURCE ASSEMBLY

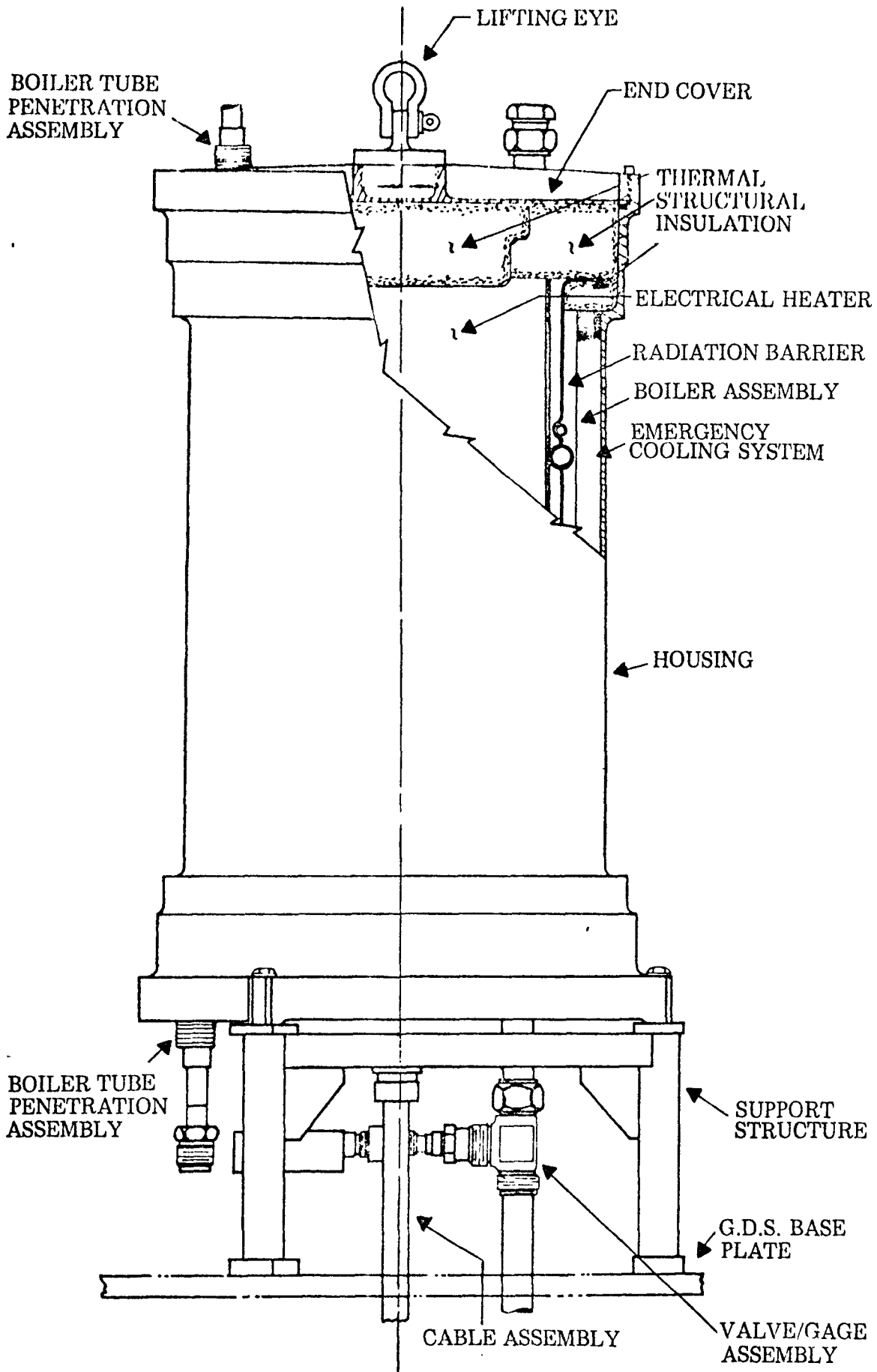


FIGURE 3.5.1.2-1B
 ELECTRICAL HEAT SOURCE
 INSTALLATION

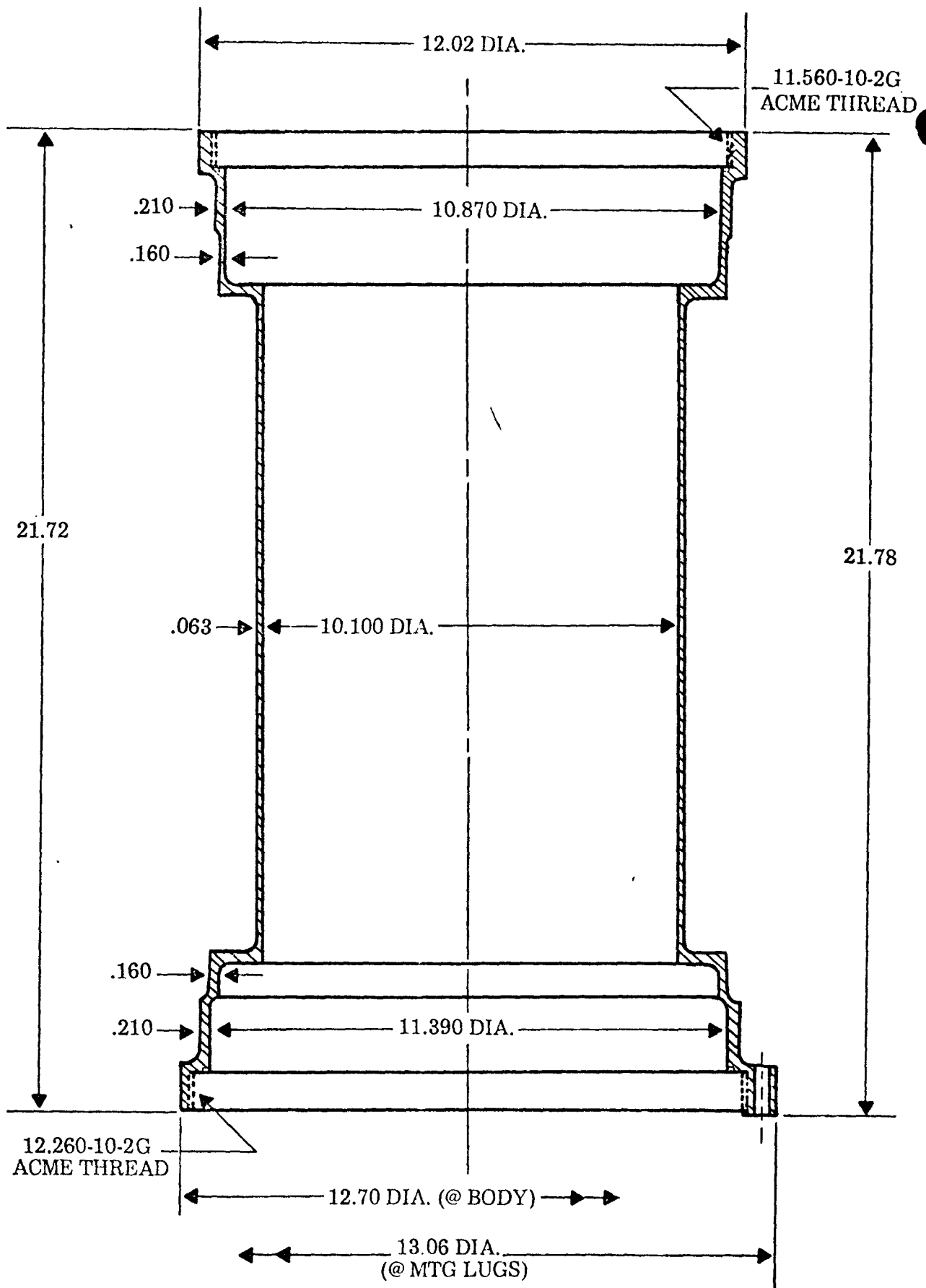


FIGURE 3.5.1.2-2
 E.H.S.A. HOUSING
 (AL ALY TYPE 6061-T6)

End Covers

Each of the end covers is machined from a disc of 6061-T6 aluminum alloy plate. Based upon structural analysis, aluminum was chosen for the cover material because of its strength to weight characteristics. Each end cover is circular shaped, with a flat, smooth underside to assist in the sealing and insulation preload process and has tapered ribs for added stiffness, machined as an integral part of the outside surface.

A single piece cover closes the upper end of the EHSA and contains the outlet connection fittings for the boiler assembly. The lower end of the EHSA is closed with an inner and outer cover which are locked together, by means of a specially machined lock ring, to form one integral assembly. The outer portion of the lower cover contains the inlet connections for the boiler assembly; the inner portion of the cover contains the electrical power input and instrumentation receptacles. The lower inner cover can be separated from the lower outer cover without having to remove the outer cover from the housing, thereby exposing a cavity of sufficient diameter to permit the electrical heat source to be installed/removed. The upper cover weight is 2.11 pounds, the lower inner cover weight is 1.41 pounds and the lower outer cover weight is 1.53 pounds. After machining and cleaning operations, a glass bead finish is applied to all exterior surfaces to remove machine tool marks and to improve surface appearance.

Boiler Tube Penetration Assemblies

The penetration assembly fittings have two functions: to minimize the heat losses from the boiler assembly tubes to the end covers (where the tubes penetrate the covers) and to form a vacuum tight closure between these tubes and the end cover. The penetration assembly consists of a type 321 stainless steel formed bellows welded to a type 304 stainless steel flange. Stainless steel was selected because of its compatibility with the type 304 stainless steel boiler assembly tube material and for its relatively low thermal conductivity properties. There are four penetration assemblies in each EHSA, two for the primary boiler tubes and two for the auxiliary boiler tubes. See Figure 3.5.1.2-3. The weight of the four penetration assemblies are 0.56 lb.

The lower end of the bellows is pre welded to the flange and is sized to allow the boiler tube to pass through the bellows at assembly with approximately 0.06 inch radial clearance. The upper end of the bellows contains a reducing collar which is sized so the boiler tube can be easily welded to the collar. This weld joint is made prior to outgassing the entire EHSA.

There is a recess in each cover which is slightly larger than the outside diameter of the penetration assembly flange. The flange is isolated from the cover by a Viton rubber gasket and the radial clearance between the cover recess and the flange body. The only metal-to-metal contact in the penetration assembly/cover connection is through the four machine screws which attach the penetration assembly flange to the cover.

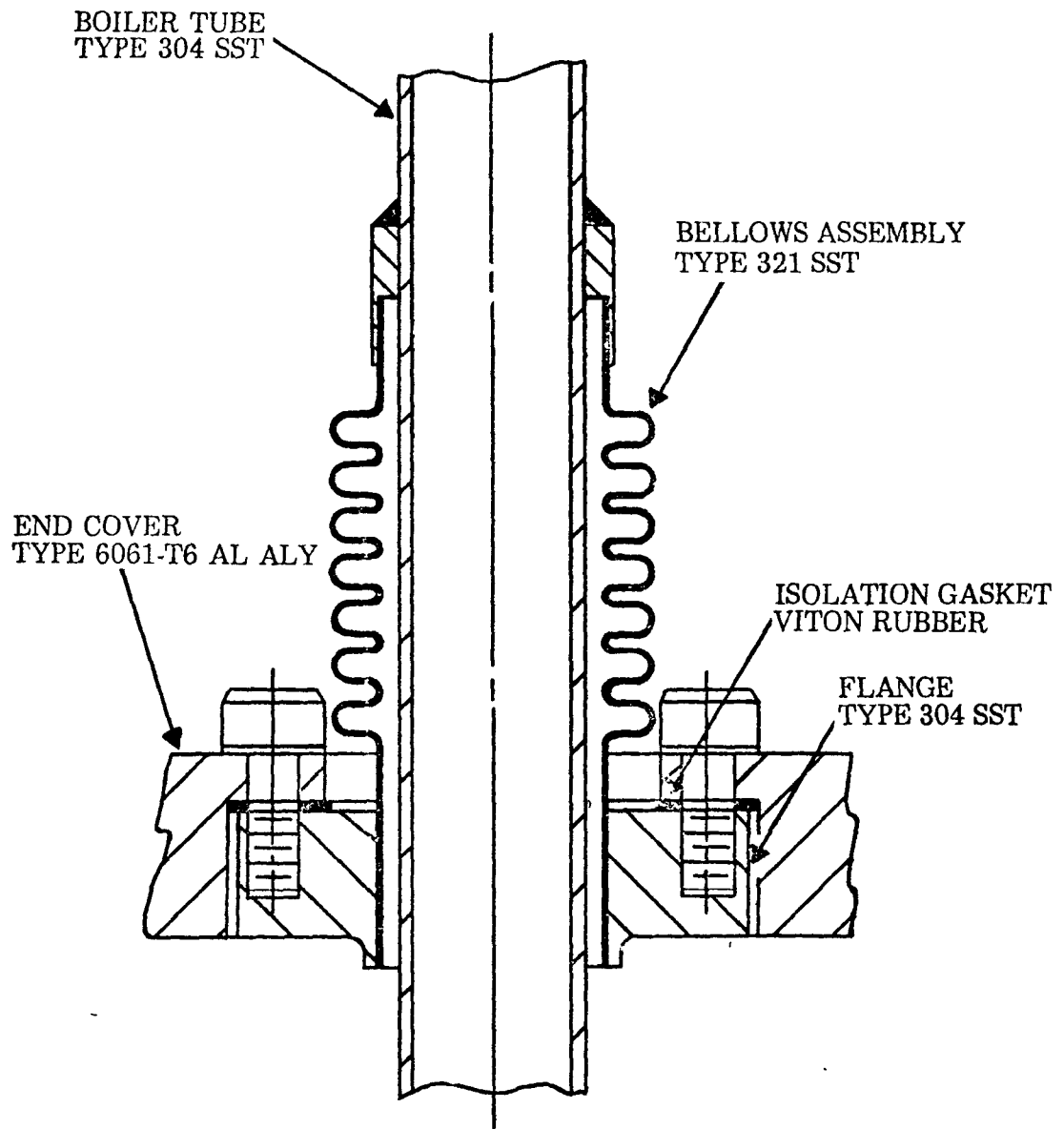


FIGURE 3.5.1.2-3
 BOILER TUBE PENETRATION ASSEMBLY INSTALLATION

Thermal/Structural Insulation

Most of the insulation in an EHSA is Min-K TE-1400, and serves three purposes: to minimize longitudinal and radial heat losses to the housing/end covers, to provide sufficient end preload for the electrical heat source and to support the boiler assembly and multifoil insulation system. Min-K TE-1400 was selected because of its temperature, thermal conductivity and compressive strength properties. Since no binder is used in its manufacture, it is easily outgassed. Prior to use in the EHSA the insulation is vacuum outgassed at 1500° F for eight hours at a level of 1000 μ or less. After outgassing, air exposure is minimized.

Emergency Cooling System

A multifoil insulation system is used in the flight system to assure that isotope heat source temperatures are maintained within tolerable limits, should Dowtherm cease to flow through the boiler assembly, by acting as an emergency heat dumping system. In such an accident situation, the heat source temperature would rise, resulting in the melting of the multifoil insulation, thereby allowing the heat source to radiate heat through the boiler assembly walls to the housing, thus maintaining tolerable heat source temperatures. Although an emergency cooling system (ECS) is not required for safety reasons for the electrical HSA as it is for the isotope HSA, it is required to simulate the same parasitic heat losses from the heat source assembly, and thus maintain the prototypicality between the two. The GDS electrical heat source temperature will always be within tolerable limits because of unique temperature controls which have been incorporated into the heater power supply. In addition to its ECS function the multifoil system (because of its excellent insulation properties) limits radial heat losses to the housing walls. The multifoil insulation system is located in the annular space between the outside of the boiler assembly and the inside of the housing.

The multifoil insulation system is a hollow right circular cylinder measuring 8.895 inches inside diameter by approximately 0.61 inch thick by 15.00 inches long. It consists of one continuous length of 0.001 inch thick type 1100 aluminum alloy foil loosely wrapped sixty times around an 0.010 inch thick type 1100 aluminum alloy foil can. Spacing between wraps is intended to be approximately 0.010 inch. However, the GDS multifoil insulation systems were wrapped tighter and as a result, their final thickness was approximately 0.44 inch instead of 0.61 inch. The foil material is lightly coated on one side with zirconium oxide (ZrO_2). The primary purpose of the coating is to insure a separation between wraps of the foil. Aluminum was selected as the foil system material because of its compatibility with the boiler assembly operating temperature and its low density.

The multifoil system is purchased as an assembly from ThermoElectron Corporation, located in Waltham, Massachusetts. Prior to procurement of the GDS systems, the vendor conducted a controlled meltdown test of a one-third actual size version of the multifoil system to verify their predicted properties of the insulation system. This test and other tests and analyses which verify its function are described in a later section.

Radiation Barrier

The radiation barrier, which is located in the annular space between the heat source and boiler assemblies, is required in order to raise* the temperature of the isotope heat source during normal operation. It is required for the GDS because the proper heater block temperatures must be achieved in order to simulate flight system parasitic heat losses. The radiation barrier is attached to each end of the boiler assembly with five sheet metal screws.

The radiation barrier is a formed, thin wall, hollow right circular cylinder which measures 7.57 inches outside diameter by 0.010 inch thick by 16.53 inches long and is made from nickel 200 sheet. After forming, the two edges of the sheet, which are butted together, are seam welded along their entire length, to form a continuous cylinder. Each side of the cylinder is grit blasted with aluminum oxide grit to provide the desired emissivity characteristics.

Electrical Heater

Each of the three electrical heat sources is a right circular cylinder which measures 7.42 inches diameter by 16.53 inches long, weighs 42.00 pounds and has a total power capability of 7200 W(e) or three times the nominal requirement of 2400 W(e) each. It simulates, as nearly as practical, the characteristics of the isotope heat source. The electrical heat source consists of two major components: the body and the cartridge heaters, see Figure 3.5.1.2-4. Extensive tests of the cartridge heaters and a heater block assembly were conducted prior to their use in an EHSA, to verify the heat source design. These tests are discussed in a subsequent section. The electrical heat source assembly was not subjected to dynamic testing. However, its design should permit the assembly to survive a KIPS qualification level dynamic test.

The heater body consists of a heater block body, which has internal Acme threads on each end and two end plugs which thread into place on each end of the body. Each component is made from EBP purified P-5710 graphite which is manufactured by Union Carbide. This grade of graphite, which is a purified grade of type ATJ graphite, was selected primarily because of its availability. After final machining, but prior to assembly, these components are vacuum outgassed at 1150°C for 6.5 hours.

The heater body serves as the housing for the twelve cartridge heaters. Initially, the body is machined oversized in length and the heater cartridge holes machined undersized. The body and end plugs are temporarily assembled and the assembly machined to the proper length. Each heater cartridge hole is reamed to match a particular heater

* The need for increasing the heat source operational temperature for impact conditions has been discussed earlier in the flight system section.

III

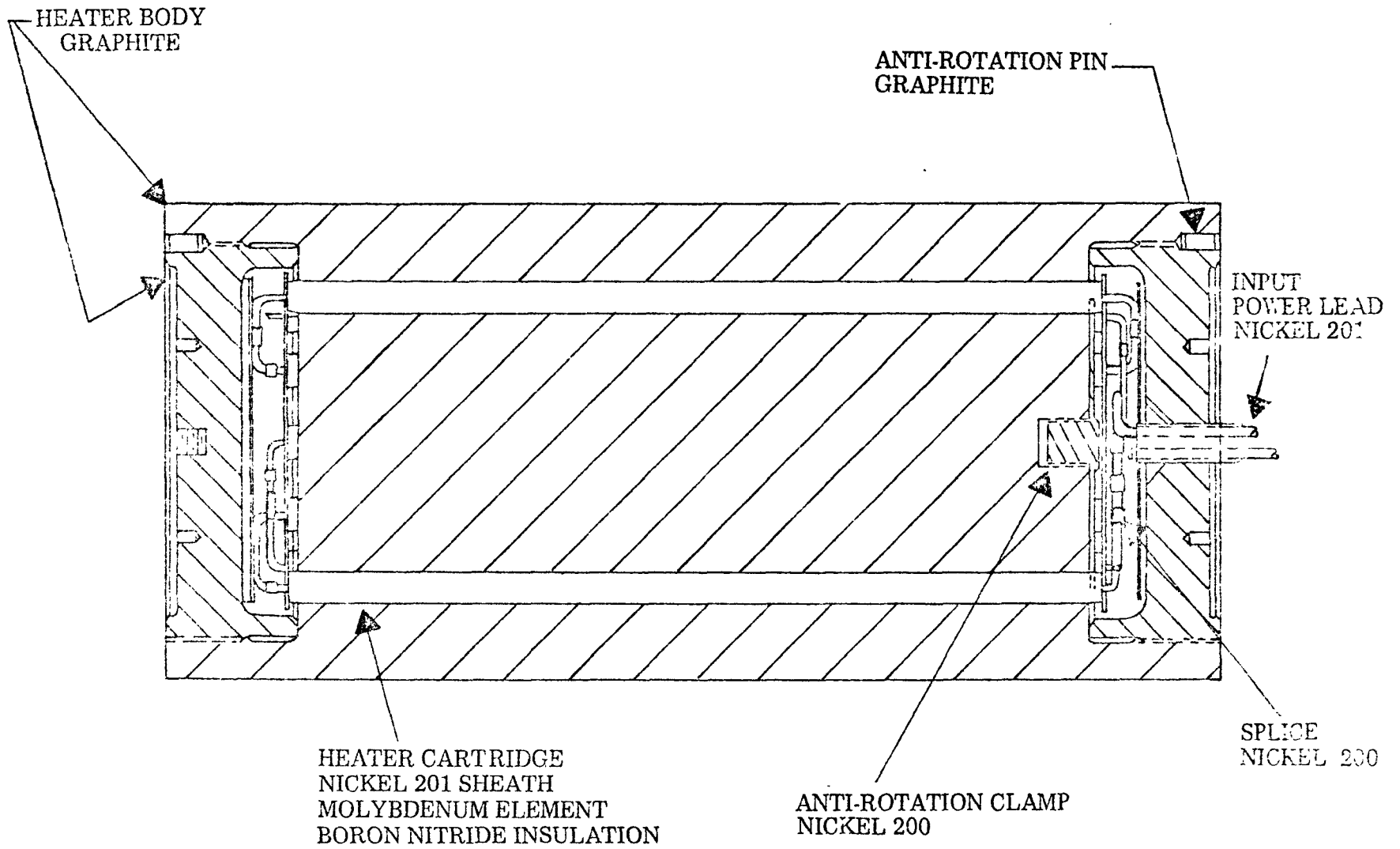


FIGURE 3.5.1.2-4
ELECTRICAL HEATER

cartridge and thereafter, they become a matched set. Cartridges cannot move during a dynamic test because their sheath is welded, on one end, to a nickel 200 anti-rotation clamp which is first threaded into the heater body.

There are twelve cartridge heaters in each electrical heat source assembly, each with a power output capability of 600 watts(e) at 19 ± 3.8 VAC. For added reliability, the twelve cartridges are connected in two parallel circuits of six cartridges each. Therefore, one circuit could cease to function and the remaining cartridges would be capable of producing the design power of 2400 watts(e). See Figure 3.5.1.2-5.

Heater Cartridges

The heater cartridges are manufactured by Watlow Electric Manufacturing Company, and measure 0.478 inch diameter by 12.75 inches long and have a heated length of 10.0 inches. The heater element is molybdenum, internal insulation is tightly compacted boron nitride, the bare #10 AWG power leads and the sheath are nickel 201.

The solid power leads are crimped internally to the molybdenum heater element, and externally to the nickel 201 stranded input power leads using nickel 200 crimps. Each power lead is crimped to a pigtail lead coming from a Deutsch 26 pin receptacle. Sample crimp splices are made before and after the actual hardware splices are made, and are pull tested, to determine the quality of the crimp splice joint. Inside the electrical heat source, the power leads are insulated using ceramic (Al_2O_3) heads. The wires and crimp splices are isolated from the heater body and end plugs by means of mica discs which rest on top of the wiring and the ends of the heater cartridges. There is also a layer (approximately 0.125 inch) of A-100 fibrous insulation between the mica disc and the end plug for additional isolation on each end of the heat source.

Prior to procuring the heater cartridges, Watlow Electric Manufacturing Company, conducted several tests to confirm their heater cartridge design. In addition to the vendor testing, eighteen heater cartridges were subjected to more rigorous testing, including life testing of six heater cartridges. One electrical heat source assembly was subjected to a rigorous test to determine its thermal profile, obtain heater circuit data and establish acceptance criteria. Each heater cartridge and electrical heat source assembly used in the GDS is subjected to a burn-in test prior to becoming a part of the EHSA assembly. The tests are discussed in detail in the next section.

Boiler Assembly

The boiler assembly consists of a 0.500 inch outside diameter by 0.035 inch wall stainless steel, copper plated tube which is wound in helical fashion around a 0.020 inch thick copper shell. A 0.250 inch outside diameter by 0.035 inch wall stainless steel, copper plated tube, for auxiliary cooling, is also wound around the shell. See Figure 3.5.1.2-6. The copper shell has helical grooves formed in it by spinning. The tubes are secured into these grooves by welding all along their lengths for the GDS units. Brazing of these tubes into the grooves was the original design, but has yet to be developed as is discussed in the next section. The entire assembly is coated on the inside and outside diameter with an iron titanate coating which is intended to assist in controlling the heat source temperature.

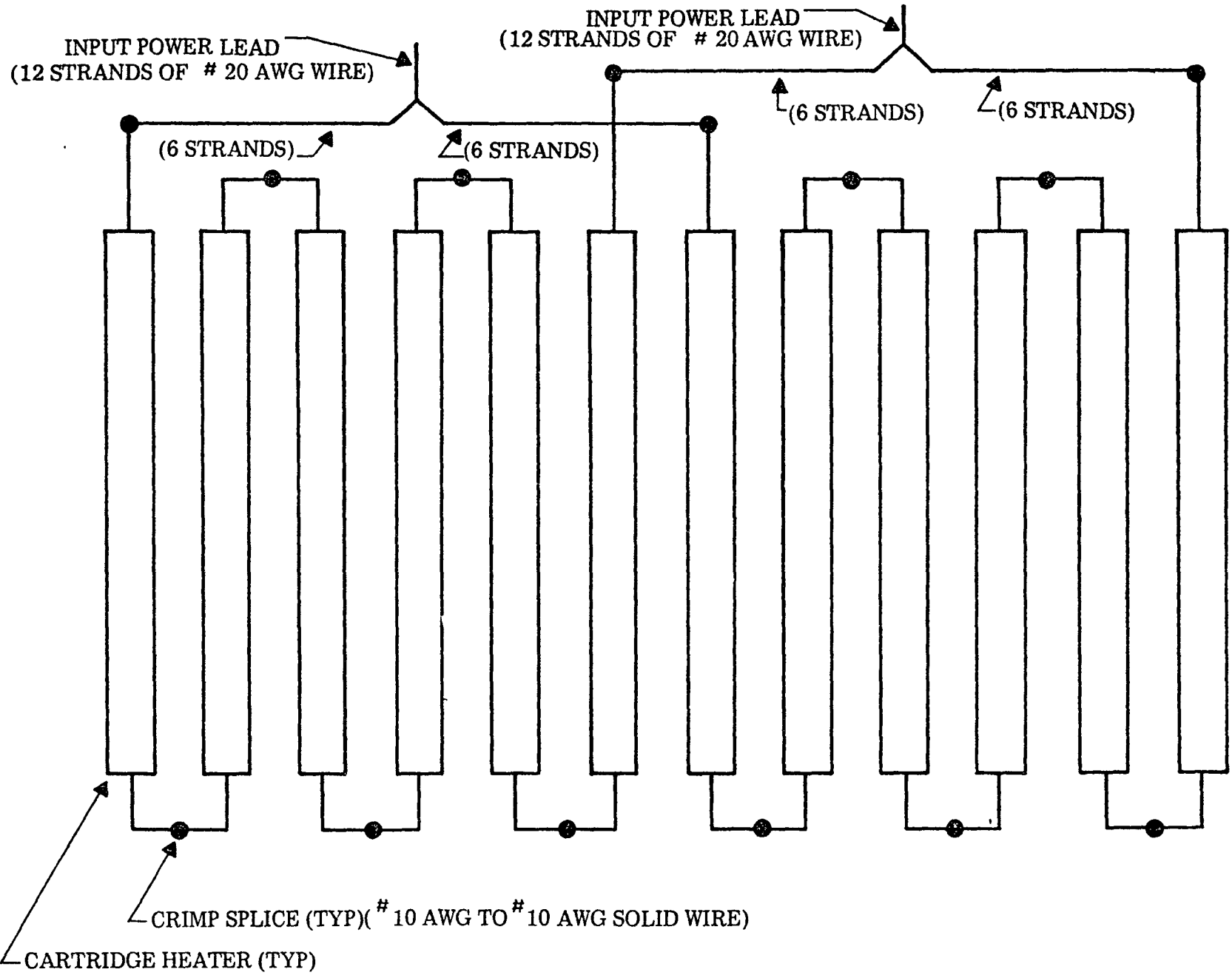


FIGURE 3.5.1.2-5
SCHEMATIC
ELECTRICAL HEATER

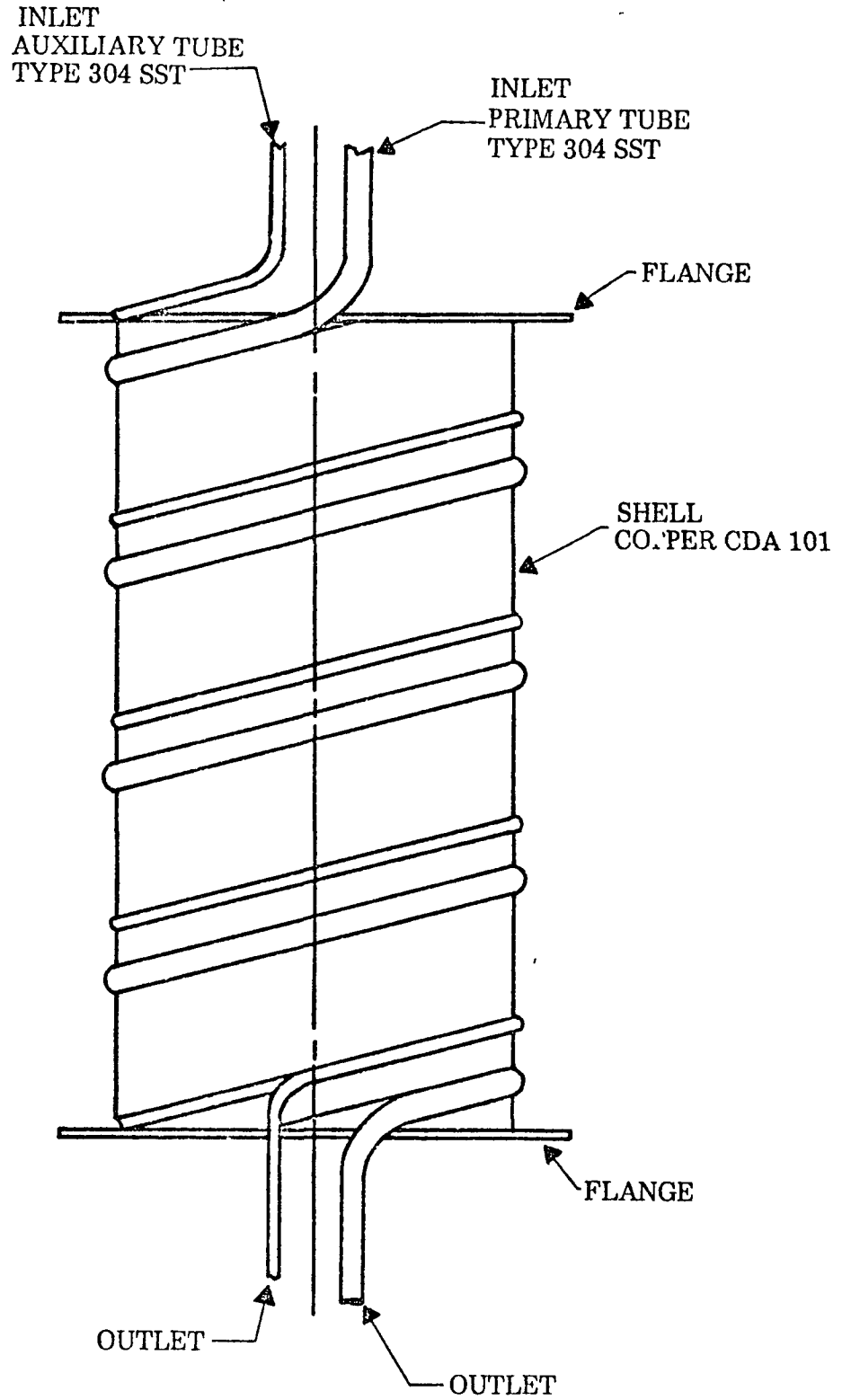


FIGURE 3.5.1.2-6
BOILER ASSEMBLY

The three GDS boiler assemblies are connected in series to form three fluid flow zones: subcooled, two phase and superheated. The inside of the 0.500 inch diameter tube, on each boiler, is fitted with a special insert which is intended to increase the film coefficient of the working fluid and to induce a high radial acceleration to maintain fluid contact on the tube wall even under the most extreme g loads. There is a different insert inside each boiler assembly.

The minimum inside diameter of the boiler shell is 7.63 inches and the maximum outside diameter, at the boiler tubes, is 8.81 inches. The boiler assembly flange to flange length is 16.53 inches. The boiler assembly fits in the annular space between the radiation barrier and the multifoil insulation system and is sandwiched between Min-K insulation at each end. The flanges are hand formed at assembly by making a series of cuts through the shell and bent to rest upon the Min-K.

The primary and auxiliary boiler tubes exit from each end of the boiler shell. They pass through the upper and lower end covers and through the penetration assemblies where they are terminated in special "vacuum-tight" (VCR-C-jon) fittings.

Instrumentation

Two components in each EHSA are instrumented. The boiler assembly is instrumented with nine chromel/alumel thermocouples which are fusion welded to the boiler shell at various locations. The thermocouples are made from bare, 24 AWG wire and then covered with fiberglass sleeving which has a maximum temperature capability of 1600°F. The wires are then routed in spiral fashion around the boiler shell and then routed through and around the Min-K insulation to the receptacle which is in the end cover. The instrumentation locations on each boiler assembly in the GDS are different. See Figure 3.5.1.2-7.

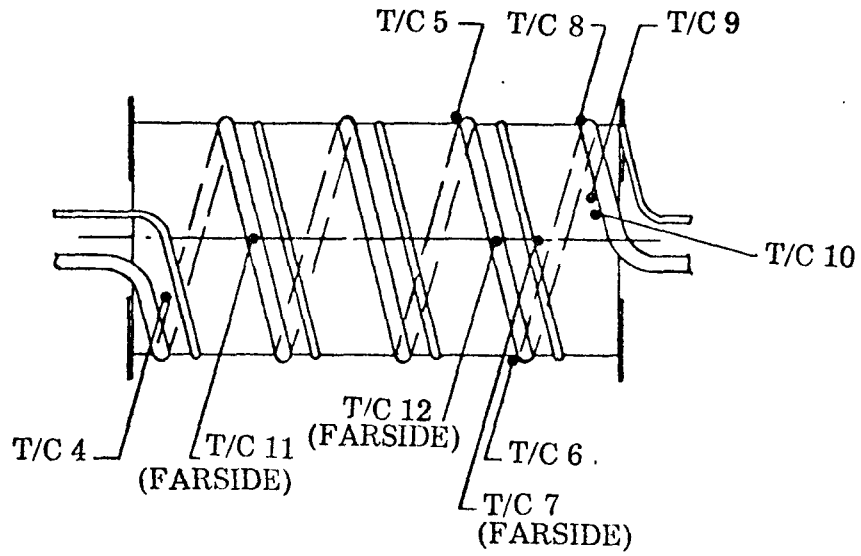
The electrical heater is instrumented with three platinum-10% rhodium sheathed thermocouples. One thermocouple is located approximately 1.75 inches from each end of the heater and one at the heater centerline. They lay in individual slots, machined into the heater body outside diameter and are retained by metal (nickel 201) clamps which are attached to the heater body. Because of the operational temperature of the electric heater, the thermocouple material is platinum-10% rhodium (+ wire) and platinum (- wire). Each wire is routed through and around the Min-K insulation and to the receptacle which is in the end cover.

All instrumentation from the boiler assembly and electrical heater is routed through a Deutsch 26 pin receptacle.

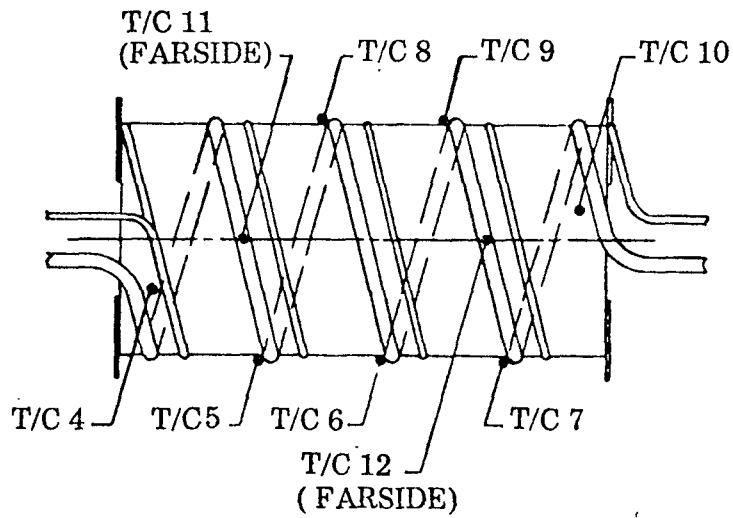
Cable Assemblies

Power input to the electrical heater is through a twelve foot cable consisting of 26 teflon insulated 16 AWG wires. One end of the cable is terminated into a Deutsch 26-pin connector (which mates with EHSA receptacle J-1) while the other end of the cable has loose wire ends.

INLET END
BOILER #3



INLET END
BOILER #2



INLET END
BOILER #1

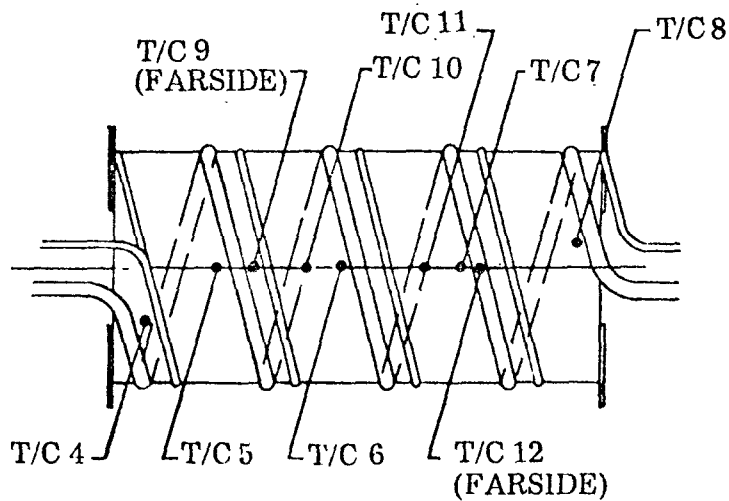


FIGURE 3.5.1.2-7
BOILER ASSEMBLY INSTRUMENTATION

The twelve foot instrumentation output cable consists of three pairs of 16 AWG, type SX stranded, asbestos insulated extension wire (calibrated for use with platinum, platinum-10% rhodium thermocouple wire) and ten pairs of 20 AWG, type K, teflon insulated chromel/alumel extension wire. One end of the cable is terminated into a Deutsch 26-pin connector (which mates with EHSA receptacle J-2) while the other end of the cable has loose wire ends.

Support Structure

Each EHSA is attached to the GDS baseplate by means of a triangular shaped, three legged, tubular, stainless steel (type 304) support structure. One end of the support structure is attached to the EHSA housing with three 0.250 inch diameter bolts. The opposite end of the support structure is attached to the GDS baseplate with three 0.375 inch diameter bolts. The support structure design limits thermal conduction to the GDS baseplate and radiation to the GDS vacuum chamber to approximately four watts (for each EHSA) as discussed in a subsequent section.

Valve Assembly

Each EHSA has a valve/pressure gage assembly attached to the 0.750 inch diameter tube which exits from the boiler inlet end of the EHSA. The purpose of the valve / pressure gage assembly is twofold. Primarily, the assembly permits monitoring of the internal environment of the EHSA in addition to providing emergency cooling for the electrical heater, in event of a loss of fluid flow through the boiler, by providing a gas backfill port through the valve assembly. Secondly, the assembly is used during EHSA outgassing and acceptance testing as described in a later section.

EHSA Power Supply Console

The EHSA power supply console provides a convenient and fail-safe method of supplying adjustable regulated AC power to the heaters of an EHSA. One power supply console is required for each EHSA in the GDS. The power supply contains appropriate instrumentation to indicate electrical power being supplied to the heaters and to indicate the heater body surface and boiler temperatures. Automatic shutdown and alarm provisions are included to facilitate unattended operation. The console is designed to operate from a 480 volts (nominal), single phase, 60 Hertz AC power source. See Figures 3.5.1.2-8 and 3.5.1.2-9.

The power supply is housed in a caster-mounted console and contains the following units:

- Instrumentation and alarm panel assembly
- Power adjustment panel assembly
- Rear connector panel assembly

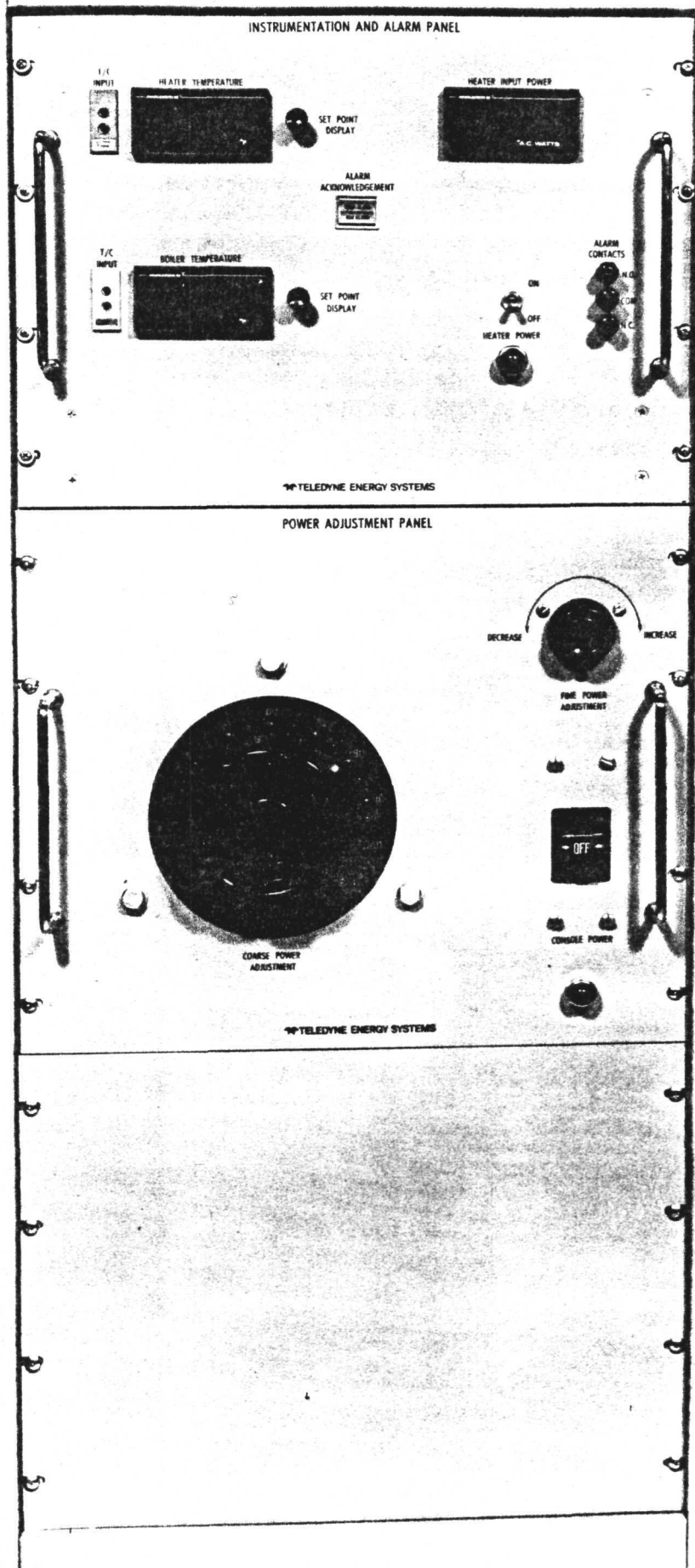


FIGURE 3.5.1.2-8
118

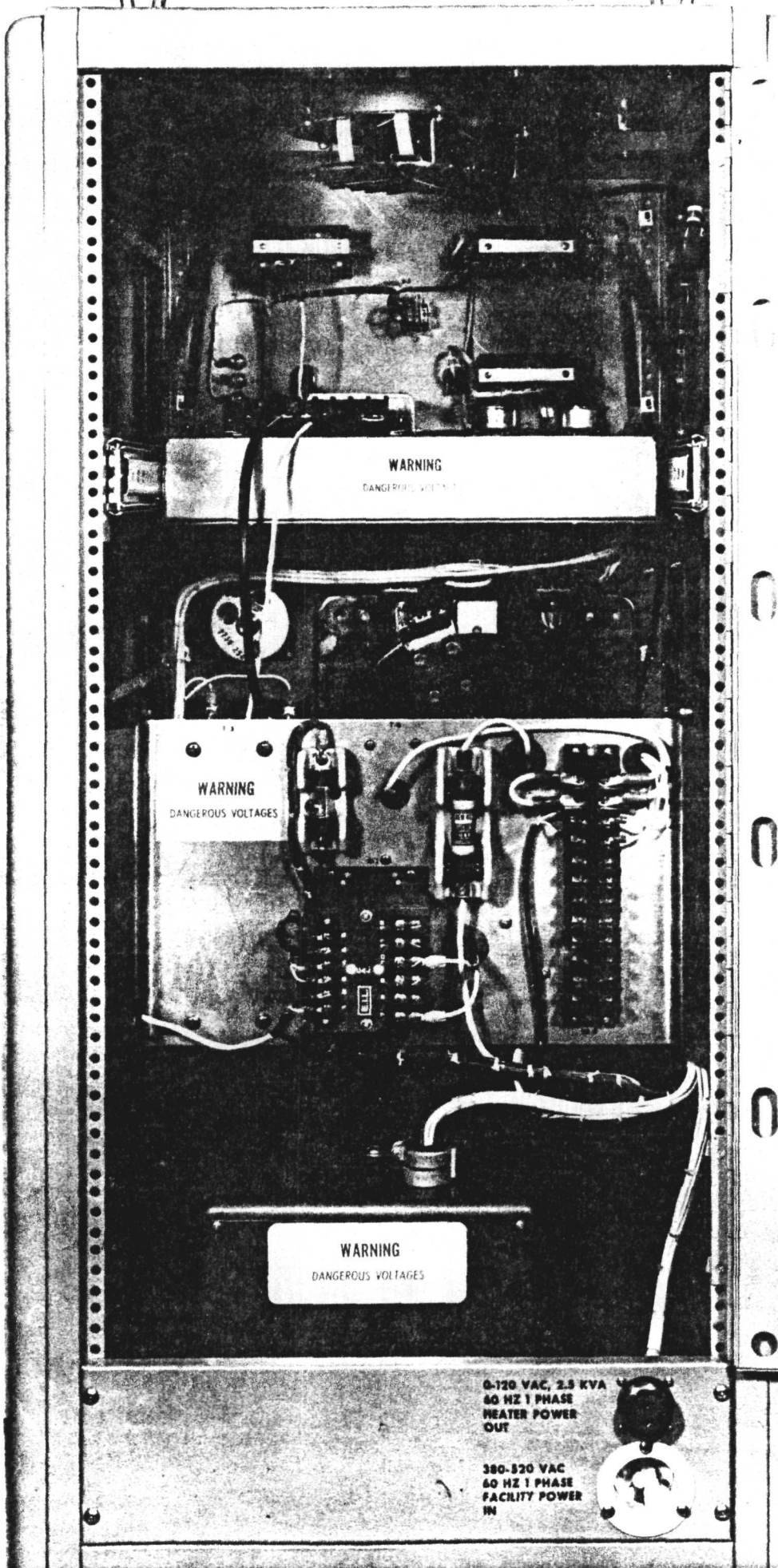


FIGURE 3.5.1.2-9
119

The instrumentation and alarm panel assembly includes a digital wattmeter system which is designed to display power supplied to the heaters and two digital temperature indicators. One temperature indicator operates from a chromel-alumel thermocouple and displays boiler assembly temperature while the other operates from a platinum-platinum 10% rhodium thermocouple and displays heater temperature. The unit is designed to slide out of the front of the console to provide access for adjustments to the set point display for the two temperature indicators.

Each temperature indicator is equipped with an overtemperature provision. If the temperature sensed by either instrument exceeds the set limit, heater power is automatically reduced to zero, an audible alarm sounds, a red alarm light comes on, and the contacts for an external alarm change state. These conditions remain until an alarm acknowledgement button is pressed. If an over-temperature condition still exists when the button is pressed, the red light changes to amber and the audible alarm stops sounding, but heater power remains at zero and the external alarm remains activated. Then, when the temperature drops below the set point, heater power comes on, the amber light goes off, and the alarm contacts return to normal condition.

The power adjustment panel assembly enables the output voltage to be continually adjusted over a range from zero to 120 volts 60 Hertz, single phase. Two knobs on the panel are used for this purpose. One is a coarse adjustment, the other is a fine adjustment.

Maximum continuous output is limited to 2700 volt-amperes with an additional restriction that the output current must not exceed 50 amperes. With these ratings, power is supplied to the heaters if all twelve heaters are operating or if a heater failure has reduced the number of active heaters to six. (The heater configuration consists of two strings in parallel, each string consisting of six heaters in series.) With all heaters operating, 2400 watts is supplied at about 66.5 volts and 36 amperes. With six heaters in operation, 2400 warts is supplied at about 94 volts and 25.5 amperes.

TABLE 3.5.1.2-I: EHSA WEIGHT

<u>Component</u>	<u>Material</u>	<u>"As Built" Weight (lbs)</u>
Housing	Aluminum Alloy 6061-T6	10.14
Cover, Lower Outer	Aluminum Alloy 6061-T6	1.53
Cover, Lower Inner	Aluminum Alloy 6061-T6	1.41
Cover, Upper	Aluminum Alloy 6061-T6	2.17
Lock Ring, Lower Outer	Aluminum Alloy 6061-T6	.81
Lock Ring, Lower Inner	Aluminum Alloy 6061-T6	.50
Lock Ring, Upper	Aluminum Alloy 6061-T6	.76
Receptacle	St. Stl. Shell Type 20CB3	.23
Penetration Assembly (Primary Tube)	St. Stl. Type 304/321	.29
Penetration Assembly (Auxiliary Tube)	St. Stl. Type 304/321	.26
Gasket	Viton Rubber	.01
Boiler Assembly	Copper Shell/ St. Stl. Tube	7.82
Electrical Heat Source	Graphite/Nickel Heaters	41.90 (w/o ext. T/C's)
Multifoil Insulation	Aluminum Alloy 1100	3.18
Min-K Insulation	Min-K TE1400	4.48
Radiation Barrier	Nickel 200	1.44
Boiler Tube Fittings (Primary)	Stainless Steel	.26
Boiler Tube Fittings (Auxiliary)	Stainless Steel	.23
Miscellaneous Hardware	(Sheathed T/C's, Screws, O-Rings, Wires, etc.)	.50
		<hr/> 77.92

3.5.1.3 Thermal Environment of Heat Source

3.5.1.3.1 Analyses

Electrical Heat Source Assembly Thermal Analysis - A thermal analysis of the GDS electrical heat source assembly operating in a vacuum chamber was performed to determine the expected heat losses and significant component temperatures. A nominal chamber wall operating temperature of 90°F was assumed for the analysis and sufficiently low chamber pressure (less than 10 mm of mercury) was assumed such that heat transport by solid (not gaseous) conduction and radiation only were important. No account was taken of manufacturing tolerances, possible interference with or deformation of the multifoil insulation or any anomalies unique to individual EHSA units. For these nominal conditions, a summary of the heat losses that were predicted from the EHSA is given below:

<u>Source</u>	<u>Quantity (watts)</u>
Support Assembly (Mounting Structure)	4.8
Power Cable	15.0
Instrumentation Cable	1.8
EHSA Internal Joule Heating (excess over isotopic heat source value)	10.2
Parasitic Heat Loss From Housing	29.2
	<hr/>
Total (per EHSA Assembly) =	61.0 Watts
	= 208.3 Btu/hr

Parasitic heat losses internal to the heat source assembly were calculated parametrically ignoring the contributions of the heater power and instrumentation cables. The heat flow path characteristics assumed for the calculations are given in Table 3.5.1.3-I. Actual calculations were accomplished with a computer program. Results of the calculations are presented in Figures 3.5.1.3-1 to 3.5.1.3-5 as graphs of the parasitic heat loss vs significant component temperatures. The assumed nominal operating condition will result in the following component temperatures and heat losses:

TABLE 3.5.1.3-I

SUMMARY OF HEAT LOSS CHARACTERISTICS

Heat Loss	Mode	Conductivity (Btu/hr-ft-°F)	Area (Ft ²)	Temperature		Path Length (Ft)	Emissivity
				Hot Side (°F)	Cold Side (°F)		
Housing + 1 end cover loss to chamber interior	Radiation	~	5.89	100 - 200	90	~	.1956
Boiler to inside (can) of multifoil insulation radiation	Radiation	~	2.95	750	735 to 745	~	.193
Through multifoil insulation	Radiation & Conduction	1.2×10^{-4}	3.00	735 to 745	100 to 160	0.020	.00418
Through Min-K end insulation (per end)	Conduction	0.0085	0.4418	1650	100 to 160	0.16667	~
From tube penetration to end covers (per tube)	Conduction	9.0	1.145×10^{-4}	700	100 to 160	0.5	~

130

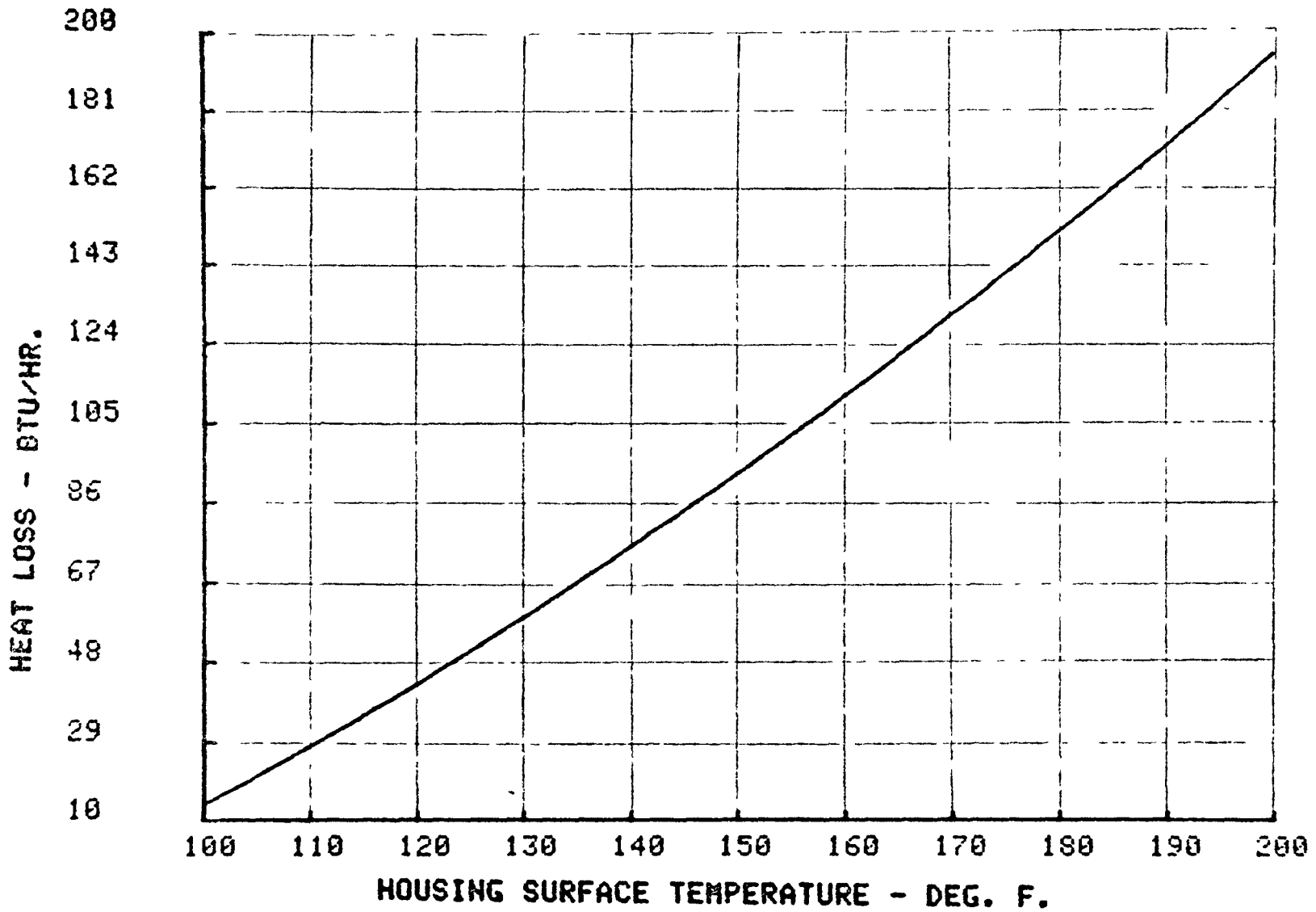


FIGURE 3.5.1.3-1

HEAT LOSS FROM HOUSING AND ONE END COVER

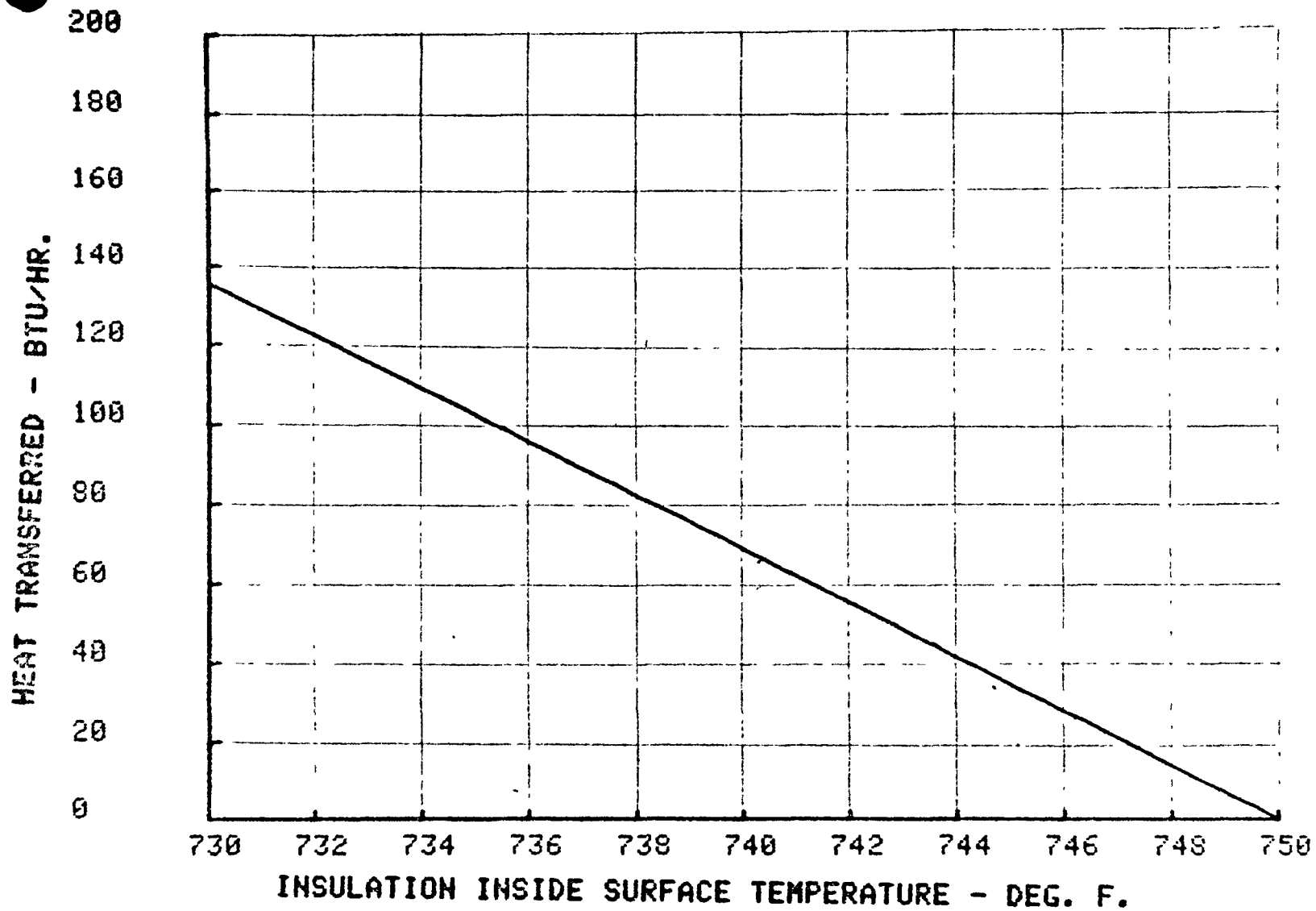


FIGURE 3.5.1.3.-2

HEAT RADIATED FROM BOILER TO INSIDE SURFACE
(CAN) OF MULTIFOIL INSULATION

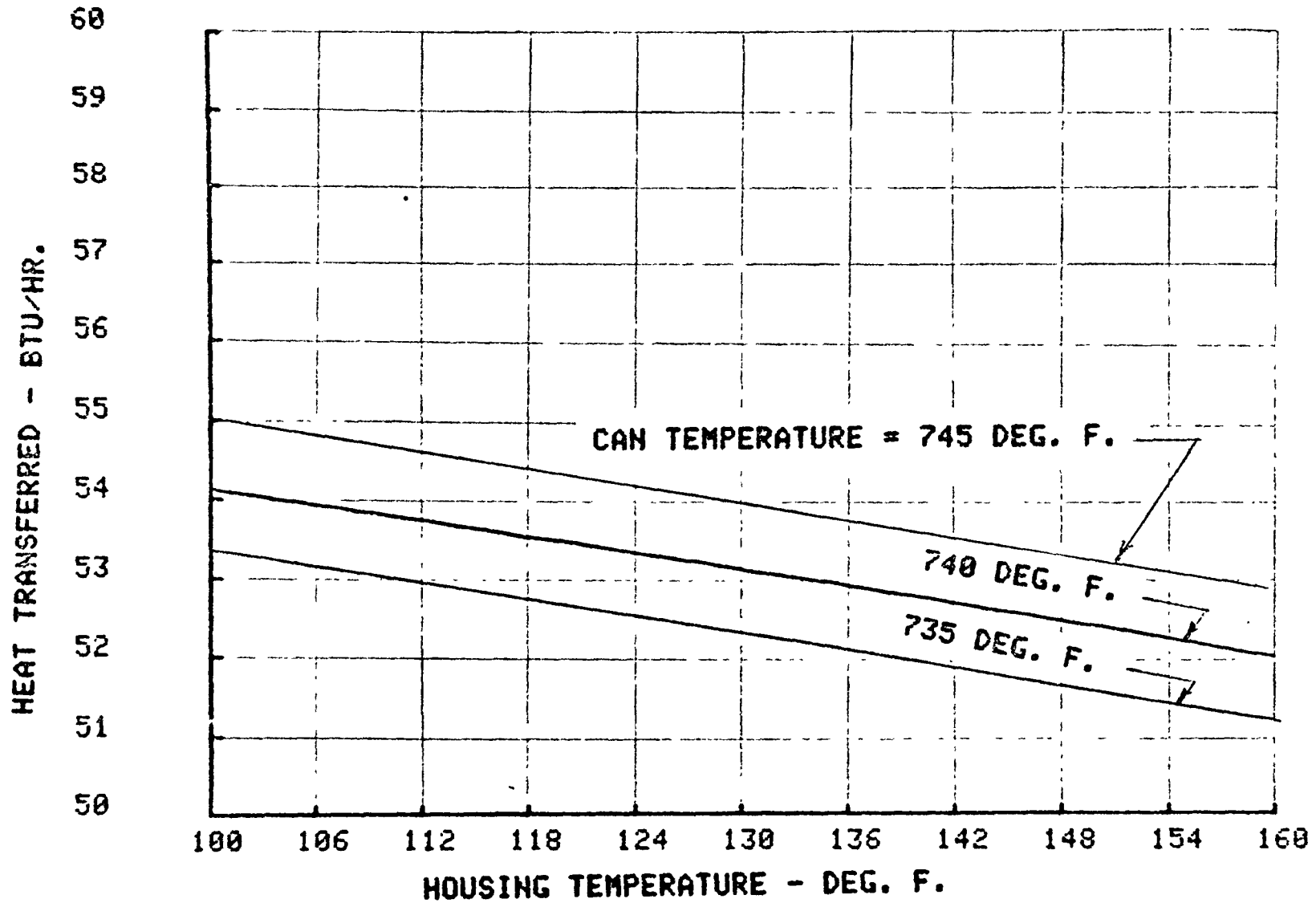


FIGURE 3.5.1.3-3

HEAT TRANSFERRED THROUGH MULTIFOIL INSULATION

HEAT TRANSFERRED - BTU/HR.

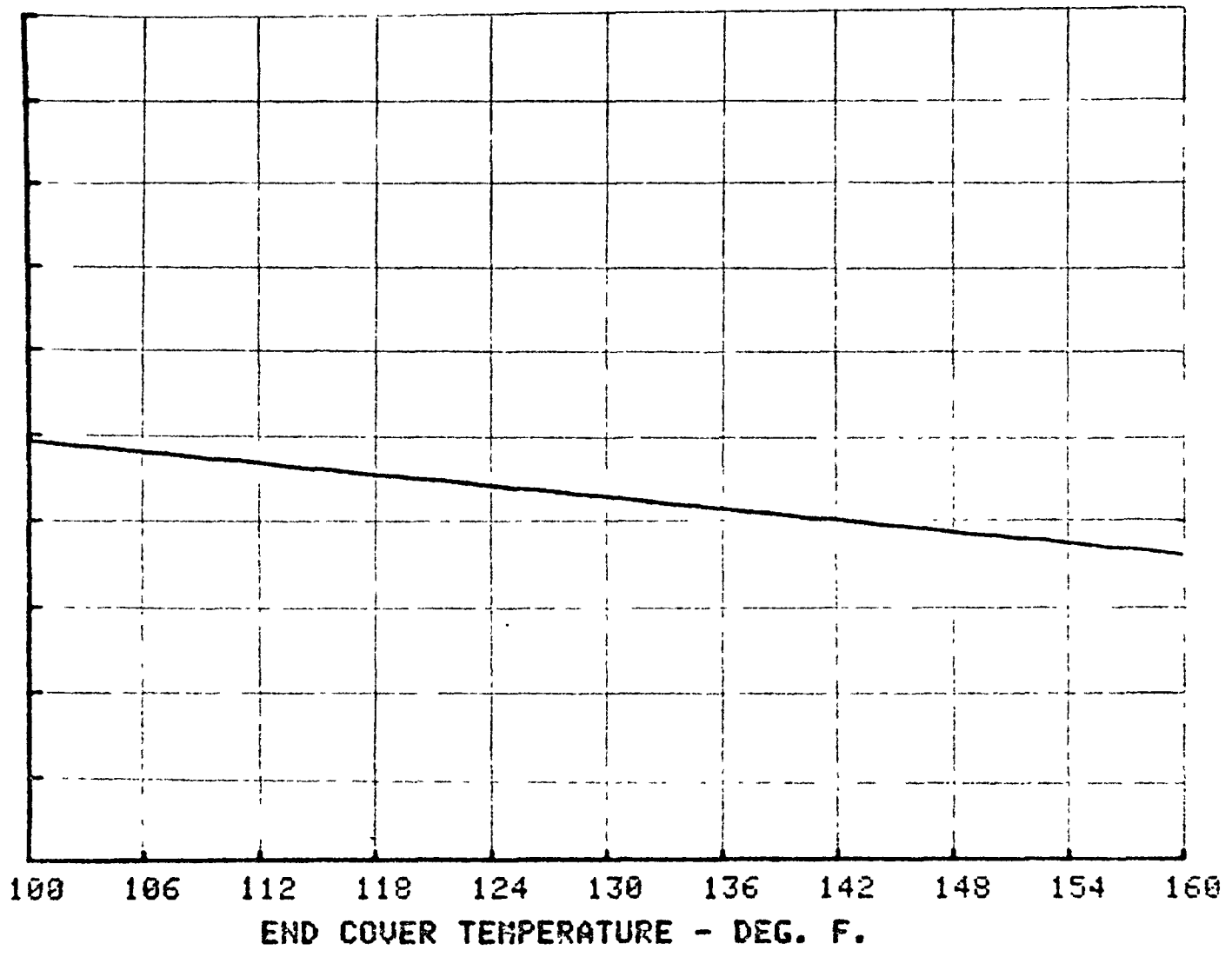


FIGURE 3.5.1.3-4

HEAT TRANSFERRED THROUGH MIN-K END INSULATION

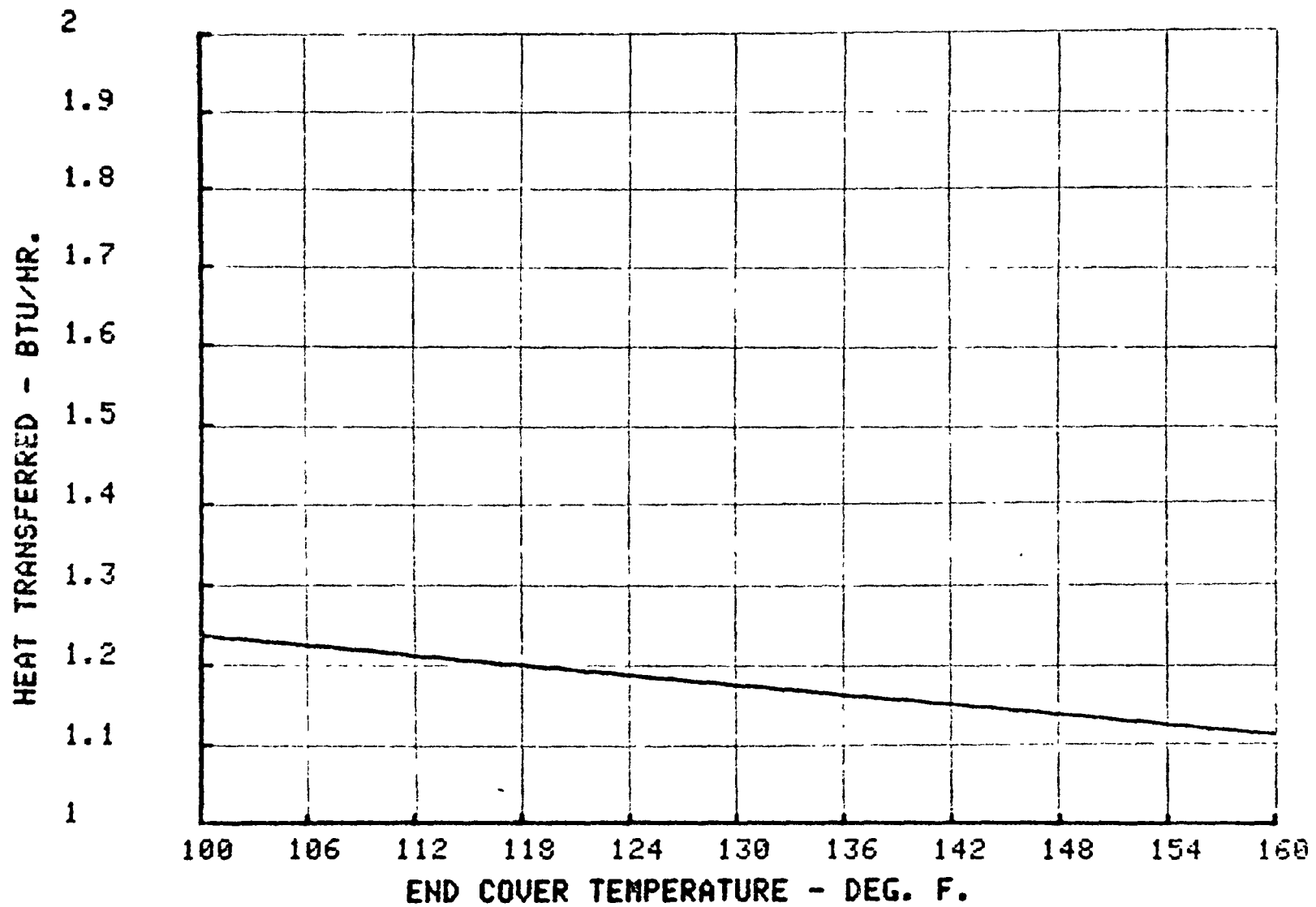


FIGURE 3.5.1.3-5

HEAT TRANSFERRED FROM TUBE TO END COVER

Housing and 1 end cover heat rejection	26.7 watts
Housing temperature	150 °F
Boiler average temperature	750 °F
Heat radiated from boiler to multifoil	15.4 watts
Multifoil inside surface (can) temperature	742 °F
Heat conducted and radiated through multifoil	15.4 watts
Heat conducted from boiler tubes to end covers	1.3 watts
Heat through Min-K end insulation (1 end)	9.9 watts
Temperature of heat source surface	1650 °F

Support System Heat Losses

The major heat conduction loss from the EHSA to the vacuum chamber occurs through the mounting bracket legs. The mounting bracket is used to support the EHSA on a baseplate during thermal vacuum testing. Figures 3.5.1.3-6 and 3.5.1.3-7 show the mounting bracket configuration.

Heat loss by conduction to the mounting plate is presented in Figure 3.5.1.3-8 as a function of the temperature difference between the plate and the housing end cover. The legs are analyzed in two stages lengthwise to account for the additional heat transport through the gussets.

$$Q_{\text{per leg}} = k \frac{\Delta T}{\frac{\Delta X_1}{A_1} + \frac{\Delta X_2}{A_2}}$$

where

$Q_{\text{per leg}}$ = heat transferred per leg, Btu/hr

k = thermal conductivity of 304 stainless steel, $9.4 \frac{\text{Btu}}{\text{hr-ft } ^\circ\text{F}}$

ΔT = temperature difference between EHSA end cover and mounting plate, °F

FIGURE 3.5.1.3-6
SIDE VIEW OF MOUNTING STRUCTURE

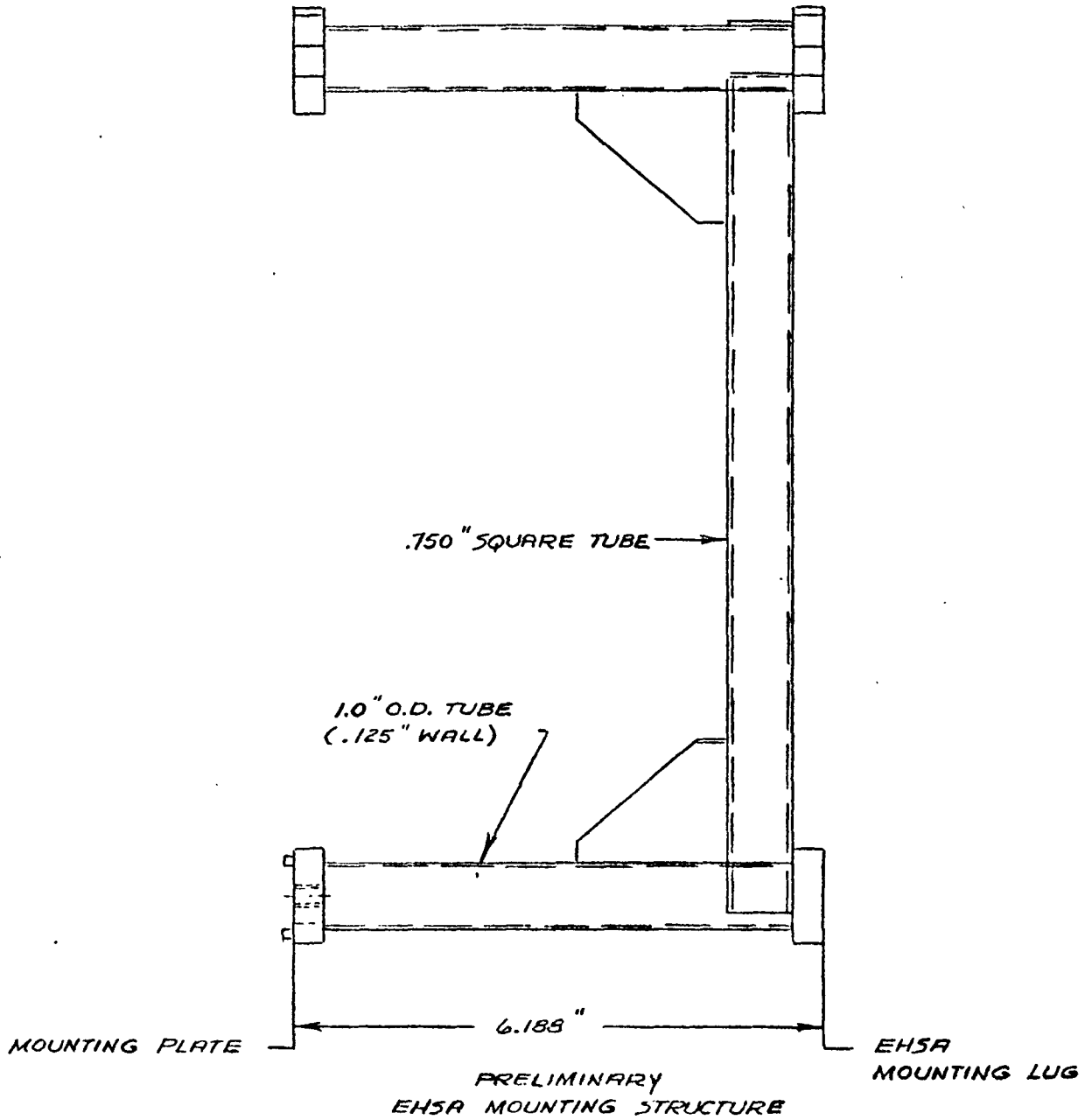
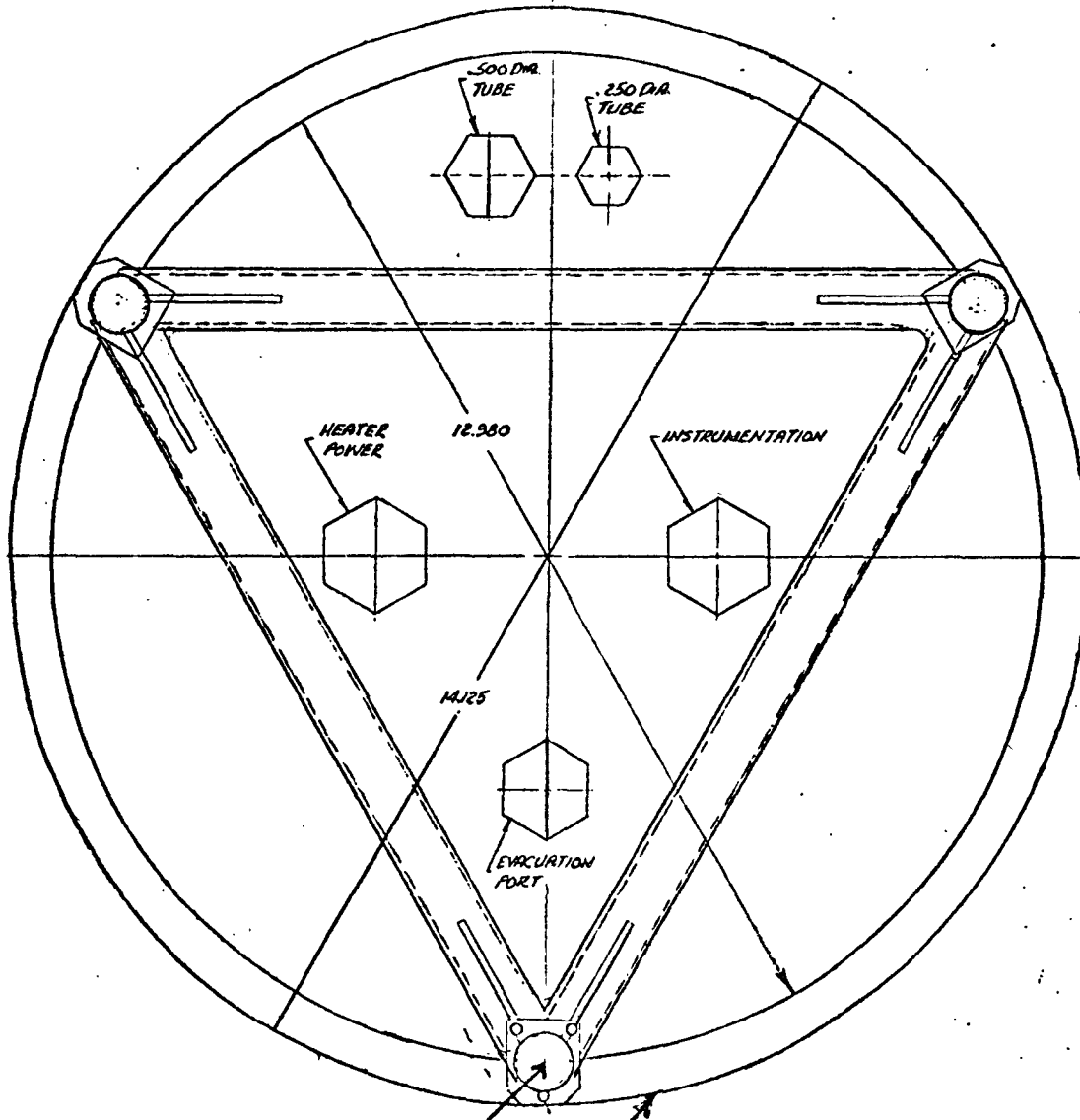


FIGURE 3.5.1.3-7

TOP VIEW OF MOUNTING STRUCTURE



.250-28 UNF-2B
3 Places

1.00 x 1.125

"Unique" Pins (.125 diameter and
.125 from edge to end)

1 Pin = Boiler Assembly #1

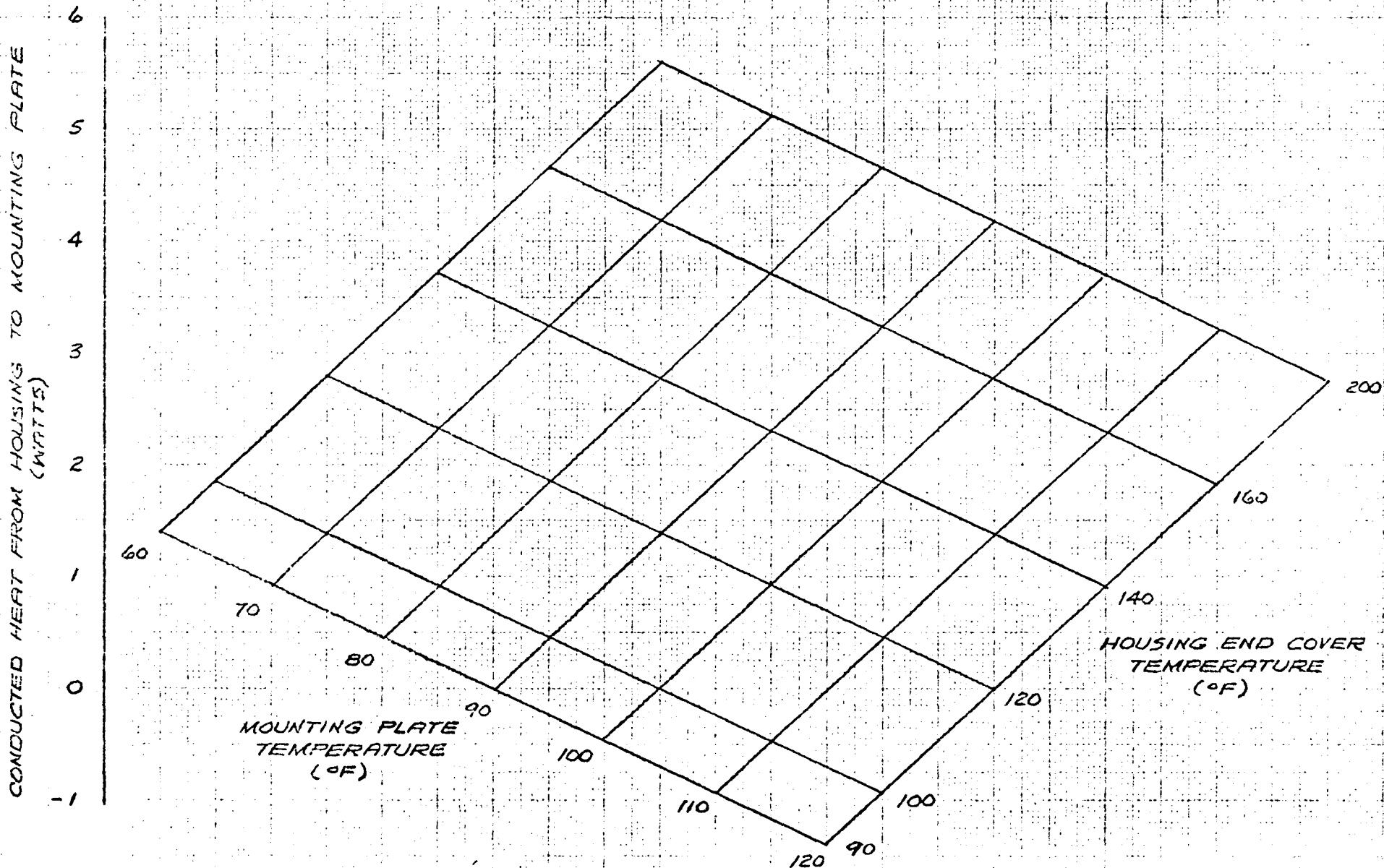
2 Pins = Boiler Assembly #2

3 Pins = Boiler Assembly #3

FIGURE 3.5.1.3-8

CONDUCTION HEAT TRANSFER FROM EHSA SUPPORT STRUCTURE

132



$$\begin{aligned} \Delta X_1 &= \text{length of leg not gusseted, } 0.250 \text{ feet} \\ \Delta X_2 &= \text{length of leg with gusset attached, } 0.208 \text{ feet} \\ A_1 &= \text{cross sectional area of leg without gussets, } 2.38619 \times 10^{-3} \text{ ft}^2 \\ A_2 &= \text{cross sectional area of leg with averaged gusset included,} \\ &\quad 2.84453 \times 10^{-3} \text{ ft}^2 \end{aligned}$$

Substitution of the values for variables gives,

$$Q_{\text{per leg}} = 0.0528409 \Delta T \text{ Btu/hr}$$

For all three legs, and converting Btu/hr to watts gives,

$$Q_{\text{total}} = 0.046427324 \Delta T \text{ watts}$$

Heat loss by radiation from the mounting bracket to the surroundings may be evaluated by means of the following equation:

$$Q = \sigma A \epsilon (T_2^4 - T_1^4)$$

where,

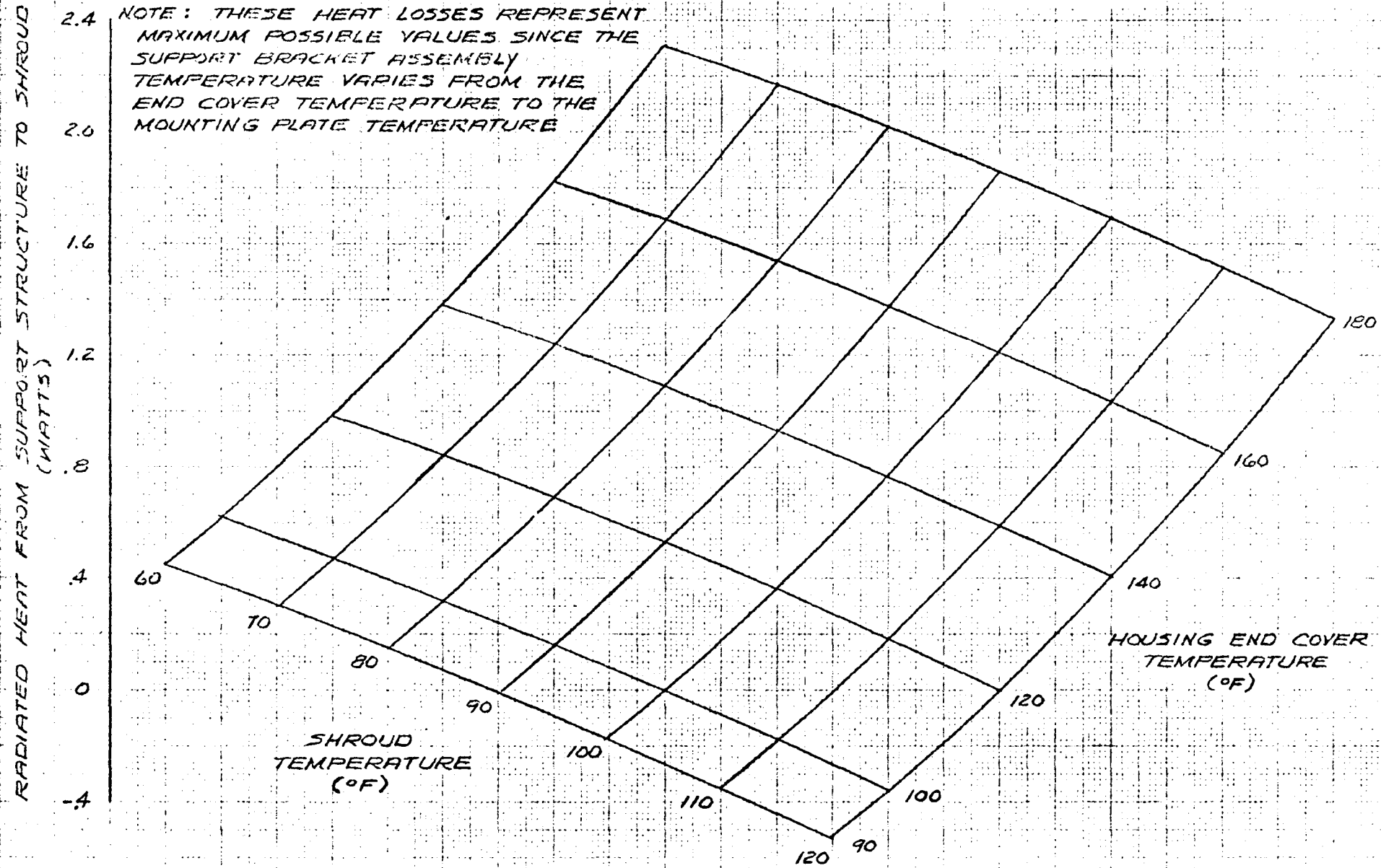
$$\begin{aligned} Q &= \text{heat lost in Btu/hr by radiation} \\ \sigma &= \text{Boltzmann's constant, } 0.172 \times 10^{-8} \frac{\text{Btu}}{\text{hr ft}^2 \text{ } ^\circ\text{R}^4} \\ A &= \text{leg plus gusset surface area, } 0.16339 \text{ ft}^2 \text{ per leg} \\ \epsilon &= \text{equivalent emissivity, considering the leg emissivity } 0.1 \text{ and the} \\ &\quad \text{chamber shroud emissivity } 0.9 \\ T_2 &= 610^\circ\text{R, } (150^\circ\text{F}), \text{ housing temperature} \\ T_1 &= 550^\circ\text{R } (90^\circ\text{F}) \text{ chamber shroud temperature} \\ Q &= 1.305 \text{ Btu/hr per leg} \end{aligned}$$

Thus, the maximum heat lost from the leg assembly to the surroundings for the assumed conditions is 0.382 watts per mounting bracket assembly. In reality, the view of the legs to space is considerably less than perfect and the leg temperature is not uniform (decreases from housing temperature to mounting plate temperature) and the shroud temperature is not far from room temperature. This heat loss is presented in Figure 3.5.1.3-9.

FIGURE 3.5.13-9

RADIATION HEAT TRANSFER FROM EHSa SUPPORT STRUCTURE

NOTE: THESE HEAT LOSSES REPRESENT
MAXIMUM POSSIBLE VALUES SINCE THE
SUPPORT BRACKET ASSEMBLY
TEMPERATURE VARIES FROM THE
END COVER TEMPERATURE TO THE
MOUNTING PLATE TEMPERATURE



134

Heat radiated from the bottom end cover of the EHSA to the base plate is determined as follows:

$$Q_r = \sigma A_c \epsilon_c (T_c^4 - T_p^4)$$

$$A_c = \text{area of end cover, } 0.919 \text{ ft}^2$$

$$\epsilon_c = \text{effective emissivity of end cover and base plate, estimated to be } 0.111 \text{ (calculated from } \epsilon = 0.2 \text{ for each surface).}$$

$$T_c = \text{end cover temperature, } ^\circ\text{R}$$

$$T_p = \text{end plate temperature, } ^\circ\text{R}$$

This equation was evaluated for various combinations of end cover and mounting plate temperatures, and the results are presented in Figure 3.5.1.3-10. Figure 3.5.1.3-11 shows the combined total loss from the EHSA lower end cover as given by the sums of the heat losses in Figures 3.5.1.3-8 thru 10. In this figure, the shroud and base plate temperatures are assumed equal.

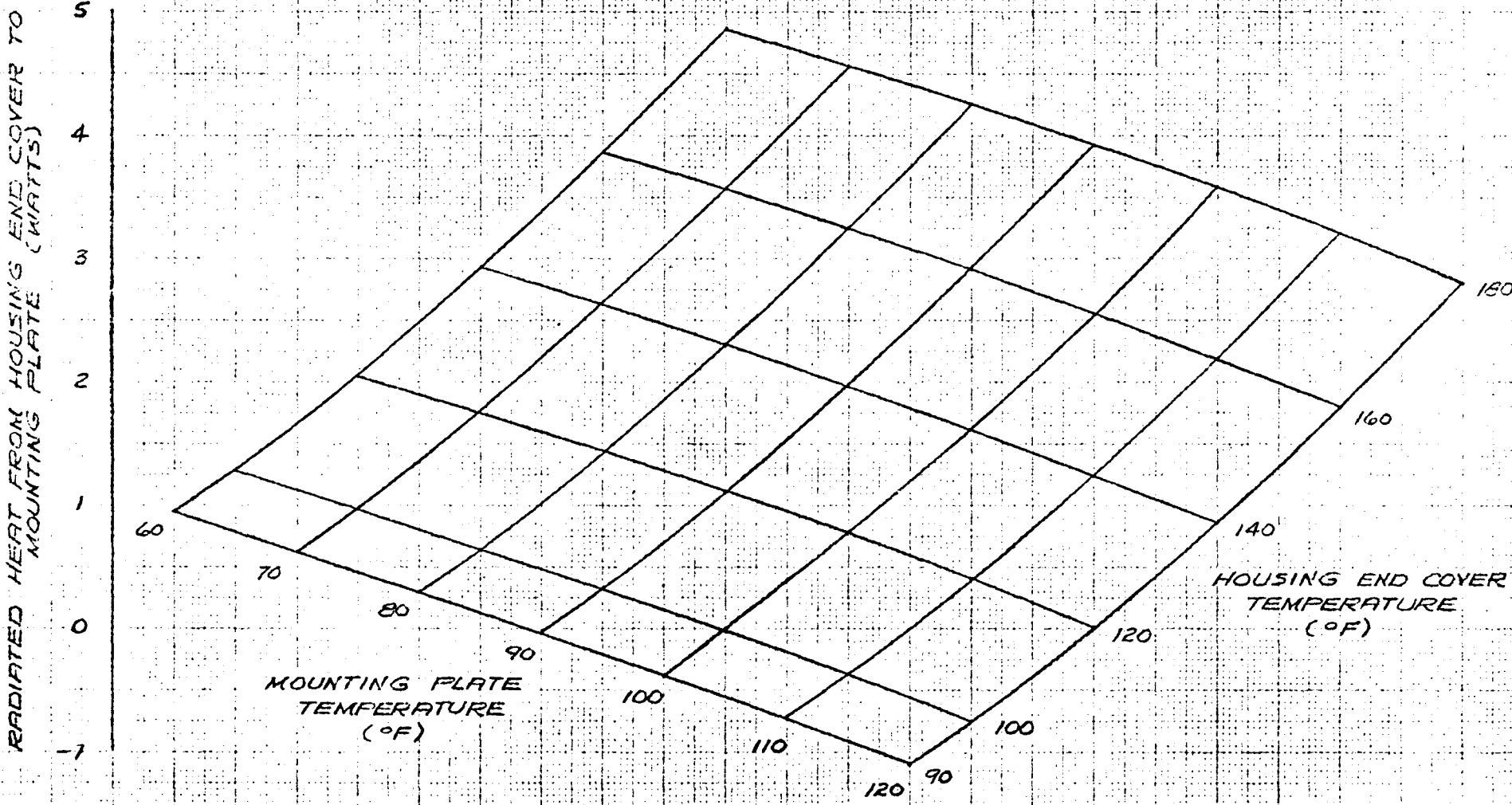
Power Cable Heat Losses

Analyses were accomplished to predict temperatures and heat flow in EHSA electrical heater power leads and housing connector to vacuum chamber cabling during GDS thermal/vacuum testing. Tolerable wire and connector temperatures are obtained with 16 gauge wire in the power cable and 20 gauge heater leads within the HSA. Total heat loss from the leads within the HSA was predicted to be about 10 watts, and the peak nickel heater lead temperature about 1650°F for a heater block temperature of 1600°F. The power cable connector on the housing and cover was predicted to reach 278°F at the connector pins. Losses of about 15 watts by radiation from the cable were predicted within the vacuum chamber. Temperatures and heat flows are essentially unaffected by the environment at or exterior to the vacuum chamber pass-through connector.

The thermal analysis was accomplished by means of two computer programs; one written specifically for the heater leads (inside the HSA) and one for the housing connector to chamber pass-through cable. Temperatures of the leads and cable predicted by these programs are shown in Figure 3.5.1.3-12, and cumulative heat losses from the leads are shown in Figure 3.5.1.3-13. Heat loss path dimensions and environment conditions are given in Table 3.5.1.3-II.

Both computer programs are based on a forward finite difference solution wherein a heat balance is achieved on a differential element. Figure 3.5.1.3-14 shows the application of the heat balance equation to a typical differential element. For a given element, heat transferred from the previous element (Q_1) plus heat generated from resistance to the passage of electric current (Q_3) is considered heat entering. Heat lost is heat radiated or conducted (Q_4) to the environment plus heat conducted forward to the next differential element (Q_2).

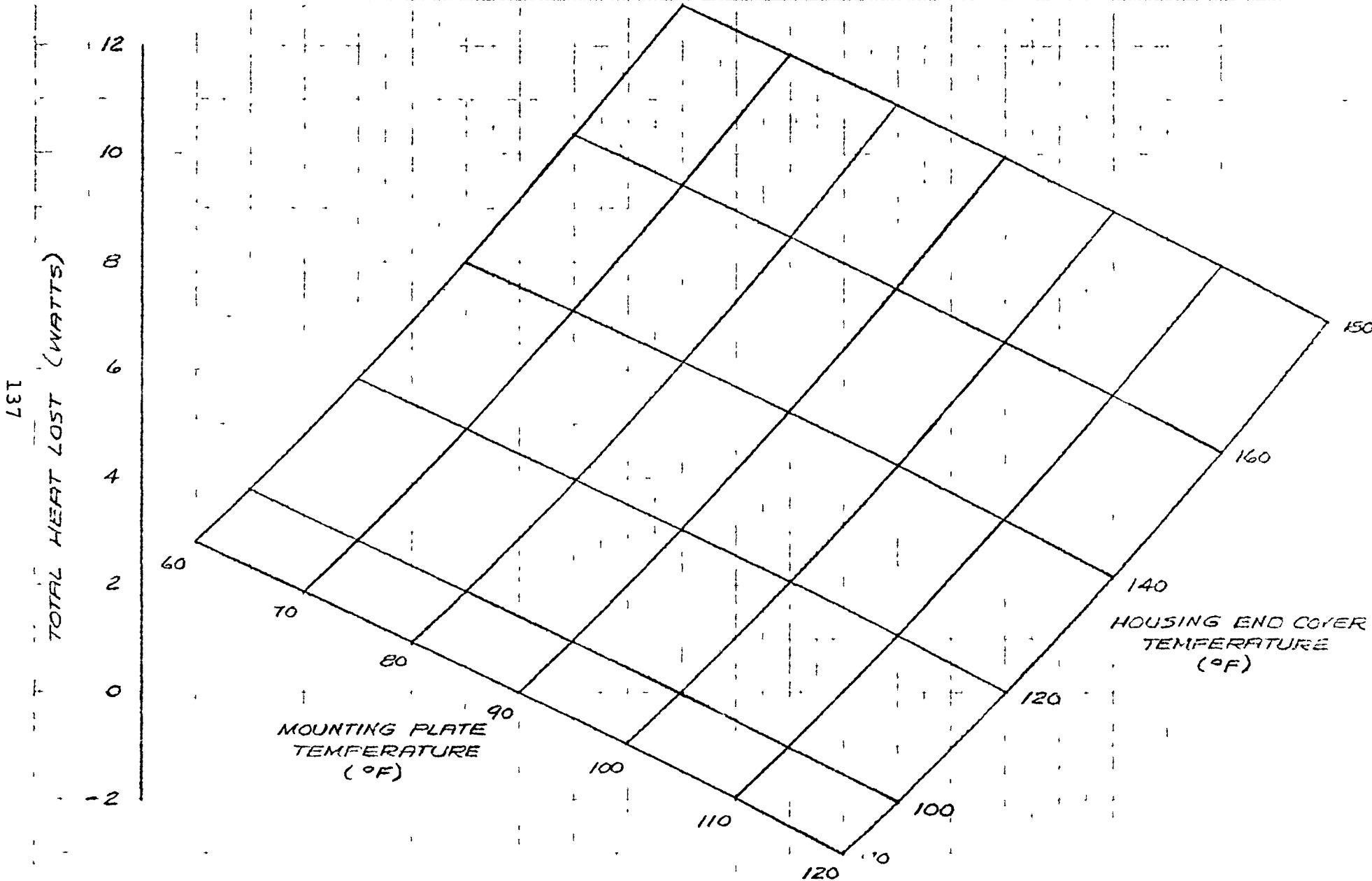
FIGURE 3.5.1.3-10
RADIATION HEAT TRANSFER FROM EHSA END COVER



136

FIGURE 3.5.1.3-11

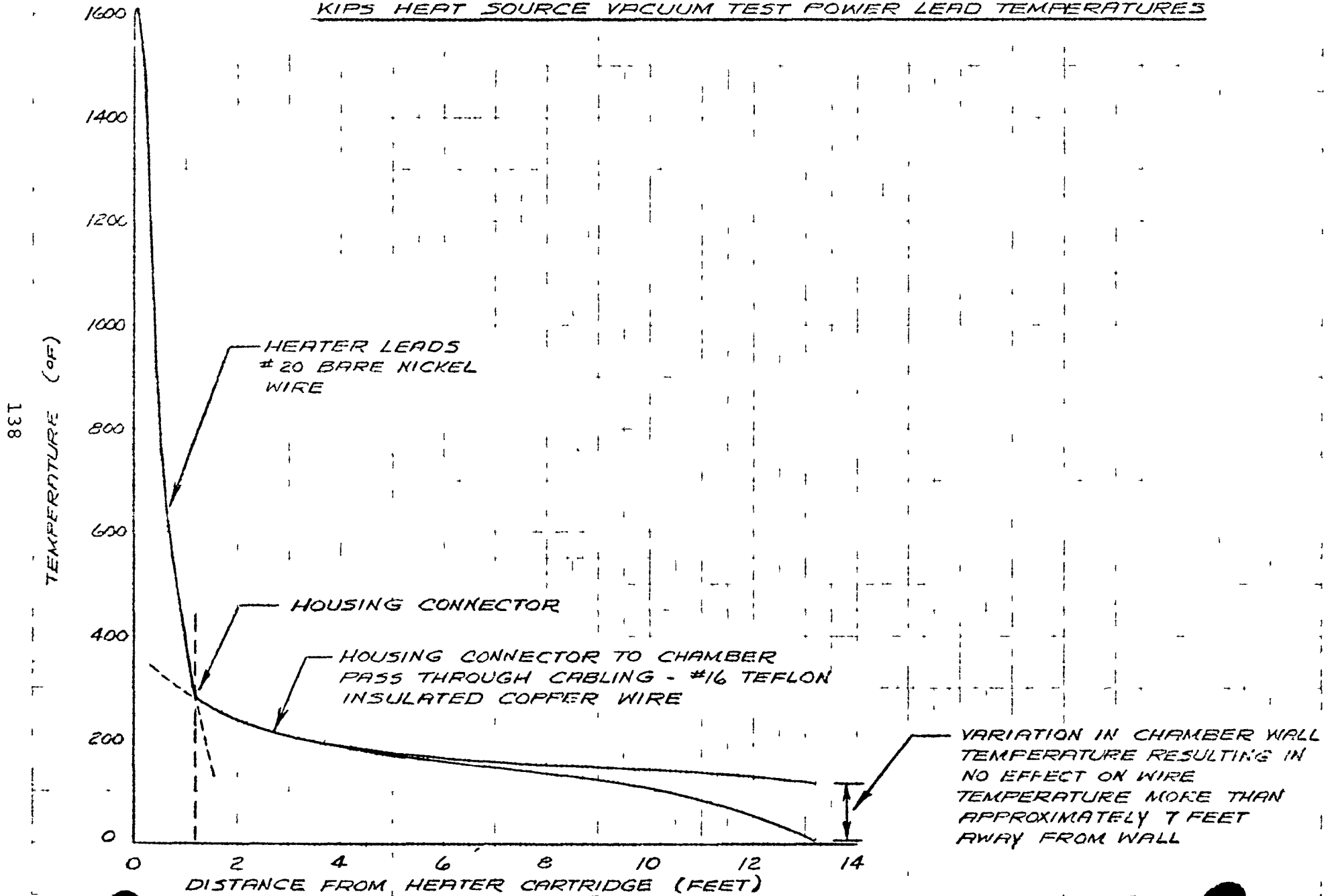
HEAT LOST FROM EHSR HOUSING LOWER END COVER TO MOUNTING PLATE AND SHROUD



137

FIGURE 3.5.1.3-12

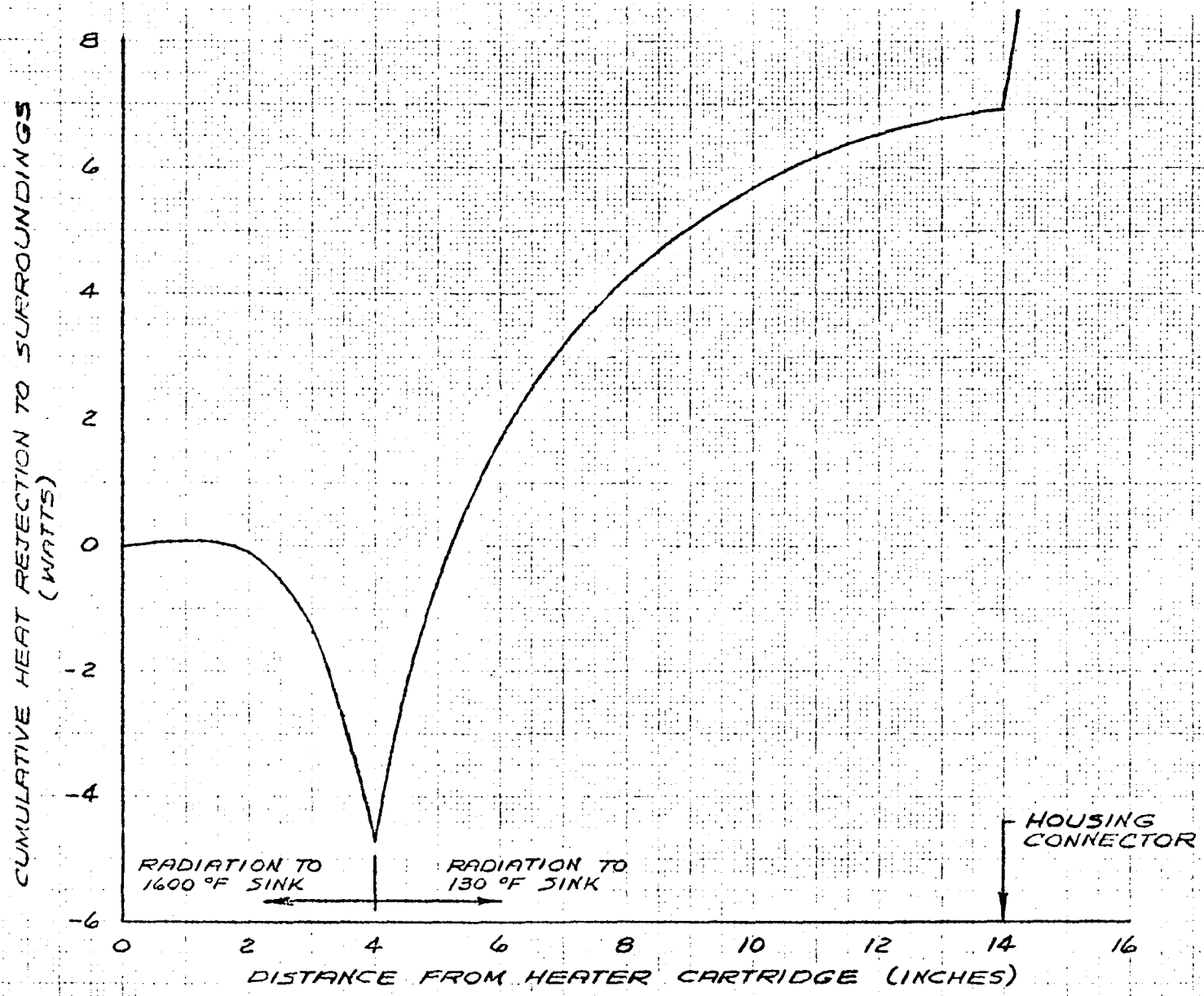
KIPS HEAT SOURCE VACUUM TEST POWER LEAD TEMPERATURES



138

FIGURE 3.5.1.3-13

KIPS HEAT SOURCE CUMULATIVE HEAT LOSS (WITHIN HEAT SOURCE)



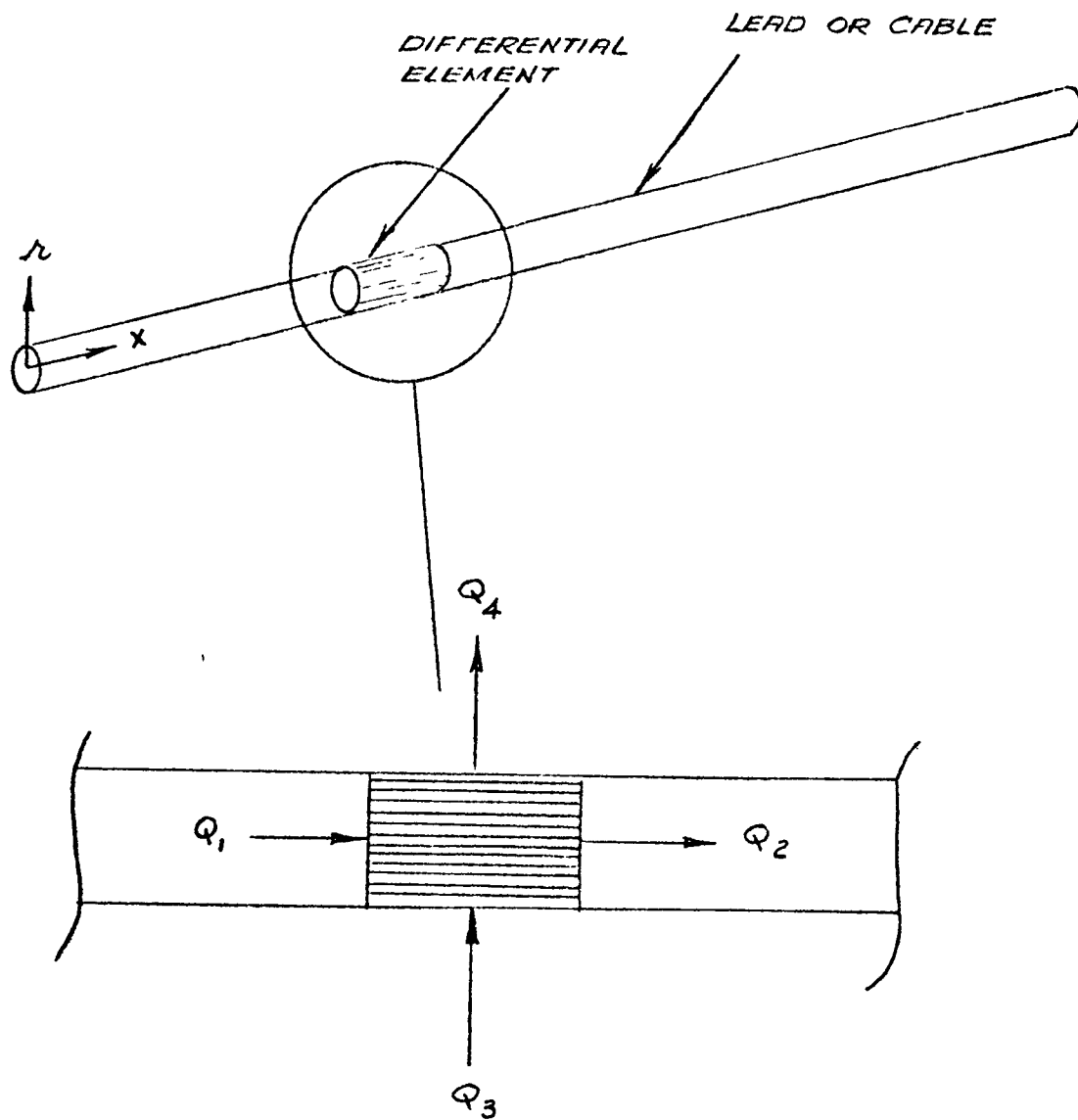
139

TABLE 3, 5. 1. 3-II

HEAT FLOW PATH AND ENVIRONMENT CHARACTERISTICS

Region	Heat Rejection Mode	Heat Flow Path Description	Environment
0 < x < 4" (heater leads)	Radiation	Area = 1/2 surface of a .375" dia. wire bundle Emissivity = .2	Constant sink at 1600°F
4" < x < 14" (heater leads)	Radiation	Area = surface of a .375" dia. wire bundle Emissivity = .2	Constant sink at 130°F
14" < x < 14.25" (connector pins)	Conduction	Area = .3924 sq. in. Length = .120 inches Conductivity = .622 Btu/hr-ft°F	Constant sink at 130°F
14.25" < x < 158.25"	Radiation	Area = surface of a .5 dia. wire bundle Emissivity = .7	Constant sink at 130°F
158.25 < x < 158.5" (connector pins)	Conduction	Area = .3924 sq. in. Length = .120 inches Conductivity = .622 btu/hr-ft°F	Variable from 0 to 100°F sink

FIGURE 3.5.1.3-14
HEAT BALANCE APPLIED TO DIFFERENTIAL ELEMENT



HEAT BALANCE : $Q_1 + Q_2 = Q_3 + Q_4$

A "buried pipe" analogy was first assumed for the heater leads inside the HSA that were completely surrounded by Min-K insulation. Resulting temperatures at the connector were unacceptably high, so rerouting of the wire next to the housing cover was requested. When this design change was incorporated, the wire was sufficiently close to the housing cover so as to lose heat to it directly by radiation. For analysis of the external cable it was assumed that 26 wires were bundled together to give a uniform cross sectional distribution of copper and insulation. An average effective conductivity in the radial direction was calculated by normalizing the conductivities of copper and teflon with their respective cross sectional areas. It was further assumed that the heat in the axial direction is conducted only by copper wires.

Code runs were made with successively smaller differential element lengths until further change had a negligible effect on temperatures and heat flows in order to assure accuracy of the answers. Solutions in the two regions (interior and exterior to the EHSA) were parameterized with respect to the housing connector temperature and heat conducted outward from the connector pins. The two solutions were matched graphically to determine the operating point.

Both the heater lead and supply cable codes divide the wiring into specific regions over which the environment is assumed constant, although several regions are considered over the total length of the wires. For the heater leads inside the housing, the first four inches of lead length are assumed to lose heat by radiation to a 1600°F constant temperature heat sink (the heater block itself is assumed to radiate to the housing end cover, which is acting as a constant 130°F sink. For the next 1/4 inch, the leads conduct through the glass and rubber connector pin potting to the 130°F housing. Total length is assumed 14-1/4 inches.

The supply cable from the housing connector to the vacuum chamber pass-through is assumed to radiate to the chamber walls over the first 12' 1/4" and then conducts heat to the vacuum chamber wall in an identical manner to the heat lost at the housing connector except that the chamber housing is not assumed to be at a fixed temperature. Code runs with various temperatures and heat flow rates at the chamber pass-through shows that the environmental effects at this point are damped out within a few feet inside the chamber. That is, the effect of radiation to the shroud overwhelms the effects of the local environment at the chamber pass-through.

Instrumentation Cable Heat Losses

In addition to the power cable heat loss, the thermocouple lead and extension wires dissipate heat from the EHSA. Temperatures of the platinum-rhodium thermocouple leads drops from 1600°F to 460°F and the copper lead extension provides a further drop of approximately 45°F. The 12 foot long copper/alloy II cable within the vacuum chamber gives another 200°F temperature drop. Total heat loss from the wires through the insulation was predicted to be about 0.23 watts, with 1.78 watts lost through the housing connector pins by conduction.

The temperature and heat flow profiles were calculated with the aid of a computer program similar to that used for analyzing the power cable. Heat flow path and environment characteristics are given in Table 3.5.1.3-III.

The thermocouple wires are assumed to be routed in a similar manner to the power leads. That is, the length of wire actually buried in the Min-K insulation is minimized by running the wire directly from the heater block assembly through the insulation to a point just below the end cover. Figure 3.5.1.2-1 shows the wire routing within the EHSA housing. Figures 3.5.1.3-15 and 3.5.1.3-16 present the temperature profile and heat loss profile for the thermocouple wire and lead wire within the vacuum chamber.

Material properties of only one leg of the thermocouple circuit are quoted. However, the same connector pin material is used for both legs, and there is little difference in the thermal conductivity of platinum 10% rhodium compared to platinum. Alloy II is pure copper with 1/2% of nickel, according to Dr. Harvey Albert of Englehard Industries, the principal manufacturer. No information could be found on the thermal conductivity of this material, so it is assumed to be the same as copper.

TABLE 3.5.1.3-III

HEAT FLOW PATH AND ENVIRONMENT CHARACTERISTICS

<u>Region</u>	<u>Heat Rejection Mode</u>	<u>Heat Flow (loss) Path Description</u>	<u>Environment</u>
0 < x < 2" (24 ga thermocouple wire)	Radiation	Area = 1/2 surface of a .020" dia. platinum - 10% rhodium wire emissivity = .2	1600°F sink
2 ≤ x < 10" (24 ga thermocouple wire)	Radiation	Area = surface of a .020" dia. platinum -10% rhodium wire emissivity = .2	130°F sink
10 ≤ x < 12" (24 ga copper extension wire)	Radiation	Area = surface of a .020" copper wire emissivity = .2	130°F sink
12 ≤ x < 12.25" (20 ga connector pins)	Conduction	Area = .3924 inches length = .120 inches conductivity - .622 Btu/hr-ft-°F	130°F sink
12.25 ≤ x < 156.25" (16 ga cable)	Radiation	Area = surface of a .5" dia. wire bundle emissivity = .7	Variable from 50 to 130°F sink

FIGURE 3.5.1.3-15

KIPS HEAT SOURCE VACUUM TEST THERMOCOUPLE WIRE TEMPERATURES

145

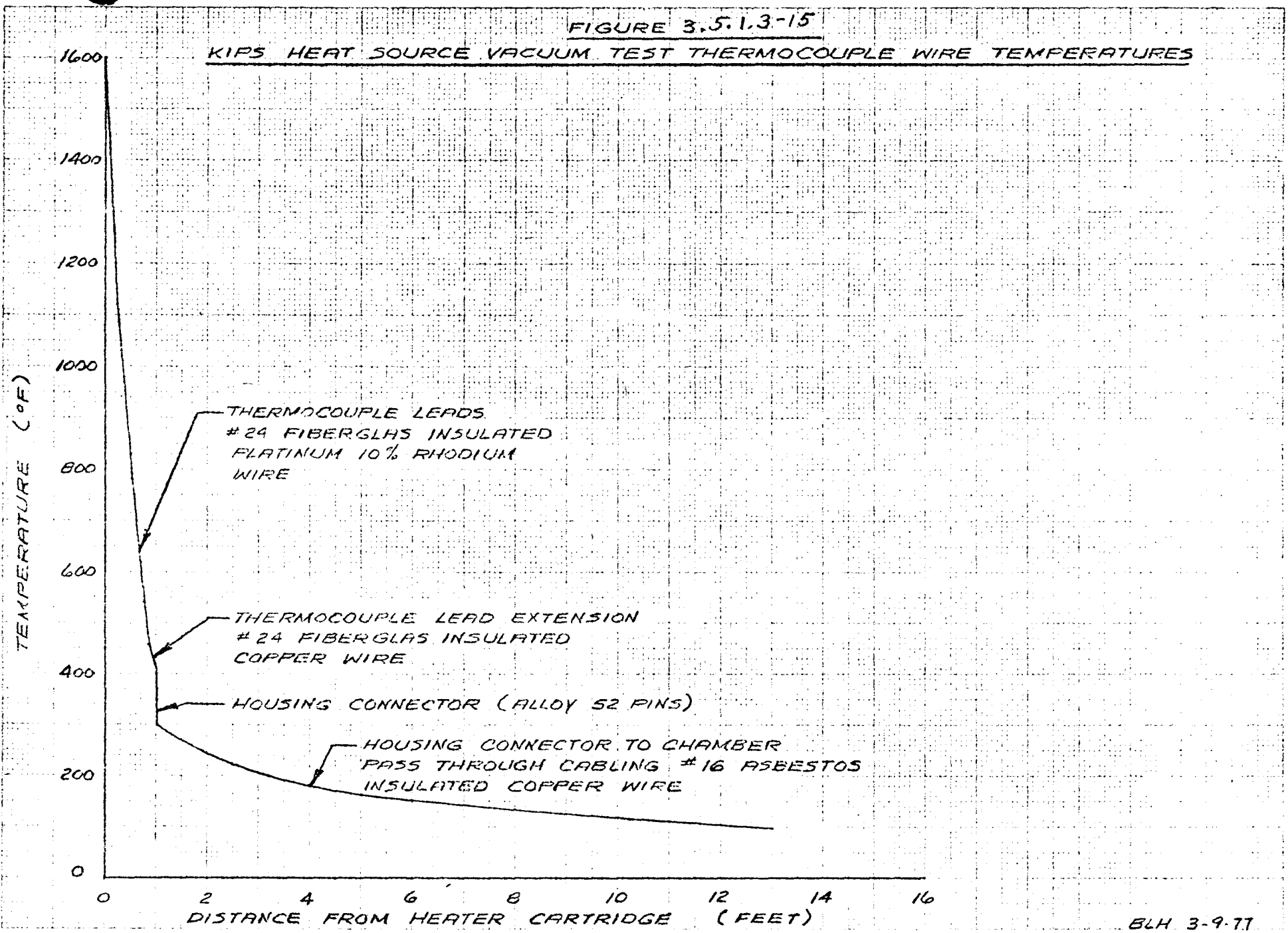
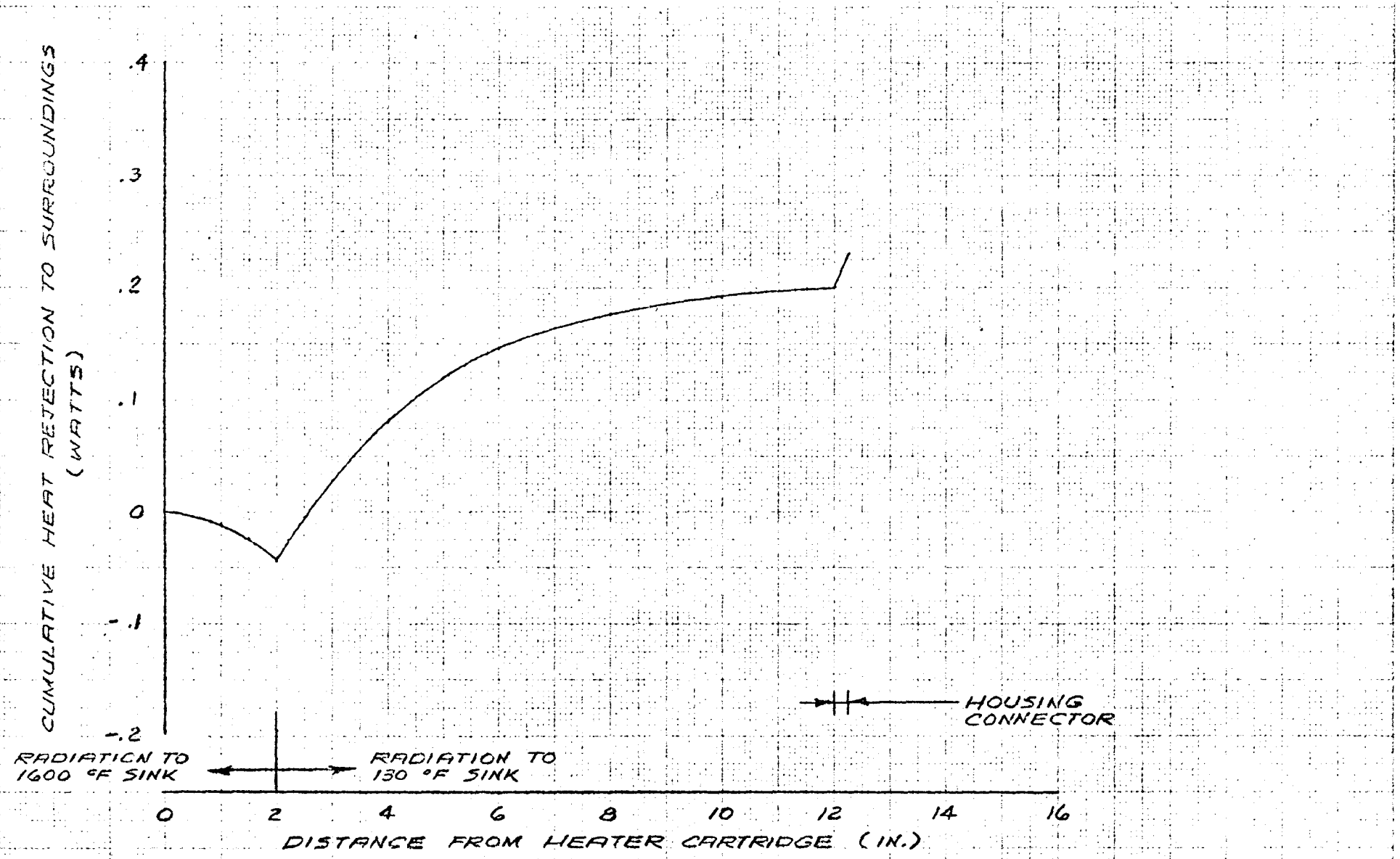


FIGURE 3.5-1.3-16

KIPS HEAT SOURCE CUMULATIVE THERMOCOUPLE WIRE HEAT LOSS
(WITHIN HEAT SOURCE)

146



3.5.1.3.2 Tests

Heater Cartridge Tests - Kips heater cartridges, when assembled inside a graphite block, are designed to provide the entire thermal input to the boiler, simulating isotope-decay heat during GDS testing of Electrical Heat Source Assembly (EHSA). In order to evaluate the capability of the heated cartridges to meet the design requirements and to establish the acceptance criteria for them, they were subjected to a series of tests. For convenience in installation in the test fixture, the first eighteen heater cartridges received from the vendor were divided into three groups of six each. The sequence of tests to which each group was subjected is indicated in Table 3.5.1.3-IV. A schematic diagram of the test setup is shown in Figure 3.5.1.3-17.

Upon receipt from the vendor all the heaters were baked-out¹ at 400° F and 1 μ vacuum inside a thermal vacuum furnace for sixteen hours; whereupon they were installed inside three bell jars. The heaters were then burned-in² under vacuum for four to six hours, first at 400° F and then at 2000° F. This initial bake-out and burn-in process was devised as heater cartridge acceptance test, so that not all the heaters would have to be subjected to the rigorous testing program planned for the first batch of eighteen heaters. Two groups of heaters were subsequently maintained at steady sheath temperature of 1800° F for a period of one week each in vacuum and argon environment respectively. At the end of two weeks test under steady state, the two groups of heaters were subjected to maximum power test, which simulates a condition of the heater cartridge performance capability, wherein one of the two parallel strings of six heaters is open circuited and the entire electrical load must be carried by the second string of six heater cartridges. The third group of heaters, after the one-week steady state test in vacuum, was passed through thermal-cycling test. The heaters were tested through thirty cycles between 500° F and 1800° F in vacuum. Subsequent to thermal cycling test, these heaters were placed on life-test, which has been in operation for ten months, as of the date of this report.

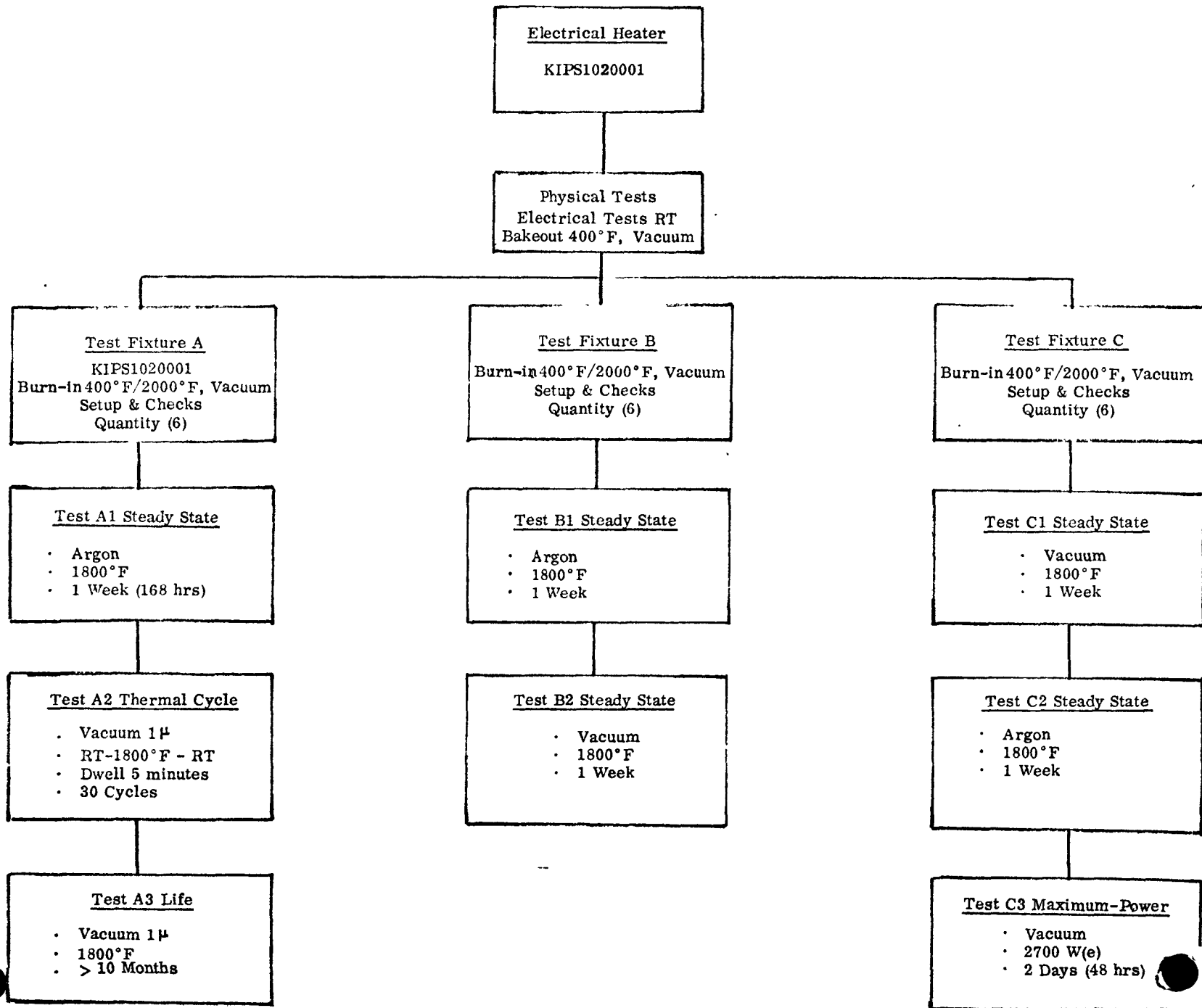
It is found after these extensive tests on the first eighteen cartridges that there was no significant change in the electrical resistance of the heaters as a result of these tests; including the case of the maximum power test. The results of the life-test under steady state conditions in vacuum are plotted in Figure 3.5.1.3-18. The evidence indicates

¹ Baked-out - Exposed to the high temperature environment without electrical current flowing through the heaters.

² Burn-in - Heated internally by passing electrical current through the heaters.

TABLE 3.5.1.3-IV

KIPS ELECTRICAL HEATER CARTRIDGE THERMAL TEST PROGRAM



149

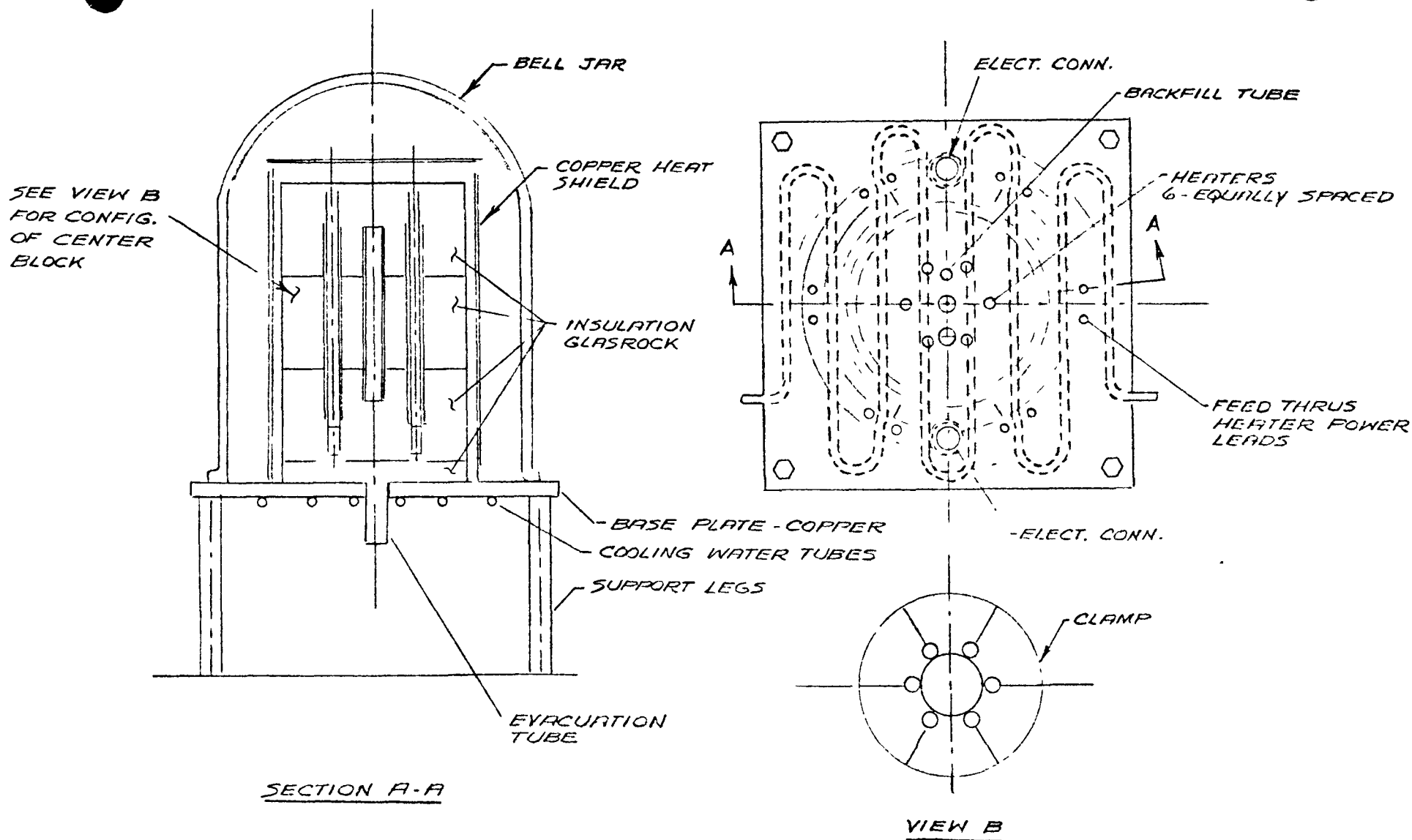


FIGURE 3.5.1.3-17
HEATER CARTRIDGE TEST SET-UP

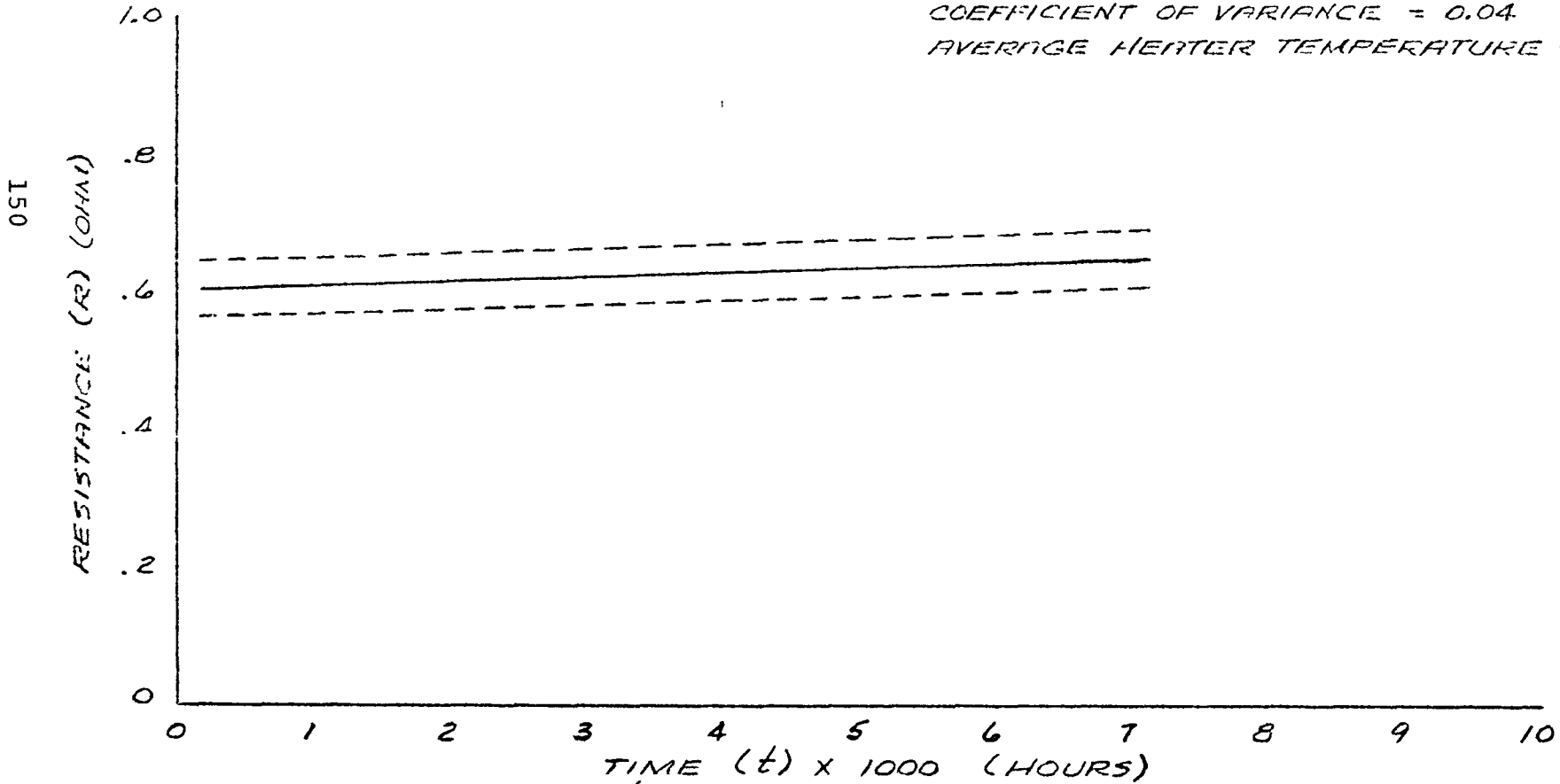
FIGURE 3.5.1.3-18
KIPS ELECTRICAL HEATER CARTRIDGE CIRCUIT RESISTANCE VERSUS
OPERATING TIME
MEAN AND 95% PROBABILITY INTERVAL
FIVE TEST SAMPLES

EQUATION:

$$R = .6029 + 6.7152 \times 10^{-5} t$$

COEFFICIENT OF VARIANCE = 0.04

AVERAGE HEATER TEMPERATURE = 1750 °F



that there is a gradual increase in resistance with time and is about 8.3% in 7000 hours. The spread in the data is relatively narrow as indicated by the coefficient of variance of less than 0.04 or 4%.

It is seen from the statistical results of the acceptance tests summarized in Table 3.5.1.3-V, that all the heater cartridges with the exception of nine (listed separately), show a change in resistance between that measured before bake-out and after burn-in, of less than 7%. The departure from the $\pm 7\%$ deviation, of these nine heaters is construed to be due to measurement difficulty and hence, it was not felt necessary to discard these heaters as unacceptable.

TABLE 3.5.1.3-V

SUMMARY OF STATISTICAL EVALUATION OF
HEATER CARTRIDGE CIRCUIT RESISTANCE

IDENTIFY		SUPPLIER	TELEDYNE ENERGY SYSTEMS			
Test Heater Block	Heater Element	KIPS1020001	KIPS1020300			Δ Chg (%)
		Post-Bake	Pre-400° F	Post-400° F	Post-2000° F	
S/N 1001 -019 (1-14)	\bar{X} s	.116 .002	- -	.118 .011	.105 .005	- -
S/N 2001 -009 (33-44)	\bar{X} s	.111 .001	.112 .003	.112 .002	.106 .001	- 4.93 2.58
S/N 2003 -009 (45-56)	\bar{X} s	.113 .002	.113 .002	- -	.109 .001	- 1.30 1.77
S/N 2004 -009 (57-68)	\bar{X} s	.114 .002	.112 .005	.109 .002	.106 .001	- 5.32 3.98
S/N 2002 -009 (69-80)	\bar{X} s	.112 .001	.112 .002	.111 .001	.106 .001	- 5.26 1.64
S/N 1002 -019 (31-92)	\bar{X} s	.111 .001	.113 .003	.110 .002	.107 .001	- 4.45 2.84
Spare (93-104)	\bar{X} s	.110 .001	.111 .003	.111 .002	.107 .001	- 3.42 1.99
105	-					\bar{X} - 4.11 s 1.55
S/N	S/N		*		*	
2001	34	.112	.120	.111	.106	- 11.67
2004	62	.115	.118	.109	.107	- 9.32
2004	63	.113	.116	.109	.107	- 7.76
2004	65	.115	.126	.109	.107	- 15.08
2002	72	.114	.117	.112	.107	- 8.55
2002	77	.113	.115	.111	.106	- 7.83
1002	81	.110	.118	.109	.106	- 10.17
1002	82	.112	.118	.111	.108	- 8.48
Spare	94	.113	.118	.112	.108	- 8.48

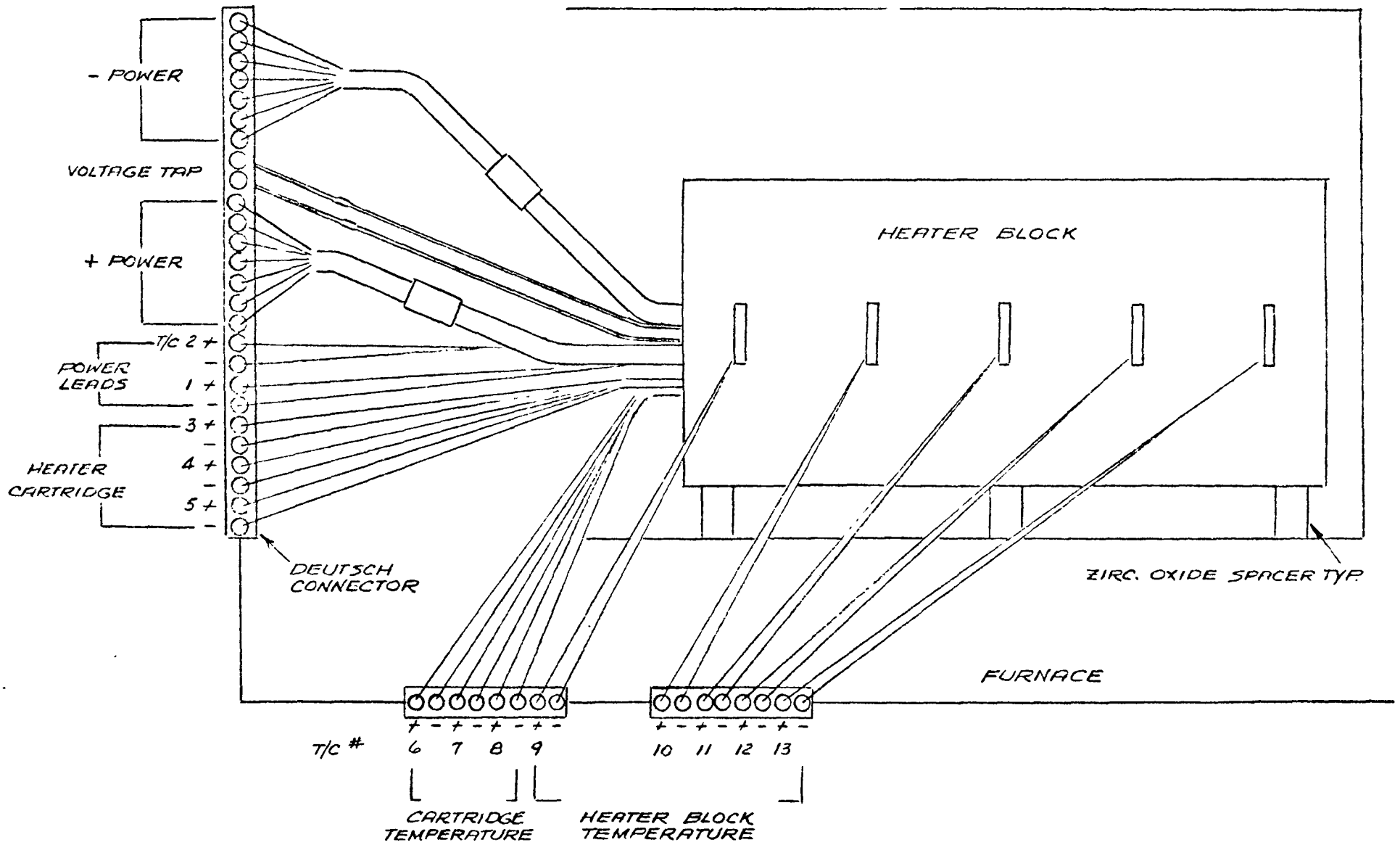
* Different measurement technique.

Electrical Heater Block Test - The first Electrical Heater Block Assembly (EHSA), consisting of twelve heater cartridges arranged in two parallel strings of six each inside a graphite block, was tested in order to determine its performance capability and to establish the acceptance criteria for subsequent assemblies. In order to obtain the temperature profile, five thermocouples were placed along the surface of the heater block and three thermocouples were attached to the heater cartridge sheath; both being in the same plane of symmetry. In addition, three thermocouples were placed on another heater cartridge sheath at 90° from the aforementioned plane. The heater block was placed inside a thermal vacuum furnace, that was evacuated to 1.5×10^{-5} torr or less. A 2400 watt electrical power input was applied to the heater block and the furnace wall heaters were adjusted until a steady state surface temperature of $1550 \pm 25^\circ\text{F}$ was reached at the heater block. This condition was maintained for a period of 24 hours, during which the circuit current and the voltage drop across the heater block were measured. A schematic diagram of the test setup is shown in Figure 3.5.1.3-19.

The steady state temperature distribution obtained during the test is shown in Figure 3.5.1.3-21. The difference between the front and the middle surface T/C's is approximately 45°F , whereas, that between the rear and the middle surface T/C's is approximately 90°F . The lesser temperature drop in front may be due to the presence of hot power leads there. An average overall temperature drop between an effective internal cylinder made of heater cartridge sheaths and the outer heater block surface was approximately 190°F . This temperature drop was found to be within acceptable levels and indicates the effectiveness of drilling the holes in the heater block by matching the diameters of the individual heaters. The 8-mil tolerance used in drilling the holes appears to be adequate. From the electrical measurements, it was noticed that the average circuit current drawn by the heater block under steady state condition was approximately 36.18 amps. The heater block circuit resistance was approximately 1.846Ω . The change in the circuit resistance before and after the heat treatment was found to be less than 1%. The insulation resistance between the power leads and the heater block surface, though reduced slightly during the heat treatment, was still very high ($300 \text{ M}\Omega$). At no time during the test was any surge in the vacuum pressure of the furnace noticed (due to outgassing of the graphite block), and the initial evacuation of the furnace to a very low vacuum level was achieved in a very short period. Thus, it can be said that the quality and condition of the graphite used in the heater block appeared to be very good.

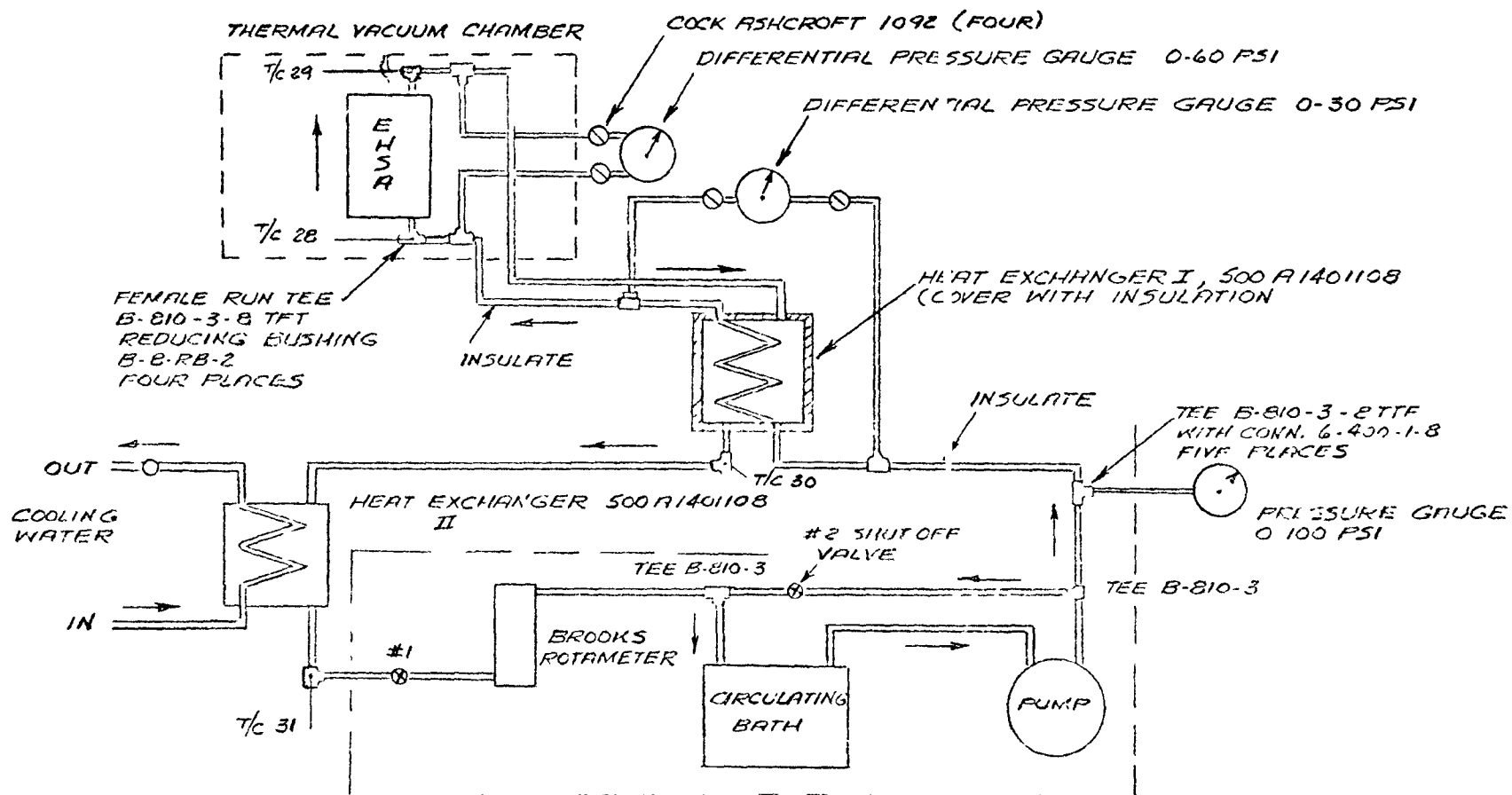
EHSA Performance Test - The Electrical Heat Source Assembly (EHSA) which consists of a radiation barrier, boiler, multifoil insulation and an electrical heater block assembly, was tested inside a thermal vacuum chamber in order to evaluate its performance and to determine the heat losses. The EHSA was connected to the Dowtherm flow loop as shown in Figure 3.5.1.3-20. The thermal vacuum chamber was evacuated to less than 1μ . The test was performed for three different flow rates. An attempt was made to keep the temperature of the fluid entering the boiler constant at three different values. Unfortunately, due to limitations imposed by the test setup,

FIGURE 3.5.1. 3-19
TEST SET-UP IN TM VACUUM FURNACE



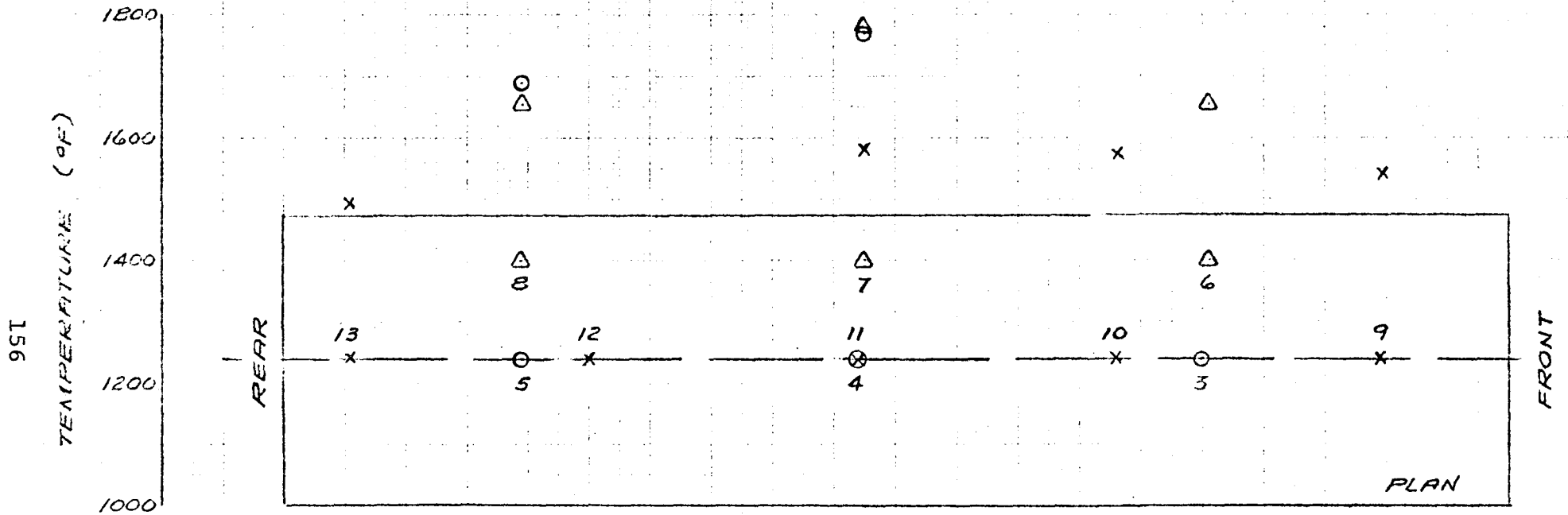
154

FIGURE 3.5.1.3-20
EH5A TEST FLOW DIAGRAM



T/Cs 28, 29, 30, 31 ARE TYPE K CHROMEL / ALUMEL THERMOCOUPLE IMMERSION PROBES
ALL TUBES EXCEPT THOSE CONNECTED TO PRESSURE GAUGES ARE 0.50 NOM. DIA.

FIGURE 3.5.1.3-21
HEATER BLOCK TEMPERATURE PROFILE



RELATIVE POSITION OF THERMOCOUPLES :

- 3, 4, 5, 6, 7, 8 - HEATER CARTRIDGE SHEATH T/C S
- 9, 10, 11, 12, 13 - HEATER BLOCK SURFACE T/C S

it became difficult to control the temperature exactly. Moreover, it was not possible to exceed 425° F at the boiler inlet. A 2400 watt electrical power input was supplied to the EHSA heaters.

The heat lost from the EHSA is that part of the total heat input to the EHSA, which is not carried away by the boiler due to change in internal energy of the fluid flowing through it. One way of determining the heat losses is to find the difference in the amount of electrical power that is supplied to the unit and the equivalent amount that is carried away by the boiler fluid. The second way, which is more involved, is to calculate the heat losses directly by knowing the temperature of the various components of the EHSA and its surroundings. Because of its inherent simplicity, the heat losses determined by the first method should give better indication of its magnitude. However, the determination of heat losses by this method is strongly dependent on the accuracy of flow measurement. In particular, it is found that the uncertainty in the measurement of heat removed by the boiler could be as large as 8%, whereas, the amount of heat loss from the EHSA is not expected to exceed 5% of the total power input.

The results of the test are summarized in Table 3.5.1.3-VI. Typical equilibrium temperatures of the various EHSA components and the amount of heat carried away by the fluid inside the boiler are indicated in that table. Most of the components of the EHSA are seen to be at their nominal temperatures. The increase in the boiler tube Reynolds number is believed to be associated with improvement in the convective heat transfer coefficient and as a consequence the boiler fin-root temperature drops and so does the boiler fin temperature. It was observed that the temperature difference between the boiler fin and the fin-root is independent of the flow rate and remains constant at $50 \pm 4^\circ \text{F}$, over the range of flow considered in the test. It is seen that at nominal flow rate (.0285 lbs/sec) the amount of heat carried away by the boiler fluid is approximately 2300 watts. The boiler in this particular EHSA did not have the center body in it. Thus, its effect on the amount of heat carried away by the boiler fluid could not be determined. However, it is believed that the presence of the center body inside the boiler tube would enhance the amount of heat removed by the boiler. It was found that, due to specific location of the thermocouples, the inside temperature of the multifoil insulation is higher than the average boiler temperature. It indicates that there is a local back flow of heat from the multifoil insulation "can" to the boiler where the boiler is relatively cooler due to the presence of tubes.

The calculated heat losses from various surfaces of the EHSA based on their average temperature are given in Table 3.5.1.3-VII. Although these heat losses are dependent on use of appropriate thermal properties of the EHSA components, they are found to be approximately 3.5% of the nominal power input. These heat losses are expected to be still lower in the production units, since in the test unit the effective thermal conductivity of the multifoil insulation is found to be slightly higher due to dimensional changes in the boiler.

TABLE 3.5.1.3-VI

SUMMARY OF THE TEST RESULTS

Average Vacuum Pressure mm Hg	Flowmeter <small>Beckman</small>		Average Boiler Inlet Temp. °F	Average Boiler Outlet °F	Diff. °F	Average Heater Block Temp. (1 + 2 + 3)/3	Average Radiation Barrier (4 + 5 + 6)/3	Average Boiler (7 + 8 + 9 + 13) 4	Multifoil (10 + 11) 2	Average Sp. Heat between Inlet & Outlet Temp. Btu/lb °F	Heat Carried Away by Boiler Watts	Average Housing Temperature (15 + 16 + 17)/3	Average T.V. Chamber Temperature (°F)
	Scale	lbs/sec											
1.336×10^{-4}	5	.0234	412	595	173	1354	1067	614	655	.539	2302	211	121
2.223×10^{-4}	6	.0285	397	543	146	1353	1054	590	632	.529	2322	204	115 I
1.86×10^{-4}	7	.0338	371	501	130	1347	1048	561	608	.513	2378	205	118
1.15×10^{-4}	5	.0234	428	557	169	1356	1070	626	666	.545	2274	214	124
$.903 \times 10^{-4}$	6	.0285	427	509	142	1355	1068	614	658	.537	2293	214	126 II
$.631 \times 10^{-4}$	7	.0338	412	538	126	1351	1063	610	643	.529	2377	213	127

NOTE: Numbers in parentheses under column titles are thermocouple numbers.

TABLE 3.5.1.3-VII

A SUMMARY OF HEAT LOSSES FROM EISA
BASED ON VARIOUS COMPONENT TEMPERATURES

From the cylindrical portion of housing	60 watts
From top of housing (inlet side)	8 watts
From bottom of housing (outlet side)	8 watts
From electrical cable	< 3 watts
From instrument cable	< 4 watts
From Dowtherm tube	< 1 watt
	<hr/>
Total	84 watts

EHSA Acceptance Tests - All the KIPS Electrical Heat Source Assemblies were performance-tested before their acceptance and delivery for use in the GDS. These tests were performed under room temperature environment after the unit had been leak-checked and outgassed. The tests were designed to verify the normal operating performance of the units. The test setup and Dowtherm flow loop are indicated in Figure 3.5.1.3-20 with the exception that in these tests Dowtherm was passed through 0.25 inch auxiliary tube of the boiler in order to avoid contamination of the main 0.5 inch tube. The tests were performed for three different flow rates of Dowtherm; in each case the temperature of Dowtherm at inlet to the boiler was maintained at $400 \pm 5^\circ\text{F}$ and 2400 watt electrical power was supplied to the heater block. Steady state conditions were maintained for a period of $1 \pm 1/4$ hour, during which circuit current, voltage drop, pressure difference, flow rate, inlet and outlet boiler temperatures were measured. The amount of heat carried away by Dowtherm flowing through the boiler was calculated as follows:

$$H = m C_p (T_2 - T_1) 3600/3.412 \text{ watt}$$

where,

m = mass flow rate of Dowtherm lbs/sec

T_2 = average boiler outlet temperature $^\circ\text{F}$

T_1 = average boiler inlet temperature $^\circ\text{F}$

C_p = average of the specific heat of Dowtherm at boiler inlet and outlet temperatures, Btu/lb- $^\circ\text{F}$

The typical values of H for four electrical heat source assemblies are given in Table 3.5.1.3-VIII. The variation in the results is within the range of uncertainty in the measurement technique. The results for the nominal flow rate of .0285 lbs/sec seem to indicate that heat losses are uniformly controlled in all the units.

TABLE 3.5.1.3-VIII

EHSA ACCEPTANCE TEST DATA

Flow Rate lbs/sec	Heat Removed by EHSA Boiler (Watt)			
	#2	#3	#4	#5
.0234	2309	2263	2252	2290
.0285	2350	2352	2327	2382
.0338	2343	2353	2262	2390

3.5.1.4 Emergency Cooling System (ECS)

The ECS for the GDS heat source assembly is identical to that proposed for the flight system. For a description and analysis see Section 2.5.1.4. In Section 2.5.1.4 the results of a full scale test of the emergency cooling system of an electrically heated heat source assembly are described. This test was conducted in support of the flight system ECS design concept and was conducted by simulating the actual failure of the working fluid loop.

3.5.1.5

Venting/Gas Management

The gas management system for the electrical heat source assembly consists of outgassing ports at each end of the EHSA, located on the covers. At the non-loading end the port is capped off for normal operations. At the EHSA loading end the outgassing assembly consists of a manual valve and a pressure/vacuum gauge. After outgassing the EHSA is backfilled with an inert gas (argon) to a nominal pressure of 5 psig. For performance testing where the unit requires evacuation to minimize parasitic heat losses the valve must be opened by hand. For Phase II the EHSA design will have a PRD incorporated into one outgassing port for gas management during T/V testing and for functional checkout tests of the PRD.

3.5.1.6 Reliability

The electrical heat source assembly is described in Section 3.5.1.2. Table 3.5.1.6-I presents the Failure Mode Effects and Criticality Analysis (FMECA) for the electrical heat source assembly. Table 3.5.1.6-II and Figure 3.5.1.6-1 presents the GDS electrical heat source assembly enclosure gas seal leak points.

TABLE 3.5.1.6-I

FAILURE MODE AND EFFECTS ANALYSIS

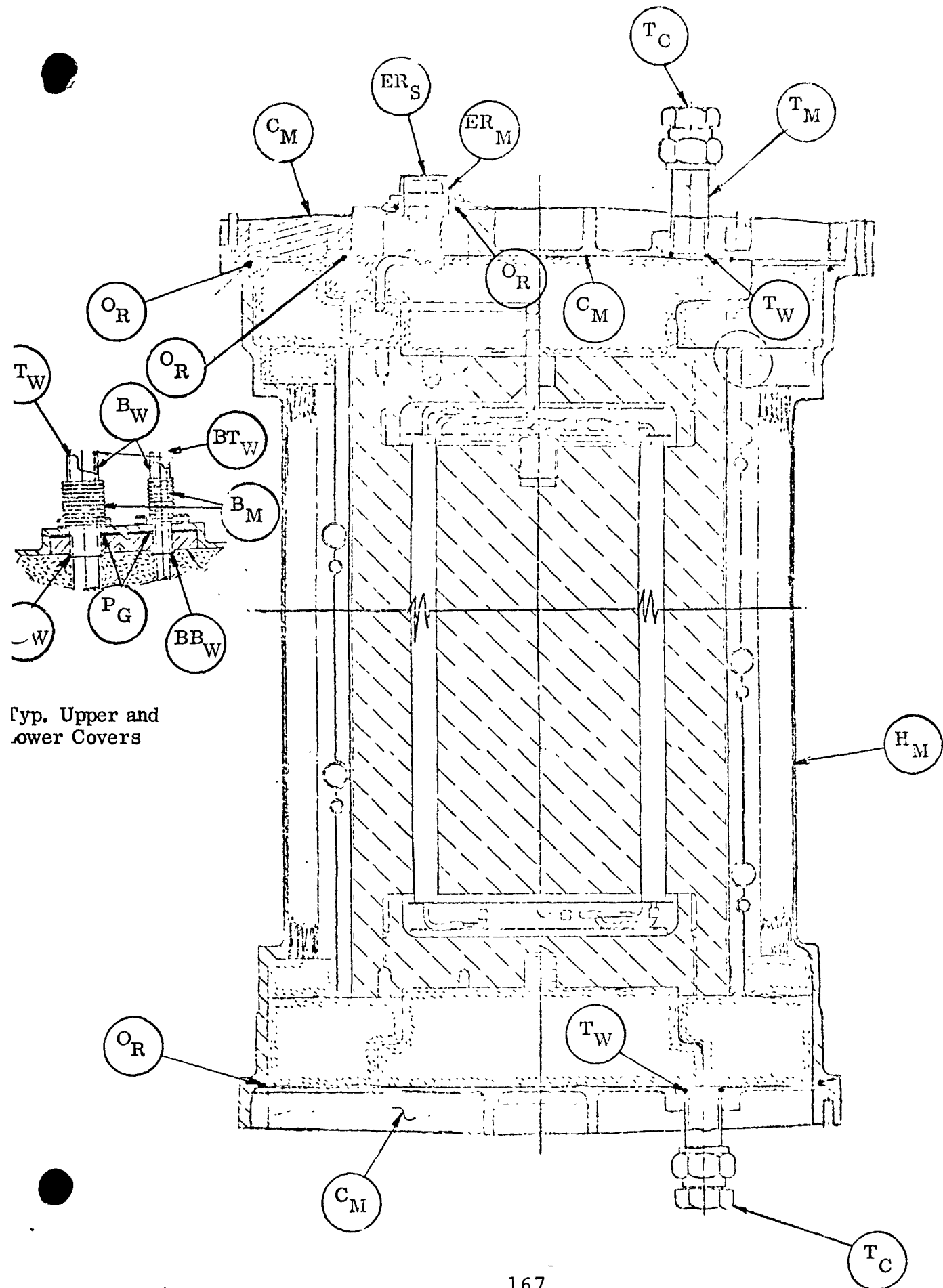
NO.	COMPONENT & FUNCTION	FAILURE MODES (FM)	POSSIBLE FAILURE CAUSES	FAILURE EFFECT (FE)	DESIGN/SAFETY CONSIDERATIONS	③ CRITICALITY RANK ① x ② = ③ ② FE RANK ① FM LIKELIHOOD		
						①	②	③
2.0	<u>Heat Source - Electric (HSE)</u>							
2.1	Supply heat for the Ground Demonstration System (GDS) (12 heater elements - parallel connected)	Open circuit (individual element lead)	Crimp splice failure	No loss of heat output - may have slight non-uniform heat distribution	Required heat can be supplied with up to 9 element failures Pre & Post crimp sample tests (pull test samples)	5	5	25
			Air exposures	Embrittlement of nickel leads due to EHDS/housing seal leak	Continuous inert gas supply to Heat Source cavity HSE can operate in air under 1400°F range	25	5	125
		Short	Fibreglass sleeving, ceramic bead failure or shift Heater sheathing burned during welding	Loss of heater element or total heater	Dielectric and insulation between heater circuits and heater block tested	5	100	500
2.2	Receptacle	Open	Broken wire handling	Reduced heat output	AC in and out redundant 8 & 9 strand per pin	5	50	250
		Short	Solder run Foreign matter	Loss of heater output	QC and N. D. T. dielectric and insulation resistance tests	5	100	500

TABLE 3.5.1.6-II

KIPS GDS HEAT SOURCE ENCLOSURE, GAS SEAL LEAK POINTS

<u>Code</u>	<u>Description</u>	<u>Quantity</u>
H _M	Housing Material	1
O _R	"O" Ring, Lower Cover	1
T _W	Tube/Lower Cover Weld	1
T _M	Tube Material	1
C _M	Cover Material, Lower	1
O _R	"O" Ring, Upper Cover - Outer	1
O _R	"O" Ring, Upper Cover - Inner	1
C _M	Cover Material - Upper, Outer	1
ER _S	Electrical Receptacle Insert Seal	2
ER _M	Electrical Receptacle Shell Material	2
O _R	"O" Ring-Receptacle	2
C _M	Cover Material, Upper Inner	1
T _W	Tube/Cover Weld - Upper Inner	1
T _M	Tube Material - Upper Inner	1
T _C	Tube Cap - Upper Inner Swageloc	1
BB _W	Bellows/Block Weld	4
B _M	Bellows Material	4
B _W	Bellows Weld	4
BT _W	Bellows/Tube Weld	4
P _G	Penetration Assembly Gasket	4

FIGURE 3.5.1.6-1: KIPS GDS ELECTRIC HEAT SOURCE ASSEMBLY ENCLOSURE
GAS SEAL LEAK FAILURE POINTS



Typ. Upper and Lower Covers

3.5.2.6 Radiator

3.5.2.6.1 Configuration

The GDS radiator assembly is an aluminum, welded/riveted assembly in the shape of a hollow right circular cylinder measuring 48.50 inches outside diameter by 111.75 inches long (at mounting feet) and weighs 80 pounds. See Table 3.5.2.6-I. It has three mounting points which extend approximately 2.81 inches below the radiator skin in order to provide clearance for tubing connections to the outlet header assembly. See Figure 3.5.2.6-1.

The radiator employs a forced convection heat transfer loop. The organic fluid passes through sixteen vertical tube extrusions which are connected, at each end through an adapter fitting, to a common header, Figure 3.5.2.6-2. Each extrusion, Figure 3.5.2.6-3, serves three purposes: as a passageway for the organic fluid, as the required frontside and backside meteoroid armor protection and as vertical stiffening for the radiator shell. The headers are made from a 0.500 inch outside diameter by 0.062 inch wall tube which is formed to a circular shape. They are protected from meteoroid puncture by a shadow shield which is attached to the radiator structure.

The 0.025 inch thick radiator skin is spliced together at four places (because the available range of standard sheet widths is limited) by means of splice plates which are riveted in place. The extruded radiator tubes are seam welded to the skin prior to the sections being spliced together. Nine circumferential channel frames are riveted to the skin for structural support.

After the radiator has been fabricated and inspected, the exterior surfaces are coated with IITRI* Z-93 thermal control coating. Z-93 is an inorganic type coating developed by IITRI which is composed of a zinc oxide (ZnO) pigment with a potassium silicate (K_2SiO_4) binder. Typical optical properties measured on 4 to 6 mil thick coating samples are summarized in Table 3.5.2.6-VI. The coating selected offers acceptable performance (material properties) coupled with ease of application, reproducibility, and ready repairability.

Evolution of the radiator design was the result of analysis and testing as described in the next section. Pressure drop flow tests were conducted in several sizes of tubing to determine the optimum radiator tube size. After the tube size was established, a four foot long, four tube section was tested. This test was followed by a test of a full length, four tube radiator section. Aside from the length differences, the sections were identical, except for the header to tube connections, see Figure 3.5.2.6-4. In addition to becoming test articles, these sections were used to develop weld parameters to be used as the basis for welding the extrusions to the skin on the full scale radiator. The tests and analysis are described more fully in a subsequent section.

NOTE: * IITRI - Illinois Institute of Technology Research Institute

TABLE 3.5.2.6-I
RADIATOR WEIGHT BREAKDOWN

<u>Component</u>	<u>Weight (lbs)</u>
Radiator Skin	40.18
Skin Splices	1.68
Tube Extrusions	10.40
Frames	10.36*
Meteoroid Shadow Shields	2.40*
Headers and Adaptor Fittings	2.79
Emissive Coating	5.80
Mounting Provisions	6.33
Total	<u>79.94 lbs*</u>

* The calculated weight of these components is based upon 0.032 inch material. The method used to fabricate these components (spinning) requires that the stock material be in one piece and to accomplish this, a piece of material approximately 52 inches square is required. Standard width sheets of aluminum, in 0.032 inch thickness, do not go beyond 48.00 inches, unless a special mill run is ordered. Therefore, in order to obtain the proper stock size material, within schedule and cost restraints, thicker (0.062 inch) material, which was in stock, had to be ordered. The increased material thickness results in a frame weight of 21.46 pounds and a shield weight of 4.80 pounds. The weight of the GDS radiator is therefore 93.44 pounds.

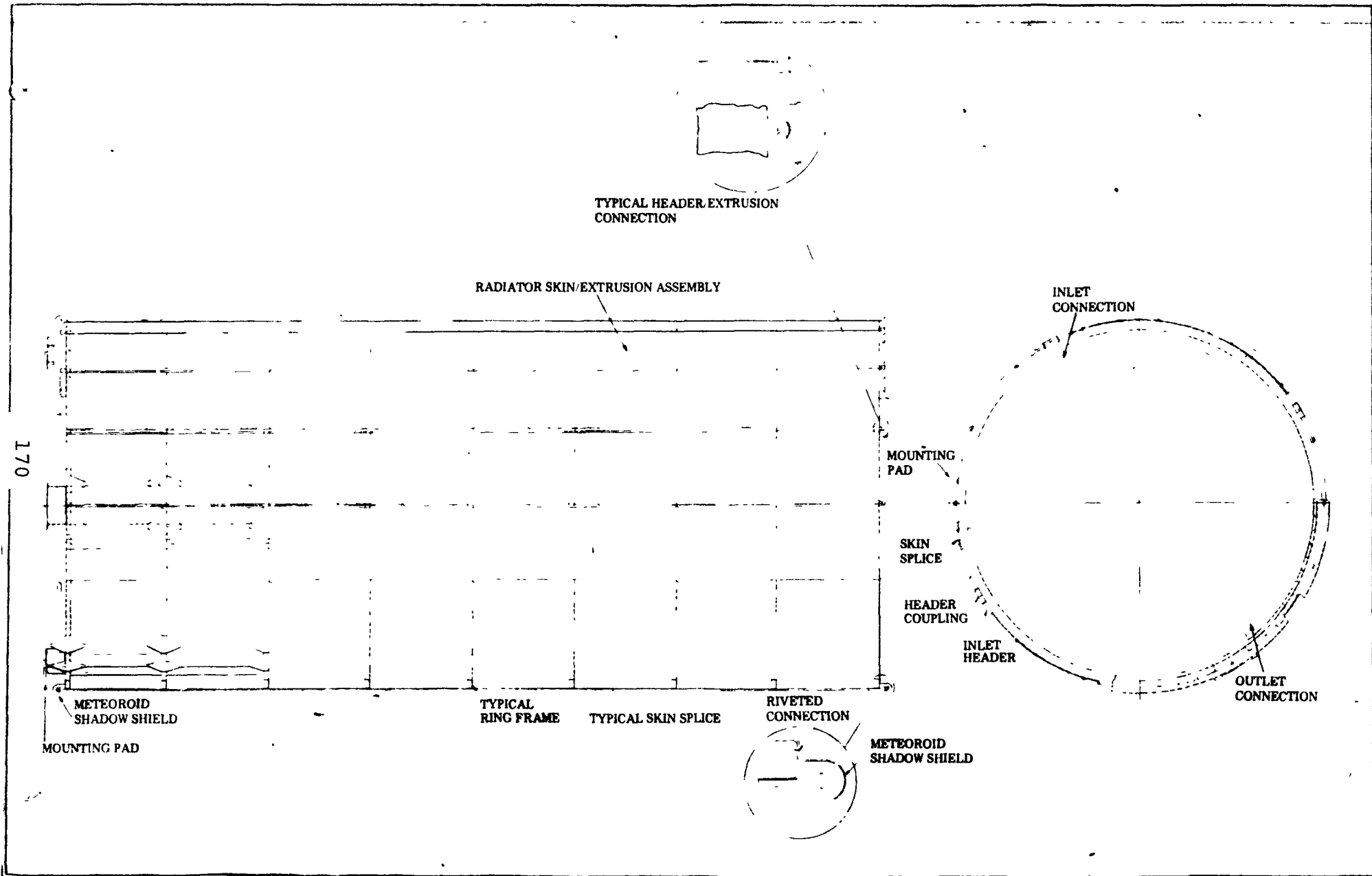


FIGURE 3.5.2.6-1 GROUND DEMONSTRATION SYSTEM RADIATOR ASSEMBLY

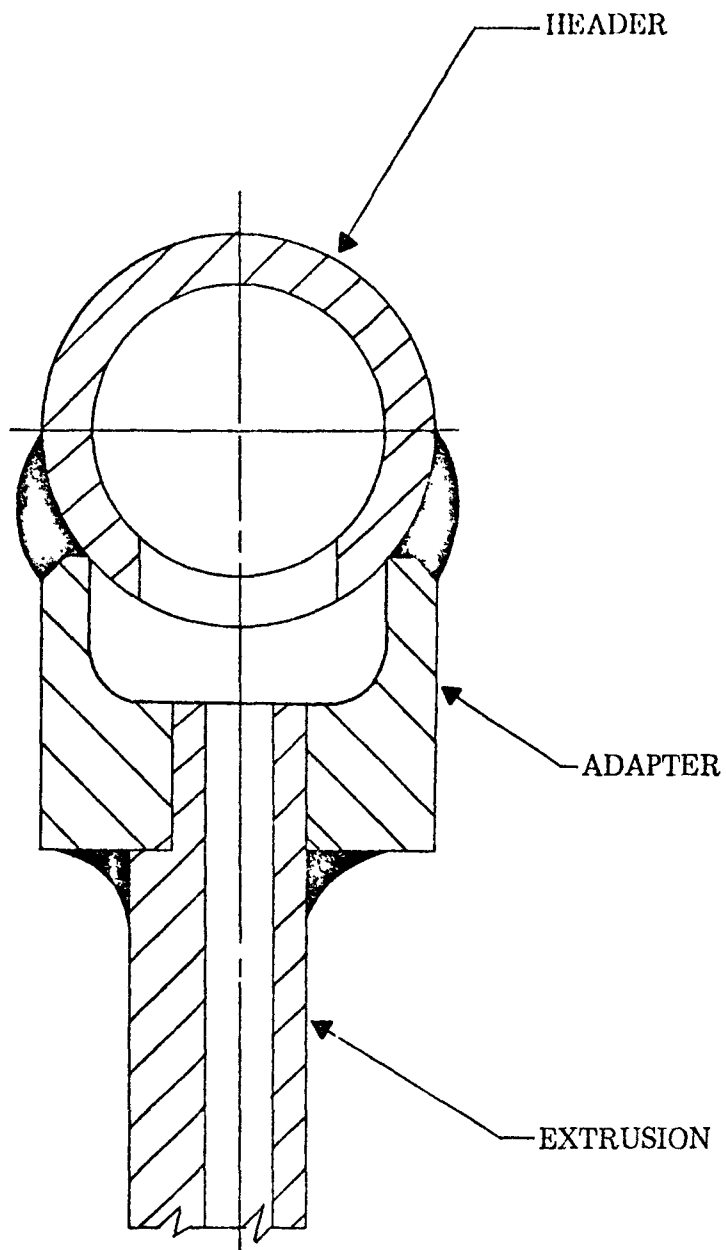


FIGURE 3.5.2.6-2
EXTRUSION/ADAPTOR TO HEADER
TERMINATION

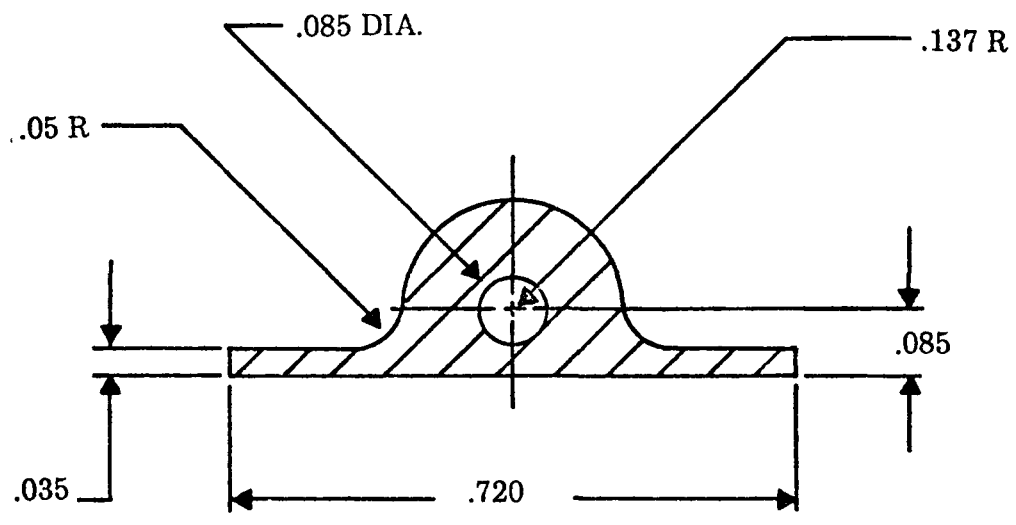


FIGURE 3.5.2.6-3
EXTRUSION

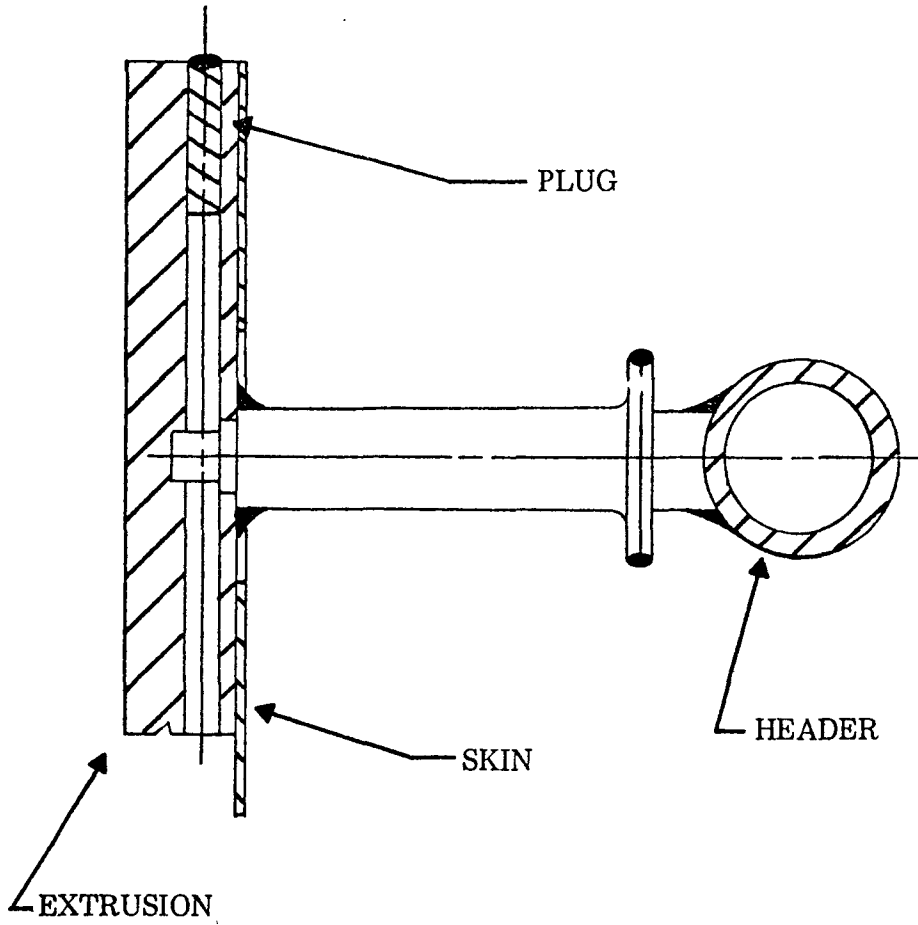


FIGURE 3.5.2.6-4
HEADER/TUBE TERMINATION
4 TUBE PANEL TEST
(OBSOLETE DESIGN)

Acceptance criteria for the tube/adaptor and adaptor/header welds was based on acceptable helium leak check data. A flight system radiator would require more elaborate non-destructive testing techniques. Therefore, to demonstrate this capability the radiator panel assemblies (extrusions/skin) and the completed assembly welds (header/adaptor tube) were radiographed. Results show that radiography of these welds can be performed and should be considered as a valid non-destructive testing method.

3.5.2.6.2 Analyses

3.5.2.6.2.1 Thermal/Hydraulic Analyses

Parametric thermal/hydraulic/weight analyses of conceptual radiator designs were performed by varying radiator geometry, skin thickness, tube size and number, header size, and meteoroid protection criterion. For the GDS design, only multiple-parallel tube between top and bottom header arrangements were considered for the studies.

The final design selections were based on obtaining the lowest weight radiator which satisfied all system performance requirements and other system design constraints as listed in Table 3.5.2.6-II. For the GDS radiator an additional consideration was that the design be capable of being manufactured and assembled without a costly manufacturing development effort.

Within those constraints listed in Table 3.5.2.6-II, the final design parameters selected for the GDS radiator are as follows:

Radiator diameter	4 feet
Radiator length	9.27 feet
Skin thickness	0.025 inch
Number of flow tubes	16
Flow tube inside diameter	0.085 inch
Flow tube frontside armor thickness*	0.094 inch
Flow tube backside armor thickness**	0.060 inch
Header inside diameter	0.375 inch
Header armor thickness	0.025 inch
Header bumper thickness	0.025 inch
ITRI Z-93 (ZnO/K_2SiO_4) coating properties	$\epsilon_H = 0.90$ (EOM) $\alpha_S = 0.3465$ (EOM)

* Original design based on $P(o) = 0.973$ allocation subsequently changed by Sundstrand for flight system to $P(o) = 0.99$.

** Provided by method of construction, actual thickness required is less.

TABLE 3.5.2.6-II

GDS RADIATOR DESIGN

PERFORMANCE REQUIREMENTS AND DESIGN CONSTRAINTS

Dowtherm flow rates:	Minimum - 0.159 lbs/sec
	Maximum - 0.358 lbs/sec
	Nominal - 0.249 lbs/sec
Waste heat load:	Nominal - 18255 Btu/hr
Radiator Coating emissivity:	ϵ - 0.90 (EOM)
Solar heat load:	Geosynchronous Orbit
	Solar absorptivity (EOM) $\alpha_s = 0.3467$
	Average solar load 48.89 Btu/hr-ft ²
Dowtherm inlet temperature:	Nominal - 212°F
Reynolds number in flow tubes at exit \geq	3000 for nominal flow and higher
Maximum fluid pressure drop $\Delta p = 20$ psi	(at nominal flow)
Meteoroid penetration criterion (total for radiator) - P(o)	= 0.99
Operations lifetime - 7 years	
Radiator diameter limit*	4 ft minimum approximately
Acoustic noise/spectrum	145 db overall (see Table 3.5.2.6-III)
Acceleration/vibration/shock	See Table 3.5.2.6-IV

* To permit installation of PCS and heat sources within the radiator envelope.

TABLE 3.5.2.6-III

ACOUSTIC SPECTRUM

Sound Pressure Level 145 db Overall*

1/3 Octave Band Center Frequency (Hz)	1/3 Octave Band Sound Pressure Level** (db)	1/3 Octave Band Center Frequency (Hz)	1/3 Octave Band Sound Pressure Level** (db)
40	124	1600	129.5
50	125.5	2000	128.5
63	127	2500	126.5
80	129	3150	125
100	130.5	4000	123
125	131.5	5000	121.5
160	132.5	6300	120
200	133.5	8000	118
250	134	630	133.5
315	134.5	800	133
400	134.5	1000	132
500	134	1250	131

* Sound pressure level spectrum

** db (Re: 0.0002 dynes/cm²)

TABLE 3.5.2.6-IV

EXPECTED LOAD ENVIRONMENTS

Environment

Acceleration 9g axial and 5g lateral simultaneous

<u>Vibration</u>	<u>Spectral Density</u>	<u>Frequency (Hz)</u>
	Increasing 3 db/oct	10-900
	0.1875 g ² /Hz	900-1400
	Decreasing 15 db/oct	1400-2000

Overall level of 15.1 grms, test duration:

3 minutes along each of the three orthogonal axes.

Shock 3 pulses in each direction along 3 orthogonal axis (18 shocks total). Pulse as follows: 775 G's peak half cycle sine, 0.2 ± .1 msec pulse width.

Pressure Sea level to 10⁻¹⁰ torr

Analysis Tools

The principal analytical tool used to generate parameter sensitivity studies was a computer program written by Sundstrand and extensively modified by TES. The program assumes the radiator is a right circular cylindrical shell with axial tubes located at a constant radius from the shell centerline. Headers supply and remove fluid from the tubes at the extreme top and bottom of the shell.

Heat rejection analysis is performed by specifying the total amount of heat to be dissipated, the solar load, and the radiator shell thickness and diameter. The code calculates the required radiator length for these conditions. Shell thickness is used to determine a fin efficiency for the area between tubes. A thermal/hydraulic analysis of the fluid flow is accomplished by specifying the axial tube inside diameter, number of tubes, and fluid flow rate. The code calculates the fluid to tube film temperature drop based on an input table of Colburn modulus vs Reynolds number. Pressure drop of the fluid in both tubes and headers are calculated from the D'Arcy equation and originally applying Moody chart data for friction factors for smooth tubes. These friction factors were subsequently modified to be consistent with measured tube data (see Section 3.5.2.6-3). Internal tube and header diameters are required input. Meteoroid armor thickness is calculated for frontside and backside of tubes and for the headers. Input required for these calculations includes constants describing the anticipated meteoroid flux (Ref. 1) and the desired no-puncture probability. Radiator weight is also calculated based on the input and calculated dimensions. Support structure such as additional stringers, frames, and mountings are not included in this weight calculation and therefore were calculated separately.

Optimization

Optimization of a radiator design involves tradeoffs between thermal efficiency and weight. Other system design constraints, in general, prevent obtaining an absolute minimum weight design. For example, increasing skin thickness and the number of flow tubes increases the fin efficiency but the weight per unit of heat rejected quickly becomes greater than optimum. In addition, because the desired flow rate is fixed, increasing the number of tubes too much lowers the Reynolds number for the tube flow into the transition flow regime which is undesirable and therefore restricts the lower limit of this design parameter to approximately $N_{Re} = 3000$, at least for nominal operating conditions. Likewise, if radiator pressure drop is a design constraint, increasing the radiator diameter will require shorter length flow tubes and the result would be a lower overall pressure drop. As the diameter increases, however, the thermal efficiency (fin) decreases unless more flow tubes are added - this adds weight because of more tubes and because of more required meteoroid protection (i.e., greater vulnerable area). In addition, increasing the diameter results in a less stable structure so weight must be added to provide greater structural stiffening.

The thermal/hydraulic tradeoffs are presented in Figure 3.5.2.6-5 for a wide range of potential radiator design parameters. The relationship between tube diameters, exit Reynolds number, tube pressure drop, and radiator shell diameter is conveniently shown on one plot. The boundaries defined by maximum desired pressure drop and minimum exit Reynolds number establish a region within which acceptable combinations of the varied parameters exist. These parameter combinations were then studied to determine the optimum set with respect to weight.

Weight Optimization

Radiator total weight was studied in three parts: structural, skin and tube/header weights. The general trend of structural (skin, stringer and frame) weight is shown in Figure 3.5.2.6-6. The minimum structure weight is obtained with skin thicknesses between 0.018" and 0.030", and with radiator shell diameter around 4'. Increasing the radiator diameter increases structural weight, and decreasing the diameter results in insufficient room for containing the rotating machinery and HSA's within the radiator envelope.

Radiator shell (skin) weight decreases with decreasing thickness. However, the practicality of manufacturing and handling the radiator becomes a significant factor as thickness drops below 0.020". And any weight saving is almost, if not completely offset by the rapid rise in required structure weight. Tube and header weights are primarily determined by meteoroid armor requirements. Contained liquid weight varies with number and diameter of radiator tubes, and is considered in overall weight calculations.

Figure 3.5.2.6-7 presents the results of the parametric weight studies for the GDS radiator. As noted in Figure 3.5.2.6-7 the studies were originally based on an overall system arrangement wherein the heat sources were horizontally mounted under the radiator circumference. This necessitated heavier mounting structure because of longer support legs. The final system arrangement consisted of the three heat sources mounted vertically inside the radiator envelope which reduced the mounting structure considerably, and thus the weights indicated in Figure 3.5.2.6-7 are high by 5 to 6 pounds. The weight breakdown of the final GDS radiator design is given earlier in Section 3.5.2.6-1.

As shown in Figure 3.5.2.6-7 the minimum weights vary as a function of radiator diameter and number of tubes but the weights tend to converge at approximately a four (4) foot diameter radiator size. Because the system arrangement (i. e., heat sources inside) constrains the minimum radiator diameter, the selection of the design is based primarily on another major system design constraint: fluid flow pressure drop. The design goal for the GDS radiator overall pressure drop was 20 psi. As shown in Figure 3.5.2.6-7 this goal can only be reached by reducing the number of tubes and increasing the tube inside diameter because of the exit Reynolds number restriction of 3000.

FIGURE 3.5.2.6-5

KIPS RADIATOR THERMAL HYDRAULIC CHARACTERISTICS

6 FT. DIAMETER
 5 FT. DIAMETER
 4 FT. DIAMETER
 — 16 TUBES
 - - - 20 TUBES
 - - - 30 TUBES

DATA FROM 9830 CODE RUNS USING
 TEST VALUES FOR FRICTION FACTOR
 18255 B/HR. Q.
 SKIN THICKNESS = 0.25 IN.

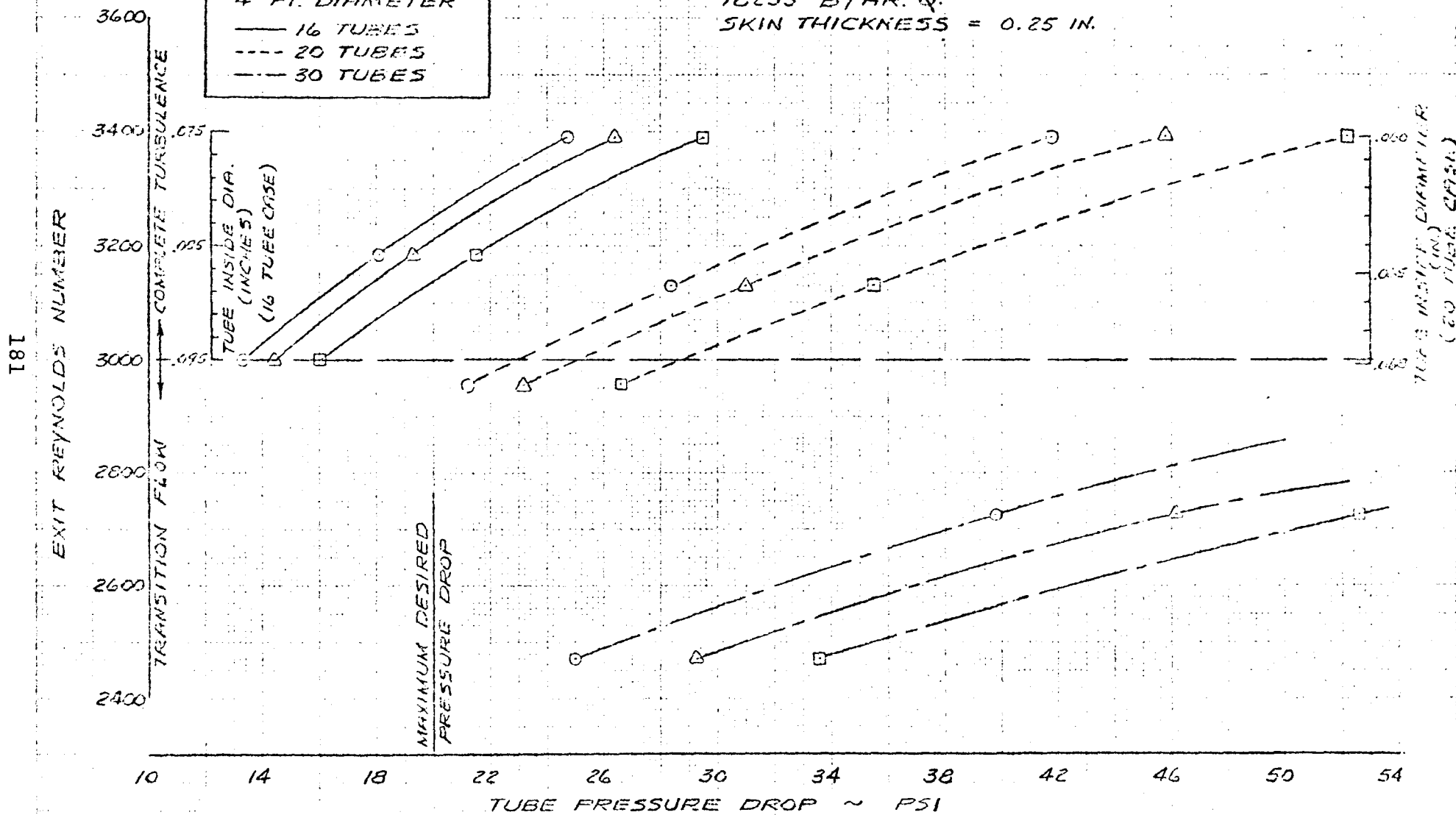
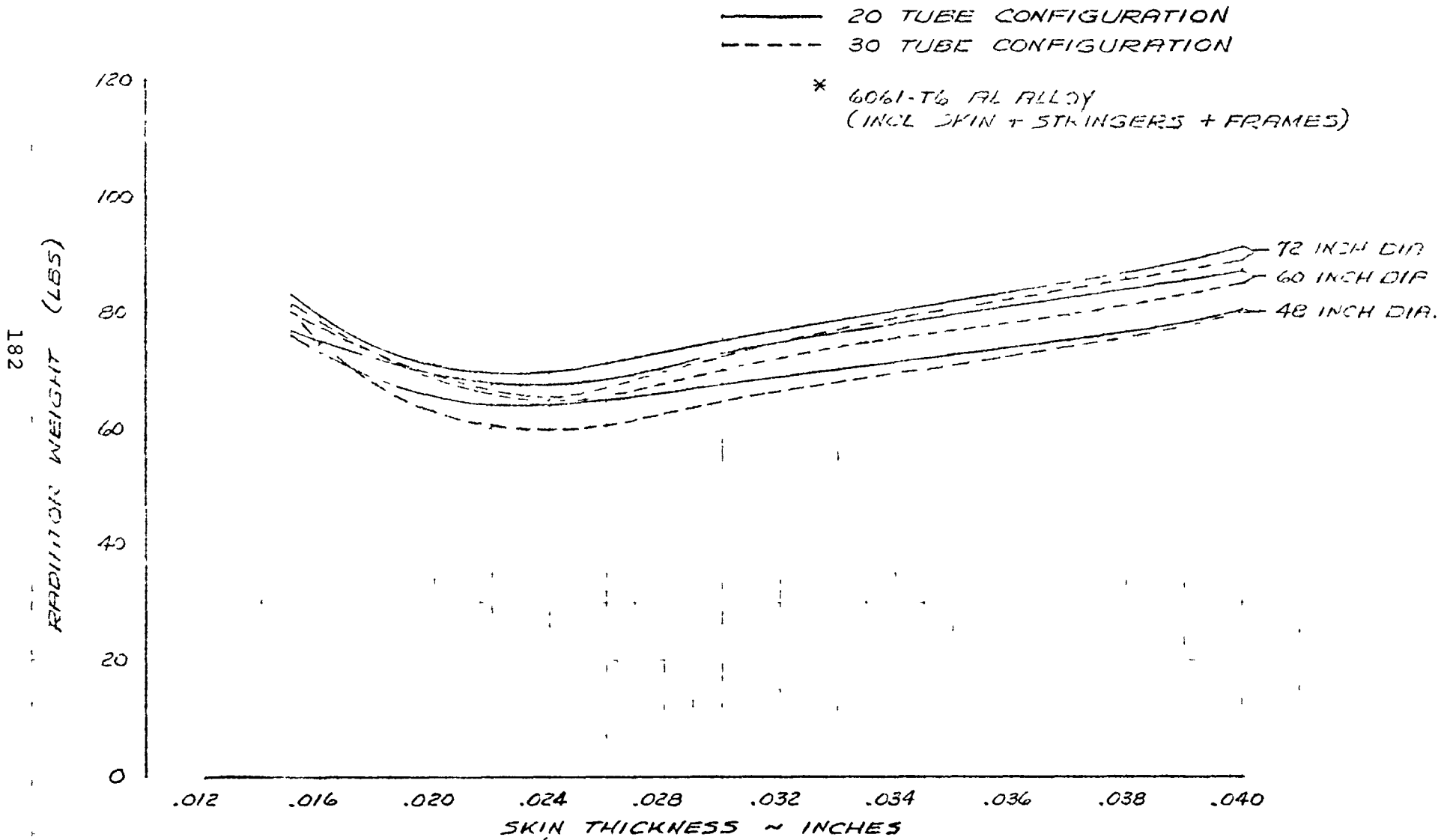


FIGURE 3.5.2.6-6
RADIATOR STRUCTURE* WEIGHT VERSUS SKIN THICKNESS
FOR VARIOUS DIAMETERS



182

FIGURE 3.5.2.6-1
MINIMUM (CONSTRAINED) RADIATOR WEIGHT

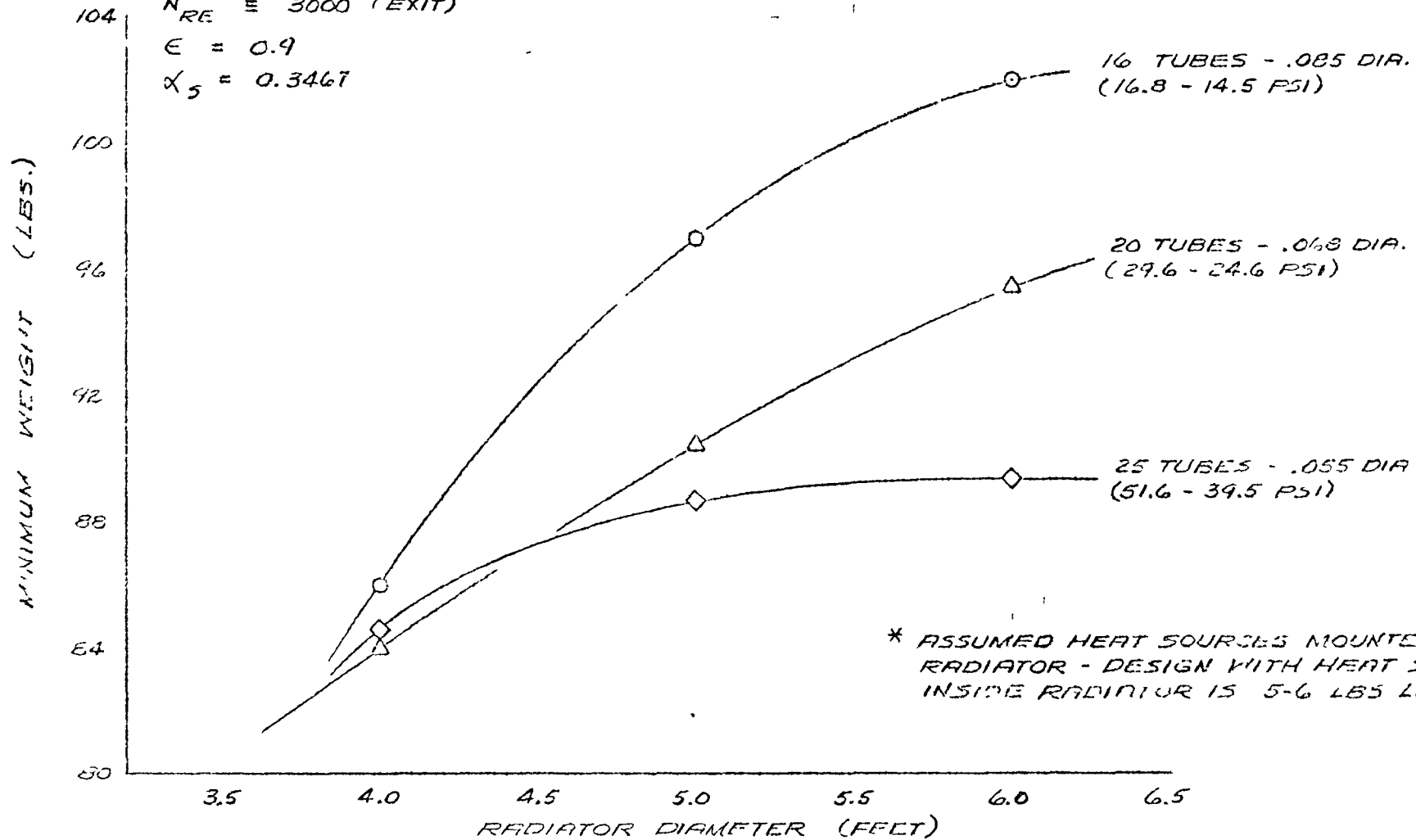
$Q_{REJ} = 18255 \text{ BTU/HR} + \text{SOLAR}$

$P_{(0)} = 0.99$

$N_{RE} = 3000 \text{ (EXIT)}$

$\epsilon = 0.9$

$\alpha_5 = 0.3467$



* ASSUMED HEAT SOURCES MOUNTED UNDER RADIATOR - DESIGN WITH HEAT SOURCES INSIDE RADIATOR IS 5-6 LBS LIGHTER

3.5.2.6.2.2 Radiator Meteoroid Protection Analysis

The radiator design is based on an overall probability of non-puncture by meteoroids of 0.99 for seven years in a synchronous geocentric orbit. Originally defined as 0.97, the non-puncture probability was increased during the development program to provide a higher overall mission reliability. The overall probability includes the probabilities of non-puncture for the frontside of the tube, the backside of the tube and the headers. The backsides of the radiator tubes are assumed to be protected by the radiator skin which acts as a so called "bumper." A modified version of an approach presented in Ref. 1 (so called Cour-Palais method) is used to evaluate the effectiveness of the skin and tube backside armor. The frontside penetration criteria is that presented in Ref. 3. The tube backside vulnerability to meteoroids entering the open end of the radiator cylinder has not been considered in the weight calculations for the GDS radiator.

Required armor thicknesses, assuming 6061-T6 aluminum construction, are as follows:

Header	0.010" (with 0.025" bumper)
Tube frontside	0.094"
Tube backside	0.020" (with 0.025" bumper)

Armor weight is a strong function of non-puncture probability. For a given probability, however, it does not vary appreciably with small changes in design (shell diameter, number of tubes, etc.), particularly near the optimum 4 foot diameter 16 tube radiator design. The dominant weight is that of the tube frontside armor, since other required armor thicknesses are less than the minimum practical thickness of manufacture. Hence, it is possible to design to extremely high probabilities of no-puncture for the header and tube backside, with the tube frontside probability of no-puncture close to the desired overall value.

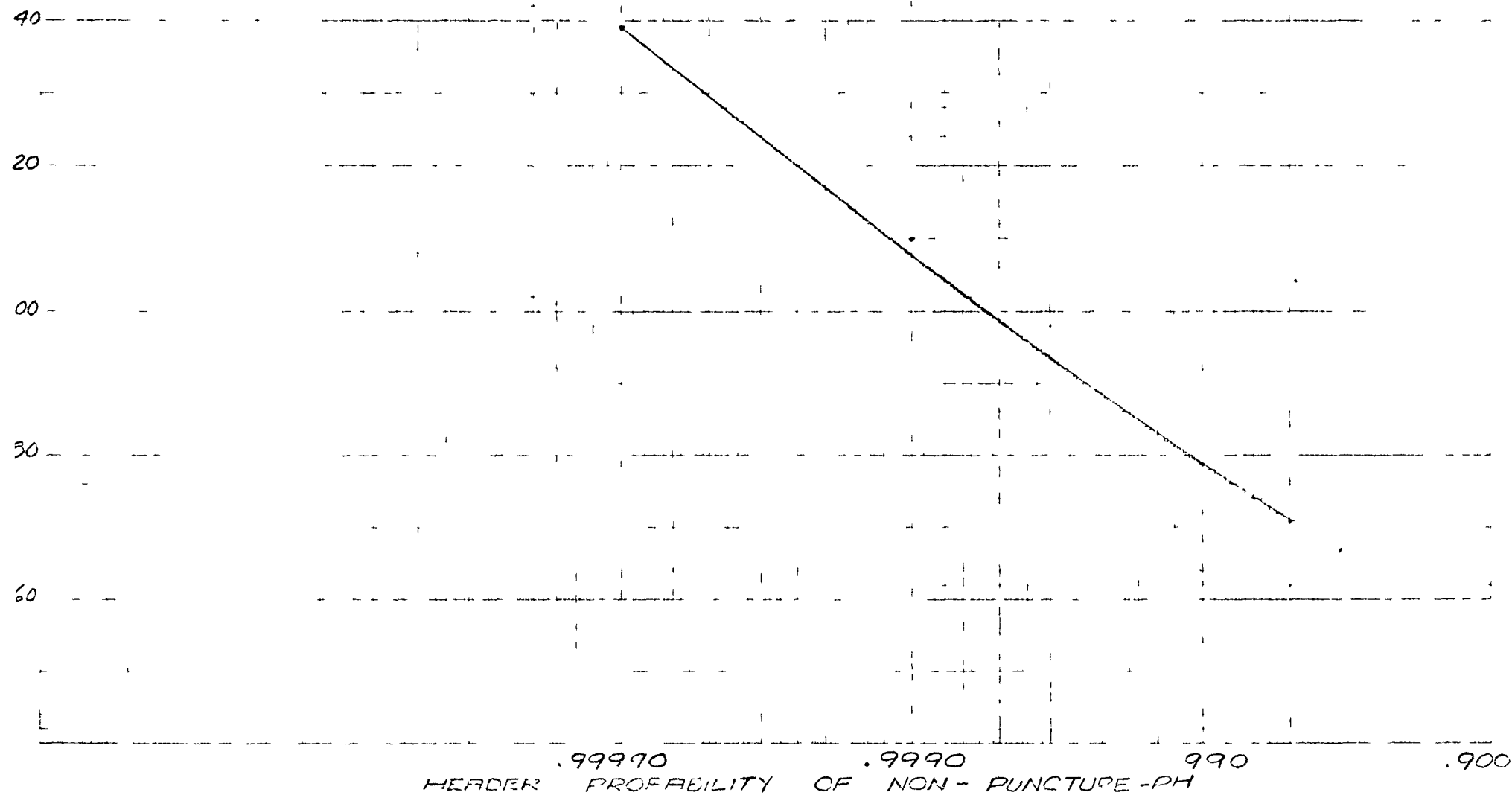
Optimization of the armor design with respect to weight was accomplished in three steps. First, a relationship was established between weight and armor thickness for the tube frontside, backside and header armors. Second, weight was studied as a function of no-puncture probability for tube and header armor. Figure 3.5.2.6-8 shows an example of header weight versus probability of no-puncture of the header for one of the typical radiator designs studied. The third and final step is to determine the optimum combination of tube frontside, backside and header non-puncture probabilities for the given overall non-puncture probability of 0.99. Figures 3.5.2.6-9 thru 11 illustrate this procedure for a typical radiator design. In Figure 3.5.2.6-9 the weights of tube frontside and backside armor are shown which combine to give the maximum tube non-puncture probability. In Figure 3.5.2.6-10 the tube and header non-puncture probabilities are combined in a similar manner to give the highest overall non-puncture probability.

Each individual value of probability of no-puncture for the tube frontside, backside and header is associated with a unique armor configuration (thickness) which determines the weight. Thus, optimization of the weight for a particular non-puncture probability defines the armor configurations.

.999999 B 7 6 54321.99999 B 7 6 54321.9999 B 7 6 54321.999 B 7 6 54321.99 B 7 6 54321.99 B 7 6 54321.9

FIGURE 3.5 2 6-8
SENSITIVITY OF HEADER
WEIGHT TO NO-PUNCTURE PROBABILITY

RADIATOR DIAMETER = 5 FT
NO. OF TUBES = 20
AVERAGE HEADER I.D. = .369"

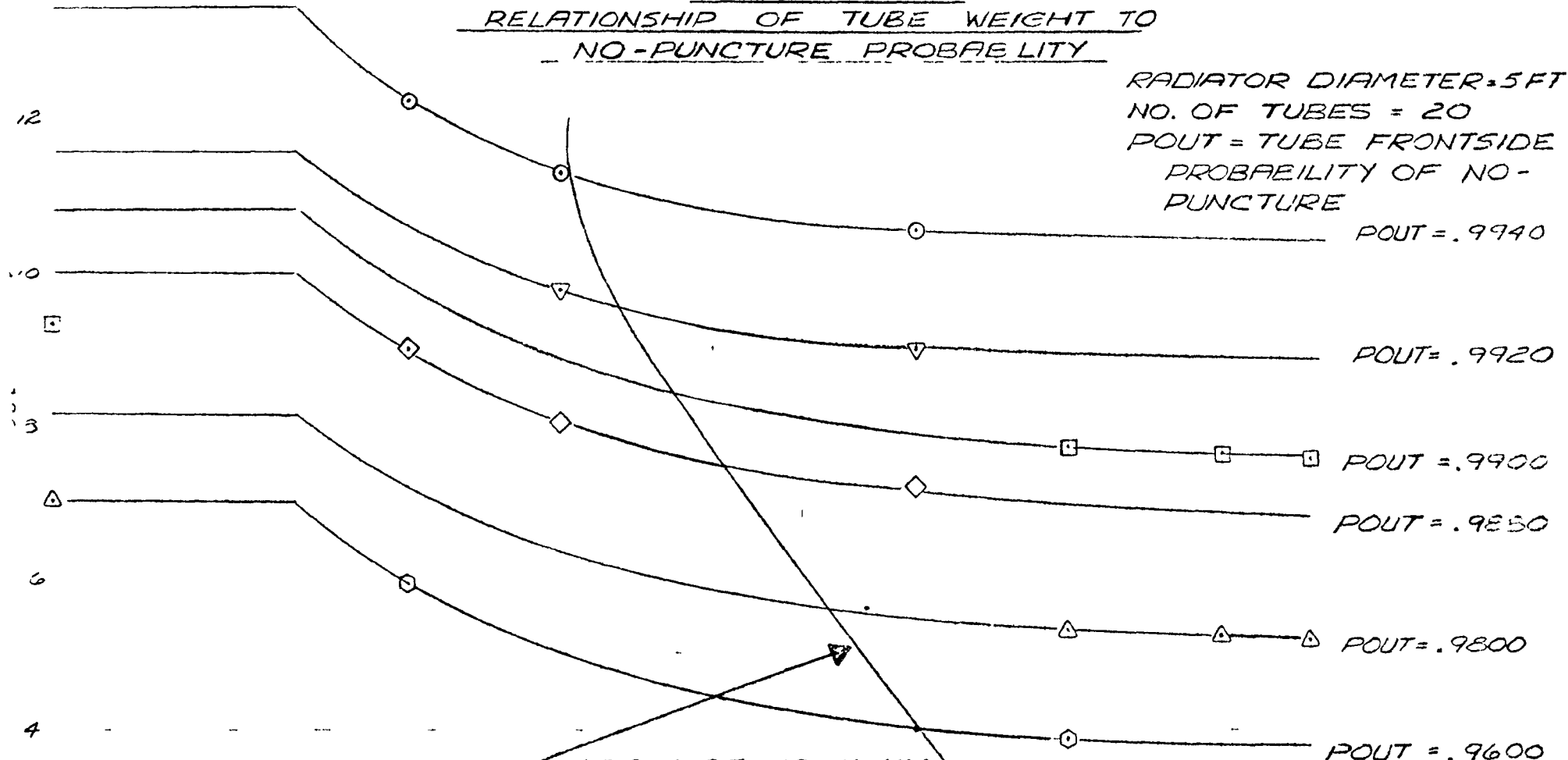


.9999 8 7 6 5 4 3 2 1 .999 8 7 6 5 4 3 2 1 .99 8 7 6 5 4 3 2 1 .9

FIGURE 3.5.2.6-9

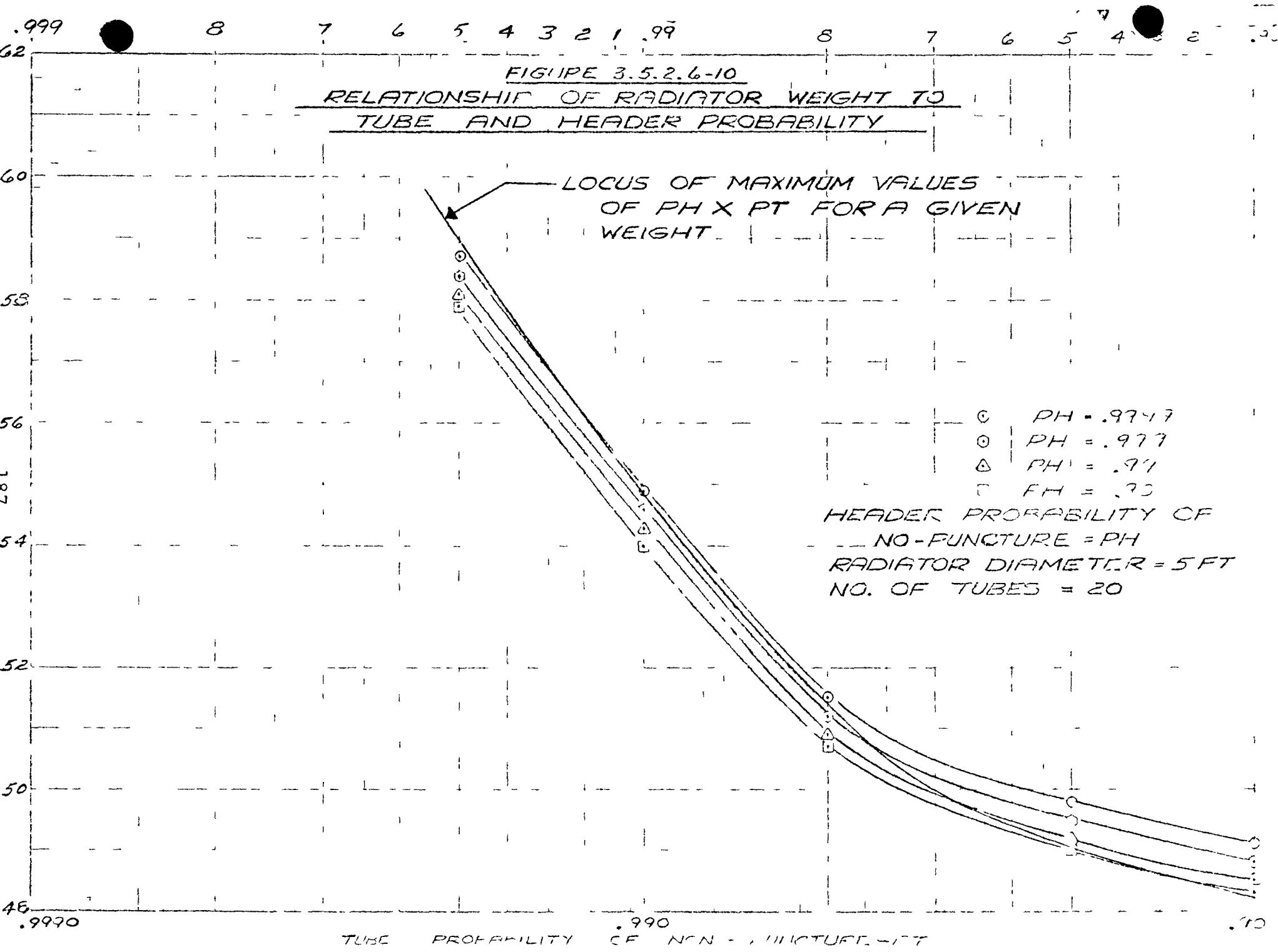
RELATIONSHIP OF TUBE WEIGHT TO
NO-PUNCTURE PROBABILITY

RADIATOR DIAMETER = 5 FT
NO. OF TUBES = 20
POUT = TUBE FRONTSIDE
PROBABILITY OF NO-
PUNCTURE
POUT = .9940



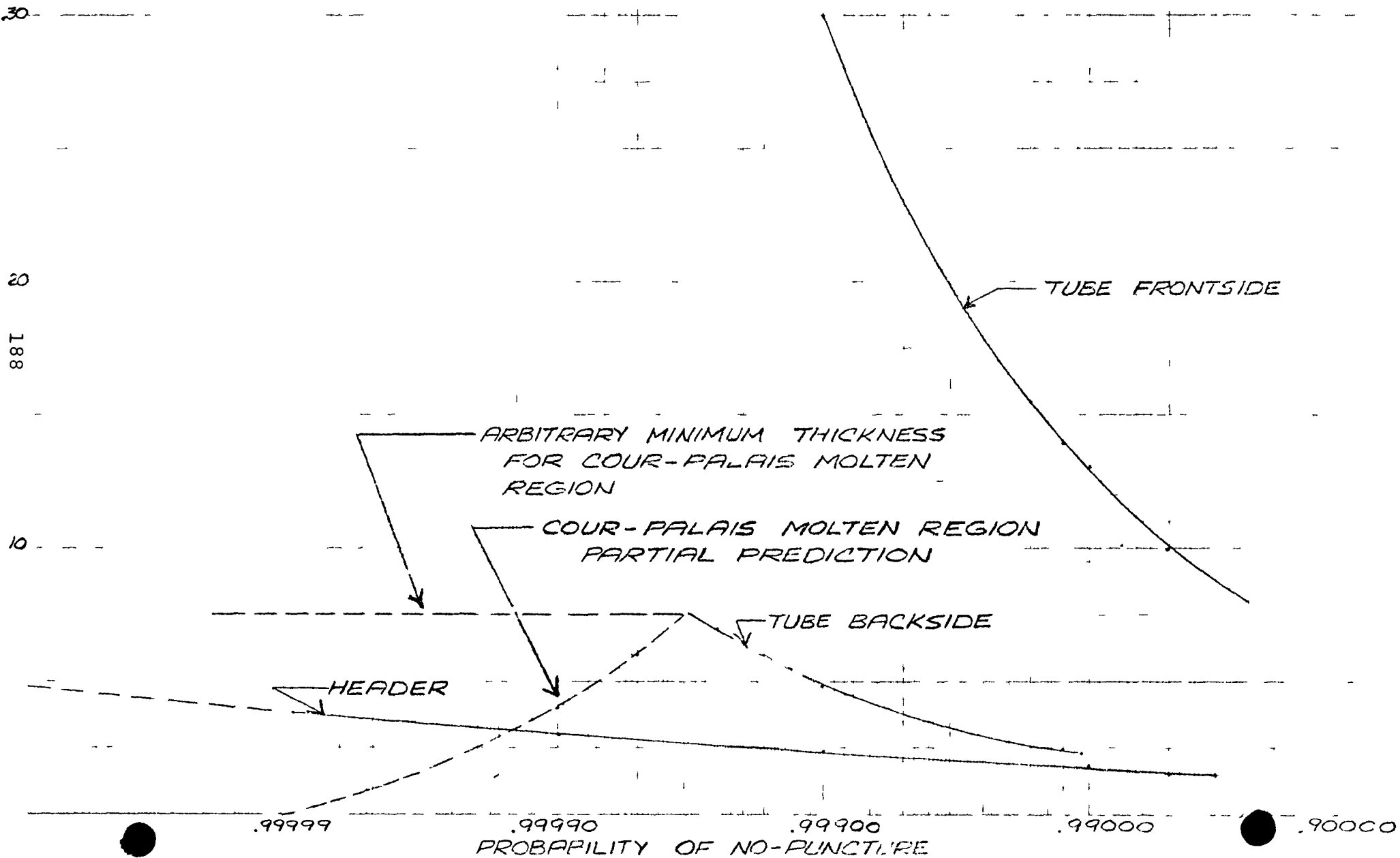
LOCUS OF MAXIMUM
VALUES OF PIN X POUT
FOR A GIVEN WEIGHT

FIGURE 3.5.2.6-10
RELATIONSHIP OF RADIATOR WEIGHT TO
TUBE AND HEADER PROBABILITY



.99999 8 7 6 5 4 3 2 1 .99999 8 7 6 5 4 3 2 1 .9999 8 7 6 5 4 3 2 1 .99 8 7 6 5 4 3 2 1 .9

FIGURE 3.5.2.6-11
ARMOR REQUIREMENT AS A FUNCTION
OF NO-PUNCTURE PROBABILITY



The GDS header is surrounded by a shield or bumper, so it has no "frontside" exposure to meteoroids.

Calculations of armor weight and non-puncture probability were all made with the Sundstrand radiator analysis computer code. The Cour-Palais method of backside armor thickness calculation described in Ref. 13 was modified to permit more realistic results. In the Cour-Palais method, design under certain condition for the optimum armor thickness at a given probability of no-puncture can result in thinner armor than would be required for a lower non-puncture probability. This anomaly was avoided by calculating the armor thickness predicted by the Cour-Palais method as a function of non-puncture probability. The actual armor thickness required was assumed to remain constant at the peak calculated value rather than decrease with increasing non-puncture probability. This relation between armor thickness and probability of no-puncture is shown in Figure 3.5.2.6-11 for a typical radiator design, and covers tube frontside, backside, and header armor configurations.

3.5.2.6.2.3 Structural Analysis

Preliminary structural analyses were conducted of the parametric radiator designs. These studies considered the use of aluminum alloys only (see Table 3.5.2.6-V) and were based on the load environment given in Table 3.5.2.6-VI. The maximum possible radiator structure temperature of 212°F was assumed for property determination. The structural analysis was performed on each radiator design by assuming the structure to be a cylindrical shell composed of thin skin stiffened by the longitudinal extrusions which carry the Dowtherm A working fluid and by circumferential ring frames. This structure when mounted at the base is subjected to overall bending and shear due to the maximum load environment specified in Table 3.5.2.6-VI. The parametric design studies showed that, in general, the armor requirements for the flow tubes (extrusions) are greater than the material required for longitudinal structural stiffness. Thus, once the required material for optimization of the structure was determined, additional material was generally required to provide adequate meteoroid protection. In addition, for those designs where the skin panels were inadequate to withstand the assumed acoustic environment, the required local panel stiffening was determined and incorporated into the weight calculations. Studies were performed to determine the optimum number of support points for a base mounted cylindrical shell radiator. The studies showed that the overall weight was insensitive to the number of support points. Therefore a three point mounting system was selected and used for the studies because this would limit the required number of attachments to the spacecraft. Typical results of these preliminary parametric structural studies were shown earlier in e.g., Figure 3.5.2.6-6. Table 3.5.2.6-VII shows a typical breakdown of the structural weights for a twenty (20) flow tube radiator configuration.

After final selection from among the radiator design variables, a detailed structural analysis was conducted to refine the design and to generate the final weight breakdown presented previously in Section 3.5.2.6.1.

TABLE 3.5.2.6-V

<u>Mechanical Properties</u>	<u>Material</u>	
	<u>3003-H14</u>	<u>6061-T6</u>
F _{tu} , @ 212°F, psi (parent material)	20,000	38,000
F _{tu} , @ 212°F, psi (as welded material)	14,000 14,000	25,000 25,000
F _{tu} , @ 212°F, psi (weld area)	12,000	20,000
F _{ty} , @ 212°F, psi (parent material)	17,000	34,000
E, @ 212°F, psi (parent material)	9.9 (10 ⁶)	9.9 (10 ⁶)

TABLE 3.5.2.6-VI
STRUCTURAL DESIGN CRITERIA

1. Load Environment

(a) Acceleration - 9g axial and 5g lateral simultaneously (limit)

(b) Vibration

<u>Spectral Density</u>	<u>Frequency (Hz)</u>
Increasing at 3 db/Oct	10-900
$0.1875 \text{ g}^2/\text{Hz}$	900-1400
Decreasing at 15 db/Oct	1400-2000

Overall level of 15.1 grms (limit)

Duration: 3 minutes along each of the three orthogonal axes.

(c) Shock - 3 pulses in each direction along 3 orthogonal axes
(18 shocks total). Pulse as follows: 775 g's peak half cycle sine,
0.2 ± .1 msec. pulse width.

(d) Acoustic noise - 145 db overall (limit).

2. Thermal Environment

The shell structure is considered to be at 212° F during exposure to maximum load environment.

TABLE 3.5.2.6-VII
RADIATOR STRUCTURE WEIGHT*
20 - TUBE CONFIGURATION

Diameter of Radiator (ft)	4				5				6			
	.015	.025	.030	.040	.015	.025	.030	.040	.015	.025	.030	.040
Thickness, Radiator Skin (in.)	.015	.025	.030	.040	.015	.025	.030	.040	.015	.025	.030	.040
Length of Radiator (ft)	9.975	9.195	9.017	8.726	9.015	8.165	7.845	7.525	8.448	7.416	7.168	6.822
Weight, Skin (lb)	25.1	39.5	46.4	59.0	29.3	44.1	50.7	64.8	33.1	48.3	55.9	70.8
Weight, Tube-Stringer (lb)	36.9	11.1	9.3	8.8	33.3	10.6	10.2	9.7	35.4	7.7	7.5	7.1
Weight, Stringer Reinforcement (lb)	8.3	7.7	7.5	7.3	7.6	6.8	6.6	6.3	7.1	6.2	6.0	5.7
Weight, Skin Stiffeners (lb)	2.9	1.9	1.0	0	2.9	2.1	1.1	0	3.2	2.1	1.1	0
Number of Frames	7	7	7	7	7	7	7	7	7	7	7	7
Weight of Frames (lb)	2.6	3.1	3.7	4.8	3.2	3.9	4.7	6.0	3.9	4.7	5.6	7.2
Weight, Miscellaneous (lb)	0.4	0.4	0.4	0.4	0.4	0.4	0.4	0.3	0.4	0.3	0.3	0.3
Weight, Total Structure (lb)	76.2	63.7	68.3	80.3	76.7	67.9	73.7	87.1	83.1	69.3	76.4	91.1

NOTE: * 6061-T6 Aluminum Alloy

3.5.2.6.3 Tests

3.5.2.6.3.1 Radiator Thermal Control (Emissive) Coating Tests

The original design basis for the radiator was the assumption of the use of the ITRI developed Z-93 emissive coating on the radiator external surface. The performance of the radiator in a geosynchronous orbit was based on estimated coating properties of infrared emittance, $\epsilon_{IR} = 0.9$ and solar absorptivity, $\alpha_s = 0.3468$ at the end of a seven year mission. For evaluation of the radiator thermal/hydraulic test results samples of the coating were sprayed at the same time as the test panels. These samples were then delivered to TRW for evaluation and property measurements. The solar absorptance (α_s) and the total hemispherical emittance (ϵ_h) of the specimens were measured. As shown in Figure 3.5.2.6-12 the spectral reflectance of two specimens were measured from which the solar absorptivity was calculated by integration over the solar spectrum. The results are presented in Table 3.5.2.6-VI together with some earlier measurements of Z-93 coating samples by TRW. The total hemispherical emittance of the sample was measured by calorimetry over a range of temperatures from -160°F to $+266^\circ\text{F}$ (the average temperature of the KIPS radiator is 145°F). These results are presented in Figure 3.5.2.6-13 and compared in Table 3.5.2.6-VII with sample measurements made earlier by TRW.

The measured hemispherical emittance of .92 to .94 at the kips radiator design temperature is somewhat higher than the assumed design value but the solar absorptivity of 0.25 average was also higher than anticipated for a beginning-of-mission value. For the ground demonstration system, this poses no problem since no ultraviolet degradation tests are planned with the radiator. In addition, because the flight system coating must be a "nuclear hardened" coating, the Z-93 coating would not be used for the flight system in any event.

3.5.2.6.3.2 Radiator Thermal/Hydraulic Test Program

Tests measuring pressure drop versus flow rate (to obtain friction factor versus Reynolds number) in single, well insulated (isothermal) tubes were conducted using heated Dowtherm A as the fluid. These tests were conducted on two different diameter tube assemblies and at several temperature levels. These tests were followed by heat rejection tests of a shortened section of a radiator panel in a thermal/vacuum chamber where space conditions were simulated by cryogenically cooled walls. The next test conducted was an in-air thermal/hydraulic test of a full length radiator panel using the final GDS design. Viewed as a whole, these tests show that design goals for the radiator have been met, indicating the GDS radiator design to be satisfactory. A test of the full size radiator in an air environment is currently planned but has not been conducted as of this report date. This test is being made to verify the overall pressure drop design goals for the radiator and to evaluate its heat rejection capability under a typical system checkout environment.

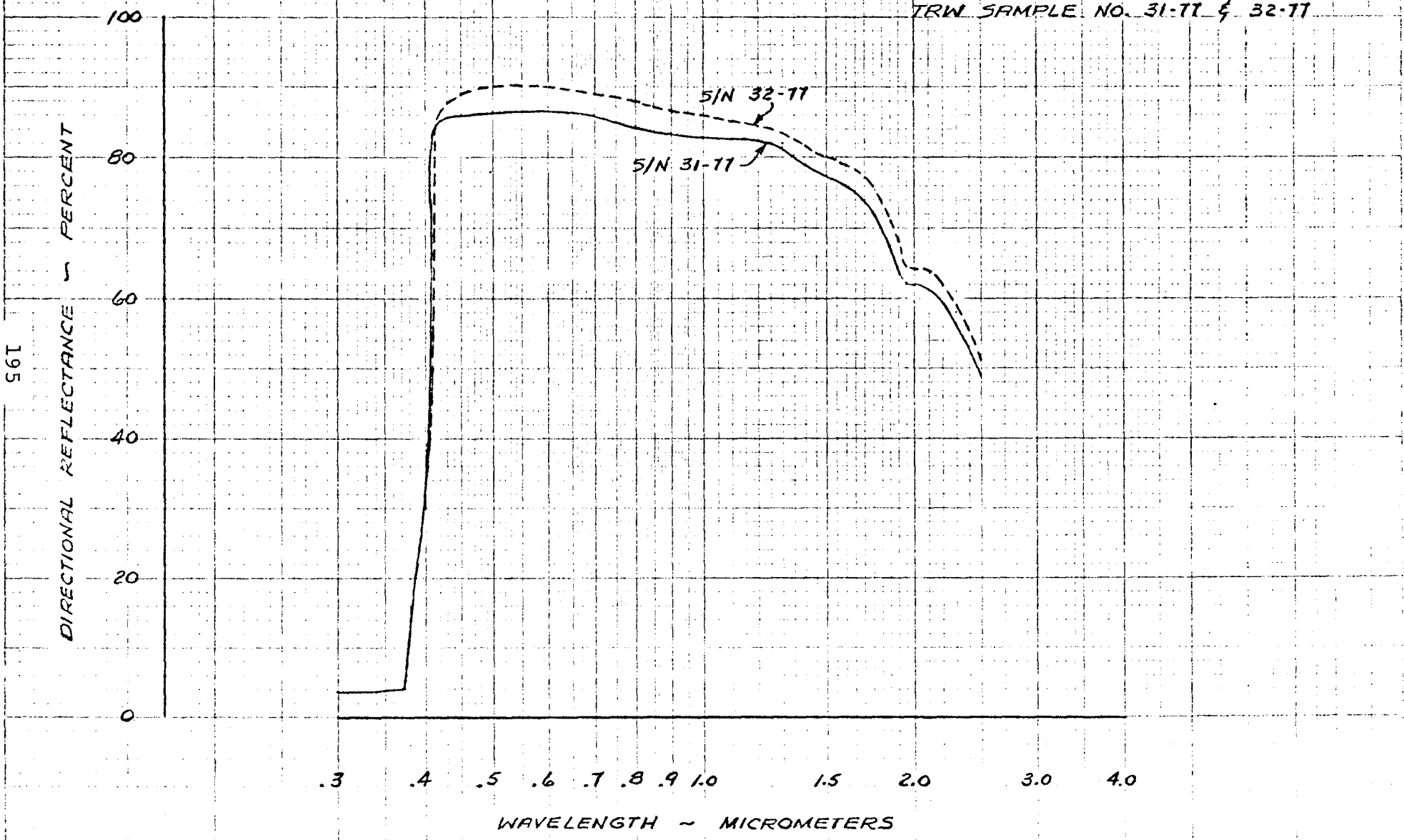
Isothermal Pressure Drop Tube Tests - Two header/radiator single tube assemblies were tested to measure friction factor data needed for both pressure drop calculations and preliminary heat transfer estimates. The tubes, with inside diameters of 0.069 and 0.085 inches, each 85.7 inches long, were instrumented with two pressure taps on the tubes at least one inch from the manifold, two pressure taps on the manifold,

10
9
8
6
5
4
3
2
1

FIGURE 3.5.2.6-12

SPECTRAL DIRECTIONAL REFLECTANCE OF TWO WHITE PAINT SPECIMENS

TRW SAMPLE NO. 31-77 & 32-77



195

FIGURE 3.5.2.6 - 13

HEMISPHERICAL EMITTANCE OF WHITE PAINT SPECIMENS
AT TEMPERATURES FROM -160 °F TO 266 °F

196

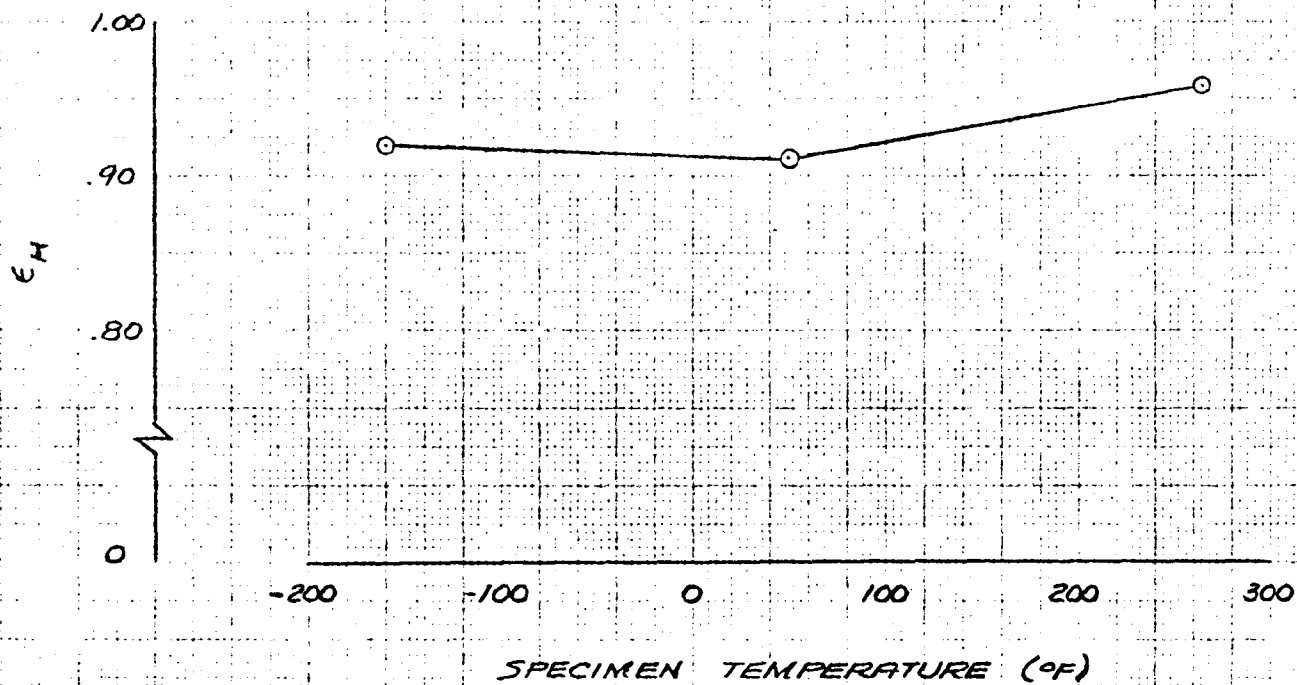


TABLE 3.5.2.6-VIII

VALUES OF SOLAR ABSORPTANCE AND NORMAL AND
HEMISPHERICAL EMITTANCE OF WHITE PAINT SPECIMENS

Specimens	Solar Absorptance α_S	Normal Emittance ϵ_N (1)	Hemispherical Emittance ϵ_H
TRW #31-77	0.25 ₉ ⁽²⁾	0.93 ₅ ⁽²⁾	0.89 (2) (3)
TRW #32-77 ⁽⁴⁾	0.23 ₃	0.93 ₇	0.89
TRW #49-77 (A)		0.93 ₂ ⁽⁵⁾	0.89
TRW #49-77 (B)		0.93 ₄ ⁽⁵⁾	0.89
TRW #49-77 (C)		0.93 ₃ ⁽⁵⁾	0.89
TRW #49-77 (D)		0.93 ₃ ⁽⁵⁾	0.89
TRW #49-77 (A) & (D) ⁽⁶⁾			(-160°F) 0.92 ₁ ⁽⁷⁾
			(+50°F) 0.91 ₂
			(+266°F) 0.95 ₈

- (1) Values of ϵ_N at 80°F were determined using a Gier Dunkle Instruments Model DB100 Infrared Reflectometer.
- (2) Although the accuracy of the measuring instruments does not justify three significant figures, the third figure is retained depressed to indicate trends.
- (3) Values of ϵ_H at 80°F were determined using the correlations of ϵ_N and ϵ_H given in Figures 13-15 of Ref. 4.
- (4) Although not requested, the solar absorptance of the duplicate specimen to that sent for α_S measurement was also determined.
- (5) Values of ϵ_N at 80°F for the four inch squares were determined using the DB100 Infrared Reflectometer. The values shown are the average of values measured at six different locations on each specimen plate.

TABLE 3.5.2.6. -VIII(Continued)

- (6) Specimens (A) and (D) were used back to back for the ϵ_H measurement. Values ϵ_H determined assume that the ϵ_H of plates (A) and (D) are identical.
- (7) These values of ϵ_H were determined by direct measurement of ϵ_H using the calorimetric technique (Ref. 3).

and five thermocouples, and was sandwiched between layers of fiberglass insulation. The flow rate was measured with a flow meter which had previously been calibrated at the four test temperatures (e.g., 212°F, 190°F, 160°F and room temperature).

Flow testing of the tubes was done using several different constant flow rates at a given fluid temperature. At each flow rate and fluid temperature pressure drop data was taken; the flow rate was then increased to give a range of Reynolds numbers from 500 to 10,000 for that fluid temperature. The flow rate was changed in small increments, such that the change from laminar to turbulent flow could be observed in the pressure drop measurements. The actual transition flow range was well defined in these isothermal measurements, and was characterized by a pressure drop which constantly oscillated between a high and low value as the flow changed back and forth from laminar to turbulent. This transition occurred in a range of Reynolds numbers above 2200 and below 3000.

Figure 3.5.2.6-14 gives typical results, in this case for a nominal 212°F fluid temperature, clearly showing the laminar, transition, and turbulent regimes. Figure 3.5.2.6-15 shows friction factor data generated by these pressure drop measurements for the 0.085 inch tube diameter selected for use in the GDS; the friction factors measured in this test were somewhat higher than were anticipated.

Two important inferences were drawn from the flow tests:

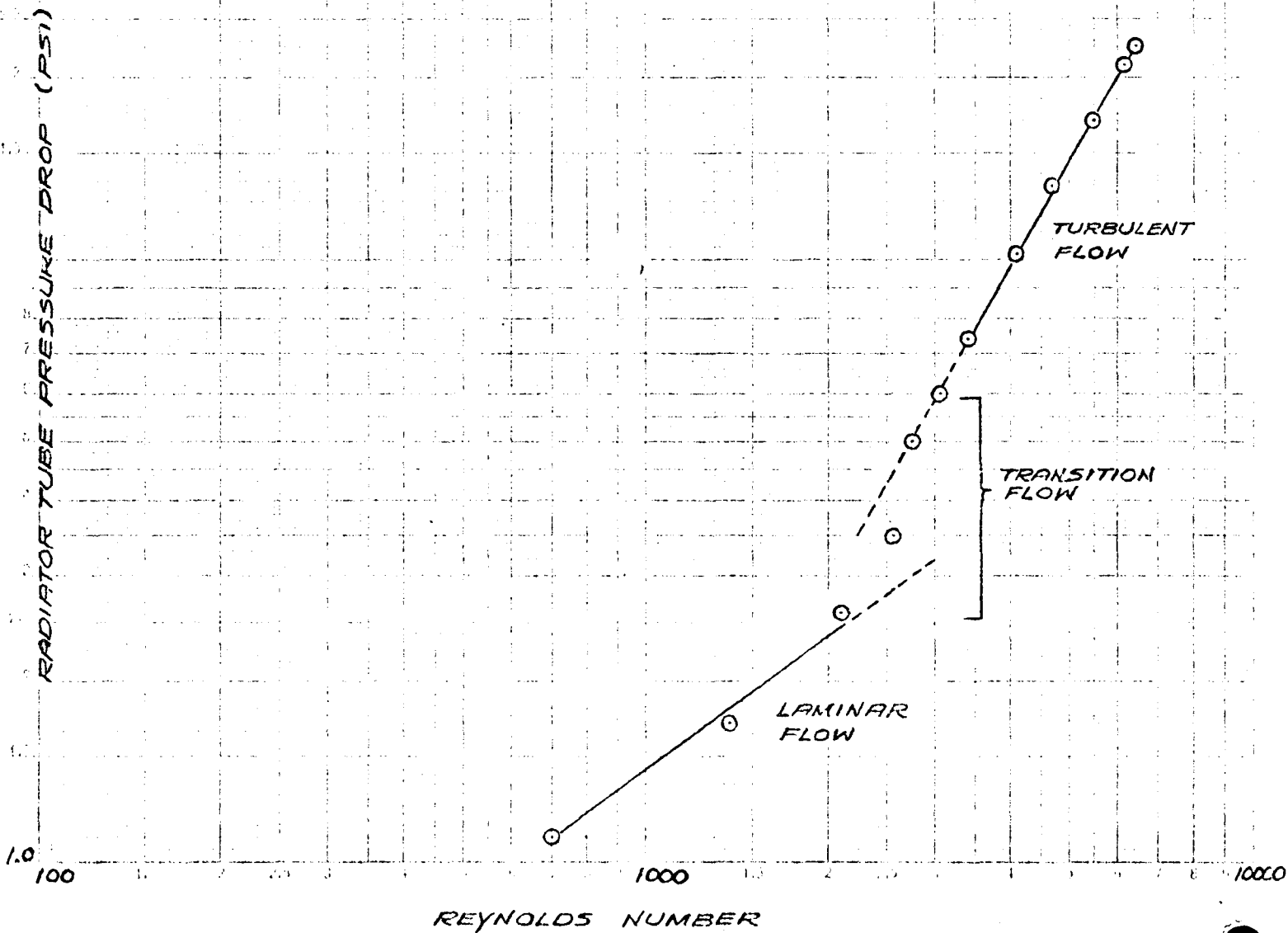
- For flow stability reasons, the design Reynolds number at any point in the tubes should be above the transition regime, i.e., the exit Reynolds number should be kept above approximately 3000.
- The higher than anticipated friction factors measured could possibly yield higher heat transfer coefficients. To evaluate this effect, Martinelli's analogy was used to determine Colburn Moduli associated with friction factor data.

Heat transfer coefficients used to predict GDS performance were determined by correlating the friction factor data using the Martinelli analogy which relates the Fanning friction factor to the Colburn Modulus (i.e., Stanton Number X Prandtl Number to the 2/3 power).

$$\text{Colburn Modulus } (N_{St} \cdot N_{Pr}^{2/3}) = \frac{(N_{Pr})^{2/3} \sqrt{f/2}}{\left[.833 \cdot 5 N_{Pr} + 5 \ln(5 N_{Pr} + 1) + 2.5 \ln\left(\frac{N_{Re} \sqrt{\frac{f}{2}}}{60}\right) \right]}$$

FIGURE 3.5.2.6-14
KIPS ISOTHERMAL TUBE TEST
PRESSURE DROP BETWEEN RADIATOR TUBE PRESSURE
TAPS VERSUS REYNOLDS NUMBER

COOLANT TEMP. AT RADIATOR TUBE INLET = 212 °F
 TUBE I.D. = 0.085 IN.
 TUBE LENGTH BETWEEN PRESSURE TAPS = 80.625 IN.



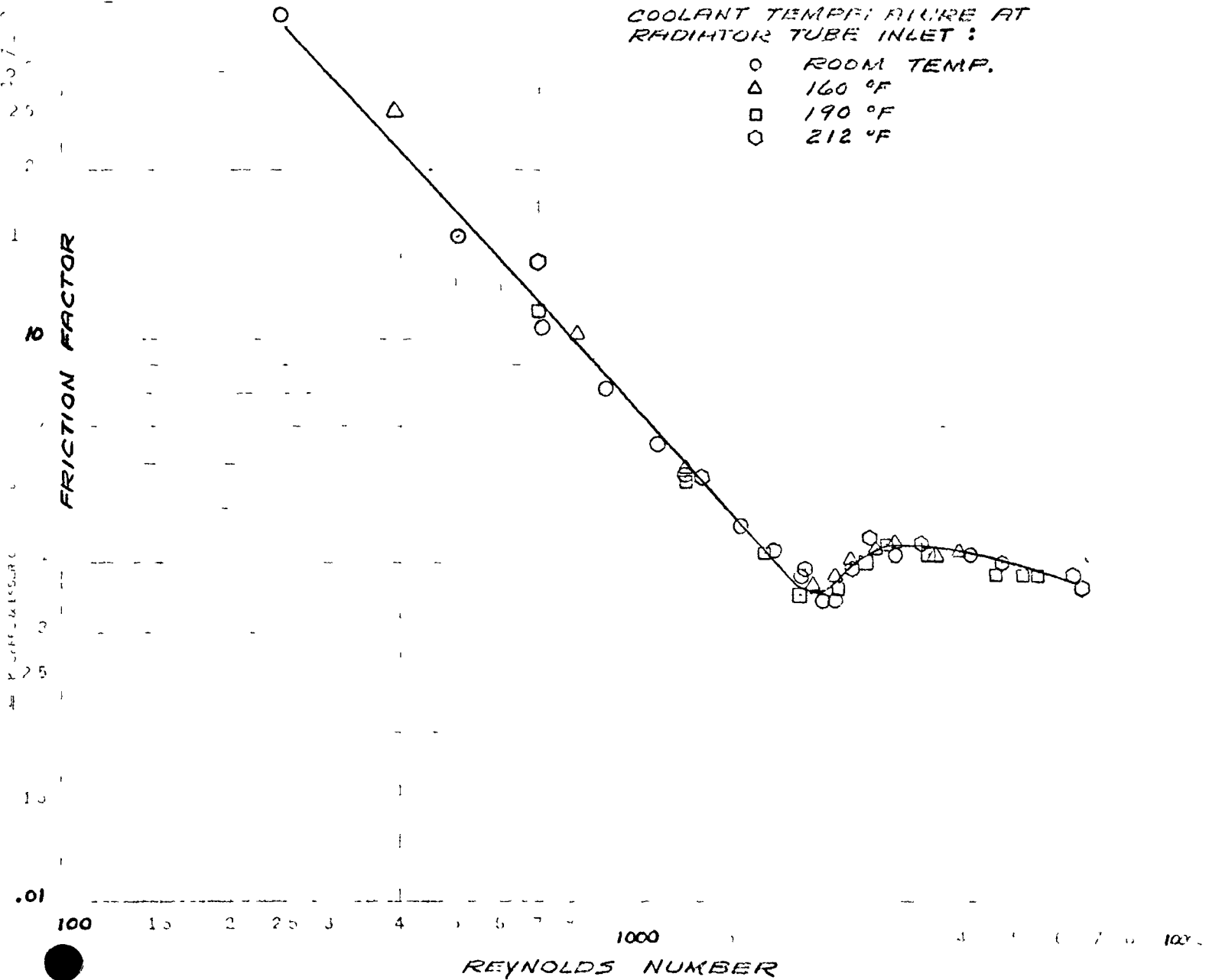
1.0

FIGURE 3.5.2.3-15
KIPS FLOW TEST

MOODY FRICTION FACTOR VERSUS REYNOLDS NUMBER

TUBE I.D. = 0.085 IN.
TUBE LENGTH BETWEEN PRESSURE
TAPS = 80.625 IN
COOLANT TEMPERATURE AT
RADIATOR TUBE INLET :

- ROOM TEMP.
- △ 160 °F
- 190 °F
- ◇ 212 °F



where:

$$N_{St} = \frac{h}{G C_p} = \text{Stanton No.}$$

$$N_{Pr} = \frac{\mu C_p}{k} = \text{Prandtl No.}$$

$$N_{Re} = \frac{DG}{\mu} = \text{Reynolds No.}$$

$$f = \text{Fanning friction factor} = \text{D'arcy factor} \div 4$$

Selected values over the range of Reynolds numbers from 600 to 10,000 are presented below.

<u>N_{Re}</u>	<u>D'Arcy Friction Factor</u>	<u>Colburn Modulus</u>
600	.035	.0099
800	.025	.0083
1000	.020	.0074
1200	.01625	.0067
1500	.01275	.0059
2000	.009375	.0051
2500	.00975	.0051
3000	.01125	.0055
4000	.0105	.0052
5000	.0100	.0051
6000	.009375	.0049
8000	.0085	.0046
10,000	.0080	.0045

Short Radiator Panel Thermal Vacuum Test - To measure the heat rejection capability of the radiator design, an actual radiator section was tested in a vacuum chamber whose walls were cryogenically cooled to simulate a deep space sink temperature (see Figure 3.5.2.6-16). Available facilities dictated that the test section be shorter and slightly less than one quarter of the circumference of the radiator. The test panel measured 48.0 inches long by 33.0 inches wide (compared to 111.24 inches by 37.7 inches for a full quarter section of the radiator) and was composed of four (0.085 inch) ID radiator tubes. The radiator thermal control coating employed on the panel was IITRI Z-93.

The test panel was instrumented with 42 chromel-alumel (type K) thermocouples, placed on the back (insulated) side and on the 0.085 inch ID tubes through small holes in the skin. Four metal sheathed thermocouple probes were installed into the manifolds to measure the Dowtherm A fluid temperatures. Pressure drop measurements were made using two sets of pressure taps. One set, placed one inch each from the inlet and outlet to the tube was used to measure the frictional pressure drop of the tube. The other set was placed on the inlet and outlet manifolds, 1.5 inches before the inlet and after the outlet of the pressure tapped radiator tube in order to measure the overall pressure drop. The manifolds had an inside diameter of 0.375 inches. Measurements were made by setting the fluid flow rate and inlet temperature, and allowing the system to come to a steady state before taking data.

Results of this test show design criteria to be met. Heat rejection rates from the short panel are given in Figure 3.5.2.6-17 which also shows the design waste heat rejection adjusted to the short panel area. Pressure drop measurements project the total pressure drop for the full length radiator to be 16.2 psi at the design flow, well below the 20 psi design goal; turning losses with the manifold-to-tube design employed in the short panel construction (which is expected to have a higher pressure drop than the final GDS radiator design) were 1.8 psi total.

Full Length Radiator Panel Flow Test - A test to determine the drop/flow characteristics of the GDS radiator design was done using a full length radiator panel. The panel skin measured 107.56 inches by 33 inches, and was instrumented with 23 chromel-alumel thermocouples on the uncoated side of the skin, with four chromel-alumel thermocouples in metal sheaths to measure Dowtherm A fluid temperatures, and with two sets of pressure taps to measure the total pressure drop and the tube pressure drop. The four extrusion tubes were 108.63 inches long, with the pressure taps 0.75 inches from the tube ends on the instrumented tube. The test panel was insulated on the uncoated side with fiberglass insulation and was mounted horizontally on a test bench as shown in Figure 3.5.2.6-18. This test panel was fabricated with a redesigned manifold-to-tube assembly attachment which eliminated one of the two right angle turns previously present in the fluid flow path (i. e., as used in the short panel test). The panel was coated with the IITRI Z-93 thermal control coating system.

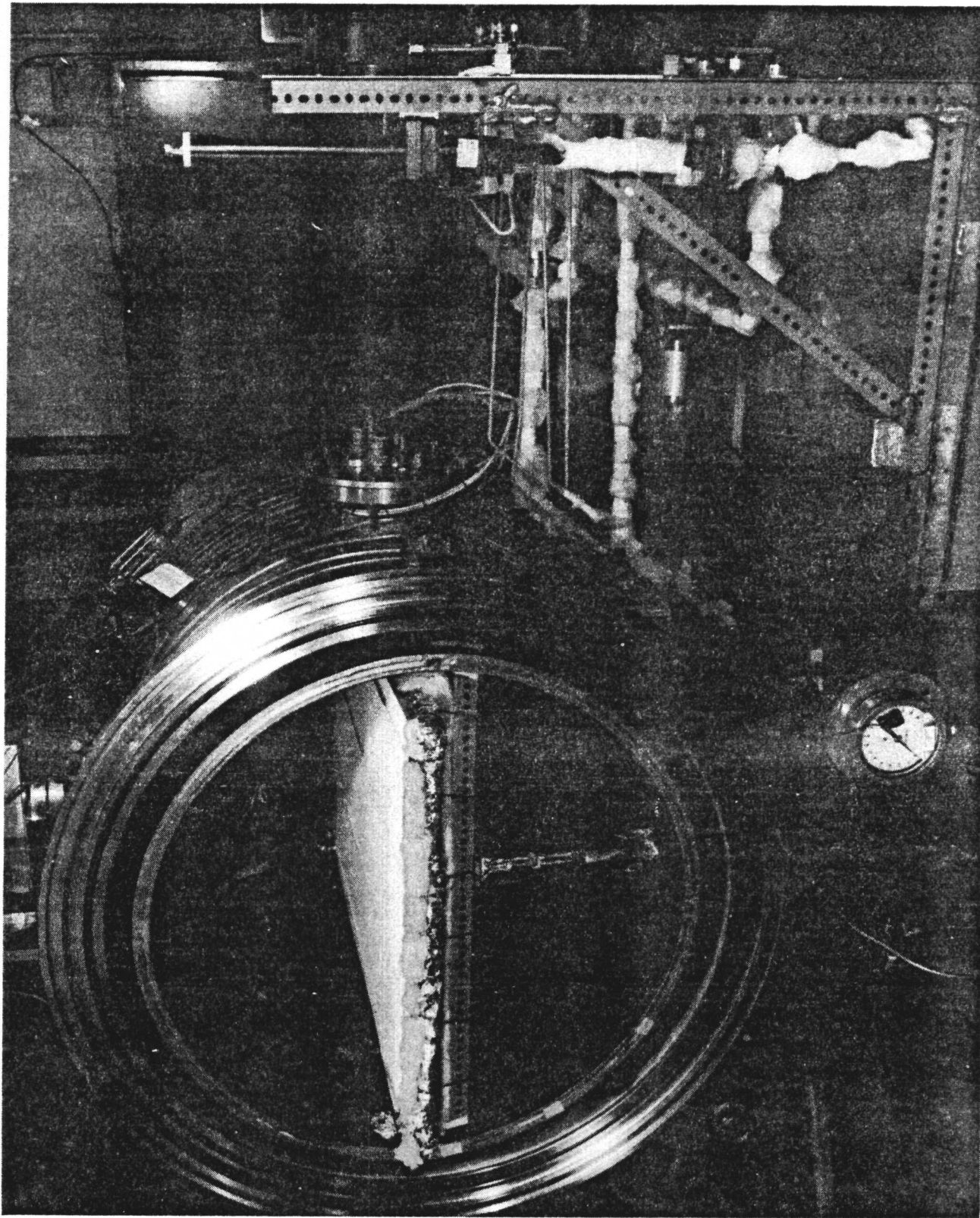
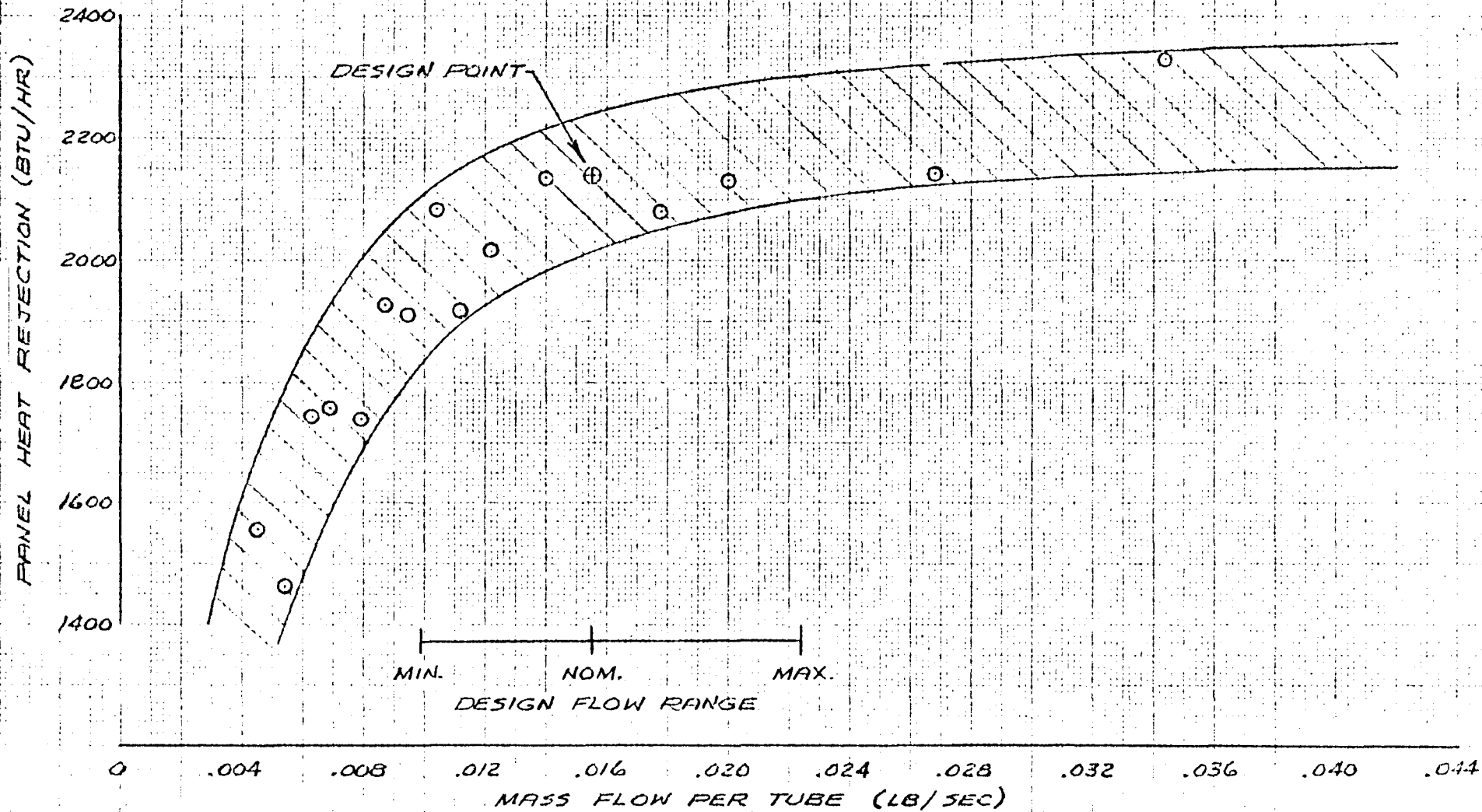


FIGURE 3.5.2.6-16. RADIATOR SHORT PANEL IN T/V CHAMBER.

FIGURE 3.5.2.6-17
KIPS SHORT PANEL T/V TEST
HEAT REJECTION VERSUS MASS FLOW PER TUBE

INLET TEMPERATURE = 212 °F
 ○ KIPS SHORT PANEL TEST DATA



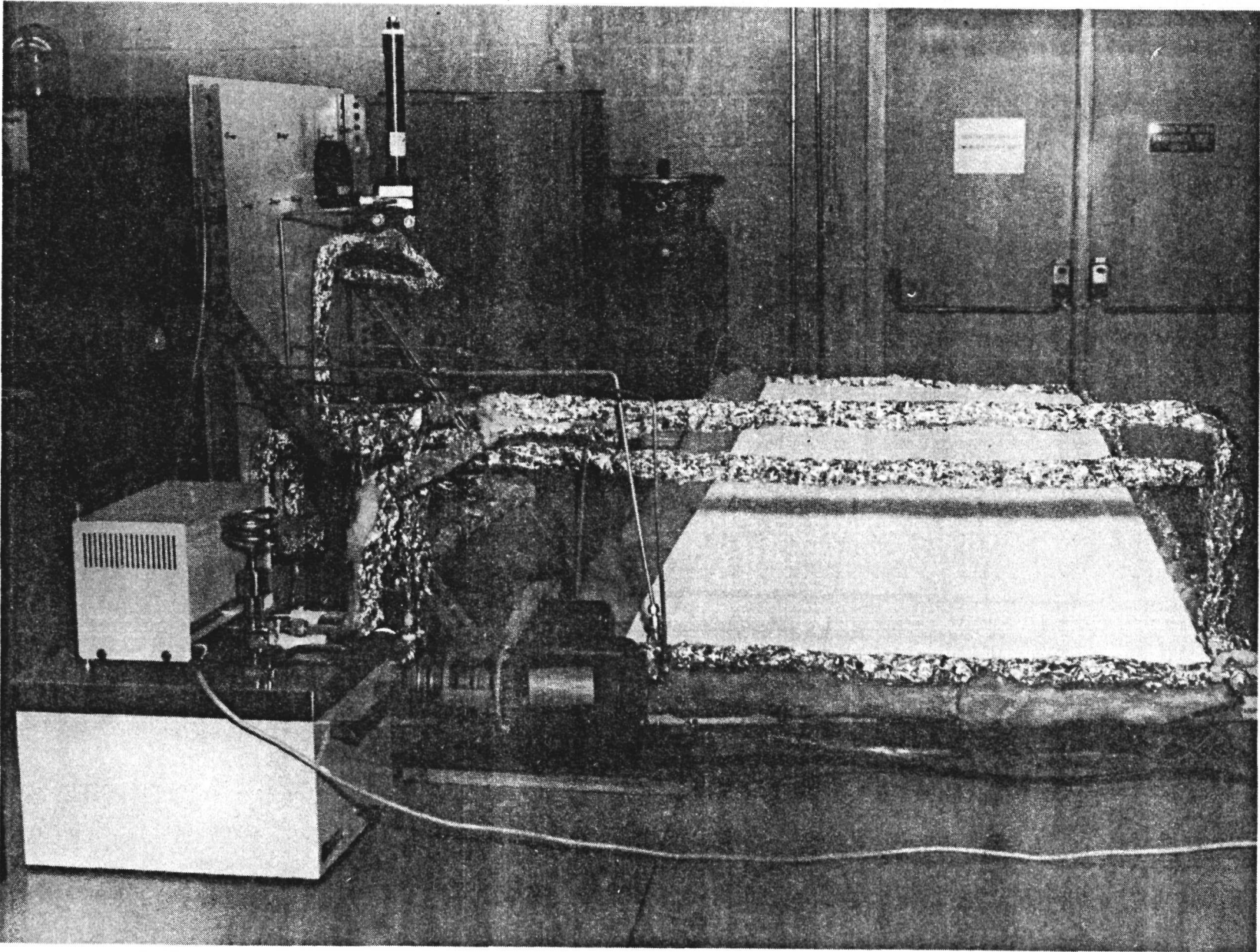


FIGURE 3.5.2.6-18. RADIATOR LONG PANEL IN-AIR TEST.

Data was taken at constant flow rates of roughly half the minimum to double the maximum flows designated for the GDS, or test flows of 0.02 to 0.14 lbs/sec per tube, and at inlet fluid temperatures of 212°F, 190°F, and 168°F. Results from this test are given in Figures 3.5.2.6-19 thru 21, which present the total pressure drop across the radiator, the pressure drop between the tube taps, and their difference, or the "header" drop. Correlation between these pressure drop results and the GDS radiator's anticipated space performance should be quite good since heat rejection under near nominal conditions (i. e. , 212°F inlet temperature and 0.015 lbs/sec per tube flow) resulted in an outlet temperature only 2°F lower than the nominal 168°F outlet temperature.

Several significant conclusions can be drawn from these test results. First, a total pressure drop of 13 to 14 psi across the radiator easily meets the design goal of less than 20 psi under nominal flow conditions. Second, the revised manifold-to-tube assembly design resulted in significant improvement in "header" pressure losses, with the revised design resulting in less than 40% of the pressure loss of the original design at any given flow rate. Third, pressure drop characteristics of the radiator appear to be only moderately temperature dependent, as could be expected from the known temperature dependence of Dowtherm properties, at least within the anticipated design temperature range.

FIGURE 3.5.2.6-19 .

KIPS LONG PANEL FLOW TEST

TOTAL PRESSURE DROP VERSUS MASS FLOW PER TUBE

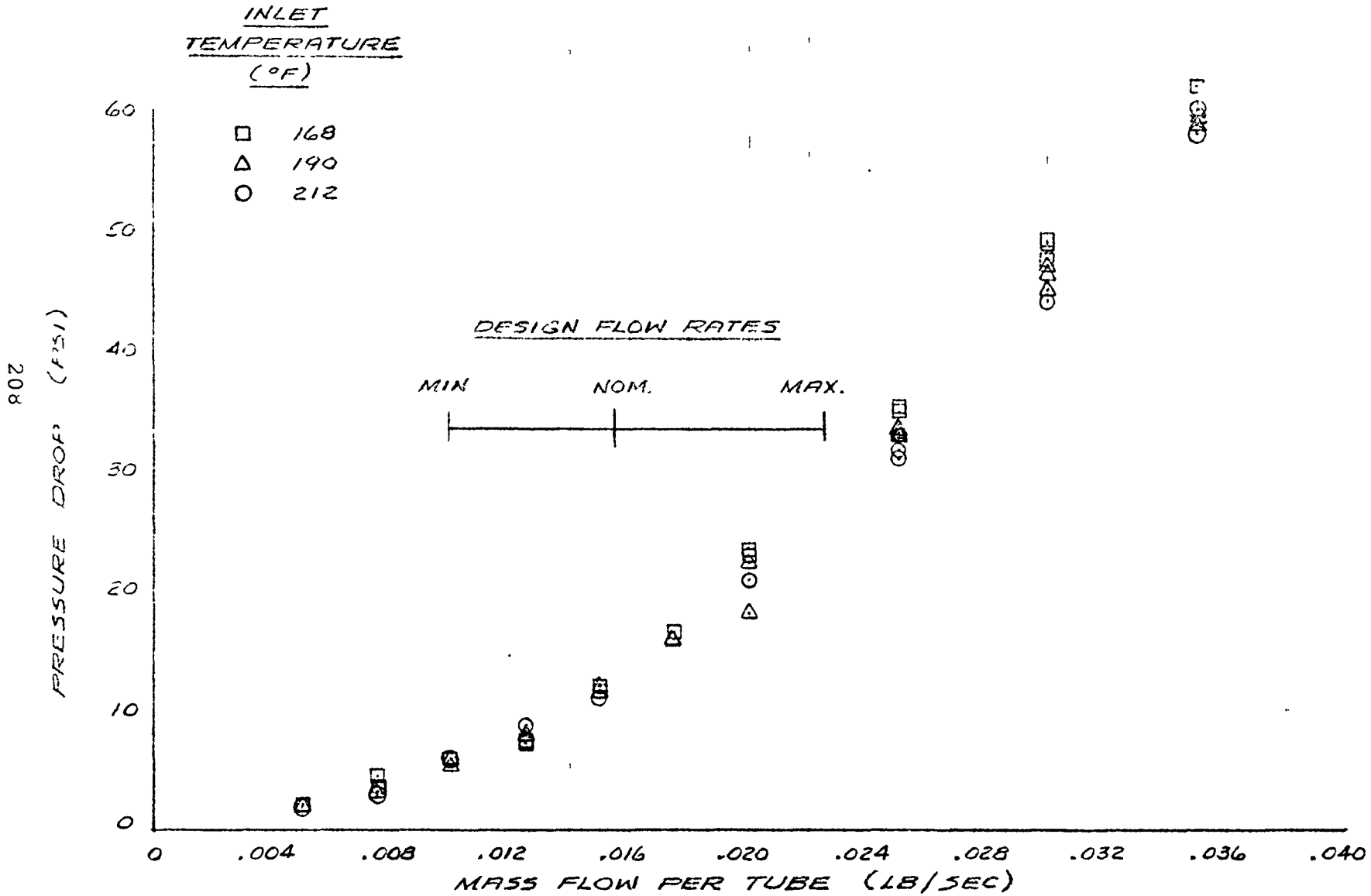
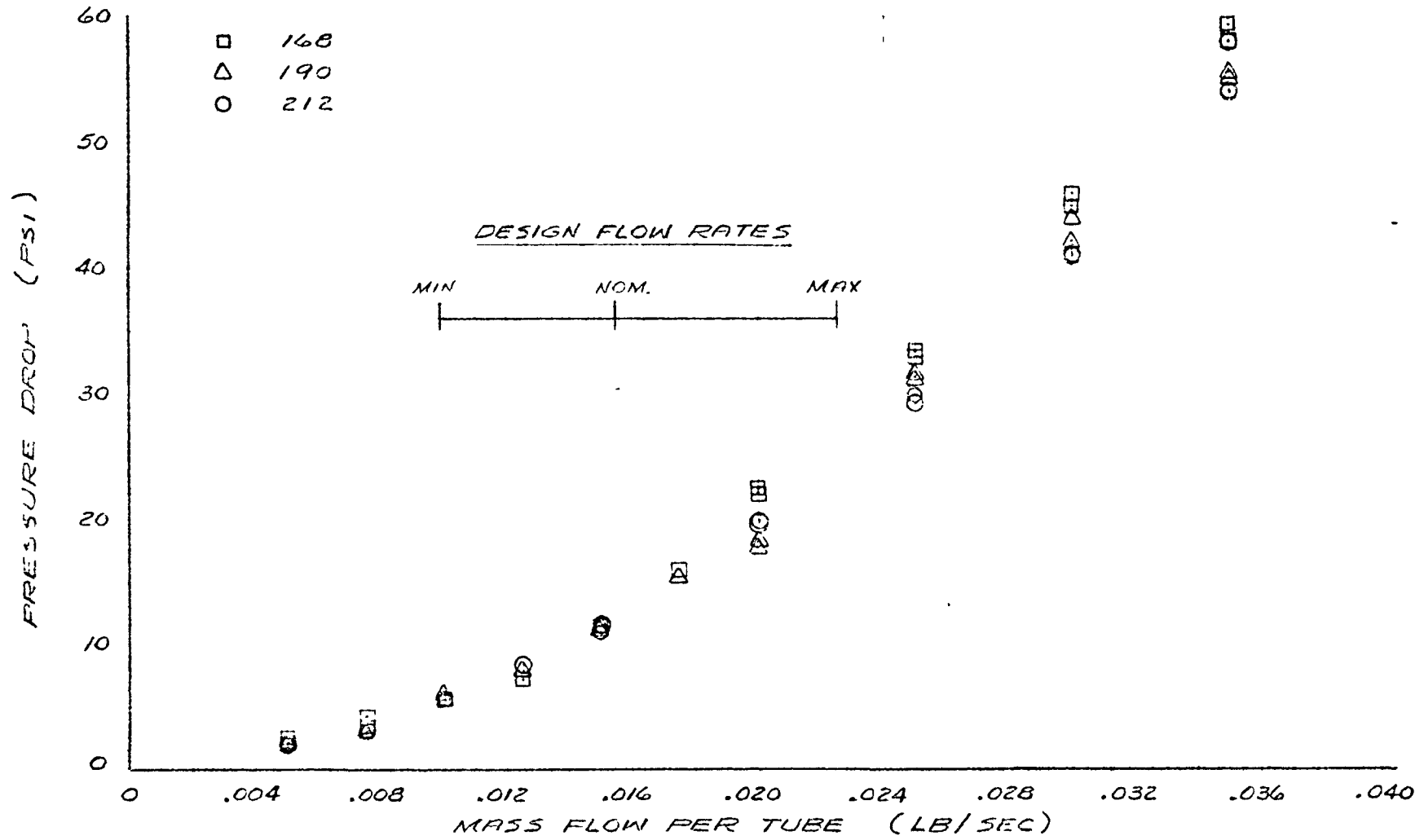


FIGURE 3.5.2.6-2.0
KIPS LONG PANEL FLOW TEST
EXTRUSION PRESSURE DROP VERSUS MASS FLOW PER TUBE

INLET
TEMPERATURE
(°F)

- 168
- △ 190
- 212



209

3.5.2.6.4 Fabrication and Inspection

The critical areas of concern with regard to the radiator fabrication efforts have been selecting the most reliable method of non-destructive testing the radiator welds and assuring that the flow tube opening has not been restricted during welding operations.

In the GDS design, there are two welds at each end of the flow tubes so that the number of welds, in fluid flow areas, in the radiator is at least $N_{\text{tubes}} \times 4$. For the GDS radiator, this amounts to 64 weld joints. The first weld attaches a saddle-like, 6061-T6 aluminum alloy adaptor fitting to each machined end of the 6063-T5 aluminum alloy extrusion (flow tube with meteoroid armor). The second weld attaches each end of the extrusion/adaptor subassembly to the 6061-T6 aluminum alloy header. Figure 3.5.2.6-22 shows the location and configuration of each weld.

The inspection technique used during the GDS fabrication was a two stage technique involving each weld at two levels of assembly with 100% of the components subjected to inspection. The first assembly level involved welding the saddle-like adaptor to each end of the machined extrusion. This subassembly is physically easy to inspect, the flow tube opening can easily be checked for restrictions and assures that only acceptable components are seam welded to the radiator skin. The second assembly level involved the radiator header to extrusion/adaptor subassembly welds and can only be performed after the radiator was fully assembled.

An evaluation of non-destructive inspection techniques for these weld joints was conducted. In addition to helium leak testing and dye penetrant inspection, a technique for radiographing these welds was developed. Several vendors were contacted and visited for discussions of techniques and a determination of capabilities. Universal Technical Testing Laboratories, located in Collingdale, Pennsylvania, was ultimately selected for this effort and weld samples were submitted for a demonstration of their technique. Figure 3.5.2.6-23 shows the weld sample configuration and Figure 3.5.2.6-24 shows the approximate film locations for the radiographs. Figure 3.5.2.6-25 is an actual radiograph of the extrusion/header weld sample.

After each assembly phase of the GDS radiator, each weld joint was helium leak checked to assure the integrity of the weld joint. Acceptance criteria was no leak greater than 1×10^{-5} scc/sec. After leak check each weld was radiographed in order to determine weld joint quality (porosity, inclusions, penetration, etc.). The GDS radiator was radiographed for information purposes only and to demonstrate a non-destructive inspection technique. Figure 3.5.2.6-26 is an actual radiograph of the GDS radiator extrusion/adaptor subassembly. Based upon the evaluation effort to date it is concluded that acceptable weld quality can be determined by these inspection methods (leak check and radiography) after acceptance criteria (i.e., porosity, inclusions, penetration, etc.) have been established as a result of a comprehensive test program based upon destructive tests, collateral analysis and radiographs. Information acquired during the GDS radiator fabrication effort will be used as a starting point for developing these criteria.

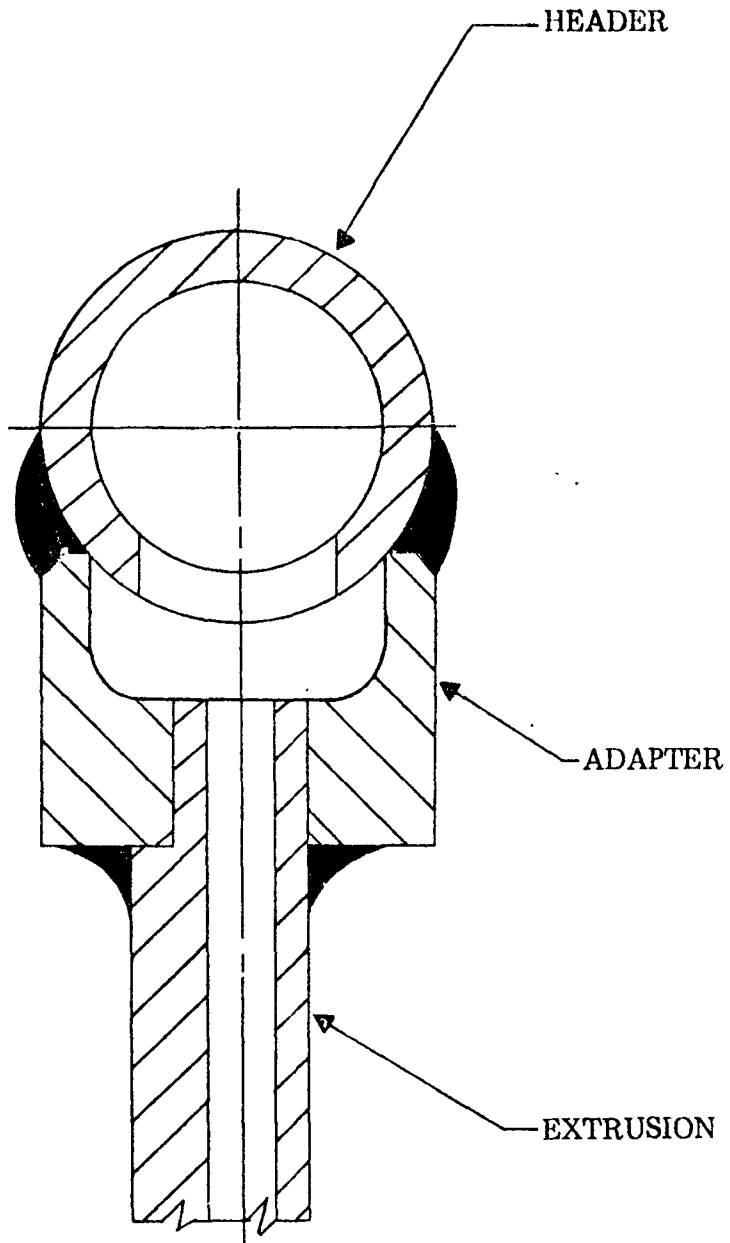


FIGURE 3.5.2.6-22
EXTRUSION/ADAPTOR TO HEADER
TERMINATION

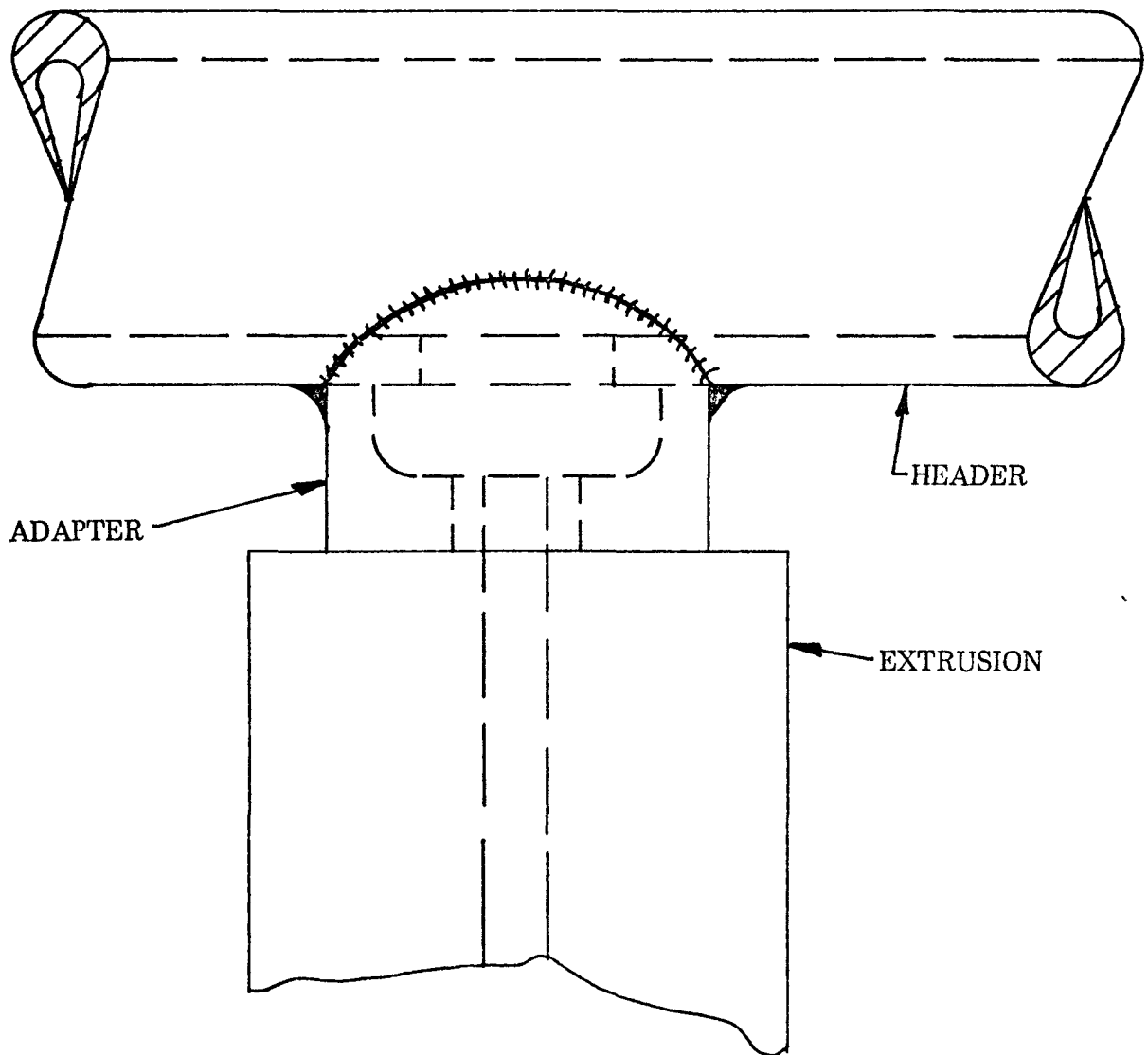
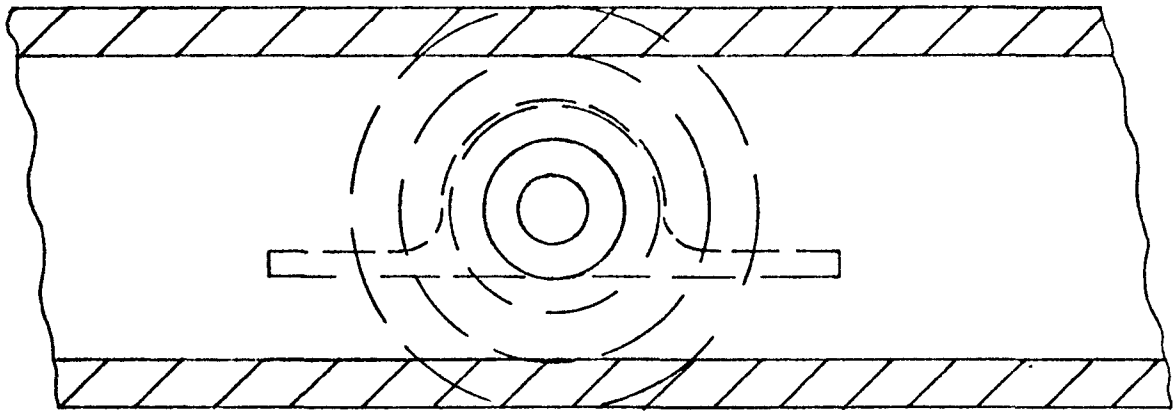


FIGURE 3.5.2.6-23
RADIOGRAPH TECHNIQUE WELD SPECIMEN

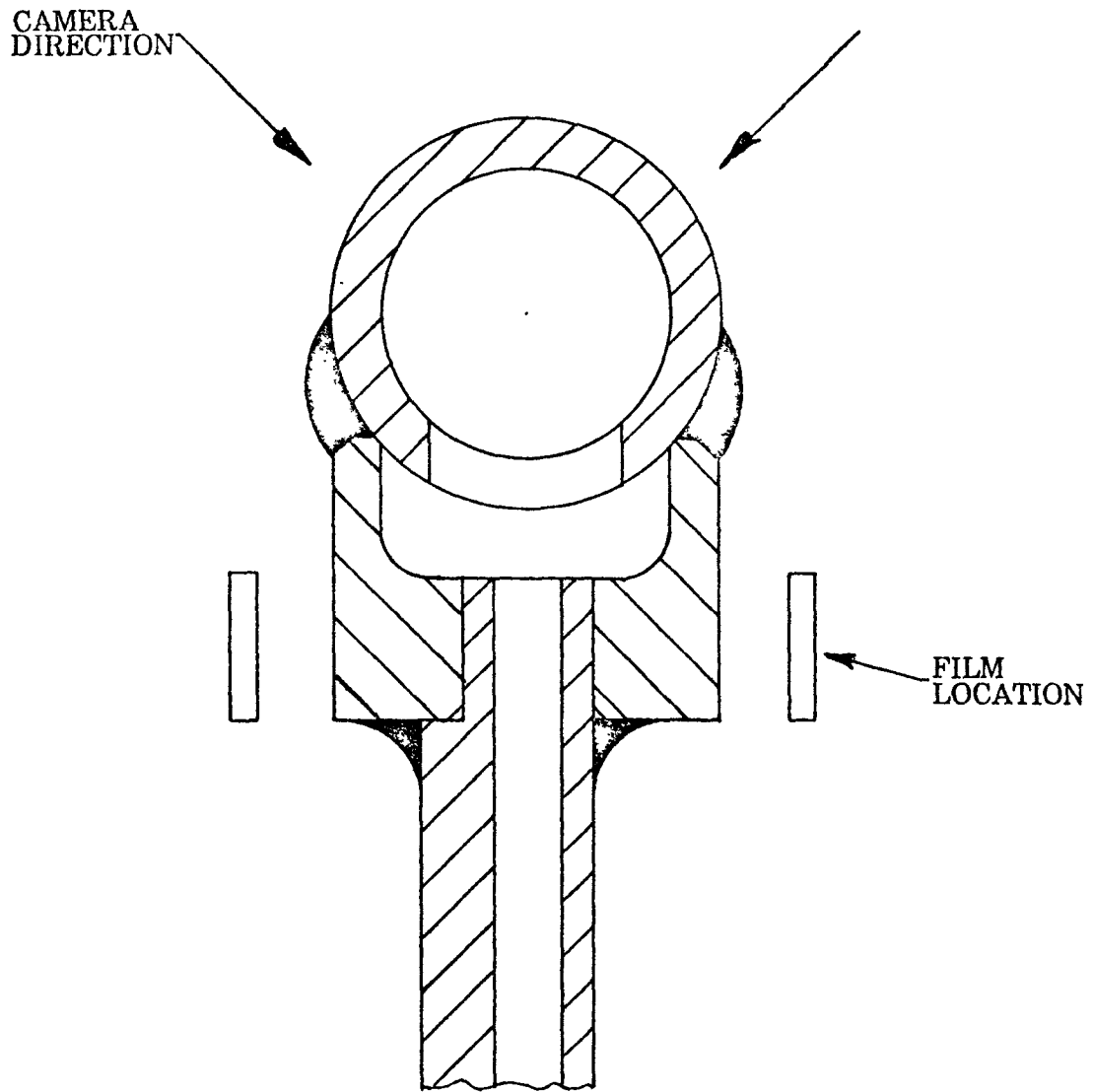


FIGURE 3.5.2.6-24
NDT RADIOGRAPH TECHNIQUE

FIGURE 3.5.2.6-26
EXTRUSION/ADAPTER WELD

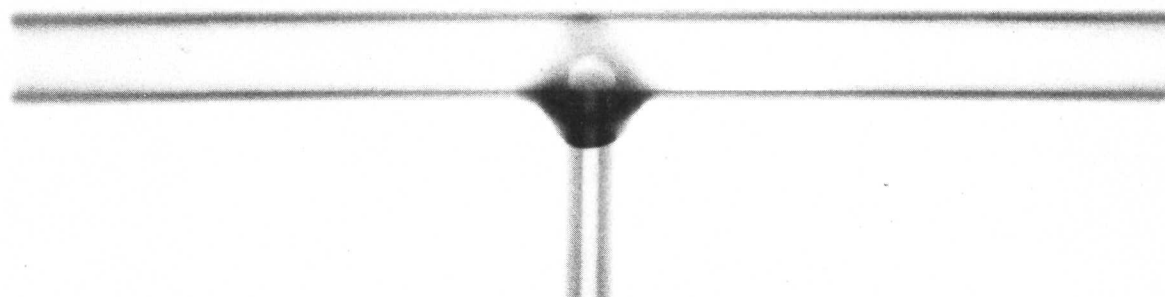


FIGURE 3.5.2.6-25
EXTRUSION/ADAPTER TO HEADER WELD
TEST SAMPLE

Figures 3.5.2.6-28 and 3.5.2.6-29 present actual metallography of extrusion/adaptor subassembly to header weld samples. Concern has been expressed about the probable entrapment of air or gases in the annular space between the machined end of the extrusion and the saddle adaptor fitting. Presumably, these gases, if not removed during the normal outgassing and evacuation of the system prior to charging the system with Dowtherm fluid, could be slowly released to the working fluid circuit.

It has been suggested that one way to preclude this entrapment is to seal weld around the top of the extrusion/adaptor interface. Initially, this was the method used to join these parts (Figure 3.5.2.6-27). However, the weld was difficult to perform because of the small dimensions involved (i.e., 0.085 inch inside tube diameter by 0.032 inch wall) and as a result of this type of edge weld, the flow tube opening became smaller by approximately 0.020 inch. Pursuing this weld method would have introduced another manufacturing operation, namely enlarging the flow tube opening to its original size. This operation is questionable because of the difficulty of picking up the exact centerline of the original flow tube opening in order not to have a mismatch of holes. This weld method was then abandoned for the present fillet weld technique.

When viewed from another direction, however, a conservatively calculated maximum gas volume which could be entrapped between these two fittings is about 0.1 cc for the entire GDS radiator (i.e., 32 welds). The system gas separator should be capable of removing this small amount of gas with no problem.

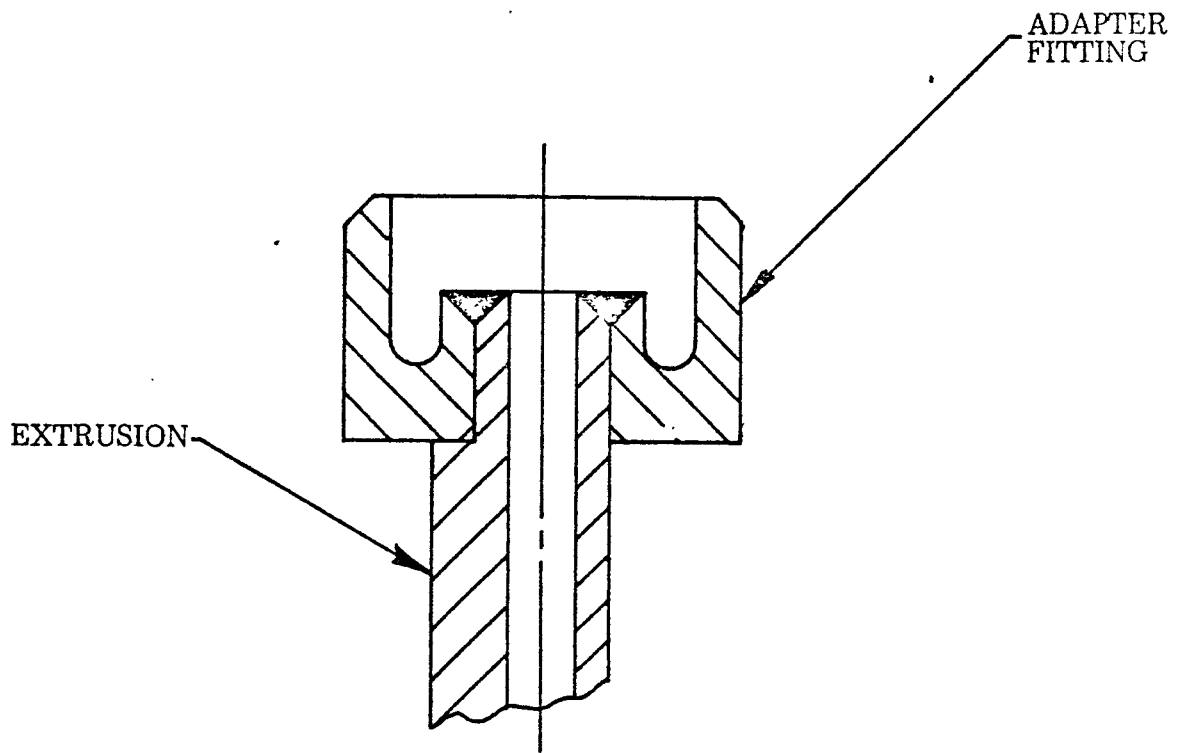


FIGURE 3.5.2.6-27
ADAPTER TO EXTRUSION WELD
(OBSOLETE DESIGN)

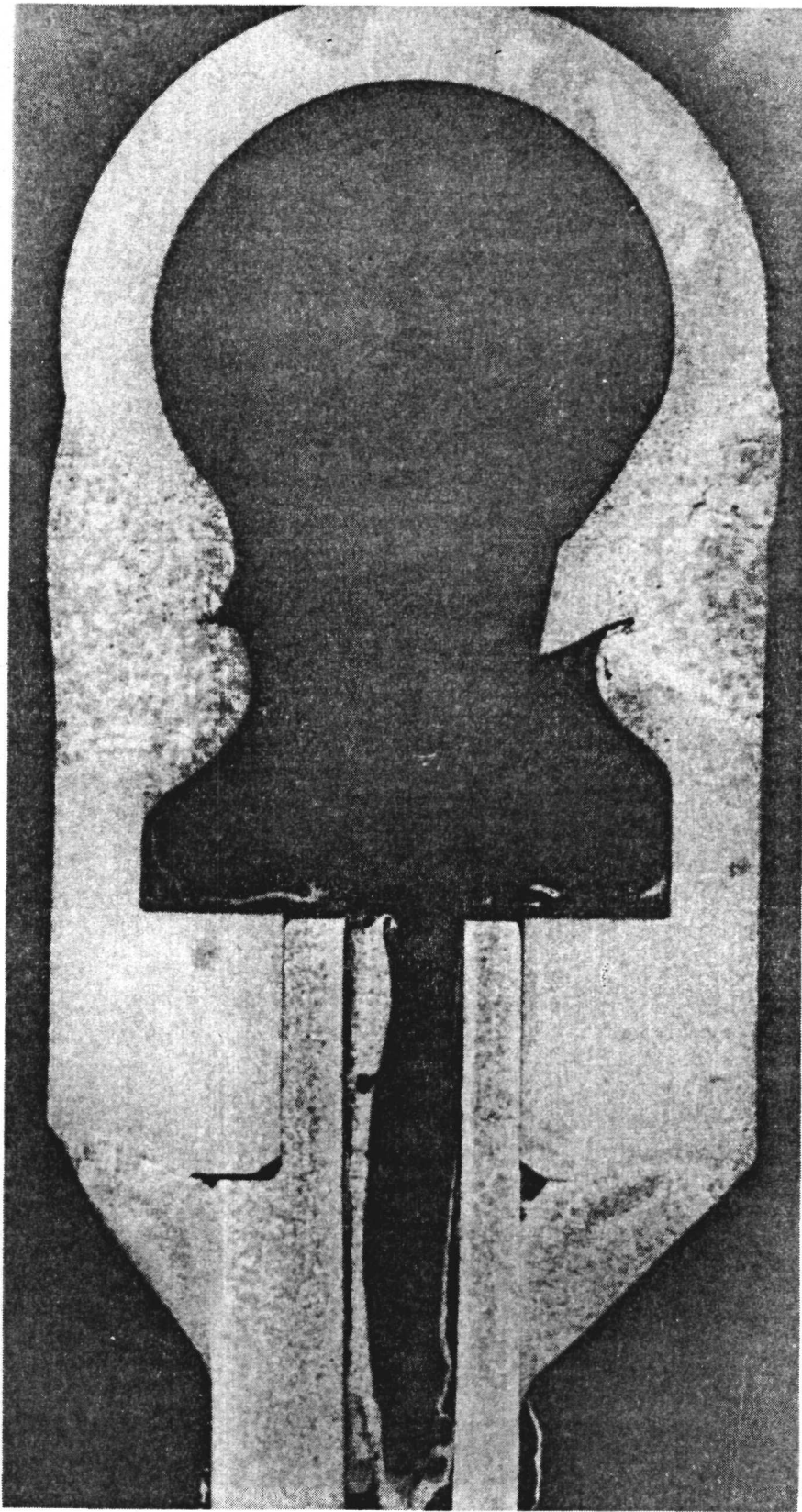


FIGURE 3.5.2.6-28.

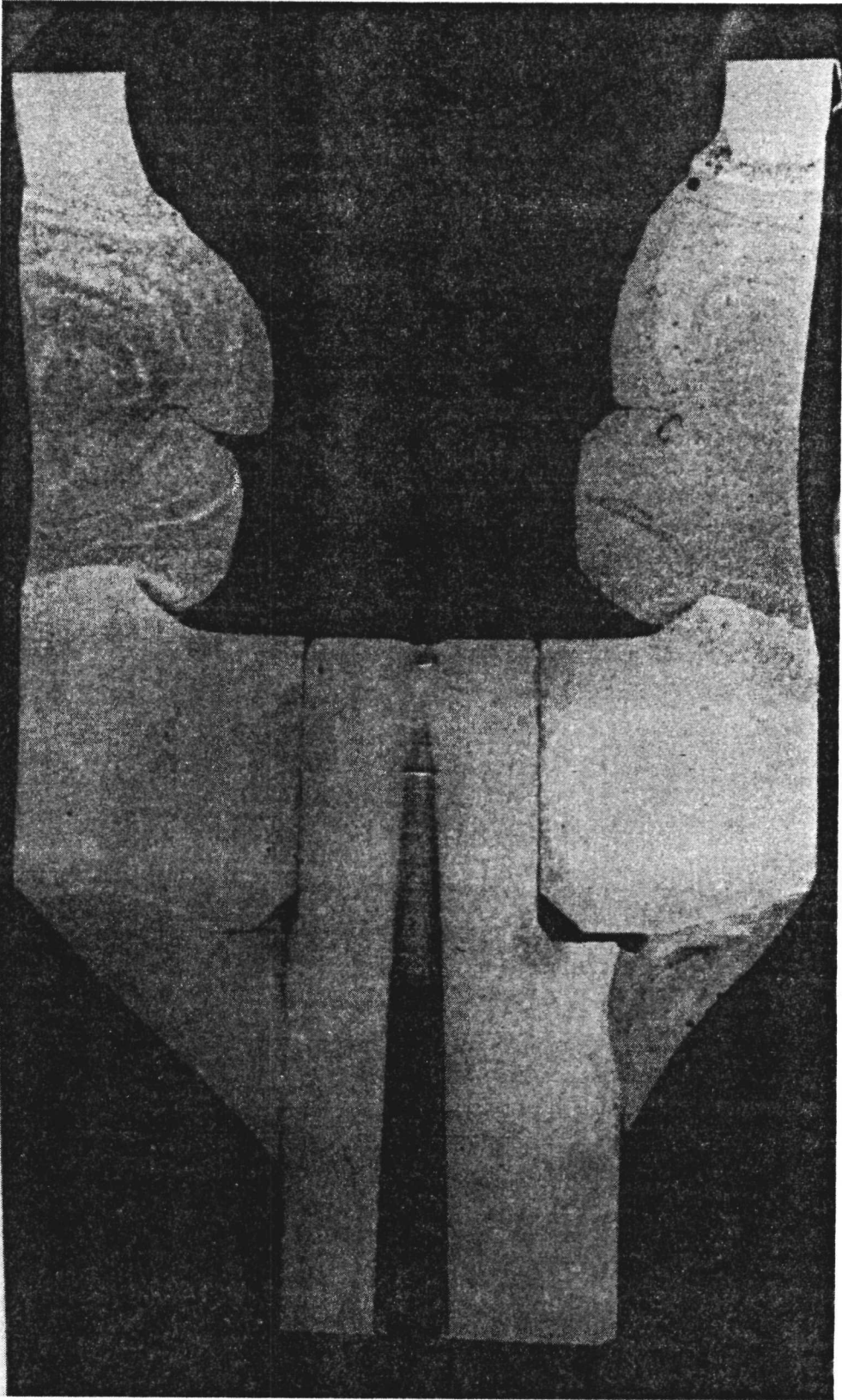


FIGURE 3.5.2.6-29

REFERENCES


1. Segletes, J. A., "Oxidation of POCO AXF-Q1 Graphite in Air," *Journal of Spacecraft and Rockets*, Vol. 10, #12, December 1973, pp. 803-806.
2. Ruwe, D. M., "User's Manual for the Thermal Analyzer Program - TAP 3," Martin-Nuclear Safety Unit, October 18, 1965.
3. K. E. Nelson and J. T. Bevans, "Errors of the Calorimetric Method of Total Emittance Measurement," NASA SP-31, pp. 55-65 (1963).
4. E. R. G. Eckert and R. M. Drake, Jr., Heat and Mass Transfer, 2nd Edition, McGraw Hill Book Co., Inc., New York (1959).
5. Anderson, R., "Trajectory Analysis of MHW HSA in Broadside and End-On Attitudes," LCIPG-RHA-623 dated October 18, 1976.
6. Anderson, R., "Aerophysics Characteristics of MHW HSA in Broadside Attitude," LCHPG-RHA-613 dated October 12, 1976.
7. Holman, J. P., "Heat Transfer," McGraw-Hill, New York, New York, second edition, 1968, pp. 166-172.
8. Seebald, J., "TRLIMP 115 User's Guide," TES-JDS-1213 dated August 6, 1975.
9. Segletes, J. A., "Ablation of Graphite in High-Speed Air Streams," *Journal of Spacecraft and Rockets*, Vol. 12, #4, April 1975, pp. 251-253.
10. Anderson, J. D., "An Engineering Survey of Radiating Shock Layers," AIAA Paper 68-1151, Williamsburg, Va., December 3-5, 1968.
11. Tarr, C. O., "BIPS Preliminary Design Review Action Item, ERDA Ltr. to J. J. Lombardo, Power System Branch, circa September 1976.
12. Roark, J. J., "Formulas for Stress and Strain," third edition, McGraw-Hill Book Co., Inc., New York 1954.
13. "Meteoroid Protection by Multiwall Structures," Cour-Palais, B. G. AIAA Hypervelocity Conference, Cincinnati, Ohio, May 1969.
14. "Radiator Response to Input Shock Load at System Shock Mounts," Telecopy Message from T. Smith (Sundstrand) to R. Hannah (TES), dated February 10, 1978.
15. "Structural Analysis of KIPS Flight System Conceptual Radiator Design," TES Memo KIPS-AA-031, 27 August 1976, A. Alexander to R. Hannah.

APPENDIX A

THERMOELECTRIC TOPPING CYCLE
FOR KIPS ORGANIC RANKINE
POWER SYSTEM

ESD-3138

February 1978

 **TELEDYNE
ENERGY SYSTEMS**

110 W. Timonium Road
Timonium, Maryland 21093

TABLE OF CONTENTS

	<u>Page</u>
I. Summary and Conclusions	1
II. Introduction	3
III. System Description	6
IV. Performance of System	11
V. Tradeoff Studies	17
VI. Safety Considerations	19
VII. Conclusions	20
VIII. References	22
Appendix A - Thermoelectric Performance Calculational Procedure	26

THERMOELECTRIC TOPPING CYCLE FOR KIPS
ORGANIC RANKINE POWER SYSTEM

I. SUMMARY AND CONCLUSIONS

A preliminary thermoelectric topping cycle design is presented herein for the Kilowatt Isotope Power System (KIPS). The design employs selenide thermoelectric modules (3M) which utilize the available thermal gradient between the KIPS Heat Source (MHW) and the boiler to generate DC electrical power supplementing the organic Rankine cycle power output. The thermoelectric subsystem performance presented herein was predicted by extrapolation of currently demonstrated (3M) thermoelectric material properties, but as better definition of the selenide conversion material properties is obtained (particularly at higher cold junction temperatures), a significant improvement in the projected topping cycle output may be realized. The significant highlights of the KIPS topping cycle design compared to the present KIPS design are presented below:

	<u>KIPS-Topping</u>	<u>Present KIPS</u>
Overall conversion efficiency	22.2%	18.05%
Weight increase (lbs) (per HSA)	25.5	0
Total weight (per HSA) ⁽¹⁾	103.2	77.7
Power output increase (watts(e)) (net gain per HSA)	100	0
Specific power (watts(e)/lb) (based on HSA weight only)	5.17	5.58
Design Voltage (VDC)	28	28
Maximum diameter* x length** (each HSA)	13.6 x 22.1	12.7 x 22.1

* Excluding mounting provisions

** Excluding tubing connections

(1) Present KIPS weight based on GDS design. Updated flight system HSA weight is lighter but corresponding topping system would be lighter weight also.

The design presented maintains heat source temperatures within acceptable limits under normal operational conditions and through transient emergency conditions resulting from failure of the thermoelectric circuit and/or failure of the organic Rankine cycle working fluid circuit. However, equilibrium PICS temperatures after loss of coolant accidents are predicted to be higher than the current acceptable values. Nevertheless it is judged that through additional design work these could be made acceptable.

It is concluded therefore that the integration of a selenide thermoelectric topping cycle with the present KIPS heat source assembly appears to be a viable means of improving the overall conversion efficiency of the KIPS system, without a serious compromise of the favorable nuclear safety characteristics of the present KIPS design, and for a small reduction in the overall power-to-weight ratio.

The reduction in organic Rankine cycle efficiency, because of the loss of heat converted to electrical power in passing through the thermoelectrics, is approximately one (1) percent. Thus, the overall efficiency improvement results in a predicted substantial rise in system electrical output of about 23%.

II. INTRODUCTION

A. Objective

The present KIPS design employs a radiation barrier in the annular space between the heat source surface and the Dowtherm A boiler inside surface. The purpose of this barrier is to increase the operational temperature of the heat source to a level where the PICS should survive an emergency reentry/impact event, at least based on present impact data.

Because of the artificial manner in which the heat source surface temperature is being elevated, it was judged that the incorporation of a thermoelectric topping system in the annular space between the heat source and the boiler might possibly be made without any penalty but weight and cost. That is, the incorporation could be made without increasing the heat source or other component temperatures appreciably, and with a significant increase in the overall system efficiency for the same thermal inventory.

The objectives of this study were to evaluate as many of the significant aspects of a topping cycle incorporation as time would permit and in sufficient detail to permit a realistic evaluation of its feasibility and potential performance. The significant potential consequences of the inclusion of a topping cycle with the KIPS rankine cycle were considered to be: (1) a performance increase; (2) a weight increase; (3) very little change in operational temperatures and heat losses; (4) considerable effect on the response of the heat source assembly to emergency conditions (both transient and long term steady state); (5) small size increase; and (6) some changes in the configuration and assembly techniques.

B. Scope of Investigation

The only thermoelectric material combination considered to be viable for the topping portion of the system is the 3M Company's selenide thermoelectric system

which consists of gadolinium selenide N type material and copper-silver-selenide P type material. A silicon germanium alloy couple was briefly considered but was discarded because of marginal efficiency increase, and a lead telluride/TAGS system is ruled out because the hot side temperatures are excessive.

The thermoelectric performance assumed for this study represents extrapolation of data from tests being currently conducted by 3M in conjunction with the Teledyne-3M-DOE SIG program. The performance is based on extrapolating the data to higher cold junction temperatures than have either been tested or evaluated analytically. The 3M Company has agreed to evaluate the performance of their couple at the higher cold junction temperature (400°C) as a check on the extrapolated performance used herein. Should any significant discrepancy exist at that point in time, an addendum to this report will be issued.

For conservatism, the cold-end hardware presently planned for use with the 3M couple in the SIG generator was assumed for this study. Although some improvement in cold-end temperature drop might be achieved by redesign of this hardware, the credibility of such a design would be questioned and perhaps tend to negate an otherwise realistic conclusion as to the potential of the topping cycle concept.

Similarly the selection of the couple geometry is not final, but the selected design is the present SIG generator couple design for credibility. Parametric evaluation of the performance of variations of the couple geometry was conducted but the lack of sufficient thermoelectric design information at this time makes the calculated performance uncertain and therefore it cannot be used until it can be confirmed. There may be, for example, some significant performance advantages to utilizing a longer (larger area) thermoelectric couple provided the weight/size penalty is acceptable, but this cannot be evaluated properly under the present circumstances.

From a configuration standpoint, only modifications to the present KIPS Heat Source Assembly design were considered in this study. The exception to this was the boiler design (which required change in any event) where two new approaches were evaluated.

The study also considered the safety aspects of incorporating a thermoelectric topping cycle in the event that one of several critical emergency conditions develops. The purpose of this portion of the investigation was to assure that certain critical heat source component (particularly the PICS) temperature constraints would not be violated.

III. SYSTEM DESCRIPTION

A. Thermoelectric Module

The thermoelectric module measures 2.50 inches by 11.56 inches and contains 192 thermoelectric couple assemblies. There are four module assemblies in each Heat Source Assembly (HSA), each with a 124 watt(e) output. The module assemblies are located between the heat accumulator ring outside diameter and the inside diameter of the boiler assembly and are equally spaced around the MHW heat source. See Figure 1. The module will be constructed of the selenide materials which are currently under development in the SIG program. The module assembly is comprised of two major components, the thermoelectric couple assembly and the heat rejection system.

The thermoelectric couple assembly is identical to the couple assembly under development in the SIG program. See Figure 2.

The heat rejection system can be broken down into two subsystems, the fin and the boiler assembly. The fin is an integral part of each module assembly and is in direct contact with the inside diameter of the boiler assembly. Each fin has two integral, longitudinal ribs which are perpendicular to the outer surface of the fin. Each of these ribs is slotted for purposes of attachment of the follower spring to the strap assembly and to enable axial growth resulting from thermal expansion of the various components. The inner surface of the fin is counterbored to accept the N-leg and P-leg springs. The conductive heat rejection path is through the strap assembly/rib interface and to the boiler assembly.

The P-leg and N-leg spring loads are reacted against the graphite heat accumulator ring on the hot side and the boiler assembly on the cold side. The thermoelectric couple assemblies are placed between the heat accumulator ring and the boiler assembly by means of special tooling.

B. Heat Source Assembly (HSA)

The addition of a thermoelectric topping cycle increases the power output of an individual HSA from 433 watts(e) to 533 watts(e) resulting in an increased of system efficiency to 22% (18% without topping).

An HSA with a thermoelectric topping cycle (Figure 1) measures 13.60 inches diameter at each end (12.40 inches diameter at center) and weighs approximately 106 pounds. A HSA without the topping cycle measures 12.70 inches diameter at one end, 12.02 inches diameter at the opposite end (10.22 inches diameter at center) and weighs approximately 80 pounds. Neither of these dimensions include mounting provisions. The major physical difference between the two HSA's is the growth in the housing and boiler assembly diameters and the additional components required for the topping cycle. A listing of individual component weights for each HSA can be found in Table I.

The hot sides of the module assemblies are in direct contact with a heat accumulator ring which fits around the isotope heat source and positions the module assemblies relative to the heat source. The ring is sized to take the spring loads from the individual couple assemblies and is supported on each end by fibrous (Min-K) insulation. The ring measures 7.47 inches inside diameter by 7.97 inches outside diameter and is 11.56 inches long. This ring replaces the radiation barrier which is required in a conventional HSA.

The inside diameter of the boiler assembly is a critical surface since intimate contact with the module assembly fin must be maintained. Therefore, this diameter must be machined to a close tolerance after the boiler tubes have been attached. There are two methods of routing the boiler tubes around the boiler shell.

One method is routing in a spiral fashion as shown in Figure 1. This corresponds to the routing presently used in the boiler assembly for the Electrical Heat

Source Assembly (EHSA). Since the boiler diameter is increased, each end of the boiler tube can exit in-line with the boiler shell. This results in a boiler and housing assembly which is symmetrical on each end. Externally, the inter-HSA piping connections are the same as now exist on the Ground Demonstration System (GDS).

The alternate method of routing the boiler tube may, in the long run, be the more desirable because of the simplified external piping arrangement. This method routes the tubes in a vertical manner around the boiler assembly, concentrating the tube locations directly over the module assemblies. See Figure 3. The boiler tube inlet and outlet would be on the same end of the HSA, thereby simplifying the external piping connections.

In order for the module assemblies to function more efficiently, the space between modules must be insulated in order to force the heat through the thermoelectrics. In an emergency overtemperature situation (i. e. , boiler fluid flow stops), it is possible for the thermoelectric materials to deteriorate, thereby eliminating the primary heat rejection path to the boiler assembly. Since Min-K type insulation will remain intact in this situation there would be high resistance to heat flow to the boiler assembly, and as a result, the heat source temperature would be excessive. Multifoil insulation, with the use of the proper metal, will prevent this excessive temperature from occurring since it will melt at a predetermined, safe temperature thereby allowing the heat source to radiate directly to the boiler assembly.

C. System Assembly

Assembly of the HSA with thermoelectric topping is slightly different than assembly of a conventional HSA and must be accomplished in an inert, oxygen free environment because of the nature of the thermoelectrics and the heat source. A special facility will be required for this operation.

Initially, the heat accumulator ring, the four module assemblies, the cold side rib and the boiler assembly will be assembled together. A special assembly tool will be required for this operation.

Min-K insulation can be installed into the lower end of the housing and the O-ring seal, lower cover and lock ring can be installed. The cover will act as a restraint for the insulation. The thermoelectric module subassembly is then lowered into the housing cavity until the boiler assembly flange bottoms on the insulation. The multifoil insulation, which fits between the boiler assembly and the inside diameter of the housing can be inserted. After installation of the multifoil insulation segments between module assemblies, the upper outer rings of insulation can be installed and hand fitted as necessary for routing of the output power wires which come from the thermoelectric module assemblies. After soldering these wires to the power output receptacle, the upper outer cover is installed. At this point the boiler assembly tubes are cut to proper length and welded to the feedthrough fittings which are in the cover assembly. Fittings are added to the boiler tubes. Tooling required to perform this portion of the assembly will be similar to the tooling used to assemble the EHSA.

Fueling of the HSA may require that the semi-completed assembly be transferred to another inert atmosphere chamber, one which has the capability of being evacuated as well as being purged with inert gas. Using tooling which will be unique for this assembly, the heat source will be lowered into its cavity, the center ring of insulation hand fitted so that the proper preload is applied to the heat source and the center cover installed. Installation of the cover will require tooling similar to the tooling used to assemble the EHSA.

TABLE I

WEIGHT BREAKDOWN PER HEAT SOURCE ASSEMBLY

	<u>HSA W/O Topping (Lbs)</u>	<u>HSA W/Topping (Lbs)</u>
Housing Assembly	10.13	10.60
Lock Ring - Upper Outer	.81	.94
Lock Ring - Upper Inner	.50	.50
Lock Ring - Lower	.76	.94
Cover - Upper Outer	1.53	2.10
Cover - Upper Inner	1.41	1.41
Cover - Lower	2.11	2.73
Receptacle	—	.11
Penetration Assembly (.25 Diameter)	.26	.26
Penetration Assembly (.50 Diameter)	.30	.30
Gasket	.01	.01
Boiler Assembly	7.82	13.02
Heat Source	42.00	42.00
Multifoil Insulation	3.08	4.24
Min-K Insulation	4.90	8.16
Radiation Barrier	1.51	—
Hardware, O-Rings, Boiler Tube Fittings, etc.	0.57	0.57
Heat Accumulator Ring	—	4.56
T/E Module Assembly & Cold Side Rib	—	7.21
Multifoil Insulation (Between Modules)	—	3.50
	<hr/>	<hr/>
} Total	77.70	103.16
} P(e)	433.3	533.3
	W/P(e) (5.58 watts/lb)	(5.17 watts/lb)

IV. PERFORMANCE OF SYSTEM

A. Steady State

Normal operating temperatures for the present KIPS design are presented in Ref. 5 and are based on the average temperature of the number two boiler in the KIPS three boiler heat source arrangement. The nominal average fluid temperature for this #2 boiler is 340°C. Maintenance of this boiler temperature was selected as a design constraint for the topping cycle performance study. The other constraint assumed for the study was a limit to the hot junction temperature of 850°C which is the current design limitation for the selenide materials. The fluid to boiler tube surface temperature difference (film drop) is assumed to be 17°C. No temperature drops are assumed within the metal of the boiler due to the substantial thickness of copper required to react the cold end hardware spring forces. End heat losses are assumed to be 100 watts due to the increased housing diameter. The thermal inventory is assumed to be 2400 watts. The resulting normal operating temperatures for the KIPS topping cycle design are compared to the present KIPS design below:

<u>Location</u>	<u>Topping Temperature ~°C</u>	<u>No Topping Temperature (°C)</u>
Fluid	340	340
Boiler	360	360
T/E Cold Junction	400	—
Heat Accumulator Ring I. D.	852	—
Heat Source Surface O. D.	885	849
PICS (Approximate)	1240	1204

Operational thermoelectric performance of the topping cycle is presented in Table 2. The calculational methodology is outlined in Appendix A. It is important to note that there is no significant impact on the amount of heat delivered to the boiler other than the direct removal of that portion of the heat converted to electrical power in the thermoelectric elements. Hence, the organic Rankine cycle output is only slightly reduced by the addition of the thermoelectric topping cycle.

TABLE 2
PREDICTED KIPS T/E TOPPING CYCLE
THERMOELECTRIC PERFORMANCE
(Current Standard Material)

Leg length (inches)	.30
Total thermal inventory (watts)	2400
End heat loss (watts) - both ends totaled	100
Module insulation heat loss (watts)	283
Heat available for conversion (watts)	2067
Calculated T/E efficiency* (%)	6.0
Electrical power output* (watts)	124
Total thermoelectric area (square inches)	46.9
N leg total area (square inches)	23.95
P leg total area (square inches)	22.95
Load voltage (volts)	28
Number of couples	190
N leg diameter (inches)	.40
P leg diameter (inches)	.39

* Neglecting 25% extraneous resistance.

B. Emergency

Two failure modes are considered: loss of T/E electrical output and loss of coolant flow. Both failures are assumed to start from the normal operating condition.

In the event the topping cycle electrical circuit becomes either shorted or opened and the organic Rankine cycle thermal operation is not primarily affected, the assumed impact on system operation is as follows:

1. The boiler sees approximately 120 W(t) more heat input.
2. The boiler will rise approximately 6°C in temperature as predicted by Figure 3 of Ref. 6.
3. The cold junction temperature rises about 6°C.
4. Sublimation of selenium due to either copper migration or increased temperature at the hot shoe results in loss of thermal contact between the hot shoe and the thermoelement.
5. The heat accumulator ring rise in temperature until the thermal inventory minus end losses can be transferred to the boiler by:
 - a. Conduction through insulation between thermoelectric modules.
 - b. Conduction through insulation between thermoelectric elements.
 - c. Radiation to thermoelements, then conduction through the elements.

For this failure, the temperature rise of the heat accumulator block would probably not be sufficient to melt our multifoil insulation between the thermoelectric modules. Hence, component temperatures would be in the same as if fibrous (Min-K type) insulation were used in place of multifoil. These component temperatures are:

<u>Location</u>	<u>Temperature ~°C</u>
Boiler	366
T/E Cold Junction	404
T/E Element Hot Side	477
Heat Accumulator Ring I.D.	912
Heat Source Surface O.D.	951
PICS (Approximate)	1306

A far more serious failure would be the loss of organic Rankine cycle working fluid flow. In this event, the boiler temperature equilibrates at about 827°C, which would melt any cold end hardware components made of aluminum. Creep and/or relaxation of the springs would occur at an accelerated rate. Also, the high hot side temperatures would promote selenide sublimation. Eventually, conductive heat transfer could be stopped at both the hot and cold ends of the element, resulting in two radiation gaps in series with the thermoelectric material thermal resistance.

This will drive the heat accumulator ring temperature up and result in melt-down of the multifoil insulation. Assuming fibrous (Min-K type) insulation present between thermoelectric modules instead of multifoil, the temperatures at significant locations are:

<u>Location</u>	<u>Temperature ~ °C</u>
Boiler	827
T/E Cold Junction	1061
T/E Element Hot Side	1143
Heat Accumulator Ring I. D.	1276
Heat Source Surface O. D.	1293
PICS	1648

In the above scenario the PICS temperature is significantly above tolerable steady state values. However, if a melting multifoil insulation is used in place of fibrous insulation between modules, the maximum PICS temperatures are established by the foil melting temperature. With a 900°C melt temperature, the final steady state temperatures, assuming incomplete foil melting and disregarding transients during the melting process are:

<u>Location</u>	<u>Temperature ~ °C</u>
Boiler	827
Hottest Remaining Foil	899
T/E Element Hot Side	918
Heat Accumulator Ring I. D.	967
Heat Source Surface O. D.	1053
PICS	1408

NOTE: The 1408°C PICS temperature presented above was calculated by assuming that one foil remained intact after the meltdown. Meltdown tests showed that this foil partially melted even in a gravity dominated test environment. Thus, the PICS temperature after meltdown is expected to be closer to 1280°C, a value predicted for complete meltdown of the foil systems.

V. TRADEOFF STUDIES

A. T/E Configuration

The thermoelectric properties of the selenide conversion materials were estimated as functions of current density and temperature using the best available* data from 3M reports. This enabled the performance of any couple configuration to be predicted. Although the baseline topping cycle design utilizes the SIG couple configuration, some advantages are evident for altering the thermoelement length and diameter. Increasing the thermoelement length requires an increase in diameter to transport the fixed thermal inventory with the desired hot to cold junction temperature difference. This diameter increase means greater total area of thermoelectric material as compared to interelement insulation; hence, higher thermal efficiency. Several element lengths were examined to determine the sensitivity of electrical power output to log length. For a change from 0.3 inch to 0.6 inch long thermoelements, about 11 watts (per heat source assembly) more electrical output can be expected considering the interelement insulation to the Min-K and the intermodule insulation multifoil.

B. Temperatures (Hot Junction/Cold Junction)

Maximum hot junction coupled with minimum cold junction temperatures provide greatest electrical output from the topping cycle. Practical considerations impose specific limits on both junction temperatures resulting in lower thermoelectric efficiency than obtained in the SIG program application. The 3M Company, suppliers of the selenide conversion material, currently recommend a hot junction temperature of 850°C. Within several years additional development of this material is expected to permit the hot junction temperature to rise to 900°C, which would result in an improvement in topping cycle electrical output.

* See page 4.

The cold junction temperature is established by the boiler operating temperature. Lowering the boiler temperature was found to have a substantial adverse impact on the efficiency of the organic Rankine cycle system. This adverse impact overwhelmed the power gain for the topping cycle, so that from a systems viewpoint the cold junction temperature is best left near the current nominal boiler operating temperature.

VI. SAFETY CONSIDERATIONS

The KIPS nuclear safety status is strongly dependent on the ability of the PICS to survive impact and subsequently contain the nuclear fuel. This places lower bounds on the allowable PICS temperature. Similarly, upper temperature limits are imposed on the PICS for full compatibility reasons. The proper functioning of the PICS requires that it be kept within a narrow range of temperatures. Hence, acceptable heat source temperatures are dictated by the range of permissible PICS temperatures.

Identification of malfunctions which affect heat source temperatures and verification that the malfunction does not drive temperatures beyond acceptable limits provides a basic demonstration of nuclear safety with respect to temperature excursions.

The most severe (with respect to heat source temperature) credible failure of the topping cycle itself is the shorting or opening of the thermoelectric circuit. Organic Rankine cycle failures are felt by the heat source only if the ability of the working fluid to remove isotopic decay heat is reduced. The worst case is total loss of coolant flow.

Both electrical failure of the topping cycle and loss of coolant accidents can be tolerated without greatly exceeding the presently accepted heat source temperature limits. Analyses demonstrating this capability are discussed in Section IV-B.

VII. CONCLUSIONS

A complete conceptual design of a thermoelectric topping cycle is presented with supporting analyses. Considerable (about 4%) increase in overall KIPS cycle efficiency is predicted without seriously violating heat source temperature constraints. The hardware analyzed is basically that being developed for the SIG program. Anticipated thermoelement improvements may further increase topping cycle electrical output. Component development required specifically for the KIPS topping cycle would include a melting multifoil insulation for use between the thermoelectric modules, acting as an emergency heat release path between the MIW heat source and the boiler.

Although the proposed topping cycle design utilizes thermoelectric modules essentially identical to those used on the SIG program, a moderate increase in power output can be obtained by increasing the thermoelement length. The electrical output of the modules would be increased about 10% by lengthening the thermoelements from 0.3 inch to 0.6 inch. The major penalties for this power increase would be the cost of developing a selenide module with the modified thermoelement dimensions and the weight increase associated with the longer elements.

Normal operating temperatures of the MIW heat source are slightly higher with the topping cycle added. This is due to the sizing of the thermoelements and modules to achieve 850°C on the hot junction in order to maximize the thermoelectric output, and the presence of a heat accumulator block for ease of system assembly.

Although inclusion of the topping cycle adds weight to the overall system, the specific weight in watts per pound is reduced by only 7 to 8% (5.17 w/lb with topping vs 5.58 without). Anticipated increases in thermoelement performance as an outgrowth of SIG development work would not affect system weight.

The major area for system growth lies in the continued development of the selenide materials. These materials are relatively new and untested at this juncture and it is not unreasonable to assume, based upon current 3M Company predictions that system efficiency can be increased as much as 5% without an additional weight increase. The increased efficiency could result in as much as 83 watts(e) additional power output, increasing the HSA power output from 533 watts(e) to 616 watts(e).

Since system efficiency would be approaching the predicted Brayton Cycle (BIPS) system efficiency, it would imply that it might be possible ultimately to eliminate one HSA from the KIPS system. Two HSA's would provide between 1030 watts(e) at the predicted efficiency) and 1232 watts(e) (future predicted efficiency) of electrical power. The obvious end result would be a decrease in system cost, weight, complexity and a savings of isotope fuel.

VIII. REFERENCES

1. Hampl, E. F., Jr., "Thermoelectric Materials Evaluation Program," Monthly Top Summary Report No. 112, MMM-2331-0481, July 20, 1977.
2. 3M Company Presentation, SIG/GDS Final Design Review, May 24-27, 1977.
3. Hampl, et. al., "TPM-217 Material Performance Characteristics," Paper No. 729040, 7th IECEC, September 25-29, 1972.
4. Brittain, Wayne, "Evaluation of a Manual Calculational Technique for Thermoelectric Couples," MS Thesis, Drexel Institute of Technology, June, 1966.
5. Loughheed, V., "Transient Thermal Response of KIPS Heat Source Assembly Assuming Loss of Coolant Flow," KIPS-VRL-057, Teledyne Energy Systems, 22 October 1976.
6. Darooka, D., "KIPS EHSA Performance Test Analysis," KIPS-DKD-086, Teledyne Energy Systems, 25 July 1977.

ESD-3138
- 2 -

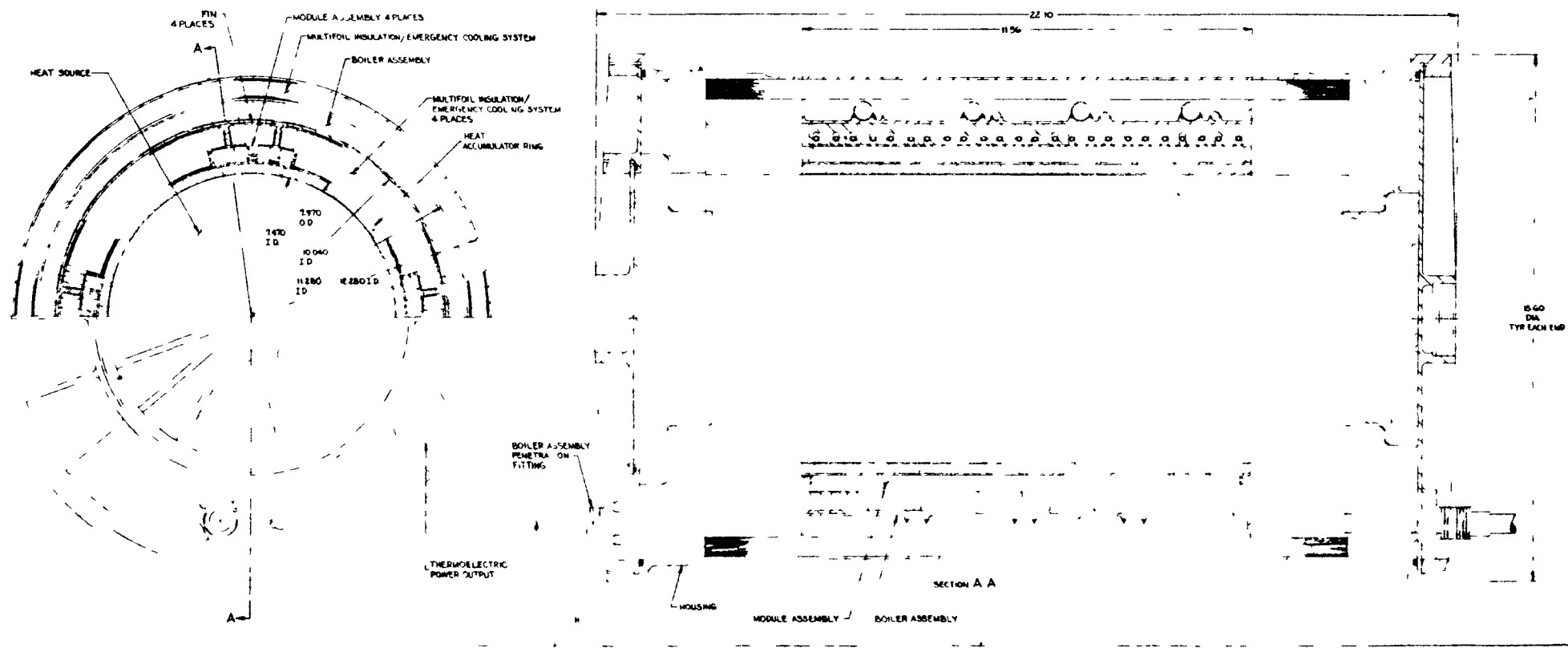


FIGURE 1 KIPS ISOTOPE HEAT SOURCE ASSEMBLY WITH THERMOELECTRIC TOPPING CYCLE

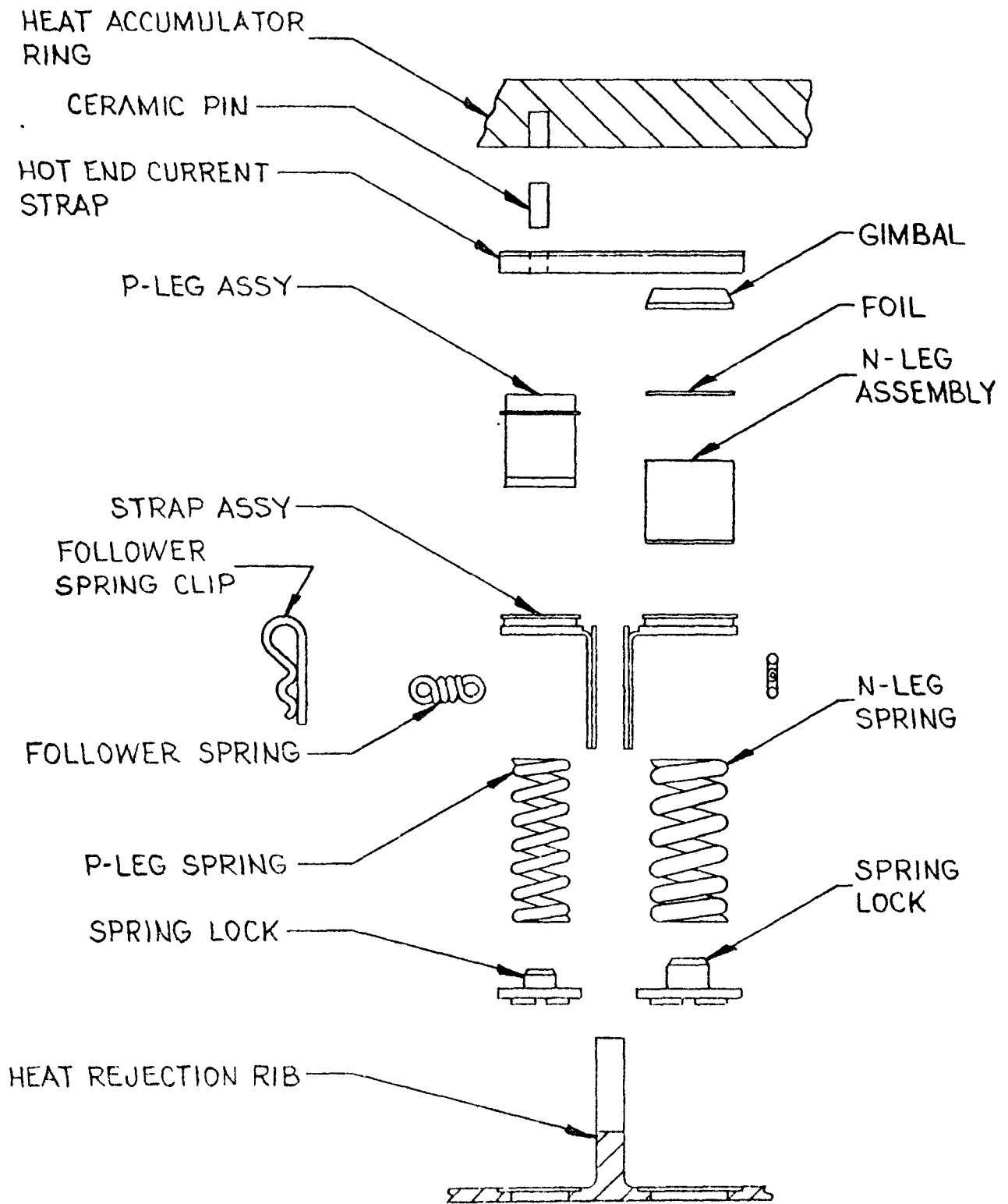
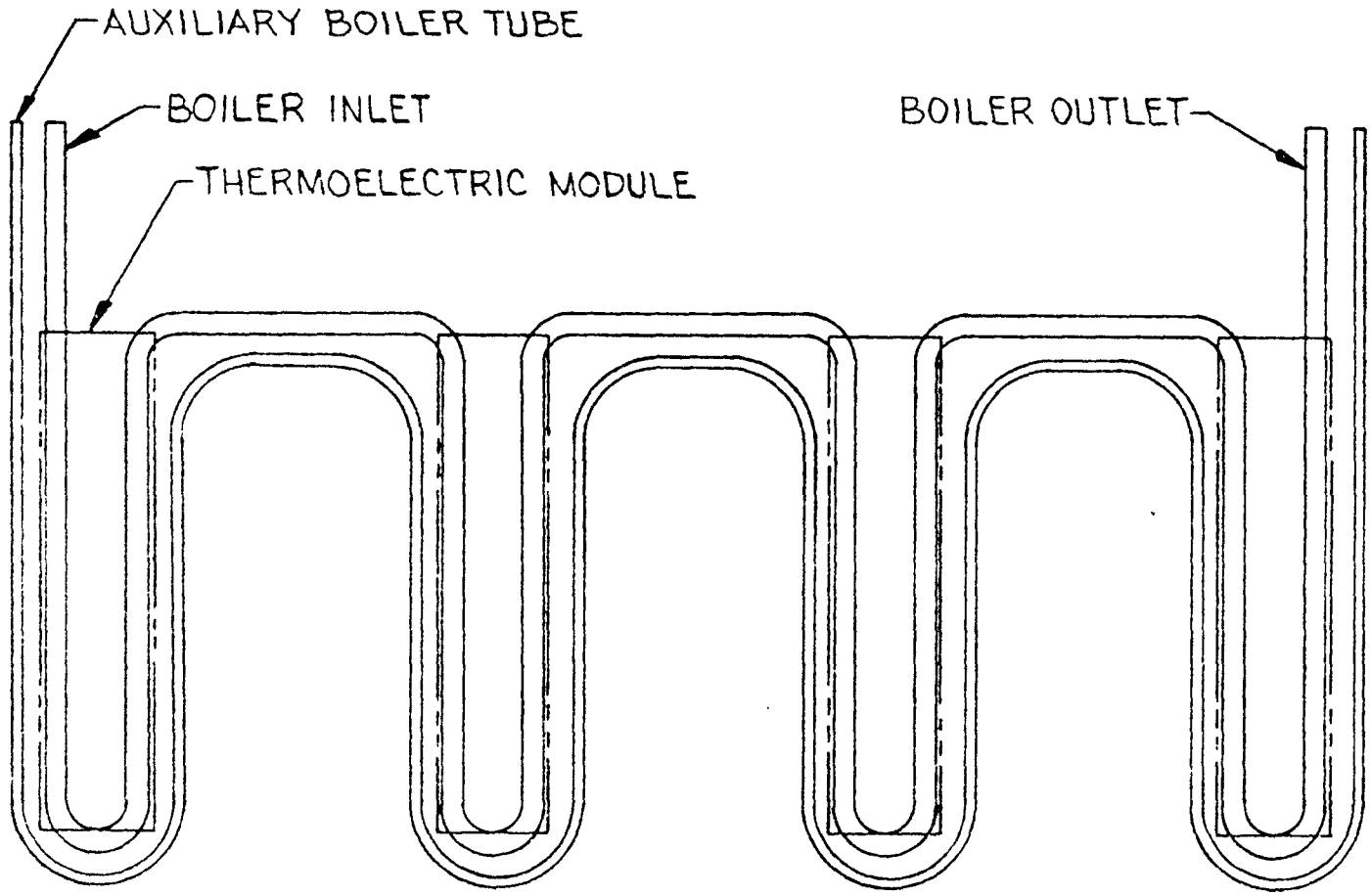


FIGURE 2
 COUPLE ASSEMBLY - EXPLODED VIEW



ESD-3138
-25-

FIGURE 3
SCHEMATIC
ALTERNATE BOILER TUBE ROUTING

APPENDIX A

The thermoelectric performance of the KIPS topping cycle was predicted in the following manner:

1. Test data and SIG GDS performance predictions were from the SIG program accumulated and reviewed. Values of Seebeck coefficient (α) and resistivity (ρ) were back calculated from open circuit voltage and resistance. This data was found in References 1 and 2.
2. Trends of α , ρ and conductivity (k) with temperature and current density (P leg only) were evaluated from Ref. 3. Absolute values of k for the P leg were quoted in this reference.
3. The test data and predicted GDS performance data were modified in accordance with the observed trends with temperature to give baseline values of α and ρ at $T_{\text{hot}} = 850^{\circ}\text{C}$ and $T_{\text{cold}} = 400^{\circ}\text{C}$. Since k_{p} is estimated at the test couple operating temperature range, k_{n} is calculated based on the test couple area ratio assuming an optimum efficiency design. k_{n} and k_{p} are then adjusted to the 850/400°C KIPS operating range.
4. Assuming a required load voltage of 28 volts at matched load operation, the required number of couples was calculated for a single string circuit.
5. Using equations presented in Ref. 4, the efficiency was determined based on best estimate values of α , ρ and k , and extrapolations of the GDS performance predictions.
6. Overall internal resistance, area ratio, and element cross sectional areas were determined. Current and P leg area were used to determine current density.

7. Values of α_p and ρ_p were corrected for the calculated current density if necessary. If significant changes in these properties occurred, the performance prediction calculations would be iterated starting at step 4.